Nano-photocatalytic Mineralization and Disinfection for Water Reclamation: From Catalyst Engineering to Process Optimization and Modelling

Meng Nan Chong

B.Eng. (Chemical Engineering)

Thesis submitted for the degree of
Doctor of Philosophy

School of Chemical Engineering

The University of Adelaide

February 2010

“The important thing in science is not so much to obtain new facts as to discover new ways of thinking about them” - *Sir William Bragg*

Table of Contents

ABSTRACT

In this thesis, a feasible photocatalytic technology for water treatment was explored using a *bottom-up* approach in four separate research and developmental stages. These include (1) the synthesis, characterizations and photocatalytic activity (PCI) evaluation of a thin nanocrystals layer of titanium dioxide (TiO_2) immobilised onto modified mesoporous kaolin clay; (2) optimization and kinetics study of the photocatalytic reaction with recalcitrant organic dye Congo red (CR); (3) optimization and kinetics study of the photocatalytic disinfection with surrogate *Escherichia coli* and (4) assessment of a sequential batch reactor (SBR) mode for semi-continuous removal of dissolved pharmaceutical organic matters from secondary municipal wastewater.

A modified two step sol-gel approach was used to immobilise layered of TiO_2 nanocrystals onto structurally stable kaolin (TiO_2-K) particles for enhanced physical properties. The TiO_2-K demonstrated a superior settling ability, adsorption capacity, PCI and stability compared to other conventional TiO_2 particles. Microscopic characterizations revealed that the modified kaolin provides a delaminated sandwich silica structure which minimizes chemical intercalation and further promotes high external surface area for heterocoagulation with microporous TiO_2 nanocrystals. Thermal regeneration cycles for the photocatalysts lifespan study examines that the PCI of TiO_2-K was improved over six treatment cycles, as a result of the change in average TiO_2 nanocrystals size and porosity.

The real operational performances of the TiO_2-K photocatalysts for the organic degradation in water were investigated in a self-designed laboratory scale annular slurry photoreactor (ASP) system. The effect of key operational factors for the ASP system, such as TiO_2-K loading, pH, aeration rate and CR concentration were investigated. Results show that pH was the most significant factor that affects the adsorption and photocatalytic reactions in the ASP system. The point of zero charge (PZC) for the TiO_2-K particles was found to shift towards more basic extent of 9.5, resulting in a detrimental PCI when the ASP was operated at pH > PZC (TiO_2-K). The optimum operating conditions of the ASP was found to be 6.0 g L^{-1} TiO_2-K loading, pH 7.0, 7.5 L min^{-1} aeration rate and 40 mg L^{-1} CR concentration. Under

these optimum ASP conditions, the CR was completely photo-degraded in 4 h along with 80% reduction in chemical oxygen demand (COD) of the LC/MS-identified intermediates species.

Owing to the lack of understanding and predictive in the singular optimum ASP condition, the Taguchi method was employed to collectively optimise the operating factor; determine the synergistic factor interactions and key influential factors, and further develop an empirical response surface model for the PCI prediction. From the Taguchi experiments, the photo-oxidation kinetics of CR exhibited saturation kinetics and thus, the Langmuir-Hinshelwood (L-H) model was applied. The Taguchi method predicted the optimum L-H apparent first order rate constant of 3.46×10^{-2} min^{-1} under the ASP operating conditions of 8.0 g L^{-1} TiO_2-K, pH 5.0, 7.5 L min^{-1} aeration rate and 40 mg L^{-1} CR. Analysis of variance revealed that the CR concentration is the most significant factor, while pH appears to be the least significant one. The aeration rate in ASP was determined to have a significant synergistic effect on the TiO_2-K loading from the 3-D response surface plot.

When the photo-oxidation of CR was referenced to the anatase titanate nanofiber (TNC) with PZC of 4.6, it was observed that the ASP operation was constrained by a narrow functional pH range. The optimum ASP operating conditions with slurry TNC were 4.0 g L^{-1} TNC loading, pH 3.0, 5 L min^{-1} aeration rate and 60 mg L^{-1} CR, resulting in a degradation rate of 3.47×10^{-2} mol L^{-1} min^{-1}. Subsequent Taguchi analysis found that the low PZC (TNC) has a profound effect on the synergistic interaction with its loading concentrations. The 3D response plots showed that the low PZC (TNC) could be compensated with a high TNC loading at pH > PZC (TNC) and low aeration rate for optimal conditions. The Taguchi method predicted that the optimum ASP operating conditions were 6.0 g L^{-1} TNC, pH 9, 5.0 L min^{-1} aeration rate and 20 mg L^{-1} CR. Analysis of variance shows that the pH, aeration rate and CR concentration were the significant factors, while TNC loading is the least significant one.

The PCI for both photocatalysts were also tested against the photo-disinfection of *Escherichia coli* (ATCC 11775) as the surrogate indicator in the batch ASP system. In both investigations, the photocatalytic inactivation kinetics was found to exhibit non-linearity in the enumerated bacteria against irradiation time. The modified Hom model was used to fit a sigmoidal-shape bacterial survivor curve with strong shoulder and tailing characteristics.

Using the TNC, the dissolved oxygen level in the open ASP system was found to be constantly replenished and further affects the photocatalytic inactivation kinetics. An L-H mechanistic model was proposed to determine oxygen transfer limitation in the photocatalytic disinfection process at different TNC loadings. A Fe^{2+} up to 1.0 mg L^{-1} could initiate the residual disinfecting effect (RDE) of the photocatalytic reaction in the ASP, with constant dissociation of hydrogen peroxide (H_2O_2) to hydroxyl radicals ($OH^{\cdot}$). The RDE was diminished with increasing COD values. To effectively suppress the bacterial regrowth, the dissolved organic carbon should be well suppressed below 16 mg COD L^{-1}.

Finally, the ASP system was operated as a SBR mode to allow semi-continuous treatment of the secondary municipal wastewater spiked with pharmaceutical Carbamazepine (CBZ) compound. A microfiltration module of 0.2 μm in porosity was fitted parallel to the reactor light source. The effects of key factors such as SBR cycles, nitrate (NO_3^-), phosphate (PO_4^{3-}), COD and photocatalysts on the effective photocatalytic CBZ removal were investigated. When the CBZ was degraded in the presence of high molecular weight effluent organic matter (EOM) in wastewater, the photocatalytic reaction appeared to have a preferential attack on the EOM that subsequently lower the degradation efficiency of CBZ. Other than this, the PO_4^{3-} in the wastewater showed a detrimental effect of photocatalyst fouling and deactivation on both TiO_2 catalysts used, resulting in a strong catalyst deactivation, and fouling of the catalysts. The deactivation and fouling are site specific and do not completely retard the photoactivity of the catalysts used. The sequential batch-annular slurry photoreactor (SB-ASP) was effectively operated up to two SBR cycles at catalyst loading (1 gL^{-1}) without any photocatalyst replacement, as the semi-continuous operation allows simultaneous water discharge and UV photocatalyst reactivation phase.

DECLARATION

NAME: Meng Nan Chong Program: PhD (Chemical Engineering)

This work contains no material which has been accepted for the award of any other degree or diploma in any university or other tertiary institution and, to the best of my knowledge and belief, contains no material previously published or written by another person, except where due reference has been made in the text.

I give consent to this copy of my thesis when deposited in the University Library, being made available for loan and photocopying, subject to the provisions of the Copyright Act 1958.

The author acknowledges that copyright of published works contained within this thesis (as listed below*) resides with the copyright holder(s) of those works. I also give permission for the digital version of my thesis to be made available on the web, via the University's digital research repository, the Library catalogue, the Australasian Digital Theses Program (ADTP) and also through web search engines, unless permission has been granted by the University to restrict access for a period of time.

*List of publications contained in this thesis and the copyright holder(s) for each work are as follows:

1. **M.N. Chong**, B. Jin, C.W.K. Chow, C. Saint. Recent developments in photocatalytic technology for water treatment: A review. Submitted to *Water Research*.

2. **M.N. Chong**, V. Vimonses, S. Lei, B. Jin, C. Saint, C. Chow. 2009. Synthesis and characterisation of novel titania impregnated kaolinite nano-photocatalyst. *Microporous and Mesoporous Materials* 117:233-242. Copyright for this paper belongs to Elsevier B.V.

3. V. Vimonses, **M.N. Chong**, B. Jin. Evaluation of the physical properties and photodegradation ability of titania nanocrystalline impregnated onto modified kaolin. Submitted to *Microporous and Mesoporous Materials*.

4. **M.N. Chong**, S. Lei, B. Jin, C. Saint, C. Chow. 2009. Optimisation of an annular photoreactor process for degradation of Congo red using a newly synthesized titania impregnated kaolinite nano-photocatalyst. *Separation and Purification Technology* 67:355-363. Copyright for this paper belongs to Elsevier B.V.

5. **M.N. Chong**, B. Jin, H.Y. Zhu, C. Chow, C. Saint. 2009. Application of H-titanate nanofibers for degradation of Congo red in an annular slurry photoreactor. *Chemical Engineering Journal* 150:49-54. Copyright for this paper belongs to Elsevier B.V.

6. **M.N. Chong**, B. Jin, C. Chow, C. Saint. 2009. A new approach to optimise an annular photoreactor system for the degradation of Congo red: Statistical analysis and modelling. *Chemical Engineering Journal* 152:158-166. Copyright for this paper belongs to Elsevier B.V.

7. **M.N. Chong**, H.Y. Zhu, B. Jin. 2010. Response surface optimization of photocatalytic process for degradation of Congo red using H-titanate nanofiber catalyst. Accepted by *Chemical Engineering Journal* 156:278-285. Copyright for this paper belongs to Elsevier B.V.

8. **M.N. Chong**, B. Jin. Photo-disinfection activity and kinetics of Escherichia coli using novel titania impregnated kaolinite catalyst. Submitted to *Chemical Engineering Journal*.

9. **M.N. Chong**, B. Jin, H.Y. Zhu, C. Saint. Bacterial inactivation kinetics, regrowth and synergistic competition in a photocatalytic disinfection system using anatase titanate nanofiber catalyst. Submitted to *Journal of Photochemistry and Photobiology A: Chemistry*.

10. **M.N. Chong**, B. Jin, C. Saint. Kinetic and mathematical modelling for the photocatalytic inactivation of Escherichia coli in an annular slurry photoreactor using titanate nanofiber catalyst. Submitted to *Chemical Engineering Journal*.

11. **M.N. Chong**, B. Jin, C.W.K. Chow, H. Zhu, C. Saint. Assessment of sequential batch photoreactor system for the removal of Carbamazepine from secondary municipal wastewater: Impacts of effluent organic matter and inorganic ions. Submitted to *Environmental Science and Technology*.

Signature…… Date……

ACKNOWLEDGEMENT

I would like to sincerely express my utmost gratitude to all who had supported and accompanied me through my Ph.D research journey to completion. Without your kind assistance and help in every phase of my study, it would have been impossible for me to cross the finish line!

First of all, I feel grateful and indebted to my principal supervisor, Associate Professor Bo Jin, where his initial and continuing trust have grounded me a doctoral scholarship and the candidature. I would say that without your academic guidance, constant encouragement, effort and sleepless nights on revising the best out of my manuscripts, I would not be in a state which I am in now! Special thanks are dedicated Professor Shaomin Lei, where without your advices in the clay catalyst preparation, this project would not get off the ground and propel like how it did now! Similar level of merits also goes to Professor Huaiyong Zhu, who has provided me with the nanofiber catalyst preparation and your manuscript revision is incomparable.

This was followed by a warmly thank to my associate industry supervisors, Professors Christopher W.K. Chow and Christopher P. Saint, who have impressed me with their enthusiasm for research and great insight into the current development in a broad range of industrial water subjects. Without you, I would say that my research is not as detailed and constructive as it looks. Many thanks also to the former colleagues in SA Water Centre for Water Management and Reuse at University of South Australia, particularly Professor Dennis Mulcahy, Dr John van Leeuwen, Mr David Pezzaniti, Mr Baden Myers, Ms Carolyn Bellamy and most of all, Mr Tim Golding for your photoreactor construction.

Countless thanks are also dedicated to a number of professional and scientific individuals, who have contributed to the success of my research project: Mr Philip Adcock (AWQC), Dr Yunfei Xi (CERAR), Dr Peter Self (Adelaide Microscopy), Dr Julie Culbert (Provisor) and Dr Daniel Jardine (Flinders University). I would like to convey my thanks to every of the past and present members of the Water Environment Biotechnology Laboratory for your shared

laughter, joy, help and our time together: Drs. Richard Haas, Zhanying Zhang, Xiaoyi Wang, Yang Yang, Qinxue Wen, Giuseppe Laera, Hongjie An and postgraduate research students; in particular, Ms Vipasiri Vimonses, Adrian Hunter, Florian Zepf, Guiqin Cai, Tzehaw Sia, Manjot Kaur and all the visiting German students.

I also wish to express my gratitude to the University of South Australia and the University of Adelaide, for accommodating me during my research candidature and provided me with an APAI scholarship. I would like to acknowledge the Australia Research Council and Australian Water Quality Centre, SA Water Corporation, which contributed to this project substantially by funding the project.

Finally, I would like to give my special thanks to my girlfriend SiewChoo Wang for her love and understanding and to my parents and friends for their encouragement, care and support during my PhD tenure.

PREFACE

This thesis contains nine chapters, of which six chapters (Chapter 2, 4, 5, 6, 7 and 8) comprise the main body. In Chapter 1, a general introduction to this project and thesis is outlined. Chapter 2 contains a comprehensive literature review, which has been submitted for publication. Chapter 3 is a general introduction to the experimental materials and methods used in this study. Specific details of the methods are given in the relevant chapters. This project aimed to develop and utilize new TiO_2 photocatalysts for the integration with an annular photoreactor system for the treatment of wastewaters. The research outcomes and findings are presented thoroughly in Chapters 4 to 8. In Chapter 4, the research focuses on the synthesis, characterisation and application of nanocrystalline titania impregnated onto modified kaolinite clay (TiO_2-K) for enhanced catalyst recovery and adsorption capacity. The durability and physical changes in the structure of the catalyst over repetitive use in water treatment was also identified. In Chapter 5, the photocatalytic activity of two different self-made photocatalysts (i.e. TiO_2-K and titanate nanofiber catalyst (TNC)) on sub-micron immobilizers were evaluated and compared in an annular slurry photoreactor (ASP) system. The influence of different photoreactor operational factors on the photooxidation rate of Congo red was studied. However, the optimized operating conditions as obtained from the studies were seen to be rather frail due to a lack of data on the factor interactions and correlations. In Chapter 6, a relatively new multi-variable optimization approach based on response surface optimization was employed to statistically identify the most significant factors, factor interactions and correlations for the two photocatalysts used. These two photocatalysts showed different isoelectric properties. The TNC catalyst with low point of zero charge experienced higher operational obligations from the factor interactions. In Chapter 7, the photo-disinfection using both photocatalysts was also evaluated under different operational conditions of the ASP system. The photo-inactivation rate of bacterial *Escherichia coli* (ATCC 11775) was evaluated using different disinfection rate models. It was observed that with the thin fibril morphology of the titanate nanofiber catalyst, an additional limiting term of dissolved oxygen should be introduced to the denominator of the mechanistic Langmuir-Hinshelwood equation. Furthermore, the residual disinfecting effect of the TNC catalyst with different ferric ion concentration was assessed and it was found that the underlying bacterial regrowth mechanism depends on the organic carbon level in water.

Chapter 8 demonstrated the possibility of using the ASP system in a sequential batch reactor (SBR) operation mode for the semi-continuous treatment process of secondary wastewater containing Carbamazepine, a pharmaceutical compound that usually penetrates through the biological activated sludge treatment. The influence of catalysts, SBR cycle, organic matter and inorganic ions on the photo-degradation performance for removal of Carbamazepine and chemical oxygen demand was assessed. Finally Chapter 9 draws the conclusions from each individual published paper and results chapters and discusses the possible future prospects for continued work in this area.

Chapters of 4, 5 and 6 have been partially published in refereed academic journals. The remaining in Chapter 2, 4, 5, 6, 7 and 8 have also been submitted for consideration of publication in different refereed academic journals. All the papers are closely related to the research field of this work.

CHAPTER 1

INTRODUCTION

1. Background

Water reclamation has become the foremost issue in most countries of the world that are facing severe water shortage problems. The main factors that contribute to the increasing water demand are varied, depending on the geographical location, population growth and distribution, activities and the availability of water resources. In the current water scenario, it is estimated that 1.2 billion people worldwide have lack of access to safe potable water, 2.6 billion have poorly sanitized water and millions of people are annually because of waterborne diseases (Malato et al., 2009). Furthermore, it is estimated that 3900 children a day face death owing to the waterborne diseases transmitted through unsafe water or human excreta. To resolve the water shortage problems and increase the clean water supply, new or viable water resources with cost-effective water treatment technologies are needed.

Reclamation of wastewater for reuse has become more popular among the developed countries, in particular countries that are geographically located in the driest continents with minimal rainfall, high evaporation rate, intense use of water for irrigation (Viessman and Hammer, 1998). The term "*reclamation*" in this instance, implies the use of a combination of conventional with advanced treatment processes that return the wastewater to nearly original quality. Such wastewater reclamation and reuse schemes have a high potential to minimize the disposal of water to the natural environment and to reduce the demand on fresh water supplies (Neal, 1996). Such augmentation using recycled water supplies for both potable and non-potable use will relieve the demand on fresh water supply with longer term benefits for the community. Among the developed countries, Australia, and in particular South Australia region is one of the driest regions that receives very low rainfall, abundant of sunlight and is also home to a highly productive horticultural business, e.g. vineyards, where an assured supply of water is a critical factor to success. The dwindling of water resources as a consequence of various external factors, coupled with the urgency to better manage the existing water resources in South Australia have driven the need for water recycling.

Different viable water resources could be reclaimed, depending on the physical, chemical and biological constituents that may impose some restrictions on their cost-effective treatment. Industrial, municipal, brackish and saline wastewaters are the potential water resources that could be reclaimed for agricultural, irrigation, aquaculture or even direct potable reuse. The treated sewage effluent from the municipal wastewater plants is one of the few attractive options that could be reclaimed to provide water for agricultural and farming activities (Lapeña et al., 1995; Bradley et al., 2002). The possible reclamation for reuse of the treated municipal sewage effluents is often associated with the presence of suspended solids, health-threatening pathogens and soluble refractory organic compounds that are both tedious and expensive to remove (Viessman and Hammer, 1998). A more cost-effective integrated technology for water reclamation to remove all the water contaminants and improve the reclaimed water quality is highly anticipated. In this instance, a large-scale example of sewage water reclamation effort was evidenced in the Virginia pipeline scheme where 22 GL of advanced treated sewage water has been contracted from the Bolivar sewage treatment plant near Adelaide (South Australia) to irrigate market gardens on the Northern Adelaide Plains (Dillon, 2000). With the beginning of such a large water reuse scheme, it is expected that more water reuse projects will be delivered into the future Australian water scene. Dillon (2000) projected that the water reuse will increase by at least 28 GL per year.

However, the currently available water treatment technologies cannot be regarded as efficient and cost-effective treatment in reclaiming the municipal sewage effluent for reuse. Before the turn of the new millennium, it was reported that no major Australian city had more advanced sewage treatment than secondary treatment, and some cities were still piping primary treated effluent into high energy coastlines and relying on dispersion (Dillon, 2000). In the current scene, advanced technologies for wastewater treatment have been adopted such as dissolved air flotation, microfiltration, adsorption with activated carbon, reverse osmosis and biological nutrient removal. The combination of conventional processes (i.e. flocculation, sedimentation and filtration) with these advanced technologies for water reclamation was proven to be effective to produce reclaimed water with better quality. On the downside, such advanced treatment technologies usually incur high costs and have retarded the overall progress in wastewater reuse over the years (Gaya and Abdullah, 2008). Furthermore, the current technologies are not environmentally friendly as the water pollutants are being transferred

from one phase to another rather than being completely mineralized from the treated wastewater stream (Padmanabhan et al., 2006). This might indirectly generate secondary toxic pollutants into the natural ecosystem. These condensed toxic pollutant streams are highly redundant and have been a concern worldwide due to increasing environmental awareness and legislations. To heighten environmental concern, chemical disinfectants such as chlorination are still in practice during the final stage of wastewater reclamation to ensure minimal water pathogens to penetrate into the ecosystems. When the chlorine reacts with the organic matter in the wastewater stream, disinfection by-products might be generated that are of mutagenic and carcinogenic hazards to human health and ecosystem (Yang et al., 2007; Lu et al., 2009; Coleman et al., 2005).

All these public and environmental concerns have led to a need of research and development in the field of "Advanced Oxidation Processes (AOPs)", as the innovative wastewater reclamation technologies. The principles of these AOPs are based on the in-situ generation of highly reactive transitory species (i.e. H_2O_2, $OH^{\cdot}$, $O_2^{\cdot -}$, O_3) for the mineralization of refractory organic compounds and pollutants, pathogens and disinfection by-products (Esplugas et al., 2002; Pera-Titus et al., 2004). Among these AOPs, heterogeneous photocatalysis employing semiconductor titanium dioxide (TiO_2) photocatalyst has demonstrated its wide applicability in the oxidation of ambiguous refractory organics into readily biodegradable compounds and eventually mineralize them into innocuous carbon dioxide and water. Generally, the semiconductor TiO_2 is the most active photocatalyst under the photon energy of $300nm < \lambda < 390nm$ and remains stable after repeated catalytic cycles (Malato et al., 2009). Other than these, the multi-faceted functional properties of semiconductor TiO_2 such as their chemical and thermal stability, resistance to chemical breakdown and their strong mechanical properties have promoted its wide application as an innovative and sustainable wastewater reclamation technology. Other important features of the heterogeneous TiO_2 photocatalysis which may have extended their feasible applications in wastewater reclamation include; (1) ambient operating conditions, such as temperature and pressure, (2) complete mineralisation without secondary pollution and (3) low capital and operation costs.

To date, the superiority of the highly reactive oxygen species (ROS) generated as a result of the photo-induced charge separation on the surface of TiO_2 for both microbial inactivation and

organic mineralisation is well-documented. At present, the application of such TiO_2 photocatalytic processes for water/wastewater treatment is still experiencing a series of technical challenges. The post-separation of the semiconductor TiO_2 catalyst after water treatment remains the major obstacle towards the practicality of an industrial process. The fine size of the TiO_2 catalyst particles, together with their large surface area-to-volume ratio and surface energy creates a strong tendency for such catalyst particles to agglomerate during the operation. Such particle agglomeration is highly detrimental in terms of the conservation of particle size, specific surface area and its reusable lifespan. Other technical challenges include the understanding and development of a photocatalytic reactor system that could be operated cost-effectively, its subsequent process optimization and modelling. When all these technical challenges can be resolved, it is expected that the operation or integration of the photocatalytic treatment technology could provide an economical, environmentally sustainable and technically robust solution to the existing wastewater reclamation technology.

2. Aims

The aim of this research was to develop a novel photocatalyst and photoreactor system to treat the different wastewaters (i.e. industrial or municipal) for wastewater reclamation purposes. Research has focused on four different research and developmental stages which comprised of:

(1) The synthesis, characterizations and photoactivity evaluation of a novel titania impregnated kaolinite nano-photocatalysts (TiO_2-K).
(2) Optimization and kinetic study of the photocatalytic reaction with recalcitrant organic dye (Congo red) molecules.
(3) Optimization and kinetic study of the photocatalytic disinfection with surrogate *Escherichia coli* and
(4) Assessment of a sequential batch reactor (SBR) mode for semi-continuous removal of dissolved pharmaceutical organic matters from secondary municipal wastewater.

3. References

Bradley, B.R., Daigger, G.T., Rubin, R., Tchobanoglous, G., 2002. Evaluation of onsite wastewater treatment technologies using sustainable development criteria. Clean Technol. Environ. Policy 4, 87-99.

Coleman, H.M., Marquis, C.P., Scott, J.A., Chin, S.S., Amal, R., 2005. Bactericidal effects of titanium dioxide-based photocatalysts. Chem. Eng. J. 113, 55-63.

Dillon, P., 2000. Water reuse in Australia: Current status, projections and research. Proc. Wat. Recycling Australia 2000, Adelaide 19-20 Oct 2000, 99-104.

Esplugas, S., Giménez, J., Conteras, S., Pascual, E., Rodríguez, M., 2002. Comparison of different advanced oxidation processes for phenol degradation. Wat. Res. 36, 1034-1042.

Gaya, U.I., Abdullah, A.H., 2008. Heterogeneous photocatalytic degradation of organic contaminants over titanium dioxide: A review of fundamentals, progress and problems. J Photochem. Photobiol. C: Photochem. Rev. 9, 1-12.

Lapeña, L., Cerezo, M., García-Augustin, P., 1995. Possible reuse of treated municipal wastewater for Citrus spp. plant irrigation. Bulletin Environ. Contamination Toxicol. 55, 697-703.

Lu, J., Zhang, T., Ma, J., Chen, Z., 2009. Evaluation of disinfection by-products formation during chlorination and chloramination of dissolved natural organic matter fractions isolated from a filtered river water. J. Hazar. Mater. 162 (2009) 140-145.

Malato, S., Fernández-Ibáñez, P. Maldonado, M.I. Blanco, J., Gernjak, W., 2009. Decontamination and disinfection of water by solar photocatalysis: Recent overview and trends. Catal. Today 147, 1-59.

Neal, J., 1996. Wastewater reuse studies and trials in Canberra. Desalination 106, 399-405.

Padmanabhan, P.V.A., Sreekumar, K.P., Thiyagarajan, T.K., Satpute, R.U., Bhanumurthy, K., Sengupta, P., Dey, G.K., Warrier, K.G.K., 2006. Nano-crystalline titanium dioxide formed by reactive plasma synthesis. Vacuum 80, 11-12.

Pera-Titus, M., García-Molina, V., Baños, M.A., Giménez, J., Esplugas, S., 2004. Degradation of chlorophenols by means of advanced oxidation processes: a general review. Appl. Catal. B: Environ. 47, 219-256.

Viessman Jr., W., Hammer, M.J., 1998. Water supply and pollution control. Addison Wesley Longman Inc. 6th Edition, California USA.

Yang, H., Cheng, H., 2007a. Controlling nitrite level in drinking water by chlorination and chloramination. Sep. Purif. Technol. 56, 392-396.

CHAPTER 2

LITERATURE REVIEW: RECENT DEVELOPMENT IN PHOTOCATALYTIC TECHNOLOGY FOR WATER TREATMENT: A REVIEW

CHAPTER 2

LITERATURE REVIEW

RECENT DEVELOPMENT IN PHOTOCATALYTIC TECHNOLOGY FOR WATER TREATMENT: A REVIEW

M. N. Chong [a,b], B. Jin [a,b,c], C. W. K. Chow [c], C. Saint [c]

[a] School of Chemical Engineering, The University of Adelaide 5000 Adelaide Australia

[b] School of Earth and Environmental Sciences, The University of Adelaide 5000 Adelaide Australia

[c] Australian Water Quality Centre, SA Water Corporation, 5000 Adelaide South Australia

Submitted manuscript to Water Research.

STATEMENT OF AUTHORSHIP

RECENT DEVELOPMENT IN PHOTOCATALYTIC TECHNOLOGY FOR WATER TREATMENT: A REVIEW

Submitted manuscript to Water Research.

Chong, M.N. (Candidate)
Performed literature review; interpreted data; manuscript evaluation; wrote manuscript.

Signed……*Date*……..

Jin, B.

Supervision of manuscript preparation; manuscript evaluation; acted as corresponding author.

I give consent for M. N. Chong to present this paper for examination towards the Doctor of Philosophy

Signed……*Date*……..

Chow, C. W. K.

Supervision of manuscript preparation; manuscript evaluation

I give consent for M. N. Chong to present this paper for examination towards the Doctor of Philosophy

Signed……*Date*……..

Saint, C.

Supervision of manuscript preparation; manuscript evaluation

I give consent for M. N. Chong to present this paper for examination towards the Doctor of Philosophy

Signed……*Date*……..

Recent Developments in Photocatalytic Technology for Water Treatment: A Review

Meng Nan Chong [a,b], Bo Jin [a,b,c*], Chow C.W.K [c], Chris Saint [b,c]

[a] School of Chemical Engineering, The University of Adelaide 5000 Adelaide Australia

[b] School of Earth and Environmental Sciences, The University of Adelaide 5000 Adelaide Australia

[c] Australian Water Quality Centre, SA Water Corporation, 5000 South Australia

[*] To whom correspondence should be addressed.

Tel.: +61 8 8303 7056. Fax: +61 8 8303 6222. Email: bo.jin@adelaide.edu.au

Abstract

In recent years, the semiconductor photocatalytic process has shown great potential as a low-cost, environmentally friendly and sustainable treatment technology to align with the "*zero*" waste scheme in the water industry. The ability of this advanced oxidation technology has been widely proven to remove persistent organic compounds and microorganisms in water. At present, the main technical barriers that impede its commercialisation remain the post-recovery of the catalyst particles after water treatment so that they may be economically re-used.

This paper reviews the recent R&D progress of engineered-photocatalysts, photo-reactor systems and the process optimizations and modelling of the photo-oxidation processes for water/wastewater treatment. A number of potential and commercial photocatalytic reactor configurations are discussed, in particular the photocatalytic membrane reactors. The effects of key photoreactor operation parameters and water quality on the photo-process performances in terms of the mineralization and disinfection are assessed. For the first time, we describe how to utilise a multi-variable approach to determine the optimum operation parameters so as to enhance process performance and photo-oxidation efficiency. Both photomineralization and photo-disinfection kinetics and their modelling associated with the photocatalytic water treatment process are detailed. A brief discussion on the life cycle assessment for retrofitting the photocatalytic technology as an alternative waste treatment process is presented. This paper will deliver a scientific and technical overview and useful information to scientists and engineers who work in this field.

Keywords: TiO_2; Photocatalysis; Water treatment; Photocatalytic Reactors; Kinetic Modelling; Water Quality; Life Cycle Analysis; Mineralization; Disinfection.

1. Introduction

Increasing demand and shortage of clean water sources due to the rapid industrialisation, population growth and long-term droughts have become an issue worldwide. With this growing demand, various practical strategies and solutions have been adopted to yield more viable water resources. The storage of rainwater for daily activities and increasing the catchment capacity for stormwater are just a few examples that could resolve the problems in the short-term. Water industries and governments in some arid areas with abundant sunlight, less rainfall and long term drought have a challenge to seek viable water resources. It is estimated that around 4 billion people worldwide experience little or no access to clean and sanitised water supply, while millions of people die annually because of severe waterborne diseases (Malato et al., 2009). These statistical figures are expected to grow in the near future, from increasing water contamination due to overwhelming discharge of micropollutants and contaminants into the natural water cycle (Wintgens et al., 2008; Richardson 2008; Suárez 2008). With a view to suppress the worsening of clean water availability, development of advanced low-cost and high efficiency water treatment technologies to treat wastewater for reuse is desirable.

One of the attractive options is the possible reuse of onsite rural wastewater or the treated municipal wastewater from treatment plants for agricultural and industrial activities (Bradley et al., 2002; Lapeña et al., 1995). Since these wastewaters constitute one of the largest possible water resources, its reuse is anticipated to offset more clean water use. Recycling wastewaters are usually associated with the presence of suspended solids, pathogens and soluble refractory organic compounds that are both tedious and expensive to treat (Viessman et al., 1998). Currently available water treatment technologies such as adsorption or coagulation merely concentrate the pollutants present by transferring them to other phases and they still remain, not being completely "*eliminated*" or "*destroyed*" (Padmanabhan et al., 2006). Other conventional water treatment methods such as sedimentation, filtration, chemical and membrane technologies involve high operating costs and could generate toxic secondary

pollutants into the ecosystem (Gaya and Abdullah, 2008). These concentrated toxic contaminants are highly redundant and are of concern worldwide due to the increasing environmental awareness and legislations. Chlorination has been most commonly and widely used during the disinfection process. The disinfection by-products generated from chlorination are mutagenic and carcinogenic to human health (Yang et al., 2007a; Lu et al., 2009; Coleman et al., 2005).

The need to resolve reuse water quality issues has led to recent R&D in the field of "Advanced Oxidation Processes (AOPs)" as a potential innovative water treatment technology. The rationale of these AOPs are based on the in-situ generation of highly reactive transitory species (i.e. H_2O_2, $OH^{\cdot}$, $O_2^{\cdot}$-, O_3) for mineralization of refractory organic compounds, water pathogens and disinfection by-products (Esplugas et al., 2002; Pera-Titus et al., 2004). Among these AOPs, heterogeneous photocatalysis employing semiconductor catalysts (TiO_2, ZnO, Fe_2O_3, CdS, GaP and ZnS) has demonstrated its efficiency in degrading a wide range of ambiguous refractory organics into readily biodegradable compounds and eventually, mineralization to innocuous carbon dioxide and water. Among the semiconductor catalysts, titanium dioxide (TiO_2) has received the greatest attention in R&D of photocatalysis technology. TiO_2 generally is the most active photocatalyst under the photon energy of 300nm $< \lambda <$ 390nm and remains stable after repeated catalytic cycles, whereas Cds or GaP are degraded to produce final toxic products (Malato et al., 2009). Other than these, the multi-faceted functional properties of TiO_2 catalysts, such as their chemical and thermal stability, resistance to chemical breakdown and their strong mechanical properties have promoted its wide application in photocatalytic water treatment.

A number of important features of heterogeneous photocatalysts have extended their feasible applications in water treatment, such as; (1) ambient operating temperature and pressure, (2) complete mineralisation without secondary pollution and (3) low operation costs. The fact that the highly reactive oxygen species (ROS) generated as a result of the photo-induced charge separation on TiO_2 surfaces are effective at microbial inactivation and organic mineralisation without creating any secondary pollution is well-documented. So far, the application of such TiO_2 catalysts for water treatment is still experiencing a series of technical challenges. The post-separation of the semiconductor TiO_2 catalyst after water treatment remains the major

obstacle towards the practicality of an industrial process. The fine particle size of the TiO_2 particles, together with the large surface area-to-volume ratio and surface energy creates a strong tendency for such catalyst particles to agglomerate during the operation. Such particle agglomeration is highly detrimental in view of particle size preservation, surface area reduction and reusable lifespan. Other technical challenges include the catalysts development with broader photoactivity range and its integration with a feasible photocatalytic reactor system. In addition, the understanding of the theory behind the common reactor operational parameters and their interactions is also lacking and presents a difficult task for process optimization. A number of commonly made mistakes in studying kinetic modelling of either the photomineralization or photo-disinfection have also been seen over the years.

This review paper aims to give an overview of the understanding and development of photocatalytic water treatment technology, from fundamentals of catalyst and photoreactor development to process optimization and kinetic modelling and eventually, the water parameters that affect the process efficiency. A short outline of the feasible application of photocatalytic water technology via life cycle interpretation and the possible future challenges are also recommended.

2. Fundamentals and Mechanism of TiO_2 Photocatalysis

2.1. Heterogeneous TiO_2 Photocatalysis

The fundamentals of photophysics and photochemistry underlying the heterogeneous photocatalysis employing the semiconductor TiO_2 catalyst have been intensively reported in the literature (Gaya and Abdullah, 2008; Fujishima et al., 2000). The semiconductor TiO_2 has been widely utilised for inducing a series of reductive and oxidative reactions on its surface. This is contributed solely by the distinct lone electron characteristic in its outer orbital. When photon energy (*hv*) of greater than or equal to the bandgap energy of TiO_2 is illuminated onto its surface, usually 3.2 eV (anatase) or 3.0 eV (rutile), the lone electron will be photoexcited to the empty conduction band in femtoseconds. Fig. 1 depicts the mechanism of the electron-hole pair formation when the TiO_2 particle is irradiated with adequate *hv*. The light wavelength for such photon energy usually corresponds to $\lambda < 400$nm. The photonic excitation leaves behind

an empty unfilled valence band, and thus creates the electron – hole pair (e^- - h^+). The series of chain oxidative-reductive reactions (Eq. 2.1 – 2.11) that occur at the photon activated surface is postulated as follows:

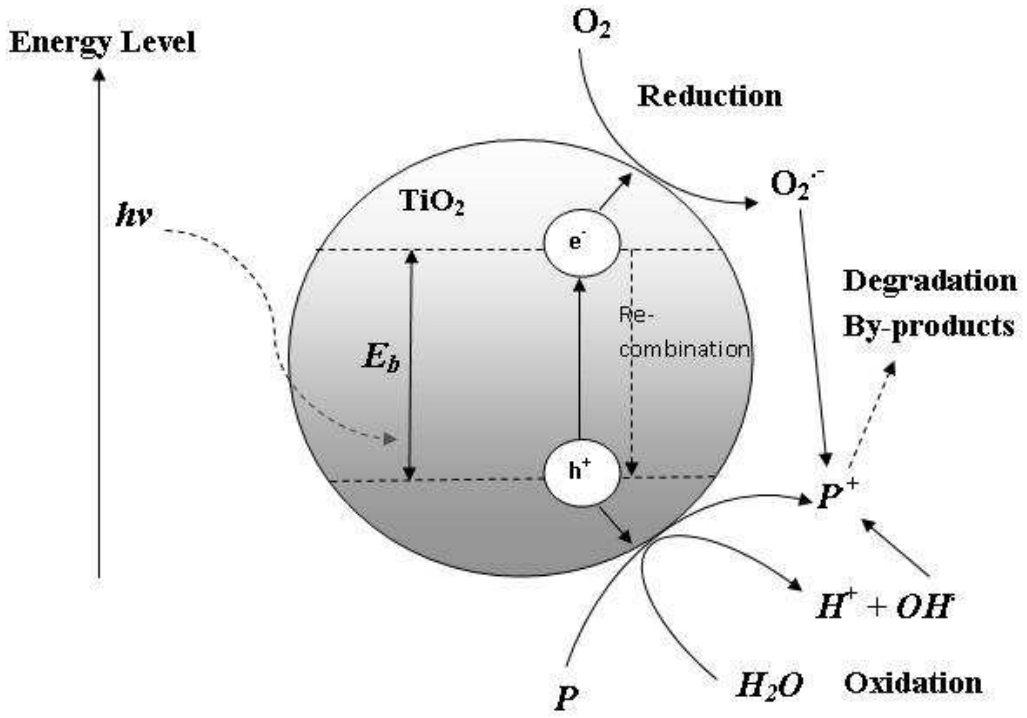

Figure 1: Photo-induced formation mechanism of electron-hole pair in a semiconductor TiO_2 particle in the presence of water pollutant (P).

Photoexcitation: $TiO_2 + hv \rightarrow e^- + h^+$ (Eq. 2.1)

Charge carrier trapping of e-: $e^-_{CB} \rightarrow e^-_{TR}$ (Eq. 2.2)

Charge carrier trapping of h+: $h^+_{VB} \rightarrow h^+_{TR}$ (Eq. 2.3)

Electron – hole recombination: $e^-_{TR} + h^+_{VB}(h^+_{TR}) \rightarrow e^-_{CB}$ + heat (Eq. 2.4)

Photoexcited e^- scavenging: $(O_2)_{ads} + e^- \rightarrow O_2^{\cdot -}$ (Eq. 2.5)

Oxidation of hydroxyls: $OH^- + h^+ \rightarrow OH^\cdot$ (Eq. 2.6)

Photodegradation by $OH^\cdot$: $R\text{-}H + OH^\cdot \rightarrow R'^\cdot + H_2O$ (Eq 2.7)

Direct photoholes: $R + h^+ \rightarrow R^{+\cdot} \rightarrow$ Intermediate(s)/ Final Degradation Products (Eq. 2.8)

Protonation of superoxides: $O_2^{\cdot -} + OH^\cdot \rightarrow HOO^\cdot$ (Eq.2. 9)

Co-scavenging of e^-: $HOO^{\cdot} + e^- \rightarrow HO_2^-$ (Eq. 2.10)

Formation of H_2O_2: $HOO^- + H^+ \rightarrow H_2O_2$ (Eq. 2.11)

The e^-_{TR} and h^+_{TR} in Eq. 2.4 represent the surface trapped valence band electron and conduction band hole respectively. It was reported that these trapped carriers are usually TiO_2 surface bound and do not recombine immediately after photon excitation (Furube et al., 1999). In the absence of electron scavengers (Eq. 2.4), the photo-excited electron recombines with the valence band hole in nanoseconds with simultaneous dissipation of heat energy. Thus, the presence of electron scavengers is vital for prolonging the recombination and successful functioning of photocatalysis. Eq. 2.5 depicts how the presence of oxygen prevents the recombination of electron–hole pair, while allowing the formation of superoxide radicals ($O_2^{\cdot -}$). This $O_2^{\cdot -}$ radical can be further protonated to form the hydroperoxyl radical ($HO_2^{\cdot}$) and subsequently H_2O_2 as shown in Eqs. 2.9 and 2.10, respectively. The $HO_2^{\cdot}$ radical formed was also reported to have scavenging properties and thus, the co-existence of these radical species can doubly prolong the recombination time of the h^+_{TR} in the entire photocatalysis reaction. However, it should be noted that all these occurrences in photocatalysis were attributed to the presence of both dissolved oxygen (DO) and water molecules. Without the presence of water molecules, the highly reactive hydroxyl radicals ($OH^{\cdot}$) could not be formed and this would impede the photodegradation of liquid phase organics. This was evident from a few reports that the photocatalysis reaction did not proceed in the absence of water molecules. Some simple organic compounds (e.g. oxalate and formic acid) can be mineralized by direct electrochemical oxidation where the e^-_{TR} are scavenged by metals ions in the system without water present (Byrne et al., 1998a). Although the h^+_{TR} has been widely regarded for its ability to oxidize organic species directly, this possibility has remained inconclusive. The h^+_{TR} are powerful oxidants (+1.0 to +3.5V against NHE), while e^-_{TR} are good reductants (+0.5 to -1.5V against NHE) depending on the type of catalysts and oxidation conditions.

Many elementary mechanistic studies on different surrogate organic compounds (e.g. phenol, chlorophenol, oxalic acid) have been extensively investigated with regard to photodegradation over TiO_2 surface. Aromatic compounds can be hydroxylated by the reactive $OH^{\cdot}$ radical that leads to successive oxidation/addition and eventually ring opening. The resulting intermediates, mostly aldehydes and carboxylic acids will be further carboxylated to produce

carbon dioxide and water. Since the photocatalysis reaction occurs on the photon activated surface of TiO_2, the understanding of the reaction steps that involves photodegradation of organics is essential in the formulation of kinetic expression. For heterogeneous photocatalysis, the liquid phase organic compounds are degraded to its corresponding intermediates and further mineralized to carbon dioxide and water, if the irradiation time is extended (Eq. 2.12).

$$Organic\ \ Conta\min ants \xrightarrow{TiO_2\ /\ h\nu} Intermediate(s) \longrightarrow CO_2 + H_2O \qquad \text{(Eq. 2.12)}$$

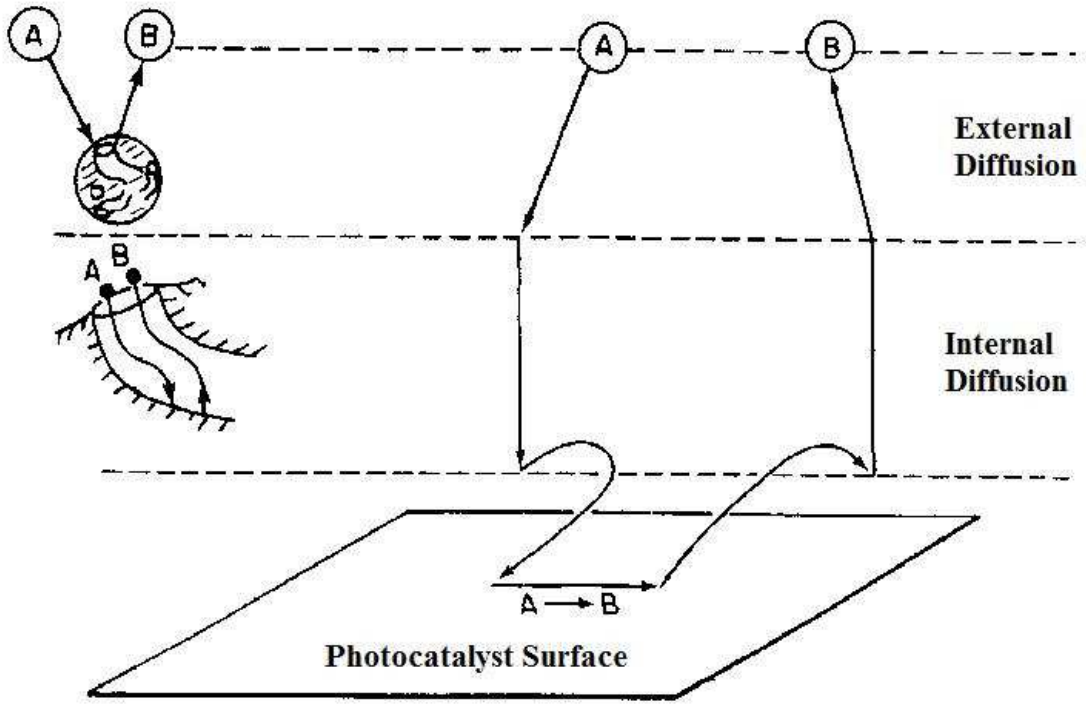

Figure 2: Steps in heterogeneous photocatalytic reaction (Fogler, 1999).

The overall photocatalysis reaction as portrayed by Eq. 2.12 can be decomposed into five independent steps, which are shown in Fig. 2 (Herrmann, 1999; Fogler, 1999):

1. Mass transfer of the organic contaminant(s) (e.g. A) in the liquid phase to the TiO_2 surface.
2. Adsorption of the organic contaminant(s) onto the photon activated TiO_2 surface (i.e. surface activation by photon energy occurs simultaneously in this step).
3. Photocatalysis reaction for the adsorbed phase on the TiO_2 surface (e.g. A → B).
4. Desorption of the intermediate(s) (e.g. B) from the TiO_2 surface.

5. Mass transfer of the intermediate(s) (e.g. B) from the interface region to the bulk fluid.

In terms of rate determination, the overall rate of reaction is equal to the slowest step. When the mass transfer steps (1 and 5) are very fast compared with the reaction steps (2, 3 and 4), the organic concentrations in the immediate vicinity of the active sites are indistinguishable from those in the bulk liquid phase. In this scenario, the mass transfer steps are not rate limiting and do not affect the overall rate of photocatalytic reaction. Vinodgopal and Kamat (1992) reported the dependence of the photodegradation rate of the organic surrogate on the surface coverage of the photocatalysts used. This outlines the importance of molecular adsorption or surface contact with the catalyst during the photocatalytic degradation. If the mass transfer steps are rate limiting, a change of the aeration or liquid flow conditions past the TiO_2 photocatalyst should alter the overall photocatalytic reaction rate.

Similarly, the surface interaction of microorganisms with the catalyst used during the photo-disinfection is essential for enhancing the inactivation rate. When the generated ROS closely contacts with the microorganisms, the cell wall will be the first site attacked by the ROS (Maness et al., 1999). The lipopolysaccharide layer of the cell external wall is the initial site attacked by the photo-induced ROS. This is followed by the site attack on the peptidoglycan layer, peroxidation of a lipid membrane and the eventual oxidation of the proteins within the membrane. All these will cause the rapid leakage of potassium ions from the bacterial cells, resulting in directly reducing the cell viability. The decrease in cell viability is usually linked to the peroxidation of the polyunsaturated phospholipid components of the cell membrane (i.e. loss of essential cell functions) and eventually leads to cell death. The formation of oxidative stress and its effects on the cell membrane can be observed using advanced atomic force microscopy or attenuated total reflection Fourier transform infrared spectroscopy. The rate of adsorption and the eventual photo-inactivation is known to positively correlate to the bactericidal effect of the TiO_2 catalyst. In this instance, the transfer of the bacterial cell to the close vicinity of the surface generated ROS site remains the rate limiting step in the photo-disinfection reaction.

2.2. Homogeneous Photo-Fenton Reaction

The Fenton reaction is a process that does not involve any light irradiation as compared with the heterogeneous TiO_2 photocatalysis reaction, whereas the photo-Fenton does react up to 600 nm in light wavelength. It was first recognised in the 1960s and remains one of the most applied AOPs for its ability to degrade high loadings of organic compounds even in highly saline conditions (Neyens et al., 2003; Bacardit et al., 2007; Machulek et al., 2007). Numerous studies on the photo-Fenton degradation of water pollutants such as chlorophenol (Pera-Titus et al., 2004), pesticides (Fallmann et al., 1999; Huston et al., 1999) and phenolic or aromatic compounds with organic loading of up to 25 gL^{-1} have been done (Gernjak et al., 2004 and 2007). A number of publications (Neyens et al., 2003; Pignatello et al., 2006; Gogate et al., 2004) have provided a comprehensive review of the basic understanding and clarity of the principles underlying the photo-Fenton reaction.

In the absence of a light source, hydrogen peroxide (H_2O_2) will be decomposed by Fe^{2+} ions in aqueous phase, resulting in the formation of hydroxyl radicals. The photo-Fenton reaction is expedited when a light source is present, causing rapid H_2O_2 decomposition by ferrous or ferric ions and resulting in the formation of radicals. All these soluble iron-hydroxy or iron complexes can absorb not only UV radiation but also visible light. However, the actual oxidizing species responsible for the photo-Fenton reaction is still under discussion (Pignatello et al., 1999). These Fenton and photo-Fenton reactions can proceed simultaneously with TiO_2 photocatalysis during UV-Vis irradiation period, post TiO_2 photocatalysis period or stand-alone photo-Fenton process. The Fenton reaction is seen to correlate strongly with the post TiO_2 photocatalysis reaction and thus, is described in detail here. The mechanism for the Fenton reaction is shown in Eq. 2.13:

$$Fe^{2+}(aq) + H_2O_2 \rightarrow Fe^{3+}(aq) + OH^- + HO^{\cdot} \quad \text{(Eq. 2.13)}$$

The Fe^{2+} can be reverted back to Fe^{3+} via different mechanisms:

$$Fe^{3+}(aq) + H_2O_2 \rightarrow Fe^{2+}(aq) + HO_2^{\cdot} + H^+ \quad \text{(Eq. 2.14)}$$

$$Fe^{3+}(aq) + HO_2^{\cdot} \rightarrow Fe^{2+}(aq) + O_2 + H^+ \quad \text{(Eq. 2.15)}$$

When a light source is present, the rate of photo-Fenton was reported to be positively enhanced compared to the dark condition. This is mainly due to the regeneration of Fe^{2+} (aq) from the photochemical effect of light and the concurrent generation of the $OH^{\cdot}$ radicals in the system. Such a reversion cycle of Fe^{2+} (aq)→ Fe^{3+} (aq)→ Fe^{2+} (aq) is continuous in generating $OH^{\cdot}$, provided the presence of H_2O_2 in the system is substantial. The regeneration of the Fe^{2+} (aq) from Fe^{3+} (aq) is the rate limiting step in the catalytic iron cycle, if a small amount of iron is present. This photoassisted reaction is termed as "photo-Fenton" reaction, where such reaction can be activated by irradiation wavelengths of up to 600 nm. It is known that this reaction is functions better under longer wavelengths as they are able to overcome the inner filter effects by photolysing the ferric iron complexes. The inner filter effect refers to the competitive adsorption of photons by other light absorbing species in the water.

Even if the photo-Fenton has higher photoactivity than the heterogeneous photocatalysis, its feasible operation is largely dependent on several water quality parameters. In the photo-Fenton reaction, the formation of the highly photoactive iron-complexes is highly dependent on the water pH and ion content (De Laat et al., 2004). It was reported that pH 2.8 was the frequent optimum pH for the photo-Fenton reaction (Pignatello, 1992). This is because at such low pH, the precipitation does not take place and further promotes the presence of dominant iron species of $[Fe(OH)]^{2+}$ in water. Such a low optimum operating pH, however, is not cost-effective for operation as it requires high chemical costs for pH rectification. The presence of different ions such as carbonate (CO_3^{2-}), phosphate (PO_4^{3-}), sulphate (SO_4^{2-}) and chlorine (Cl^-) also affects the iron equilibrium in water. These ions have the potential to raise the water pH and effectively lower the photo-Fenton reaction rate. Both CO_3^{2-} and PO_4^{3-} have a double detrimental effect on the reaction, as they precipitate the iron as well as scavenge the $OH^{\cdot}$ radicals. A higher pH of 4.0-5.0 was determined to be sufficient to sustain the photo-Fenton reaction with 2-6 mM of iron for the initiation of the treatment (Gernjak et al., 2007). To date, the maximal iron loading reported was 450 mgL^{-1} (Oliveros et al., 1997; Torrades et al., 2003).

Although H_2O_2 may be generated via the TiO_2 photocatalysis (Eq. 2.11), its relative low amount in the system is inadequate to drive the Fenton reaction. Many researchers have reported the addition of H_2O_2 as enhancing both the photo-Fenton and TiO_2 photocatalysis

reactions. The H_2O_2 can inhibit the recombination of the electron-hole pair, while further provides additional $OH^{\cdot}$ radicals through the following mechanisms:

$$H_2O_2 + e^- \rightarrow HO^{\cdot} + HO^- \quad \text{(Eq. 2.16)}$$

$$O_2^{\cdot -} + H_2O_2 \rightarrow O_2 + HO^{\cdot} + HO^- \quad \text{(Eq. 2.17)}$$

This combined TiO_2 photocatalysis – Fenton reactions are particularly useful for the disinfection process (Domínguez et al., 1998; Marugán et al., 2006 and 2007). The addition of H_2O_2 to the photocatalysis and Fenton systems results in a residual disinfection to avoid microbial regrowth. Rincon and Pulgarin (2006) performed trials with TiO_2 photocatalysis and photo-Fenton reaction for the disinfection of water contaminated with *Escherichia coli*. They found that the bacterial inactivation rate was higher than the photocatalysis alone and the decrease in bacterial number continued under dark conditions without significant regrowth within the following 60 h. However, it was outlined that such a residual disinfection effect was highly dependent on the light intensity used during the irradiation period, as well as the relative concentrations of Fe^{3+} and H_2O_2. Further addition of H_2O_2 was found to decrease the overall reaction rate in several studies, owing to the formation of less penetrative $HO_2^{\cdot}$ radicals, as described by Eq. 2.18:

$$HO^{\cdot} + H_2O_2 \rightarrow HO_2^{\cdot} + H_2O \quad \text{(Eq. 2.18)}$$

Other combined photo-Fenton and oxidative processes have also been proposed in the literature, such as; ozone (Beltrán-Heredia et al., 2001) and ultrasound (Torres et al., 2008). However, their significance compared to the TiO_2/photo-Fenton will not be discussed in detail here.

3. Advancements in Photocatalyst Immobilization and Supports

Since the discovery of the photocatalytic effect on water splitting by Fujishima and Honda (1972) using a TiO_2 electrode, numerous studies have been evolved to synthesis TiO_2 catalysts of different scale, characterise its physical properties and determine its photo-oxidation

performance to the surface-oriented nature of the photocatalysis reaction (Fujishima et al., 1972; Kondo et al., 2008; Hosono et al., 2004; Joo et al., 2005; Wang et al., 1999). The TiO_2 catalyst in nano-dimensions permits a large surface area to volume ratio and can further promote the efficient charge separation and trapping at the physical surface (Nagaveni et al., 2004a and 2004b). The light opaqueness of this nanoscale TiO_2 catalyst was reported to have an enhanced oxidation capability compared to the bulk TiO_2 catalysts (Siddiquey et al., 2008). Although the nanoscale TiO_2 catalysts show considerable improvement in terms of their physical and chemical properties, the particle size and morphology remains the main problem in a large-scale water treatment process (Byrne et al., 1998b; Yu et al., 2002). In this section, the current technical challenges that prevent the application of slurry TiO_2 photocatalytic systems are discussed together with the possible engineering solutions to resolve the problem. We will have a brief discussion on the modified TiO_2 catalyst with dopants for enhanced photoactivity under solar irradiation.

3.1. Challenges in the Development of Photocatalytic Water Treatment Process

To date, the most widely applied photocatalyst in the research for water treatment is Degussa P-25 TiO_2 catalyst. This catalyst is used as a standard reference for comparisons of photoactivity under different treatment conditions (Serpone et al., 1996). The fine particles of Degussa P-25 TiO_2 have always been applied in a slurry form. This is usually associated with a high volumetric generation rate of ROS as proportional to the amount of surface active sites when the TiO_2 catalyst is in suspension (Pozzo et al., 1997). On the contrary, the fixation of catalysts into a large inert substrate reduces the amount of catalyst active sites and also enlarges the mass transfer limitations. Immobilization of the catalyst results in increasing the operational difficulty as the photon penetration might not reach every single site for photonic activation (Pozzo et al., 1997). Thus, the slurry type of TiO_2 catalyst application is usually preferred.

With the slurry TiO_2 system, an additional process step would need to be utilised for post-separation of the catalysts. This separation process is crucial to avoid the loss of catalyst particles and introduction of TiO_2 into the treated water stream (Yang et al., 2007b). The catalyst recovery can be achieved through process hybridization with conventional sedimentation (Fernández-Ibáñez et al., 2003), cross-flow filtration (Doll et al., 2005) or

various membrane filtrations (Choo et al., 2001; Zhao et al., 2002; Zhang et al., 2008a). Coupling with the pH control strategy close to the isoelectric point for induced coagulation, it was reported that microfiltration (MF) hybridization can recover the remaining 3% of the catalyst particles for reuse (Malato et al., 2009). Several important operating issues with slurry TiO_2 still remain even with a membrane integration process. These include the types of membrane, pore size and blockage, regeneration or back-washing and fouling (Lee et al., 2001; Molinari et al., 2002; Xi et al., 2001). A number of studies have utilized micron size immobilizers for catalyst fixation that enhanced surface contact with the contaminants and prevent the membrane fouling or pores blocking which requires rapid back-washing (Xi et al., 2001; Zhang et al., 2009). These immobilisers include catalyst fixation onto activated carbon (Lee et al., 2004), mesoporous clays (Chong et al., 2009a), fibers (Zhu et al., 2004) or even onto the membrane itself (Kwak et al., 2001. The following subsections outline a few catalyst immobilization strategies that are suitable for use with slurry reactors, membrane reactors or both.

3.2. Mesoporous Clays

Natural clays have been used intensively as the support for TiO_2 owing to their high adsorption capacity and cost-effectiveness. Fig. 3 shows the TiO_2 crystal being deposited on a clay material (Chong et al., 2009). Different types of clays have been investigated, which include bentonite (Sun et al., 2002), sepiolite (Xie et al., 2009), montmorillonite (Kun et al., 2006), zeolite (Fukahori et al., 2003) and kaolinite (Chong et al., 2009a). Although these clays are catalytically inactive, their superior adsorption capacity has been attractive for increasing the surface contact during the photocatalysis reaction. It was proposed that natural clays should not be used directly to immobilise TiO_2. This is due to the presence of different surface or lattice-bounded impurities that might diffuse and further affect the TiO_2 efficiency of the immobilised layer (Chong et al., 2009a). In addition, if these impurities are not removed, the polar molecules in the aqueous environment might initiate an internal reaction within the clay structure, resulting in clay swelling (Chong et al., 2009a). The swelling will be profound in certain type of clays, where Van der Waals forces hold the entire clay in a turbostatic array. This is undesirable, particularly if the photocatalytic reactions take place in a reactor where the hydrodynamics can be strongly affected, consequently leading to the loss of photoactivity. Other factors that might need to be taken into consideration if pillared clays are used as the

immobiliser substrate include the density of the clays, particle size distribution range and the complementary photoreactor system used. The use of mesoporous clays as the support for nano-size TiO_2 have been successfully demonstrated in a number of studies, including the slurry or membrane processes (Chong et al., 2009b; Sun et al., 2004).

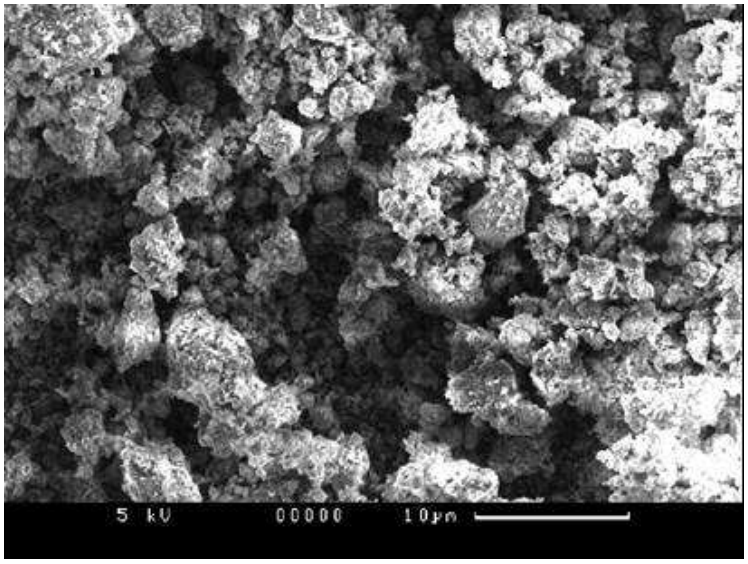

(a)

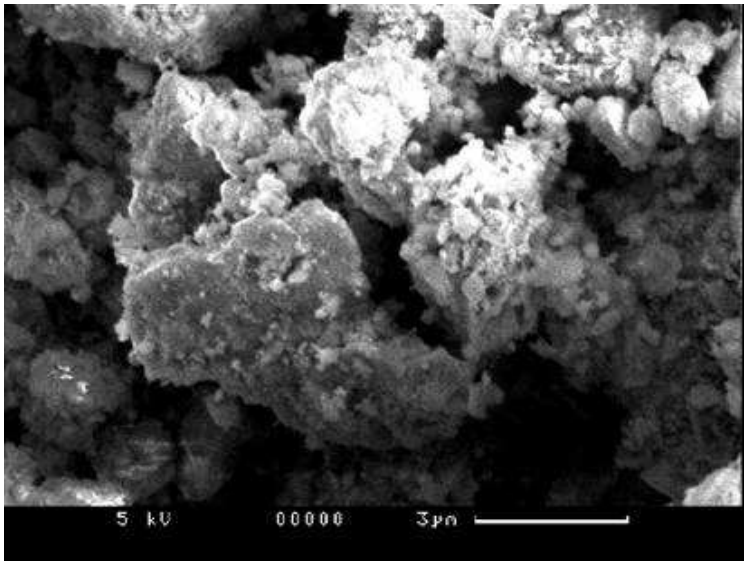

(b)

Figure 3: Nanocrystals of TiO_2 deposited on clay materials by SEM imaging. (a) 10 μm resolution; (b) 3 μm resolution.

3.3. Nanofibers, Nanowires or Nanorods

Glass, optical, carbon, titanate and woven cloths fibers have also been studied as support materials in the photooxidation of various organic contaminants for water purification (Pozzo et al., 1997). Most of these fibers have a protruded rod-shape or longitudinal morphology. Using the nanofibers, nanowires or nanorods, mass transfer limitations can be resolved by their thin longitudinal morphology. The use of less durable immobilizer fibers (e.g. of glass or woven cloths) however, may lead to a low durability as the deposited anatase crystals might wear-off, resulting in a loss of photoactivity over time. Such immobilizer fibers also increase the pressure drop in the reactor system. In contrast, a good benefit of nanofibers for commercial success is that they can be fabricated into MF, ultrafiltration (UF) and photocatalytic membranes (PMs). The MF fibers membrane is of particular interest as it shows high pollutant removal rate at low transmembrane pressure (< 300 kPa). A commercial success of such fabricated MF and UF membranes has been demonstrated by Zhang and co-workers (Zhang et al., 2008a and 2008b). Further details on the fabricated nanofibers or nanowires MF membranes can be obtained in the literature.

3.4. Photocatalytic Membrane

Recently, the use of the PMs has been targeted owing to the fact that the photocatalytic reaction can take place on the membrane surface and the treated water can be continuously discharged without the loss of photocatalyst particles. The PMs can be prepared from different materials and synthesis methods. These include the TiO_2/Al_2O_3 composite membranes (Bosc et al., 2005; Zhang et al., 2006a and 2006b; Choi et al., 2005 and 2007), TiO_2 supported on polymer and metallic membranes (Kim et al., 2003; Bellobono et al., 2005a and 2005b) or doted polymer membranes containing TiO_2 particles entrapped within the membrane structure during the membrane fabrication process (Artale et al., 2001; Kleine et al., 2002; Molinari et al., 2004). Also, possible TiO_2 organic and inorganic ceramic membranes have been investigated (Kwak et al., 2001; Kim et al., 2003; Yang et al., 2006). Fig. 4 shows different types of photocatalytic membranes for water treatment application (Zhang et al., 2008b; Albu et al., 2007). In most studies, however, PMs may encounter technical problems such as membrane structure deterioration, low photocatalytic activity and loss of deposited TiO_2 layer over time. To prevent the problems associated with the TiO_2 membrane coating, an approach

using membranes without any deposited TiO_2 layer can be configured into a slurry-membrane hybrid system, which will be outlined in the Section 4.

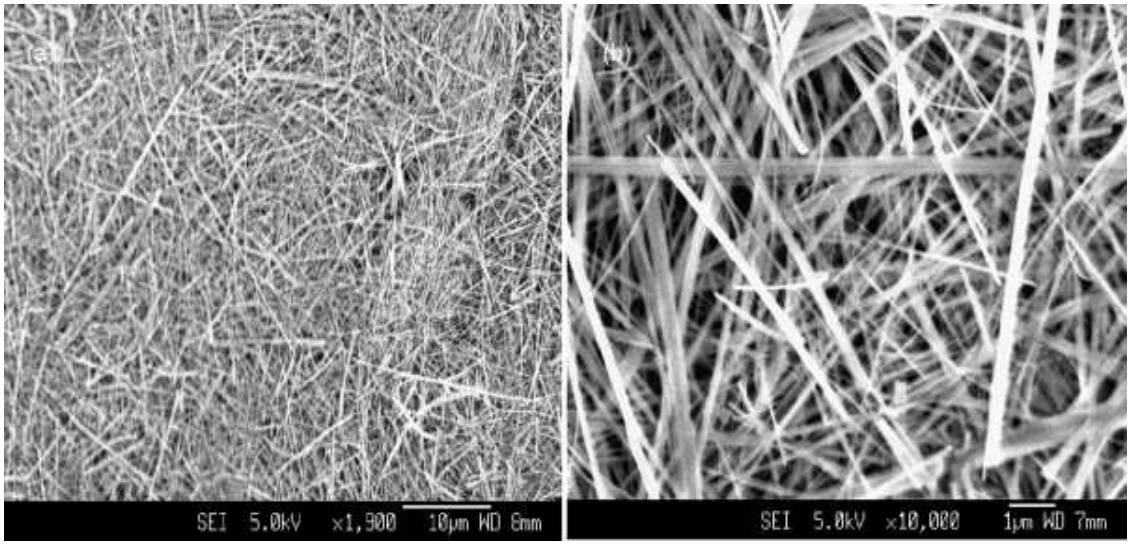

(a)

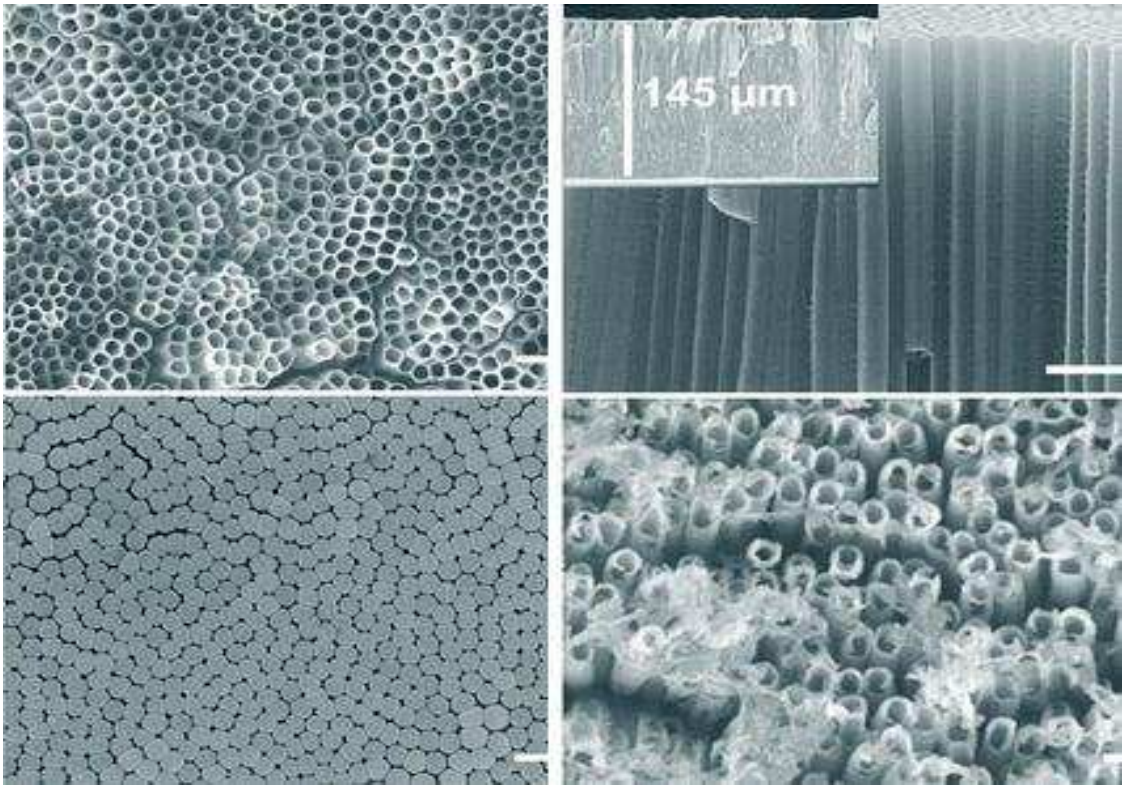

(b)

Figure 4: (a) FESEM images of the TiO_2 nanowire membrane (Zhang et al., 2008b); (b) SEM images of TiO_2 nanotube layer formed free-standing membrane (Albu et al., 2007).

3.5. Photocatalyst Modification and Doping

As TiO_2 photocatalytic reactions take places under ambient operating conditions, photoactivity is usually constrained by the narrow energy spectrum for the photonic activation of catalysts. The higher-end of the UV spectrum required for catalyst activation is usually accompanied by increased operating costs. One attractive option is to utilize the vast abundance of outdoor solar irradiation for catalyst activation in an appropriately designed photoreactor system. To broaden the photoresponse of TiO_2 catalysts, various material engineering solutions have been devised including composite photocatalysts with carbon nanotubes (CNTs) (Yu et al., 2006), dyed sensitizers (Vinodgopal et al., 1996), noble metals or metal ion incorporation (Ni et al., 2007), transition metals (Litter, 1999) and non-metal doping (Fujishima et al., 2008).

The rationale in utilizing these strategies is to balance both the half-reaction rates of the photocatalytic reaction by adding an electron acceptor or modifying the catalyst structure and composition. Fig. 5 presents the use of different mechanisms to enhance the photoactivity of the catalysts. The strong presence of electron acceptors can scavenge the excited electrons and altogether, prevent the recombination of electron-hole pairs. Recent studies showed that modified TiO_2 catalysts have an enhanced photoactivity under solar irradiation (Li et al., 2006; Ishibai et al., 2008; Shaban et al., 2008). CNTs coupling with TiO_2 have shown potential prolongation of electron-hole pairs by capturing the electron within their structure (Yu et al., 2006). As for dye sensitized coupling, the excited dye molecules under solar illumination can provide additional electrons to the CB for enhancing the formation of electron-hole pairs (Fig. 5a) (Vinodgopal et al., 1996). Dyes such as Methylene Blue, Azure, Erythosin, Rhodamin and Crystal Violet have been widely functionalized under solar irradiation (Vinodgopal et al., 1996).

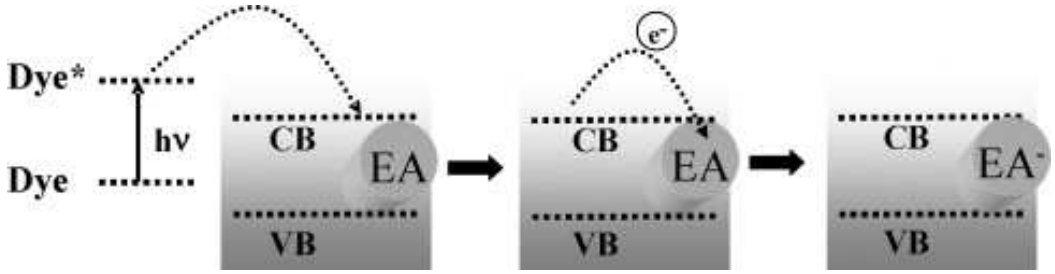

(a)

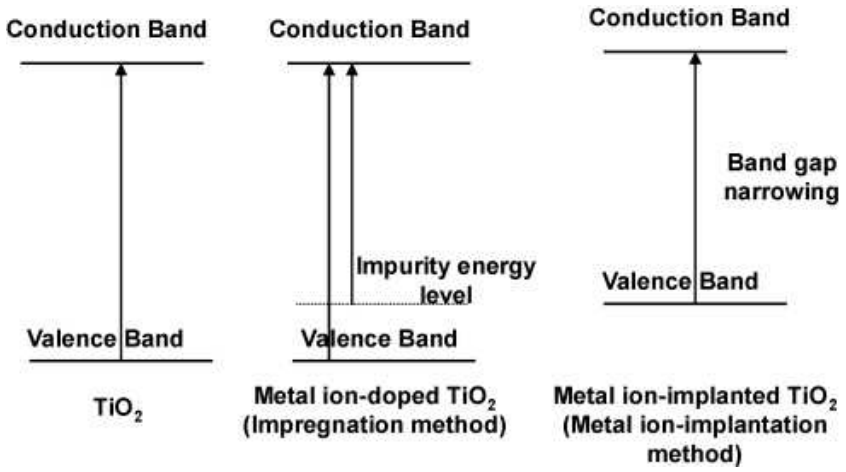

(b)

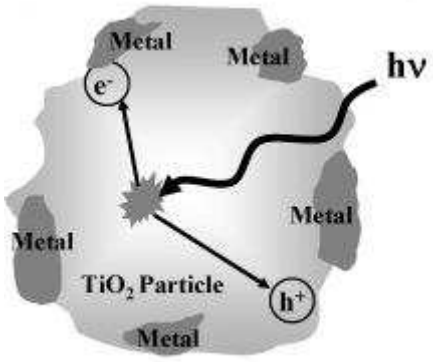

(c)

Figure 5: (a) Steps of excitation with a sensitizer in the presence of an adsorbed organic electron acceptor (EA); (b) Scheme of TiO_2 band structures, chemically ion-doped TiO_2 and physically ion-implanted TiO_2; (c) Electron capture by a metal in contact with a semiconductor surface (Malato et al., 2009).

Similarly, noble metals (e.g. Ag, Ni, Cu, Pt, Rh, and Pd) with Fermi levels lower than TiO_2 catalysts have also been deposited on the TiO_2 surface for enhanced charge separation (Fig. 5b) (Ni et al., 2007). These metals were reported to enhance electron transfer, but require knowledge about the optimal deposited amount needed during the fabrication process. Although noble metal coupling could be efficient in prolonging the surface charge separation, their cost-effectiveness for an industrial application is usually replaced by more economical transition or non-metal doping. The mechanism of such transition and non-metal doping is different from the noble metal coupling, as the TiO_2 is incorporated into the TiO_2 crystal lattice (Asahi et al., 2001; Irie et al., 2003; Ihara et al., 2003). Such incorporation introduces impurity in the bandgap of TiO_2 and thus, reduces the photonic energy requirements (Fig. 5c). More recently, the use of non-metal dopants (e.g. N, C, F, S and etc.) can improve the photoactivity and feasibility of TiO_2 catalysts for industrial applications (Fujishima et al., 2008). Further research efforts maybe needed to get a better understanding of the photoactivity kinetics, so as to improve the photooxidation efficiency for water treatment.

4. Photocatalytic Reactor Configuration

Photocatalytic reactors for water treatment can generally be classified into two main configurations, depending on the deployed state of the photocatalysts: (1) reactors with suspended photocatalyst particles and (2) reactors with photocatalyst immobilised onto a continuous inert carrier (Pozzo et al., 2000). Various types of reactors have been used in photocatalytic water treatment, including the annular slurry photoreactor (Chong et al., 2009b), cascade photoreactor (Chan et al., 2003) and downflow contactor reactor (Ochuma et al., 2007). The disparity between the two main configurations is that the first one requires an additional downstream separation unit for the recovery of photocatalyst particles while the latter permits a continuous operation.

Pareek et al. (2008) addressed that the most important factors in configuring a photocatalytic reactor are the total irradiated surface area of catalyst per unit volume and light distribution within the reactor. Slurry-type photocatalytic reactor usually has a high total surface area of photocatalyst per unit volume, while the fixed bed configuration is often associated with mass transfer limitation over the immobilised layer of photocatalyst. The light photon distribution

through either *direct* or *diffuse* paths within the reactors needs to be decided (Cassano et al., 2000). Direct photon utilisation means that the photocatalysts are directly activated with light photons, rather than with the assistance of various parabolic light deflectors to concentrate and transfer the photons. To achieve uniformity in photon flux distribution within the reactor, the correct position of light source is essential to ensure maximal and symmetrical light transmission and distribution. Nowadays, the use of photo-reactors with assisted parabolic light deflectors has become unfavourable, owing to the need for special configuration and high operating costs. This type of reactor needs to be designed to ensure the maximal illuminated reactor volume with minimal pressure requirement for good catalyst mixing and dispersion. Until recently, the slurry photocatalytic reactor was still the preferred configuration owing to its high total surface area of photocatalyst per unit volume and ease of photocatalyst reactivation. The photocatalyst particles can be separated by settling tanks or external cross-flow filtration systems to enable continuous operation of the slurry reactor. A technically promising solution for solving the downstream separation of photocatalyst particles after treatment is by the application of hybrid photocatalysis-membrane processes. Application of such a hybrid system prevents the use of a coagulation, flocculation or sedimentation to separate the catalyst particles from the treated water stream. Other benefits include further energy saving and size of process installation and site area required.

Hybrid photocatalytic-membrane reactor systems are generally known as "photocatalytic membrane reactors" (PMRs). This is owing to the nature of the hybrid system where the membrane filtration unit can be configured into different positions with the photocatalytic reactor. Fu et al. (2006) designed a submerged membrane reactor (Fig. 6) with two different reaction zones; UV slurry TiO_2 zone with a movable baffle that separates the submerged membrane module. These PMRs can be generalised by (1) irradiation of the membrane module and (2) irradiation of a feed tank containing photocatalyst in suspension (Molinari et al., 2001 and 2002). For the former configuration, the photocatalyst can be either deposited onto the membrane or suspended in the reaction water. The PMRs allow a continuous operation of the slurry-type reactor without any loss of photocatalyst particles as well as the ability to control the water residence time independently. This enables the treated water to achieve the predefined level before being membrane filtered through the hybrid system. In the PMRs with immobilised PMs, the membrane module functions as the support for the

photocatalyst particles and barrier against the different organic molecules exist in the reaction water. Similarly, the membrane also acts as a physical barrier against the photocatalyst particles and organic molecules or photocatalytic intermediates to be degraded in the slurry PMRs.

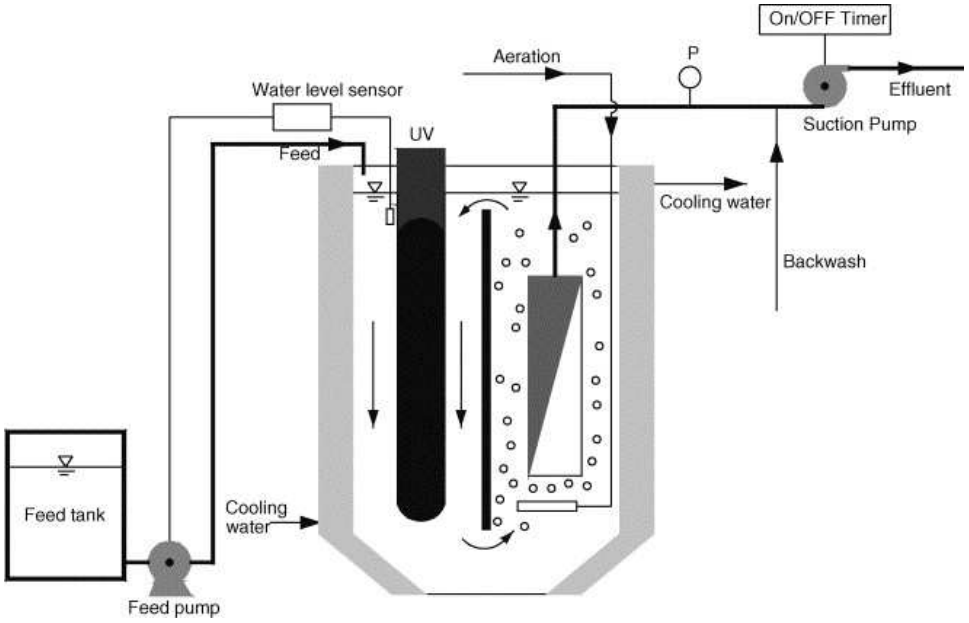

Figure 6: Schematic of submerged membrane photocatalytic reactor (Fu et al., 2006).

In the PMRs with immobilised photocatalysts, the photocatalytic reaction takes place on the surface of the membrane or within its pores. The PMs used maybe of MF (Ryu et al., 2005; Meng et al., 2005; Rivero et al., 2006; Jung et al., 2007; Chin et al., 2007; Huang et al., 2007), UF (Molinari et al., 2002; Tsarenko et al., 2006; Sun et al., 2004; Sopajaree et al., 1999a and 1999b) or NF (Molinari et al., 2001, 2002, 2004 and 2006; Augugliaro et al., 2005) dimensions, depending on the targeted colloidal size and final water quality requirement. The MF membrane is useful when the colloidal size is in the range of 0.1 – 5 µm, while both UF and NF targeted smaller particle size ranges. The photooxidation efficiency of the contaminants was reported to be higher when an immobilised PM was used, than in the case of PMRs with suspended catalyst particles (Molinari et al., 2004). It was reported that immobilising the photocatalyst particles might cause severe destruction to the membrane structure owing to their close contact with both UV light and hydroxyl radicals (Chin et al., 2006). In view of this, the hybridization configuration of the membrane process using

photocatalysts in suspension appears to be the more promising arrangement. This PMR configuration has been well described in the literature for water phase degradation of humic (Sun et al., 2004; Ryu et al., 2005; Jung et al., 2007; Tsarenko et al., 2006) and fulvic acids (Fu et al., 2006), bisphenol A (Chin et al., 2006), phenol (Molinari et al., 2002), 4–nitrophenol (Molinari et al., 2001), 4–chlorophenol (Ryu et al., 2005), grey water (Rivero et al., 2006), para-chlorobenzoate (Huang et al., 2007), river water (Meng et al., 2005) and dyes (Molinari et al., 2002 and 2004; Ryu et al., 2005; Sopajaree et al., 1999a and 1999b).

With these PMRs, one of the main operational issues is the transmembrane pressure, which determines both the filtration rate and operating costs. It is known that the PMR treatment costs increase if photocatalysts with small particle and colloidal size are used. With both the MF and UF membrane filtration, the fine photocatalyst particles can cause membrane fouling and subsequently, reduce the membrane permeate flux. Fu et al. (2006) utilised spherical ball-shaped TiO_2 particles that promote separation, recovery and reuse, while prolonging the membrane lifespan as these particles do not cause pore blockage. Besides, the surface charge properties of the photocatalyst particles can be manipulated to prevent membrane pore blockage. Xi and Geissen (2001) integrated a thermoplastic membrane module of cross-flow MF and found that low permeate flux occurred when the operating pH varied from the isoelectric point of the TiO_2 particles used. This is owing to the pH induced coagulation-flocculation state of TiO_2 that declines the rate of permeate flux. This was resolved by maintaining the operating pH close to the isoelectric point of TiO_2 by adding certain electrolytes to the TiO_2 slurry. Even with such control strategies, the quality of permeate is low owing to the rapid penetration of small molecules through the membrane used.

Recently, different hybridizations of PMRs with dialysis (Azrague et al., 2006), pervaporation (Camera-Roda et al., 2007) and direct contact membrane distillation (MD) (Mozia et al., 2009) have been used (Fig. 7). Pervaporation is a physical process where a selective organophilic membrane is used to act as a selective barrier for the molecules to be degraded. Augugliaro et al. (2001) observed that a synergistic effect occurs when pervaporation is used, where the intermediates from the degradation of 4-chlorophenol (i.e. hydroquinone, benzoquinone) can be selectively permeable without competing with 4-chlorophenol for photocatalytic reaction. Other types of organophilic membrane have also been investigated, such as polymeric UF

membranes and polyethersulfonate NF membranes (Bae et al., 2005; Lee et al., 2008). A stronger rejection impact on the membrane is usually associated with the use of the UF or NF membranes. The choice of membrane for an efficient hybridization depends on the organic molecular size, pH or electrostatic interaction and Donnan exclusion phenomenon (Meares, 1986).

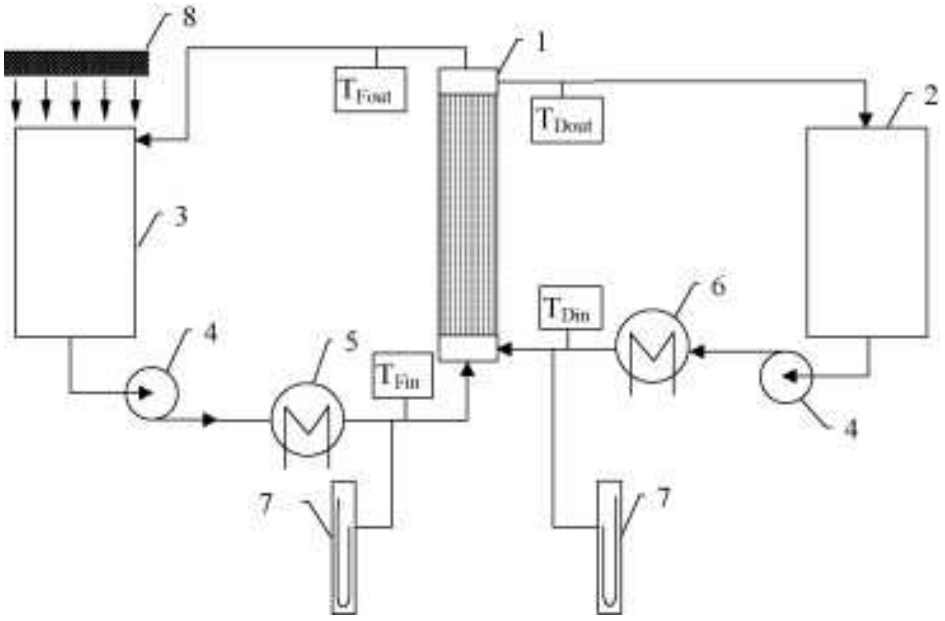

Figure 7: Schematic diagram of the apparatus for hybrid photocatalysis–MD process: (1) membrane module; (2) distillate tank; (3) feed tank (V = 2.9 dm^3); (4) pump; (5) and (6) heat exchangers; (7) manometers; (8) UV lamp; T_{Fin}, T_{Din}, T_{Fout}, T_{Dout} – inlet and outlet temperatures of feed and distillate, respectively (Mozia et al., 2009).

The MD is where the feed volatile components in water are evaporated through a porous hydrophobic membrane to produce high quality distillate products (Mozia et al., 2009). Its main advantage is that there is no membrane fouling when TiO_2 is present. During the process, the volatile stream is maintained inside the membrane pores. The vapour pressure difference on both sides of the porous membrane remains as a driving force for the process. This force, however, largely depends on the temperatures and solution composition in the layer adjacent to the membrane (Tomaszewska et al., 1998; Gryta et al., 2001). It was reported that the feeding temperature in MD can range from 303 to 363 K. Similar scaling-up operational

constraints of low permeate flux and high energy demand have rendered redundant its current full scale development. However, some efforts to utilise alternative energy sources such as solar energy to enable MD application are detailed in the literature (Lawson et al., 1997; Bouguecha et al., 2005).

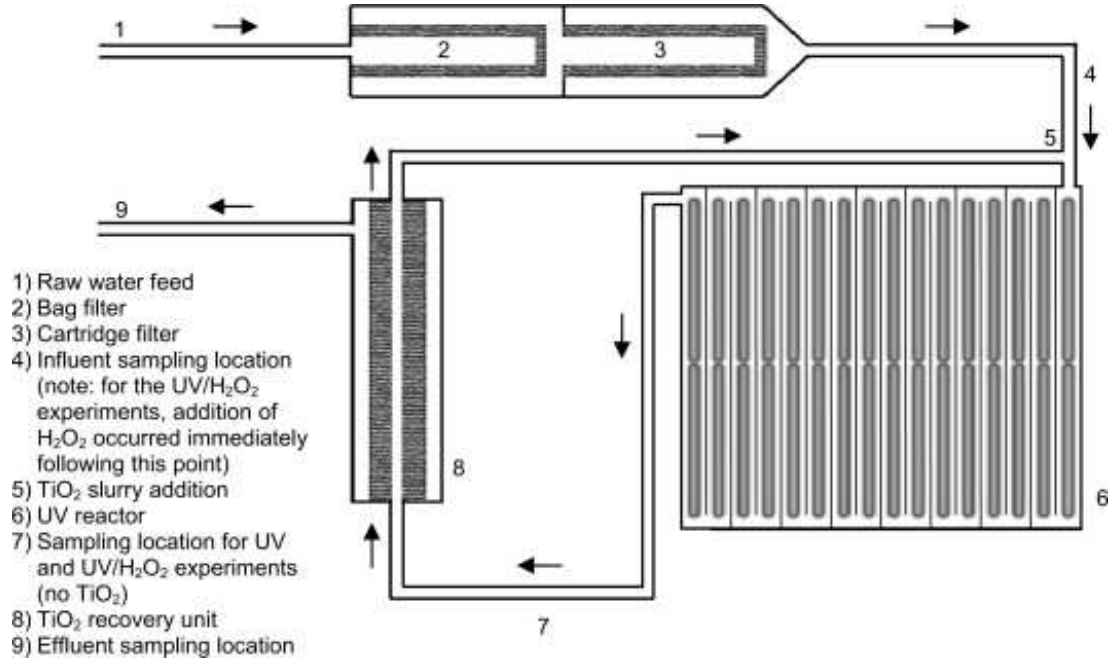

Figure 8: General schematic of photocatalytic reactor membrane pilot system (Benotti et al., 2009).

Among all the hybrid PMR systems, the pilot Photo-Cat^{TM} system (Fig. 8) (manufactured by Purifics Inc., Ontario, London) has shown the best potential application. Benotti et al. (2009) evaluated its ability in the removal of 32 pharmaceuticals, endocrine disrupting compounds and estrogenic activity from water. They found that 29 targeted compounds and estrogenic activity of greater than 70% were removed while only 3 compounds were less than 50% removed at the highest number of UV passes. In the Photo-Cat^{TM} system, the water stream passes through a pre-filter bag and a cartridge filter before being mixed with a nanoparticle TiO_2 slurry stream. The mixed stream then passes through the reactor within the 3 mm annulus of the 32 UV lamps aligned in series, which can be individually controlled for varying water quality. The overall hydraulic residence time for the 32 UV passes is between 1 to 32 s, depending on the number of UV lights turned on. A cross-flow ceramic membrane TiO_2

recovery unit is hybridized downstream of the reactor to remove the TiO_2 from the flow stream, while allowing the treated water to exit. The retentate TiO_2 stream is recycled and remixed with the fresh TiO_2 slurry stream that enters the reactor stream.

5. Operational Parameters of the Photocatalytic Reactor

After the integration of the semiconductor catalyst with a photoreactor, the oxidation rates and efficiency of the photocatalytic system are highly dependent on a number of the operation parameters that govern the kinetics of photomineralization and photo-disinfection. This section will discuss the significance of each operation parameter on the corresponding kinetics and some recent methods to optimize the photocatalytic system via response surface analysis. The following outline a range of parameters that affect the photocatalytic performance of TiO_2 photocatalysts in water treatment.

5.1. TiO_2 Loading

Concentration of TiO_2 in the photoreactor water treatment system affects the overall photocatalysis reaction rate in a true heterogeneous catalytic regime, where the amount of TiO_2 is directly proportional to the overall photocatalytic reaction rate (Gaya and Abdullah, 2008). A linear dependency holds until the extent when the reaction rate starts to aggravate and becomes independent of TiO_2 concentration. This is attributed to the geometry and working conditions of the photoreactor where the surface reaction is initiated upon light photon absorption (Bamba et al., 2008). When the amount of TiO_2 increases above a saturation level (i.e. highly turbid), the light photon absorption coefficient usually decreases radially. However, the light attenuation over the radial distance could not be well correlated with the *Beer-Lambert Law* owing to the strong absorption and scattering of light photons by the TiO_2 particles (Chen et al., 2007). The excess TiO_2 particles can create a light screening effect that reduces the surface area of TiO_2 being exposed to light illumination and thus, the photocatalytic reaction. Therefore, any chosen photoreactor should be operated below the saturation level of the TiO_2 photocatalyst used to avoid excess catalyst and to ensure efficient photon absorption. In this sense, both catalyst loading and light scattering effect can be considered as a function of optical path length in the reactor.

A large number of studies reported the effect of TiO_2 loadings on process efficiency (Gaya and Abdullah, 2008; Herrmann 1999; Chong et al., 2009b and 2009c; Ochuma et al., 2007; Chin et al., 2006). These results are mostly independent and a direct comparison cannot be made, as the working geometry, radiation fluxes, intensity and wavelengths used were different. It was reported that the optimum catalyst loading for photomineralization and photo-disinfection are varied, and mainly depend on the dimension of the photoreactor. The determination of photoreactor diameter is crucial in not only the effective photon absorption, but also the water flow hydrodynamics (Malato et al., 2009). A uniform flow can ensure that a steady state residence time is obtained; while turbulence removes catalyst deposition or reaction dead zone (Malato et al., 2003). Diameters smaller than 20-25 mm were not feasible for turbulent flow while diameters larger than 50-60 mm are impractical. This is because large diameters usually have lower saturated catalyst loading and efficiency. In this instance, the amount of catalyst should be considered. Usually the TiO_2 catalysts can be mixed uniformly with the targeted water prior to introduction into the reactor system. During the dark homogenization period of the catalyst, a low concentration of organic pollutants is observed owing to the strict adsorption of organics onto the catalysts surface (Xu and Langford, 2001). Similarly, catalyst-bacteria interaction was reported in the photo-disinfection treatment of microorganisms (Gogniat et al., 2006).

5.2. pH

In heterogeneous photocatalytic water systems, pH is one of the most important operating parameters that affect the charge on the catalyst particles, size of catalyst aggregates and the positions of conductance and valence bands. Due to the nature of TiO_2 catalysts used, any variation in the operating pH is known to affect the isoelectric point or the surface charge of the photocatalyst used. Many reports have used the point of zero charge (PZC) of TiO_2 to study the impact of pH on the photocatalytic oxidation performance (Chong et al., 2009b and 2009c; Ochuma et al., 2007; Chin et al., 2006; Toor et al., 2006). The PZC is a condition where the surface charge of TiO_2 is zero or neutral and lies in the pH range of 4.5–7.0, depending on the catalysts used. At PZC of TiO_2, the interaction between the photocatalyst particles and water contaminants is minimal due to the absence of any electrostatic force. When the operating pH<PZC(TiO_2), the surface charge for the catalyst becomes positively charged and gradually exerts an electrostatic attraction force towards the negatively charged

compounds. Such polar attractions between TiO_2 and charged anionic organic compounds can intensify the adsorption onto the photon activated TiO_2 surface for subsequent photomineralization and photo-disinfection reactions (Xu and Langford, 2001; Gogniat et al., 2006). This is particularly significant when the anionic organic compounds are present at a low concentration level. However, at pH>PZC(TiO_2), the catalyst surface will be negatively charged and repulse the anionic compounds in water. Different pH will affect the surface charge density of the TiO_2 catalyst (Rincón and Pulgarin, 2004), according to the following water equilibrium equations (Eq. 5.1-5.2);

At pH<PZC: $TiOH + H^+ \leftrightarrow TiOH_2^+$ (Eq. 5.1)

At pH > PZC : $TiOH + OH^- \leftrightarrow TiO^- + H_2O$ (Eq. 5.2)

The surface charge density distribution for these TiO_2 catalyst clusters is highly dependent on the operating pH. It was reported that the distribution of TiOH is ≥ 80% at 3 < pH < 10; TiO^- ≥ 20% at pH > 10 and $TiOH_2^+$ ≥ 20% at pH < 3. The equilibrium constants for these reactions at different pH are pK_{TiOH2}^+ = 2.4 and pK_{TiOH} = 8.0 (Kormann et al., 1991). During photocatalytic reaction, the initial operating pH usually drops slightly from the formation of multitude intermediate by-products that may possess different chemical functional groups that affect the water pH (Stylidi et al., 2003).

A similar electrostatic interaction enhancement for photo-disinfection of microorganisms was observed during the photocatalytic process (Gogniat et al., 2006). During photo-disinfection, the initial photo-induced damage to the microorganisms takes place on the lipopolysaccharide layer of the external cell wall and on the peptidoglycan layer. This is followed by lipid membrane peroxidation and the subsequent oxidation of the membrane proteins and polysaccharides. An increased density of $TiOH_2^+$ (at low pH) can form electrostatic links with the bacteria through their negatively charged surfaces, resulting in increasing rates of photo-disinfection. Herrera Melián et al. (2000) observed that the bacterial inactivation rate was enhanced at pH 5.0. It should be noted that the enhanced bactericidal activity of TiO_2 at a low pH is due solely to the TiO_2 mediated photo-killing and not acidification of the cell. Heyde and Portalier (1990) explained that the negligible *E.coli* reaction to acid conditions was from the presence of an acid tolerance response by the bacterium itself, which secretes acid-induced

proteins for acid-shock protection. However, Rincon and Pulgarin (2006) did not find any differences in *E.coli* inactivation rates when the initial pH varied between 4.0 and 9.0. To date, various types of microorganisms have been inactivated successfully using TiO_2 photocatalysis, which include *Lactobacillus acidophilus, Escherichia coli, Saccharomyces cerevisiae, Chlorella vulgaris, Streptococcus faecalis and aureus, Enterobacter cloacae, total coliforms, C. albicans, F.solami, Aspergillus niger* and others (Matsunaga et al., 1985; Herrera Melián et al., 2000; Ibáñez et al., 2003; Seven et al., 2004; Lonnen et al., 2005).

Although an electrostatic link between the catalyst particles and microorganisms was reported, a subsequent microbial cell adsorption and eventual penetration of the catalysts through the cell wall depend on the mean particle size. Since the relative sizes between the bacteria and catalysts are significantly different, the charged $TiOH_2^+$ clusters might not come into full contact with the bacteria. Sichel et al. (2007) found that TiO_2 catalyst is actually adsorbed onto fungal spores rather than the reverse. This is because fungal spores are larger (a few order of magnitudes) than the catalyst particles. A small decrease in microbial loadings was observed during the initial dark homogenization period with catalyst particles. This is from the catalyst agglomeration and subsequent sedimentation of the agglomerates. The rate of bacterial adsorption in this instance is directly related to the bactericidal activity of the catalyst used. It was also reported that the adsorption phenomena during the dark and irradiated phase will act indifferently and thus, a direct comparison between these two irradiated phases cannot be made.

Interaction between catalyst particles themselves also exists and is dependent on the operating pH. The particle distribution size of the catalysts can vary from 300 nm to 4 μm depending on the distant from the PZC of TiO_2 (Malato et al., 2009). At pH = PZC, the neutral surface charge of the catalyst particles is unable to produce the interactive rejection for solid-liquid separation. Thus, this induces catalyst aggregation where the catalyst becomes larger and leading to catalyst sedimentation (Blanco et al., 2001). This physical property is usually manipulated in the hybridized PMR system, where the pH of the treated wastewater is neutralized to pH 7 for subsequent recovery of catalyst particles. The larger TiO_2 clusters can settle faster than the smaller clusters. With such a neutralization strategy, almost 97% of the catalysts can be recovered in the settling tank. The remaining TiO_2 catalysts can be recovered

via the downstream MF system. Similarly, the water pH will also affect effective separation in the PMR system where inappropriate control promotes electrostatic repulsion, the Donnan exclusion phenomena and thus, the rejection tendency for the membrane used (Seffaj et al., 2005; Molinari et al., 2005). It must be stressed that appropriate pH control strategies must be implemented at every different location of a photocatalytic water treatment process for efficient photomineralization or photo-disinfection reaction to proceed.

5.3. Temperature

Numerous studies have been conducted on the dependence of photocatalytic reactions on the reaction temperature (Muradov et al., 1996; Fu et al., 1996; Chen and Ray, 1998; Rincón and Pulgarin, 2003; Evgenidou et al., 2005). Although heat energy is inadequate to activate the TiO_2 surface, the understanding on such dependency could be extrapolated when operating the process under natural sunlight illumination. Most of the previous investigations stated that an increase in photocatalytic reaction temperature (> 80^oC) promotes the recombination of charge carriers and disfavours the adsorption of organic compounds onto the TiO_2 surface (Gaya and Abdullah, 2008). At a reaction temperature greater than 80^oC, the photocatalytic reaction is interpreted with the Langmuir-Hinshelwood (L-H) mechanism, where the adsorption of the reactants is disfavoured resulting in *KC* becoming ‹‹ 1. This will reduce the L-H expression (Eq. 6.1) into the apparent rate equation $r = k_{apparent}C$. All these drastically reduce the photocatalytic activity of TiO_2 when the reaction temperature rises. The desorption of degraded products from the TiO_2 surface is the rate limiting step when temperatures rise. On the contrary, a temperature below 80^oC actually favours adsorption which is a spontaneous exothermic phenomenon, resulting in achieving *KC* of L-H model (Eq. 6.1) ›› 1 and further enhanced the adsorption of final reaction products. A further reduction in temperature to 0^oC will cause an increase in the apparent activation energy. As a consequence, the optimum reaction temperature for photomineralization is reported to be in the range of 20^oC to 80^oC (Malato et al., 2009).

For photo-disinfection using TiO_2 photocatalysis, the increase in reaction temperature will increase the inactivation rate of microorganisms (Rincón and Pulgarin, 2003). This is consistent with the Van't Hoff-Arrhenius equation (Eq. 5.3), where the rate constant *k* is linearly proportional to the exponential (-1/T);

$$\ln\left(\frac{k_1}{k_2}\right) = -\frac{E_a}{R}\left(\frac{1}{T_2} - \frac{1}{T_1}\right) \quad \text{(Eq. 5.3)}$$

In which k_1 and k_2 are the constants for temperatures T_1 and T_2, E_a is the energy of activation and R is the universal gas constant. The sensitivity of a microbe to the catalyst activity depends on its incubation temperature, type and resistance of the microorganism to temperature change. The order of resistance of microorganisms to conventional disinfection treatment is: *Non-spore forming bacteria < Viruses < Spore forming bacteria < Helminths < Protozoa (oocysts).* To date, there is no comprehensive study conducted to compare the effect of TiO_2 photo-disinfection of each microorganism type under different operating temperatures. Thus, the photo-disinfection using TiO_2 catalyst is usually conducted below temperature of 80^{o}C to prevent high water heating costs (high heat capacity) (Herrmann, 2005).

5.4. Dissolved Oxygen

Dissolved molecular oxygen (DO) plays an important role in the TiO_2 photocatalysis reaction to assure sufficient electron scavengers are present to trap the excited conduction-band electrons from recombination (Chong et al., 2009b). The oxygen does not affect the adsorption onto the TiO_2 catalyst surface as the reduction reaction takes place at a different location from where oxidation occurs (Malato et al., 2009). Other roles for DO may involve the formation of other ROS and the stabilization of radical intermediates, mineralization and direct photocatalytic reactions. The total amount of DO in a reactor depends on a few technical considerations. For a photoreactor, the total delivered DO not only acts as an electron sink but also provides sufficient buoyant force for complete suspension of TiO_2 particles. Photoreactor sparging with pure oxygen in TiO_2 slurry reactor is usually a cost-ineffective solution, as the amount of DO being held-up is a function of the photoreactor geometry. The difference between the two sparging media of air and oxygen is usually not very drastic as the mass transfer of oxygen to the close vicinity of the surface is the rate dependent step (Habibi et al., 2005). Generally Henry's Law can be assumed to give a good approximation of the amount of oxygen dissolved under the experimental conditions, provided the oxygen sparging rate and the photoreactor gas hold-up are known (Chong et al., 2009c). In this equilibrium law, it is also necessary to account for the fact that the oxygen solubility decreases with increasing

reaction temperature. As discussed, it is preferential to operate the photoreactor under ambient conditions to prevent the elevated cost of air or oxygen sparging for enhanced electron sink.

The presence of dissolved molecular oxygen was also suggested to induce the cleavage mechanism for aromatic rings in organic pollutants that are present in the water matrices. Wang and Hong (2000) proposed that during aromatic ring cleavage in the degradation of a dioxyl compound, the molecular oxygen will follow the cleaving attack of a second hydroxyl radical. The analogous partial pressure of oxygen applied during the reaction for a closed reactor system is also important. A significantly higher partial pressure of oxygen will result in a higher initial organics photomineralization rate than its structural transformation (Chen and Ray, 1998; Wang and Hong, 2000). It was reported that at low oxygen pressure of 0.5 kPa, 75% of the original 2-CB compounds were transformed, but only 1% of them was mineralized to CO_2 after 5 h of UV irradiation (Wang and Hong, 2000). Though elevated partial pressures of oxygen are imperative, it is difficult to quantify their influence on the surface activity of TiO_2, owing to the polyphasic nature of the photocatalytic liquid phase reaction (Herrmann, 1999).

The detrimental effect of DO on the photocatalysis reaction was reported by Shirayama et al. (2001). They observed an elevated photodegradation rate of chlorinated hydrocarbons in the absence of DO. This could be explained by the strong absorption characteristics for UV photons at intensities of 185 and 254 nm, respectively. The DO molecules act as an inner filter in this case and caused a sharp attenuation in UV light intensity, mainly at the UV-C germicidal region. There is no report found to determine the DO impact on a photocatalysis process using UV-A or UV-B light sources. To date, the effect of DO on the efficiency of photo-disinfection rate has been paid little attention. The formation of various ROS under the series of redox reactions on the catalysts surface was assumed to be similar in both photomineralization and photo-disinfection reaction. If sufficient nutrients are available, the constant sparging of DO will generally promote microbial growth and offset the photo-disinfection rate. This indirectly prolongs the irradiation time necessary to achieve the desired inactivation level. It is thus, recommended that the effect of DO on microbial inactivation should be investigated thoroughly in a particular photoreactor system before improvising DO sparging strategy.

5.5. Contaminants and their Loading

Previous investigations have reported the dependency of the TiO_2 photocatalytic reaction rate on the concentration of water contaminants (Ochuma et al., 2007; Toor et al., 2006; Chong et al., 2009b and 2009c). Under similar operating conditions, a variation in the initial concentration of the water contaminants will result in different irradiation time necessary to achieve complete mineralisation or disinfection. Owing to the photonic nature of the photocatalysis reaction, excessively high concentrations of organic substrates are known to saturate the TiO_2 surface and reduce the photonic efficiency, leading to photocatalyst deactivation (Saquib and Muneer, 2003).

Not all organic substrates will have such profound effects on the irradiation time and this also depends on the corresponding chemical nature of the targeted compounds to TiO_2 photocatalysis reaction. For instance, 4-chlorophenol will undergo a degradation pathway with constant evolution of intermediate(s) product (i.e. hydroquinone and benzoquinone) while oxalic acid will undergo direct transformation to carbon dioxide and water (Bahnemann, 2004). Such evolution of intermediate(s) in the case of 4-chlorophenol further prolongs the irradiation time necessary for total mineralisation, owing to direct competition for photocatalysis over unselective TiO_2 surfaces. In the development of a mathematical model that represents the kinetics of mineralisation while relating to the TiO_2 loading required, commonly used water quality parameters such as chemical oxygen demand (COD), total organic carbon (TOC) or dissolved organic carbon (DOC) could be more appropriate to account for such competitiveness of intermediate(s) with its predecessor compounds. Also, organic substrates with electron withdrawing nature such as benzoic acid and nitrobenzene were found to strongly adhere and are more susceptible to direct oxidation than those with electron donating groups (Bhatkhande et al., 2004). Most of the TiO_2 studies conducted to date utilise a range of model organic substrates with different substituent groups but these rarely convey any useful information and merely test the photo-efficiency of a new photocatalyst or an integrated reactor column. Some field kinetics of the photomineralization of real wastewater has also been reported (Marugán et al., 2007; Radjenovíc et al., 2009; Vilar et al., 2009; Malato-Rodríguez et al., 1996). Owing to the persistence of dissolved organics in the real wastewater, slow photomineralization kinetics is attained with prolonged irradiation times to achieve complete mineralization. Slow kinetic turnover of photocatalytic water treatment as a stand-

alone process means a higher initial cost on the reactor volume and site area is required. Recently, this heterogeneous photocatalytic technology has been coupled with biological treatment to increase its industrial feasibility (Parra et al., 2002). Such coupling allows the retention time in biological treatment stages to be reduced, where the non-biodegradable compounds of the wastewater can be turned into biodegradable compounds with the photocatalytic treatment.

Similarly, the efficiency of photo-disinfection of various microorganisms has been assessed for possible application of photocatalytic technology to replace chemical disinfection methods. In general, the mechanism involved in microbial disinfection includes the destruction of microbial protein structures and inhibition of their enzymatic activities (Maness et al., 1999). Compared to the persistency during organic photomineralization, a general classification for bacterial resistance to the disinfectant used has also been proposed. Among all, the most resistant infectious type of microorganism are prions, followed by coccidia (*Cryptosporidium*), bacterial endospores (*Bacillus*), mycobacteria (*M. tuberculosis*), viruses (poliovirus), fungi (*Aspergillus*), Gram-negative (*Pseudomonas*) and eventually Gram-positive bacteria (*Enterococcus*) (Malato et al., 2009). Their differences in resistance are explained by their cell wall permeability, size and complexity. These all contain members that are capable of causing human disease when ingested from contaminated water. Most bacteria can be killed easily with TiO_2 photocatalysis, but complete inactivation (bactericidal rather than bacteriostatic effect) might have to be ensured as they are highly infectious. Similarly, this infectious nature can also be found in viruses (adenoviruses, enteroviruses, hepatitis A and E viruses, noroviruses and saproviruses, rotaviruses) and many protozoa (*Acanthamoeba spp, Cryptosporidium parvum, Cyclospora cayetanensis, Entamoeba histolytica, Giardia intestinalis, Naegleria fowleri, Toxoplasma gondii* (WHO, 2006)*).* All these protozoa are highly infectious in low numbers and the photocatalytic treatment should be targeted on these groups as the surrogate indicators. This is to ensure that adequate photocatalytic treatment can be assured to prevent the outbreak of epidemic diseases following consumption of treated water.

5.6. Light Wavelength

The photochemical effects of light sources with different wavelength emitting ranges will have a profound consequence on the photocatalytic reaction rate, depending on the types of photocatalysts used – crystalline phase, anatase-to-rutile composition and any state of photocatalyst modifications. Using commercial Degussa P-25 TiO_2, which has a crystalline ratio of anatase 70/80: 20/30, a light wavelength at $\lambda < 380$ nm is sufficient for photonic activation (Hermann 1999; Bahnemann, 2004). The crystalline phase of rutile TiO_2 has smaller bandgap energy of $E_B \sim 3.02$ eV, compared to the anatase TiO_2 of 3.2 eV (Gaya and Abdullah, 2008). This dictates that rutile TiO_2 will be activated with a light wavelength of up to 400 nm, depending on the bandgap threshold of the type of rutile TiO_2 used.

For UV irradiation, its corresponding electromagnetic spectrum can be classified as UV-A, UV-B and UV-C, according to its emitting wavelength. The UV-A range has its wavelength spans from 315 – 400 nm (3.10 – 3.94 eV), while UV-B has a wavelength range of 280 – 315 nm (3.94 – 4.43 eV) and the germicidal UV-C ranges from 100 – 280 nm (4.43 – 12.4 eV) (Rincón et al., 2005). In most of the previous studies, the UV-A light provides light photons sufficient for photonic activation of the catalyst (Bhatkande et al., 2004; Chin et al., 2006; Ochuma et al., 2007). As with outdoor solar irradiation, the UV-C is usually absorbed by the atmosphere and does not reach the earth's surface. Only the lamp-driven photoreactor system can utilize UV-C irradiation synthetically for catalyst photonic activation and reduction of viable microorganisms. The mechanism of UV-C cell destruction action involves the direct induction on pyrimidine and purine and pyrimidine adducts on the cell DNA. However, not all microorganisms are susceptible to UV-C radiation and some highly resistant microorganisms can survive through the disinfection process. These include *Legionella pneumonphila* and *Cryptosporidium parvum* oocysts (Malato et al., 2009).

The natural UV radiation that reaches the surface of earth consists of both UV-A and UV-B spectrums. The photolysis mechanism for both UV irradiations on cell inactivation is dissimilar to the discussed UV-C mechanism. Both UV-A and UV-B irradiation can be absorbed by cellular components called intracellular chromophores. L-trytophan is the best known intracellular chromophore and is thought to contain unsaturated bonds such as flavins, steroids and quinines (Tyrrell and Keyse, 1990). Among these UV irradiations, UV-A

irradiation is toxic only in the presence of oxygen. The ROS or oxidative stress generated from the chromophore light absorption can damage cells and cellular components, leading to peroxidation, pyrimidine dimer formation and eventually DNA lesions. The contact between the ROS and DNA results in single strand breaks and nucleic acid modifications. Such damage to the DNA is usually lethal or mutagenic irreversible. With the presence of TiO_2 catalyst as the light sensitizer, a high degree of cell damage is seen as the amount of ROS generated increases. A few microorganisms that are resistant to UV-A photolysis have been successfully inactivated by TiO_2 photocatalysis, namely; *Enterobacter cloacae, E.coli, P.aeruginosa* and *S.Typhimurium* (Ibáñez et al., 2003).

A longer wavelength of irradiation (λ > 400 nm) has also been used in solar disinfection (SODIS) study (Sichel et al., 2007; Lonnen et al., 2005; Berney et al., 2006; Kehoe et al., 2004; McGuigan et al., 2006. However, the photo-killing mechanism is as yet unclear as it involves a mixed spectrum of UV-A and solar irradiation. A similar cell destruction mechanism to the one proposed for UV-A irradiation is thought to take place in this mixed light spectrum. In the SODIS, the pathogens in the drinking water contained in PET bottles were found to be inactivated within 6 h of sunlight exposure. However, significant research and developments on disinfection using photocatalytic-mediated processes need to be conducted to broaden the photoactivity of current TiO_2 catalysts used.

5.7. Light Intensity

The photonic nature of the photocatalysis reaction illustrates the dependency of the overall photocatalytic rate on the light source used. Light intensity is one of a few parameters that affect the degree of photocatalytic reaction on organic substrates. Fujishima et al. (2000) indicated the initiation of TiO_2 photocatalysis reaction rates is not highly dependent on light intensity, where a few photons of energy (i.e. as low as 1 $\mu W\ cm^{-1}$) can induce the surface reaction. To achieve a high photocatalytic reaction rate, particularly in water treatment, a relatively high light intensity is required to adequately provide each TiO_2 surface active site with the photon energy required. However, when using the nominal TiO_2 particles without modifications, the surface reaction is restricted to photons with wavelengths shorter than the absorption edge of approximately 400 nm. The organic conversion in the presence of UV wavelength (λ < 400 nm) in many studies obeyed the linear proportionality correlation to the

incident radiant flux. This was evidenced by Glatzmaier et al. (1990 and 1991), where they observed that the destruction of dioxin and polychlorinated biphenyls was enhanced in the presence of high intensity photons. A similar finding was reported in Magrini et al. (1990) where the organic decomposition rate was reported to increase with the radiation intensity.

Later, it was discovered that the dependency of the reaction rate on radiant intensity behaves indifferently under different lighting conditions (Curcó et al., 2002; Qamar et al., 2006; Karunakaran and Senthilvelan, 2005). The linear dependency of the photocatalytic reaction rate on radiant flux (Φ) was found to change to square-root dependency ($\Phi^{0.5}$) above a certain value. Such a shift in dependency form was postulated to be due to the amount of photo-generated holes available during the electron-hole pair formation. In the nature of the TiO_2 catalyst used, the photo-induced generation of valence band holes are much lower than the conduction band electrons available. In this instance, the photo-generated holes are the rate-limiting step and the detailed derivation of the square-root dependency can be obtained from Malato et al. (2009). At high intensities, the dependency of the photocatalytic reaction rate on radiant flux reduced to zero (Φ^0). This was explained by the saturated surface coverage of the catalyst, resulting in a mass transfer limitation in the adsorption and desorption and thus, preventing the effect of light intensity to set in. In this case, an increase in the fluid turbulence might help to alleviate the mass transfer problem on the surface of the catalyst. The desorbed final products might also affect the dependency of reaction rate on radiant flux, as they might scavenge the electron acceptors and further promote the electron-hole pair recombination.

Rincón and Pulgarin (2004) reported that the residual disinfecting ability of the photocatalyst largely depends on the duration of light intensity without any temporal interruptions. They investigated the effect of light intensities at 400 and 1000 W/m^2 on bacterial lethality and regrowth and found that the higher intensity without any temporal interruptions caused irreversible damage to *E.coli*. In the intermittent light irradiations with constant interruptions, the bacteria regrew during the subsequent 24 or 48 h. Some studies suggested that this regrowth is for dark-repair mechanism where the partially damaged cells recover in the presence of nutrients (Sun et al., 2003; Shang et al., 2009). Others have suggested that the damaged but not totally inactivated cells could recover their viability through photo-repairing under radiation of 300-500nm or on the re-synthesis and post replication of cells (Rincón and

Pulgarin, 2003; Sichel et al., 2007). In this case, it must be noted that when using different light intensity in photo-disinfection, a final conclusive point cannot be made directly. The disinfection results of 400 W/m^2 at 2.5 h irradiation might not be the same as the result arising from 1000 W/m^2 for 1 h. Thus, in order to predict the minimum irradiation required at constant irradiance, preliminary studies into both the photoreactor performance and microbial consortia (different resistances) is important.

5.8. Response Surface Analysis

From the earlier discussions on the effect of the operational parameters on the reaction rate, several parameters affect the system indifferently. Overall, a multi-variable (MV) optimisation approach is actually required to optimize a photoreactor system as parameter interactions might exist. Parameter interactions refer to the relationship between operating parameters such as TiO_2 loading on pH or pH on radiant flux. Given the optimization of photoreactor systems, the conventional one-parameter-at-a-time approach is mostly used to unveil the effects of one parameter after another. Although such studies on the effect of common parameters on the reaction rate are acceptable, the outcomes could be insignificant and have less predictive power if one parameter changes.

This has lead to the application of effective design of experiments (DOE), statistical analysis and response surface analysis for photocatalytic studies (Chong et al., 2009d; Liu and Chiou, 2005; Lizama et al., 2002; Korbahti and Rauf, 2008; Calza et al., 2006; Fu et al., 2007). Using this approach, different permutations of experimental design are involved and the operational parameters and spans are defined. Compared to the conventional one-parameter-at-a-time approach, the MV optimization approach has pre-determined experimental points that are dispersed uniformly throughout the study domain, i.e. only a small region is covered in the domain of conventional study. This allows the optimization process to be more time-effective and enhances the identification of parameter interactions when they can be interpreted using commercial statistical software such as Design Expert® Software.

Chong et al. (2009d) proposed the use of Taguchi-DOE approach, together with analysis of variance, statistical regression and response surface analysis to study the combined effects of 4 key operation parameters that affect the photocatalytic reaction rate in an annular photoreactor.

They utilized 9 experimental permutations to analyse the 81 possible parameter combinations. It was reported that the interaction between the TiO_2 loading and aeration rate had a positive synergistic effect on the overall reaction rate. A response surface model was developed to correlate the reaction rate dependency on the 4 different parameters according to the statistical regression shown in Eq 5.4;

$$R_o = b_0 + \sum_{i=1}^{k} b_i X_i + \sum_{i=1}^{k} b_{ij} X_i^2 + \sum_{i_{i<j}}^{k} \sum_{j}^{k} b_{ij} X_i X_j \qquad \text{(Eq. 5.4)}$$

where R_o is the predicted response output of the photo-mineralization rate, and i, j are linear, quadratic coefficients, respectively. The parameters of b and k are the regression coefficient and the number of parameters studied in the experiment, respectively, and X_i, X_j (I = 1, 4; j = 1, 4, $i \neq j$) represent the number of independent variables in the study. This model (Eq. 5.4) is empirical and independent of the photoreactor system. Subsequent verification works is required to determine the accuracy and applicability of such model for the prediction of photoreaction rate under the variation of its parameters. Other DOE approaches to photocatalytic reactor optimization have also been applied including central composite design (Cho and Zoh, 2007), Bayesian (Jaworsji et al., 2008) and Plackett-Burman designs (Wu et al., 2006).

6. Kinetics and Modelling

Kinetics and mechanistic studies on the photomineralization or photo-disinfection rate of the water contaminants are useful for process scale-up. The appropriate utilization of kinetic models for the interpretation of experimental data enables the latter design and optimization of photoreactor system with sufficient capacity and minimal non-illuminated reactor volume. In this section, the different kinetics and rate models for both photomineralization and photo-disinfection will be discussed along with common misconceptions in kinetic modelling.

6.1. Photomineralization Kinetics

In most of the photocatalytic, kinetic and mechanistic studies over the irradiated TiO_2 surfaces studies usually only involve a single constituent model organic compound. The kinetics of different organic compounds ranging from dye molecules, pesticides, herbicides and phenolic compounds to simple alkanes, haloalkanes, aliphatic alcohols and carboxylic acids have been investigated (Herrmann 1999; Bahnemann 2004; Gaya and Abdullah, 2008; Malato et al., 2009). The non-selective nature of the $OH^{\bullet}$ radicals means that the disappearance rate of the studied compound with irradiation time should not be referenced as a standard for reactor design purposes. This is because numerous intermediates are formed en-route to complete mineralization and neglecting this is a common mistake in portraying the photomineralization kinetics. In this instance, the organic concentrations can be expressed collectively in COD or TOC to yield an in-depth understanding on the photomineralization kinetics.

As the L-H model is surface-area dependent, the reaction rate is expected to increase with irradiation time. Since less organic substrate will remain after increased irradiation times with higher surface availability. A zero rate of degradation is associated with the total decomposition achieved. Numerous assumptions for the L-H saturation kinetics type exist and for the applicability in the rate of photomineralization, any of the four possible situations is valid: (i) reactions take place between two adsorbed components of radicals and organics; (ii) the reactions are between the radicals in water and adsorbed organics; (iii) reactions take place between the radical on the surface and organics in water and (iv) reactions occur with both radical and organics in water.

Some researchers have found that simpler zero- or first-order kinetics is sufficient to model the photomineralization of organic compounds. This was, however, only applicable for a limited condition where the solute concentration is sufficiently low. In most kinetic studies, a plateau-type of kinetic profile is usually seen where the oxidation rate increases with irradiation time until the rate becomes zero (Minero 1999; Cunningham and Sedlak, 1996). The appearance of such a kinetic profile usually fits the L-H scheme. According to the L-H model (Eq. 6.1), the photocatalytic reaction rate (r) is proportional to the fraction of surface coverage by the organic substrate (θ_x), k_r the reaction rate constant, C the concentration of organic species and K is the Langmuir adsorption constant:

$$r = -\frac{dC}{dt} = k_r \theta_x = \frac{k_r KC}{1 + KC} \qquad \text{(Eq. 6.1)}$$

The applicability of Eq. 6.1 depends on several assumptions, which include (i) the reaction system is in dynamic equilibrium; (ii) the reaction is surface mediated and (3) competition for the TiO_2 active surface sites by the intermediates and other reactive oxygen species is not limiting (Chong et al., 2009c). If these assumptions are valid, the reactor scheme only consists of adsorption surface sites, organic molecules and intermediates, electron-hole pairs and the reactive oxygen species. The rate constant (k_r) for most of the photocatalytic reaction in water is usually reported to be in the order of 10^6 to 10^9 $(Ms)^{-1}$ (Malato et al., 2009). This k_r-value is proportionality constant for the intrinsic reactivity of the photo-activated surface with *C*. Others have also suggested the k_r is proportional to the power law of effective radiant flux (i.e. $\Phi_e^{\,n}$) during the photomineralization reaction (Cunningham and Sedlak, 1996; Monllor-Satoca et al., 2007). The *K*-parameter is the dynamic Langmuir adsorption constant (M^{-1}) that represents the catalysts adsorption capacity. Eq. 6.1 can be solved explicitly for *t* using discrete change in the *C* from initial concentration to a reference point:

$$\ln\left(\frac{C}{C_o}\right) + K\left(C - C_o\right) = -k_r K t \qquad \text{(Eq. 6.2)}$$

The *K*-value can be obtained using a linearized form of Eq. 6.1, where 1/*r* is plotted against 1/*C*:

$$\frac{1}{r_0} = \frac{1}{k_r} + \frac{1}{k_r K C_0} \qquad \text{(Eq. 6.3)}$$

The real *K*-value obtained from the linearized plot of 1/*r* against 1/*C* is significantly smaller and was explained by the differences in adsorption-desorption phenomena during the dark and the illumination period (Malato et al., 2009). When the organics concentration is low (in mM), an "apparent" first order rate constant (Eq. 6.4) could be expressed where *k'* (min^{-1}) = $k_r K$:

$$r = -\frac{dC}{dt} = k_r KC = k'C \quad \text{(Eq. 6.4)}$$

Rearranging and integration of Eq. 6.4 yields the typical pseudo-first order model as in Eq. 6.5 and 6.6:

$$C = C_o e^{-k't} \quad \text{(Eq. 6.5)}$$

$$\ln\left(\frac{C_0}{C}\right) = -k_r Kt = -k't \quad \text{(Eq. 6.6)}$$

The apparent rate constant, however, only serves as a comparison and description for the photocatalytic reaction rate in the reactor system. Fig. 9 shows a typical saturation kinetic plot for the degradation of organic dye molecules in an annular photoreactor system, where the reaction rate increases to a point where the rate plateaus off. To interpret the maximal photomineralization rate, the tailing regime of the L-H saturation profile should be neglected. Only the slope of the tangent to the inflexion point should be used to obtain the maximal photomineralization rate. The unit for the slope in this instance has the same chemical reaction order as the zero-order rate constant.

A lump-sum L-H saturation kinetics profile has also been used to simplify the approximation for end photocatalytic reactor system (Minero et al., 2006). In such an empirical lump-sum L-H approach, the degree of organics mineralization is actually expressed in terms of TOC (Eq. 6.7):

$$r_{TOC,O} = \frac{\beta_1[TOC]}{\beta_2 + \beta_3[TOC]} \quad \text{(Eq. 6.7)}$$

This Eq. 6.7 allows the prediction of TOC degradation as a function of irradiation time. Similar reciprocal plots of $1/r$ against $1/[TOC]$ can be used to determine the empirical parameters, β_1, β_2 and β_3 as Eq. 6.3. The irradiation time taken to achieve the fractional degradation of TOC can also be estimated when Eq. 6.7 is expressed as in Eq. 6.2. Such an

empirical lump-sum L-H model has greatly summarized the need for precise kinetic measurement and made a great approximation for any particular photoreactor system, provided sufficient data are collected for the determination of rate parameters.

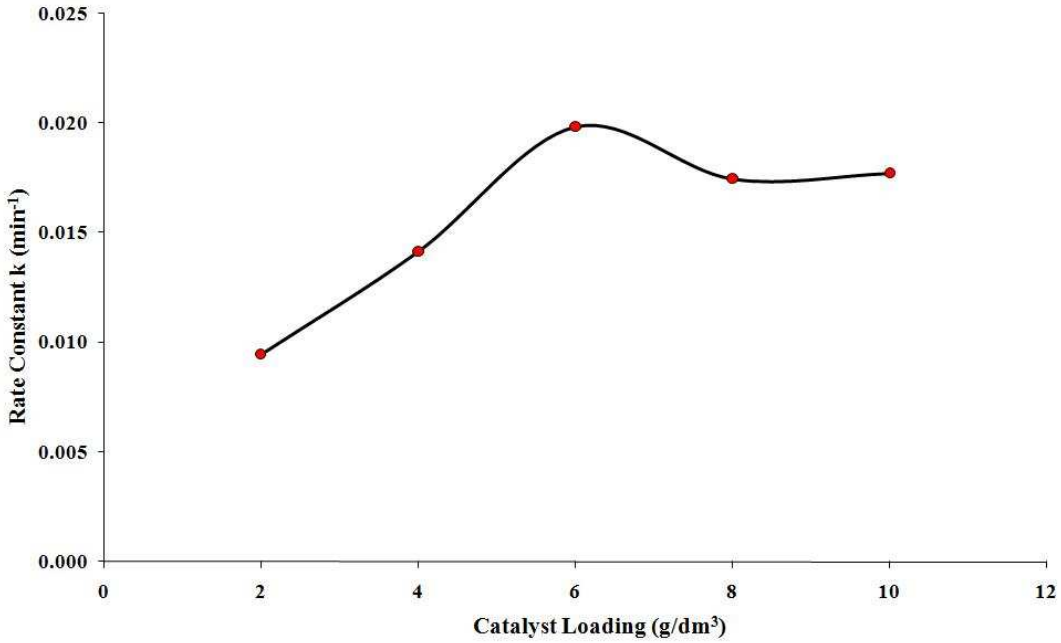

Figure 9: Typical saturation kinetics plot for the degradation of organic dye molecules in an annular photoreactor system (Chong et al., 2009b).

6.2. Photo-Disinfection Kinetics

Since the first application of semiconductor catalysts for disinfection by Matsunaga et al. (1985), few studies have been found in the literatures which comprehensively study the kinetic modelling of photo-disinfection of microorganisms in a water treatment process. Empirical kinetic models have been the mostly applied for interpretation of photo-disinfection data, because of process complexity and variability. The general expression for the empirical photo-disinfection models for demand-free condition is expressed in Eq. 6.8. In this instance, demand-free conditions assume that the catalyst concentration is constant with irradiation time.

$$\frac{dN}{dt} = -kmN^{x}C^{n}T^{m-1} \qquad \text{(Eq. 6.8)}$$

where *dN/dt* = rate of inactivation; *N* = number of bacterial survivors at irradiation time *t*; *k* = experimental reaction rate; *C* = concentration of photocatalyst used; *m*, *n* and *x* are the empirical constants. However, the most commonly employed disinfection model in photo-disinfection studies to date is the simple mechanistic Chick-Watson (C-W) model (Eq. 6.9) (Cho et al., 2004 and 2008).

$$\log\frac{N}{N_O} = -k'T \qquad \text{(Eq. 6.9)}$$

In this C-W model, the photo-disinfection rate is expressed as a linear function of the enumerated bacteria and catalyst loading. The combined kinetic parameter of *CT* between the catalyst concentration and irradiation time required to achieve complete inactivation is widely used as a reference for process design. Other than this, this *CT*-values concept is used to compare the efficacy of different disinfectant used in water treatment (Finch et al., 1993). This C-W model, however, may not always be applicable as many studies may have experienced a curvilinear or non-linear photo-disinfection profile. Hom (1972) reproduced a useful empirical modification of the C-W model after having observed that the disinfection plots of natural algal-bacterial systems were curvilinear, rather than typical log-linear type (Eq. 6.10). In the Hom model, the bacterial inactivation level is predicted in a non-linear function of *C* and *T*, depending on the empirical parameters of *n* and *m*, respectively. Since this Hom model is a two-parameter model, it should be stressed that it is only applicable to a photo-disinfection profile with a maximum of two non-linear regions. For *m*-values greater than unity, the inactivation curve displays an initial “shoulder” while “tailing” is seen when the *m*-value is less than unity.

$$\log\frac{N}{N_O} = -k'C^nT^m \qquad \text{(Eq. 6.10)}$$

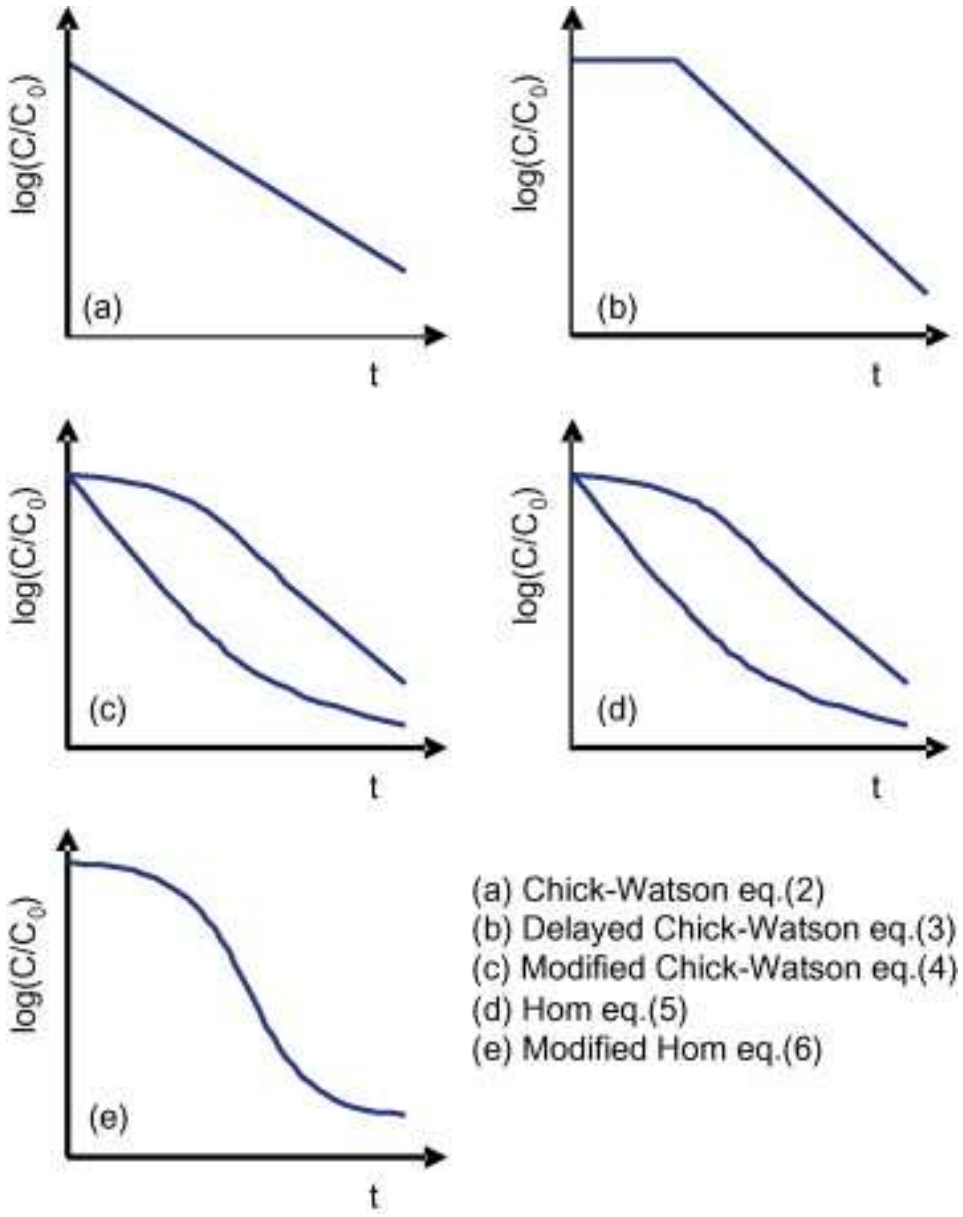

Figure 10: Common non-linearity in the photo-disinfection kinetics profile using TiO_2 catalyst, along with the appropriate disinfection models used (Marugán et al., 2008).

Marugán et al. (2008) have outlined the common non-linearity found in the photo-disinfection kinetics profile using Degussa P-25 TiO_2 catalyst fitted with common disinfection models (Fig. 10). In their study, they found that three different inactivation regions in the photo-disinfection profile, namely (i) a lag or initial smooth decay, known as the "shoulder", followed by (ii) a typical log-linear inactivation region and ends with (iii) a long deceleration process at the end of the disinfection, which is known as the "tailing". The presence of "shoulder" was justified

by the cumulative damage nature of photo-disinfection treatment on the cytoplasmic membrane rather than an instantly lethal (Gyürék and Finch, 1998). The "tailing" during the photo-disinfection, however, is not well understood. Benabbou et al. (2007) proposed that the "tailing" region was related to the competition for photocatalysis between organic products released from constant cell lyses and the remaining intact cells. Others have proposed that the "tailing" deviations from the log-linear reduction were due to the presence of variations in the bacterial population resistant to the disinfectant used (Lambert and Johnston, 2000). Nevertheless, the use of *CT* concept or Hom model can lead to an over-design for a photo-disinfection system (Gyürék et al., 1998). A further modification to the Hom model was made to account for the simultaneous presence of shoulder, log-linear reduction and tailing (Eq. 6.11) (Marugán et al., 2008; Cho et al., 2003);

$$\log\frac{N}{N_O} = -k_1\left[1-\exp(-k_2 t\right]^{k_3} \qquad \text{(Eq. 6.11)}$$

Eq. 6.11 is known as the modified Hom model and it expands the applicability of the Hom model for the fitting of the initial shoulder, log-linear reduction and prolonged tailing behaviours. Another detailed empirical model that can detail the different bacterial inactivation regions is a power law expression (Eq. 6.12), when m=1 for the generalized differential equation (Eq. 6.8) (Gyürék et al., 1998);

$$\frac{dN}{dt} = -kN^x C^n \qquad \text{(Eq. 6.12)}$$

Integration of Eq. 6.12 yields the Rational model (Eq. 6.13). If x=1, this Rational model can be reverted back to the C-W model. In this instance, the Rational model assumes that $x \neq 1$;

$$\log\frac{N}{N_O} = -\frac{\log\left[1+N_O^{x-1}(x-1)kC^n T\right]}{(x-1)} \qquad \text{(Eq. 6.13)}$$

The Rational model (Eq. 6.13) can describe both "shoulder" and "tailing" characteristics for x less than or greater than unity respectively. Similarly, the Hom model (Eq. 6.10) can also be integrated according to the Rational Model with the introduction of both x and $m \neq 1$ to yield the Hom-Power model (Eq. 6.14):

$$\log\frac{N}{N_O} = -\frac{\log\left[1 + N_O^{x-1}(x-1)kC^nT^m\right]}{(x-1)} \qquad \text{(Eq. 6.14)}$$

Anotai (1996) reported that this Hom-Power model may provide a better fit than both the Hom and Rational models. However, the existence of four empirical parameters in the model may result in an over-parameterization with null physical meanings for each parameter within the model. To reduce the number of null parameters, the Selleck model (Eq. 6.15) was proposed. This model assumes that the catalyst concentration remains constant during the irradiation period:

$$\frac{dS}{dt} = \frac{kCS}{1+KCT} \qquad \text{(Eq. 6.15)}$$

where S is the survival ratio = N/N_o at irradiation time t; k and K are the rate constants. In this model, the "shoulder" was assumed to be a result of cumulative effects of the chemical disinfectant on the microbial target during the contact time. A gradual decrease in the permeability of the outer cell membrane of *E.coli* as an action of the catalysts can be idealized by a series of first order reaction steps on a single *E.coli* cell that leads to lethality. This model can be modified to account for the disinfection of coliform bacteria in water/wastewater effluent (Eq. 6.16) (Gyürék et al., 1998):

$$\log\frac{N}{N_o} = -n\log\left[1+\frac{CT}{K}\right] \qquad \text{(Eq. 6.16)}$$

Although empirical models provide a simple correlation of the photo-disinfection data, the mathematical nature of their relevant terms yields null or misinterpret physical meaning. For instance, the m-value > 1 in the Hom model actually suggests that photocatalytic reactivity

increases with irradiation time in the ASP. If the vitalistic assumption of bacterial population resistance distribution is valid, this actually indicates that the most resistant bacteria are killed first prior to the least resistant one (Lambert and Johnston, 2000). This shows that the rationale for the applicability of Hom model is contradictory.

It was proposed that mechanistic models could convey a better physical meaning in their kinetic terms. It was hypothesised that the photo-disinfection mechanism can be viewed as a pure physicochemical phenomenon and preceds in a similar way to a chemical reaction (Lambert and Johnston, 2000). The classical C-W model is a typical example of the mechanistic photo-disinfection kinetics model. In the model, the apparent exponential decay curves for bacterial survival ratios with irradiation times follow a similar decay mechanism of a chemical reaction and are thus, applicable for both phenomena. This can be visualised when the C-W model is integrated mathematically with *N,* assuming to be the number of moles of reactant generated to yield the log-linear curve of a first-order reaction.

To formulate a mechanistic model for photo-disinfection kinetics, the occurrence of both "shoulder" and "tailing" region should be rationalized idealistically. The presence of "shoulder" can be justified mechanistically by the single-hit multiple targets or a serial phenomenon event (Gyürék et al., 1998). Under mechanistic assumption, the damage to the microbial cell is viewed as cumulative rather than instantly lethal. This dictates that a large number of critical molecules need to be denatured prior to cell inactivation (Gyürék et al., 1998). Severin et al. (1984) proposed that the cumulative inactivation of a single bacterium can be collectively represented by a series of integer steps. These disinfection steps were thought to pass on a bacterium from one level to another in a first order reaction with respect to the catalyst used until a finite number of lethal (*l*) events was reached. The microorganisms which accumulate less than the postulated number of lethal steps are considered to survive the photo-disinfection process. As for the "tailing" region, many have regarded that it resulted from the presence of a microbial subpopulation resistant to thermal sterilisation. Najm (2006) also suggested that the "tailing" is due to the intrinsic distribution of bacterial resistance to the sterilisation method, making the bacteria more resistant, adapted and inaccessible to heat treatment. Marugán et al. (2008) reviewed that such "tailing" was not a common phenomenon in water disinfection treatment. So far, no justifiable explanation has been proposed to account

for the occurrence of "tailing" in the water disinfection treatment with well-mixed conditions and equally resistant cloned-bacterial population. It was suggested that the "tailing" was a result of gradual deterioration in the rate of disinfection and total inactivation was achievable only after a sufficient retention time. The random collisions between the catalyst and bacteria can be expressed by the Poisson probability, as the number of collisions supercede prior to the number of microbial death (Gyürék et al., 1998). If the destruction rate of the microorganisms is assumed to be the same for the first and *l* th target at the κth bacteria site, thus, the rate of destruction for the microorganisms is given by;

$$\frac{dN_{\mathrm{K}}}{dt} = kCN_{\mathrm{K}-1} - kCN_{\mathrm{K}} \qquad \text{(Eq. 6.17)}$$

Solving for κ = 0 to κ = l – 1 gives the log fraction of microbial survival, not exceeding l – 1 at the end of the contact time;

$$\ln\frac{N}{N_o} = -kCT + \ln\left[\sum_{\mathrm{K}=0}^{l-1}\frac{(kCT)^{\mathrm{K}}}{\mathrm{K}!}\right] \qquad \text{(Eq. 6.18)}$$

Lambert et al. (2000) stated in the formulation of all mechanistic models that take into account the "shoulder" and "tailing", an intermediate population stage is usually suggested with different rates of disinfection for each microbial state. Typically, two different microbial states for the number of damaged bacterial and undamaged bacteria (i.e. C_{dam} + C_{undam}) were introduced to account for such non-linearity in bacterial survivor curves. A similar Langmuir-Hinshelwood (L-H) type of mechanistic model (Eq. 6.19 and 6.20) can also be applied to represent the photo-disinfection kinetics to yield more meaningful kinetic terms (Marugán et al., 2008). Johnston et al. (2000) showed that the inoculum size of the bacteria has a large impact on resistance distribution and thus, the errors associated with this term should be given attention during the mechanistic modelling.

$$\frac{dC_{undam}}{dt} = \frac{-k_1 K_{undam} C_{undam}^{\eta_{undam}}}{1 + K_{undam} C_{undam}^{\eta_{undam}} + K_{dam} C_{dam}^{\eta_{dam}}} \qquad \text{(Eq. 6.19)}$$

$$\frac{dC_{dam}}{dt} = \frac{k_1 K_{undam} C_{undam}^{\eta_{undam}} - k_2 K_{dam} C_{dam}^{\eta_{dam}}}{1 + K_{undam} C_{undam}^{\eta_{undam}} + K_{dam} C_{dam}^{\eta_{dam}}} \quad \text{(Eq. 6.20)}$$

where k_i is the true log-linear deactivation rate constant for the reaction between generated ROS with bacteria. The pseudo-adsorption constant, K_i, represents the surface interaction between the catalyst and bacteria. This constant is similar to the adsorption equilibrium constant in a conventional L-H model. Due to the significant size differences between *E.coli* cells and the catalyst agglomerates, these constants do not represent strict adsorption phenomena but a more general surface interaction during photo-disinfection. These adsorption constants allow the "shoulder" representation in the photo-disinfection kinetics data. The inhibition coefficient, η_i is a power coefficient that accounts for the "tailing" in the bacteria inactivation curve. Marugán et al. (2008) proposed that η_i is needed to account for the inhibition produced by the increasing concentrations in the medium of cell lysis and oxidation products strongly competing for the ROS. This is particularly important towards the end of photo-disinfection, as high concentrations of these compounds and small amount of viable bacteria are present in the suspension. In this instance, the η_i in the proposed L-H model essentially means that the reaction order with respect to the microbial population is higher than one.

Both Eq. 6.19 and 6.20 have six independent parameters that describe photo-disinfection rates. This constitutes a high risk of over-fitting the experimental data, where the statistical significance of parameters and the plausibility of the model are low. By taking into account the intrinsic kinetics of ROS attack, the catalyst-bacteria interaction and the inhibition by-products are similar for both undamaged and damaged bacteria, the following are assumed:

$$k_1 = k_2 = k \quad \text{(Eq. 6.21)}$$

$$K_{undam} = K_{dam} = K \quad \text{(Eq. 6.22)}$$

$$\eta_{undam} = \eta_{dam} = \eta \quad \text{(Eq. 6.23)}$$

With these, the Eq. 6.19 and 6.20 are reduced to Eq. 6.24 and 6.25. The three independent parameters allow a simultaneous fitting of three different inactivation regimes of "shoulder", "log-linear" and "tailing. Fitting of the Eq. 6.24 and 6.25 to the experimental measurements of

(C_{undam} + C_{dam})/C_o can be achieved using a non-linear regression algorithm coupled with a fifth-order Runge-Kutta numerical approach. Marugán et al. (2008) showed good fitting of such a mechanistic L-H model to the photo-disinfection of *E.coli* under different loadings of Degussa P25 TiO_2 catalyst.

$$\frac{dC_{undam}}{dt} = \frac{-kKC_{undam}^{\eta}}{1 + KC_{undam}^{\eta} + KC_{dam}^{\eta}} \quad \text{(Eq. 6.24)}$$

$$\frac{dC_{dam}}{dt} = k\frac{KC_{undam}^{\eta} - KC_{dam}^{\eta}}{1 + KC_{undam}^{\eta} + KC_{dam}^{\eta}} \quad \text{(Eq. 6.25)}$$

7. Water Quality

In a full-scale plant for water treatment, a number of technical issues have to be sorted out. Water quality of the influents in the treatment plant can vary with time. In this section, the implication of TiO_2 photocatalytic processes for treatment of water sources of different qualities will be discussed. This enables a fuller understanding of the effects of various key water quality parameters on the suitability of applying such advanced TiO_2 photocatalytic processes.

7.1. Turbidity

Turbidity often refers to the insoluble particulates that are present in the targeted water (Viessman Jr. and Hammer, 1998). These are highly detrimental to the TiO_2 photocatalysis based process, as they can affect the optical properties and further impede the penetration of UV light by strong scattering and absorption of the rays (Chin et al., 2004; Tang and Chen, 2004). This will cause a variation in the predicted use of TiO_2 loading, UV penetration path and light intensity. Also, excessive levels of turbidity can reduce both the photomineralization and photo-disinfection efficiency of the pollutants present in water from shielding effects that attenuate the light penetration causing those pollutants to survive from the treatment (Rincón and Pulgarin, 2005; Chin et al., 2004; Tang and Chen, 2004). Suspended solids will also shield target pollutants from oxidation reactions. In such cases, suspended solids refer to the non-

filterable residue that is retained on the filter medium after filtration. All these factors ultimately decrease the overall photocatalytic efficiency for water treatment. To ensure rapid photocatalytic reaction rate, the turbidity of the targeted water should be kept below 5 nephalometric turbidity units (NTU) for optimal UV light utilisation and photocatalytic reaction (Gelover et al., 2006; Fernándezs-Ibáñez et al., 2009). Rincón and Pulgarin (2003) observed that the water turbidity higher than 30 NTU will affect negatively the rate of photocatalytic disinfection. The limit of 5 NTU is arbitrary and depends on the receiving water bodies and the treatment levels required. Since TiO_2 photocatalytic processes are retrofitted to the advanced water treatment stage, prior reduction in turbidity could be achieved via conventional treatment processes such as screening, filtration, sedimentation, coagulation and flocculation. The standard for 1 NTU is a 1.0 mgL^{-1} of specified size of silica suspension and can be prepared for laboratory investigation. The turbidity standard can be calibrated using a photoelectric detector or nephalometry for the intensity of scattered light.

7.2. Inorganic Ions

The presence of inorganic ions in the targeted water for TiO_2 photocatalytic treatment is expected. To functionalise a TiO_2 water treatment process, the basic understanding of these inorganic ions on the photocatalytic performance is essential. Crittenden et al. (1996) reported that when a photocatalyst is utilised in either slurry or fixed-bed configuration to treat real waters with different inorganic ions, photocatalyst deactivation was usually observed. This resulted from a strong inhibition from the inorganic ions on the surface of the TiO_2 semiconductor used. Thus, the presence of these inorganic ions together with their permissible levels on the photocatalytic performance of TiO_2 in water treatment has to be determined to ensure minimal disturbances on the efficient operation of the TiO_2 based treatment process. With such data, a cost effective fouling prevention with inorganic ions and photocatalyst regeneration strategies can be customised.

A number of studies have been conducted on the effects of different inorganic anions or cations, on both TiO_2 photomineralization and photo-disinfection reactions (Rincón and Pulgarin, 2004; Habibi et al., 2005; □zkan et al., 2004; Schmelling et al., 1997; Leng et al., 2000; Wong and Chu, 2003; Wang et al., 2004; Chen et al., 1997; Riga et al., 2007; Guillard et al., 2003). It must be emphasized, however, that most of these studies have concentrated on

how different inorganic ions affect rates of photocatalytic reactions with a model surrogate organic compound. The surrogate model organic compound can be biased towards its photocatalytic performance owing to its underlying chemical properties and the main constituent groups that form the compound. For instance, the model compounds with either electron-withdrawing or donating groups will contribute different degree of interaction to degradation pathways (Herrmann, 1999). Due to the zwitterionic nature of the TiO_2 particles used, it is also possible that the operating pH might have a profound effect on the selective inhibition of inorganic ions on the surface of the TiO_2 particles (Guillard et al., 2003). However, few discussions have been centred on considering how the chemical nature of the model organic used and the operating pH in the photocatalytic reactor inhibits different inorganic ions in photocatalytic water treatment.

The effects of both inorganic cations (i.e. Na^+, K^+, Ca^{2+}, Cu^{2+}, Mn^{2+}, Mg^{2+}, Ni^{2+}, Fe^{2+}, Zn^{2+}, Al^{3+}) and anions (i.e. Cl^-, NO_3^-, HCO_3^-, ClO_4^-, SO_4^{2-}, HPO_4^{2-}, PO_4^{3-}) on the photocatalytic water treatment have been investigated (Rincón and Pulgarin, 2004; Habibi et al., 2005; □zkan et al., 2004; Schmelling et al., 1997; Leng et al., 2000; Wong and Chu, 2003; Wang et al., 2004; Chen et al., 1997; Riga et al., 2007; Guillard et al., 2003). A general consensus from these studies concludes that Cu^{2+}, Fe^{2+}, Al^{3+}, Cl^-, PO_4^{3-} at certain levels may decrease photo-mineralization reaction rates while Ca^{2+}, Mg^{2+}, Zn^{2+} may have negligible effects. This is because the Ca^{2+}, Mg^{2+} and Zn^{2+} are at their maximum oxidation states resulting in their inability to inhibit the photocatalysis reaction. The presence of Fe^{2+} can catalyse both the Fenton and photo-Fenton reactions. Choi et al. (1994), however, observed that Fe^{2+} fouled the photocatalysts surface by introducing an rusty orange colour change with the formation of $Fe(OH)_3$ while PO_4^{3-} in the nominal pH range remains strongly adsorbed onto the TiO_2 surface and further inhibits its photoactivity (Kerzhentsev et al., 1996; Abdullah et al., 1990). Some groups report that NO_3^-, SO_4^{2-}, ClO_4^- and HCO_3^- inhibit the surface activity of the photocatalysts, while others may not have such impact. Both NO_3^- and SO_4^{2-} have detrimental effect on the photo-disinfection rate and Cu^{2+} enhances the photocatalytic activity up to 0.1 mM, while further increases in its concentration reduce the reaction rates (Okamoto et al., 1985; Habibi et al., 2005). Nitrogen-containing molecules are mineralized into NH_4^+ and mostly NO_3^-. Ammonium ions are relatively stable and their proportion depends mainly on the initial oxidation degree of nitrogen on the irradiation time. Pollutants containing sulfur atoms

are mineralized into sulphate ions. While Cl^- has no inhibition on the photocatalytic degradation of trichloroethylene at a concentration up to 3.0 mM. On contrary, the addition of oxyanion oxidants such as ClO_2^-, ClO_3^-, IO_4^-, $S_2O_8^-$ and BrO_3^- increased photo-reactivity by scavenging conduction-band electrons and reducing the charge-carrier recombination (Martin et al., 1995). The presence of salts is also known to diminish the colloidal stability as screening effects become more profound. This was followed the double layer compression and surface charge neutralisation, which increases the mass transfer limitations and reduces surface contacts between the pollutants and catalysts. Other inorganic ions also affect photodegradation rates, where the presence of SO_4^{2-} in a TiO_2 coated glass spiral reactor could double the disappearance rate of the pesticide monocrotophos, and Mn^{2+} improved photoactivity by simultaneously increases the electron-hole pairs and preventing their recombination (Zhu et al., 1995; Mu et al., 2004).

Several mechanisms for fouling effects of inorganic ions on TiO_2 photoactivity have been proposed (Burns et al., 1999; Rizzo et al., 2007). These include UV screening, competitive adsorption to surface active sites, competition for photons, surface deposition of precipitates and elemental metals, radical and hole scavenging and direct reaction with the photocatalyst. The NO_3^- ion was reported to screen the photocatalyst than inhibiting the TiO_2 surface (Burns et al., 1999). The competition for surface active sites involves the constant displacement of hydroxide ions from TiO_2 surface and thus further reduces the generation of radicals. Quantum yield is reduced as a result of the direct competition of inorganic ions for light photons (lowered number of photons entering the reactor). A similar decrease in photonic efficiency was observed when precipitates were formed and deposited onto the TiO_2 surface, blocking accessibility of both photons and organic compounds. The ultimate inorganic anions that were determined to scavenge both the hole and radicals include Cl^-, HCO_3^-, SO_4^{2-} and PO_4^{3-} (Diebold, 2003). A mechanism for Cl^- and HCO_3^- in inhibiting photocatalysis via hydroxyl radical and holes scavenging was proposed by Matthews and McEnvoy (1992); Lindner et al. (1995), respectively:

$$Cl^- + OH^\cdot \rightarrow Cl^\cdot + OH^- \qquad \text{(Eq. 7.1)}$$

$$Cl^- + h^+ \rightarrow Cl^\cdot \qquad \text{(Eq. 7.2)}$$

The Cl^- accounted for its inhibitory effect on TiO_2 photocatalysis through a preferential adsorption displacement mechanism over the surface bound OH^- ions. This reduces the number of OH^- ions available on the TiO_2 surfac, and the substituted Cl^- further increases the recombination of electron-hole pairs. Among other chlorinated molecules, Cl^- ions are readily released in the solution. This effect could be of benefit in a process where photocatalysis is associated with a biological depuration system, which is generally not efficient for chlorinated compounds (Herrmann, 1999). Other ions such as PO_4^{3-} are known to avert adsorption of amino acids over the TiO_2 catalysts, while CO_3^{2-} and other ionic species react with $OH^{\cdot}$ radicals to compete with microorganisms and further reduce efficiency. Thus, the presence of inorganic ions in water subjected to TiO_2 photocatalytic treatment is an important factor in determining its successful implementation.

To resolve TiO_2 photocatalyst fouling issue, preventative or regenerative strategies can be adopted, depending on the nature of deactivation. Fouling preventative strategies by means of water pre-treatment, complexation and photocatalyst surface modifications can be addressed, while rinsing the TiO_2 surface with different chemical solutions constitutes the regenerative strategies. Water pre-treatment with ion exchange resins is one method that can be employed to ensure minimal disturbances by inorganic ions. Burns et al. (1999) discussed that the operational cost of water pre-treatment with ion exchange resins can be minimised if the fouling ions were identified and selectively removed. Other preventative strategies such as complexation of fouling agents after "escorting" the ions through the reactor can be utilised, provided that the strong fouling ions are hard to remove from the feed water stream. Modifications of the TiO_2 surface to increase the hydrophobicity and adsorption capacity is an upstream preventative way to enhance the rate of photodegradation in the presence of fouling ions. However, this method is unstable and impractical compared to the others, where the modifications were reported to be displaced away with time. As for the regenerative strategies, different types of chemical rinsing are reported to potentially resolubilize surface deposits, precipitates and reduced metals. The fouled ions usually do not form strong surface complexes and can be easily displaced by an ion exchange rinse. Abdullah et al. (1990) reported that TiO_2 fouling with SO_4^{2-} and PO_4^{3-} can be displaced by NaOH, KOH and $NaHCO_3$, while Cl^- can be easily regenerated with water. More complex mixtures of inorganic ions need to be

investigated to better mimic real water matrices in photocatalytic water treatment or after investigation of water matrices with one known inorganic ion composition at a time.

7.3. Heavy and Noble Metals

Heavy metals that might be present in trace amount in the wastewater stream are highly toxic in some of their valence states (Kabra et al., 2004). Due to the pliable nature of biological treatment, these metals can remain and permeate through the treatment process. To treat such metals, TiO_2 photocatalytic process has been reported to simultaneously convert these metals into non-toxic ionic states and further converted them into their corresponding elemental form on the TiO_2 surface for metal recovery. Prairie et al. (1994) reported that Ag(I), Cr(IV), Hg(II) and Pt(II) were easily treated with TiO_2 of 0.1 wt% whereas Cd(II), Cu(II) and Ni(II) could not be removed. The extent of such metals conversion and recovery process are highly dependent on the standard reduction potential of the metals for the reduction reactions. For an efficient removal, a positive potential of greater than 0.4 V or the flat band potential of TiO_2 was required (Herrmann, 1999; Kabra et al., 2004). Since the rates of both oxidation (organics) and reduction (metals) on the TiO_2 surface are intrinsically interrelated, the present of sufficient organics in the water matrices were found to facilitate the metal recovery. The redox process for the metal reduction on the TiO_2 surface is given below:

$$Mn^+ + H_2O \xrightarrow{TiO_2\,(h\nu)} M^o + nH^+ + \frac{n}{4}O_2 \qquad \text{(Eq. 7.3)}$$

Herrmann et al. (1988) reported that small crystallites of silver (3 and 8 nm) were initially deposited and began to agglomerate (few hundreds of nm) when the conversion increased. Since the photosensitive surface was not masked, a relatively large amount of silver was recovered, leaving behind concentration of lower than the detection limits of atomic absorption spectroscopy ($\leq$ 0.01 ppm) in solution. The effect of various factors on the photoreduction of silver on TiO_2 surface were further investigated (Huang et al., 1996). Angelidis et al. (1998) also reported that even at low concentration of metal ions, the photodeposition of metals on the TiO_2 surface from solution was still performed effectively. However, they noted that the rate of photodeposition was enhanced when Pt-loaded was used

instead of unloaded TiO_2 particles. This metal photodeposition property on TiO_2 surface is particularly useful when the water legislation limit on the metal contents is stringent.

8. Life Cycle Assessment of Photocatalytic Water Treatment Processes

In the current development of photocatalytic water/wastewater treatment processes, their application is still investigated at pilot plant scale. A few pilot plants have been established to obtain feasibility data like treatment efficacies, site area requirements for targeted volume, electrical energy consumption, process emissions and chemical costs. The heterogeneous photocatalysis and photo-Fenton plants located at the INETI (Instituto Nacional de Engenharia, Technologia Industrial e Inovacao, Portugal) and PSA (Plataforma Solar de Almeria, Spain) are two pilot plants that have delivered most of these data for technical analysis. Both plants consist of compound parabolic collectors (4.16 m^2 aperture area) exposed to sunlight, a reservoir tank, a recirculation pump and connecting tubing, amd are operated in batch mode (Munoz et al., 2006). Further technical details can be found in the literature (Gernjak et al., 2006; Lapertot et al., 2006).

In order to assess these photocatalytic processes as emerging technologies for large scale water/wastewater treatment, a life cycle assessment (LCA) should be evaluated based on the currently available data. LCA is one of the most widely accepted tools that not only consider the environmental impact of the emergent photocatalytic water treatment, but also its technical feasibility and costs. Andreozzi et al. (1999) also pointed out that the potential application of ROS-based oxidation processes entails high costs for energy and reactants consumption. Thus, to consider the feasibility of photocatalytic water treatment on the whole, a comprehensive LCA based on viable technical data should be carried out. Munoz et al. (2005) carried out a simplified LCA based on small-scale laboratory data of heterogeneous photocatalysis and other AOPs. However, they found that small-scale laboratory data interpretation in their LCA study can lead to inconclusive results.

Using LCA, the environmental burdens from a product, process or activity via materials and energy balances can be defined and reduced as well as the waste discharges, its impacts on the environment and the environmental improvement opportunities over the whole life cycle

(Consoli et al., 1993). This holistic LCA approach in decision making over other environmental assessment approaches includes all the burdens and impacts, and focuses on the emissions and wastes generated (Azapagic and Cliff, 1999).

Munoz et al. (2006) carried out a LCA based on two pilot plants of INETI and PSA, which treated 1 m^3 of methy-phenylglycerine (MPG) to destroy non-biodegradable and toxic compounds to a level that met the quality of aquatic ecosystems with both homogeneous photo-Fenton and heterogeneous photocatalysis. Other technically rationale assumptions were also made to facilitate the estimation of energy and materials consumed and produced. Nine impact categories of the possible large scale photocatalytic water treatment process were included in the analysis, namely; global warming potential, ozone depletion potential, human toxicity potential, fresh-water aquatic toxicity potential, photochemical oxidant formation potential, acidification potential, eutrophication potential, non-renewable energy consumption and land use.

Fig. 11 shows the LCA results for possible large scale water application using photocatalytic technology. They show that the retrofitting of heterogeneous photocatalysis process to the existing biological wastewater treatment can lower eutrophication potential, but require higher site area requirement and electricity consumption. These technical constraints are result from requirements for a large land area and the raw materials to build the parabolic collector infrastructure and high power needed to pump the wastewater through the system. However, the results from the impact categories cannot be compared directly to each other as they were expressed in different measurement units. From the engineering point of view, these constraints mainly arise from the low photo-activity of the catalyst used under solar irradiation. Further materials engineering solutions and studies should be carried out to resolve such technical issues to permit the scale-up of the technology to a commercially viable process.

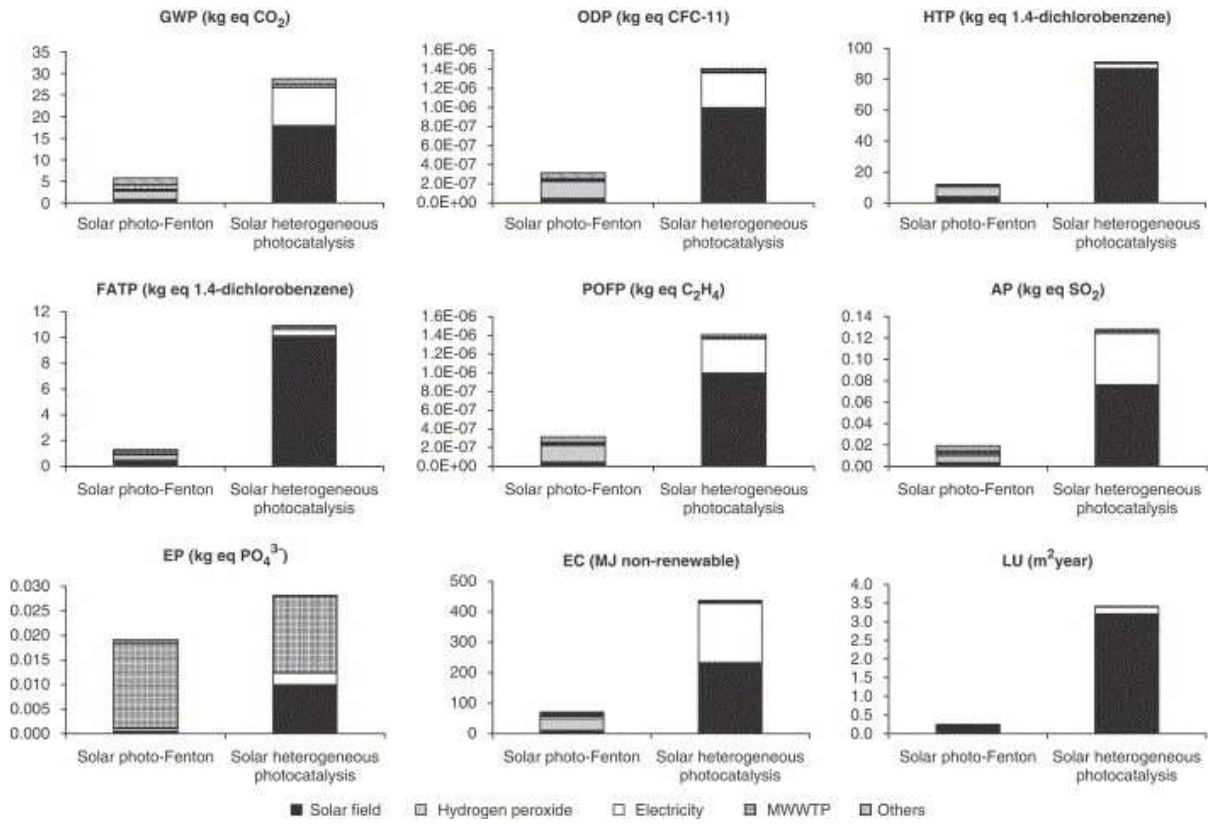

Figure 11: Life cycle impact assessment results for the alternatives under study (Muñoz et al., 2006).

9. Future Challenges and Prospects

Semiconductor photocatalytic technologies using either UV light or solar have become more prominent because of the advantages of the use of vast additive chemicals or disinfectants and its mineralization aspects. These are particularly important, as the recalcitrant organics are mineralized rather than transformed to another phase. Coupled with the ambient operation of the process, all these make photocatalytic water treatment technology a viable alternative for commercialisation in the near future. Different water contaminants ranging from hazardous contaminants of pesticides, herbicides and detergents to pathogens, viruses, coliforms and spores are effectively removed by this photocatalyzed process.

The applicability of the heterogeneous photocatalytic technology for water treatment is constrained by several key technical issues that need to be further investigated. The first would

be whether the photocatalytic process is a pre-treatment step or a stand-alone system. The non-selective reactivity on the non-biodegradable water soluble pollutants means the photocatalytic process can be used effectively as a pre-treatment step to enhance biodegradation of recalcitrant organic pollutants prior to biological water treatment. The residence times and reaction volumes for the biological treatment could be reduced. If the photocatalytic process is used as a stand-alone treatment system, the residence time required might be prolonged for total bacterial inactivation or mineralization. As discussed, this is hindered by slow kinetics, low photo-efficiency and a need for continuous (without interruption) illumination to achieve the required total organic carbon removal or microbial inactivation. For the stand-alone system, the site area requirement might be proportionally high for an increased reaction volume required.

In order to promote the feasibility of photocatalytic water treatment technology in the near future, several key technical constraints ranging from catalyst development to reactor design and process optimization have to be addressed. These include (i) catalyst improvement for a high photo-efficiency that can utilize wider solar spectra; (ii) catalyst immobilisation strategy to provide a cost effective solid-liquid separation; (iii) improvement in the photocatalytic operation for wider pH range and to minimize the addition of oxidant additives; (iv) new integrated or coupling system for enhanced photomineralization or photo-disinfection kinetics and (v) effective design of photocatalytic reactor system or parabolic solar collector for higher utilization of solar energy to reduce the electricity costs. Currently, the utilization of solar energy is limited by the photo-efficiency of the TiO_2 catalyst bandgap to only 5% of the solar spectrum. The need for continuous illumination for efficient inactivation of pathogens has diverted solar utilization to employ artificial UV lamp-driven process. In addition, the low efficacy design of current solar collecting technology (0.04% capture of original solar photons) has encouraged the developmental progress of photocatalytic technology in water treatment industry. Further pilot plant investigations with different reactor configurations are needed to ensure that the photocatalytic water technology is well-established and presents vast techno-economic data for any LCA study. Finally, a large scale photocatalytic treatment process with high efficacy, solar-driven and low site area requirements can be realized in the short future with rapid evaluation of different possible pilot plant configurations.

Acknowledgement

This work was supported by the Australian Research Council Linkage Grant (LP0562153) and Australian Water Quality Centre, SA Water Corporation through the Water Environmental Biotechnology Laboratory (WEBL) at the University of Adelaide.

References

Abdullah, M., Low, G.K.C., Matthews, R.W., 1990. Effects of common inorganic anions on rates of photocatalytic oxidation of organic carbon over illuminated titanium dioxide. J. Phys. Chem. 94, 6820-6825.

Albu, S.P., Ghicov, A., Macak, J.M., Hahn, R., Schmuki, P., 2007. Self-organized, free-standing TiO_2 nanotube membrane for flow through photocatalytic applications. Nano Lett. 7, 1286-1289.

Andreozzi, R., Caprio, V., Insola, A., Marotta, R., 1999. Advanced oxidation processes (AOP) for water purification and recovery. Catal. Today 53, 51–59.

Angelidis, T.N., Koutlemani, M., Poulios, I., 1998. Kinetic study of the photocatalytic recovery of Pt from aqueous solution by TiO_2, in a closed-loop reactor. Appl. Catal. B: Environ. 16, 347-357.

Anotai, J., 1996. Effect of calcium ion and chemistry and disinfection efficiency of free chlorine at pH 10. Ph.D dissertation, Drexel University, Philadelphia.

Artale, M.A., Augugliaro, V., Drioli, E., Golemme, G., Grande, C., Loddo, V., Molinari, R., Palmisano, L., Schiavello, M., 2001. Preparation and characterisation of membranes with entrapped TiO_2 and preliminary photocatalytic tests. Ann. Chim. 91, 127–136.

Asahi, R., Morikawa, T., Ohwaki, T., Aoki, K., Taga, Y., 2001. Visible-light photocatalysis in nitrogen-doped titanium dioxides. Science 293, 269-271.

Augugliaro, V., García-López, E., Loddo, V., Malato-Rodríguez, S., Maldonado, I., Marcí, G., Molinari, R., Palmisano, L., 2005. Degradation of linomycin in aqueous medium: Coupling of solar photocatalysis and membrane separation. Sol. Energy 79, 402-408.

Augugliaro, V., Litter, M., Palmisano, L., Soria, J., 2006. The combination of heterogeneous photocatalysis with chemical and physical operations: A tool for improving the photoprocess performance. J. Photochem. Photobiol. C: Photochem. Rev. 7, 127-144.

Azapagic, A., Clift, R., 1999. Life cycle assessment and multiobjective optimisation. J. Cleaner Production 7, 135–143.

Azrague, K., Aimar, P., Benoit-Marquié, F., Maurette, M.T., 2006. A new combination of a membrane and photocatalytic reactor for the depollution of turbid water. Appl. Catal. B: Environ. 72, 197-205.

Bacardit, J., St□tzner, J., Chamarro, E., 2007. Effect of salinity on the photo-Fenton process. Ind. Eng. Chem. Res. 46, 7615-7619.

Bae, T.H., Tak, T.M., 2005. Effect of TiO_2 nanoparticles on fouling mitigation of ultrafiltration membranes for activated sludge filtration. J. Membr, Sci. 249, 1-8.

Bahnemann, D., 2004. Photocatalytic water treatment: Solar energy applications. Sol. Energy 77, 445-459.

Bamba, D., Atheba, P., Robert, D., Trokourey, A., Dongui, B., 2008. Photocatalytic degradation of the diuron pesticide. Environ. Chem. Lett. 6, 163-167.

Bellobono, I.R., Morazzoni, F., Bianchi, R., Mangone, E.S., Stanescu, R., Costache, C., Tozzi, P.M., 2005a. Solar energy driven photocatalytic membrane modules for water reuse in agricultural and food industries. Pre-industrial experience using s-triazines as model molecules. Int. J. Photoenergy 7, 87–94.

Bellobono, I.R., Morazzoni, F., Tozzi, P.M., 2005b. Photocatalytic membrane modules for drinking water purification in domestic and community appliances, Int. J. Photoenergy 7, 109–113.

Beltran-Heredia, J., Torregrosa, J., Dominguez, J.R., Peres, J.A., 2001. Comparison of the degradation of *p*-hydroxybenzoic acid in aqueous solution by several oxidation processes. Chemosphere 42, 351-359.

Benabbou, A.K., Derriche, Z., Felix, C., Lejeune, P., Guillard, C., 2007. Photocatalytic inactivation of Escherischia coli: Effect of concentration of TiO_2 and microorganism, nature, and intensity of UV irradiation. Appl. Catal. B: Environ. 76, 257-263.

Benotti, M.J., Stanford, B.D., Wert, E.C., Snyder, S.A., 2009. Evaluation of a photocatalytic reactor membrane pilot system of pharmaceuticals and endocrine disrupting compounds from water. Wat. Res. 43, 1513-1522.

Berney, M., Weilenmann, H.U., Siminetti, A., Egli, T., 2006. Efficacy of solar disinfection of Escherichia coli, Shigella flexneri, Salmonella Typhimurium and Vibrio cholera. J. Appl. Microbiol. 101, 828-836.

Bhatkhnade, D.S., Kamble, S.P., Sawant, S.B., Pangarkar, V.G., 2004. Photocatalytic and photochemical degradation of nitrobenzene using artificial ultraviolet light. Chem. Eng. J. 102, 283-290.

Blanco, J., Malato, S., de las Nieves, J., Fernández, P., 2001. Method of sedimentation of colloidal semiconductor particles, European patent application EP-1-101-737-A1, European Patent Office Bulletin 21.

Bosc, F., Ayral, A., Guizard, C., 2005. Mesoporous anatase coatings for coupling membrane separation and photocatalyzed reactions. J. Membr. Sci. 265, 13–19.

Bouguecha, S., Hamrouni, B., Dhahbi, M., 2005. Small scale desalination pilots powered by renewable energy sources: Case studies. Desalination 183, 151-165.

Bradley, B.R., Daigger, G.T., Rubin, R., Tchobanoglous, G., 2002. Evaluation of onsite wastewater treatment technologies using sustainable development criteria. Clean Technol. Environ. Policy 4, 87-99.

Burns, R., Crittenden, J.C., Hand, D.W., Sutter, L.L., Salman, S.R., 1999. Effect of inorganic ions in heterogeneous photocatalysis. J. Environ. Eng. 125, 77-85.

Byrne, J.A., Eggins, B.R., 1998a. Photoelectrochemistry of oxalate on particulate TiO_2 electrodes. J. Electroanal. Chem. 457, 61-72.

Byrne, J.A., Eggins, B.R., Brown, N.M.D., McKinley, B., Rouse, M., 1998b. Immobilisation of TiO_2 powder for the treatment of polluted water. Appl. Catal. B: Environ. 17, 25-36.

Camera-Roda, G., Santarelli, F., 2007. Intensification of water detoxification by integrating photocatalysis and pervaporation. J. Sol. Energy Eng. 129, 68-73.

Calza, P., Sakkas, V.A., Medana, C., Baiocchi, C., Dimou, A., Pelizetti, E., Albanis, T., 2006. Photocatalytic degradation study of diclofenac over aqueous TiO_2 suspensions. Appl. Catal. B: Environ. 67, 197-205.

Cassano, A.E., Alfano, O.M., 2000. Reaction engineering of suspended solid heterogeneous photocatalytic reactors. Catal. Today 58, 167-197.

Chan, A.H.C., Chan, C.K., Barford, J.P., Porter, J.F., 2003. Solar photocatalytic thin film cascade reactor for treatment of benzoic acid containing wastewater. Wat. Res. 37, 1125-1135.

Chen, H.Y., Zahraa, O., Bouchy, M., 1997. Inhibition of the adsorption and photocatalytic degradation of an organic contaminant in an aqueous suspension of TiO_2 by inorganic ions. J. Photochem. Photobiol. A: Chem. 108, 37-44.

Chen, D., Ray, A.K., 1998. Photodegradation kinetics of 4-nitrophenol in TiO_2 suspension. Wat. Res. 32, 3223-3234.

Chen, C.C., Lu, C.S., Chung, Y.C., Jan, J.L., 2007. UV light induced photodegradation of malachite green on TiO_2 nanoparticles. J. Hazard. Mater. 141, 520-528.

Chin, M.L., Mohamed, A.R., Bhatia, S., 2004. Performance of photocatalytic reactors using immobilized TiO_2 film for the degradation of phenol and methylene blue dye present in water stream. Chemosphere 57, 547-554.

Chin S.S., Chiang, K., Fane, A.G., 2006. The stability of polymeric membranes in TiO_2 photocatalysis process. J. Membr. Sci. 275, 202-211.

Chin S.S., Lim, T.M., Chiang, K., Fane, A.G., 2007. Hybrid low-pressure submerged membrane photoreactor for the removal of bisphenol A. Desalination 2002, 253-261.

Cho, M., Chung, H., Yoon, J., 2003. Disinfection of water containing natural organic matter by using ozone-initiated radical reactions. Appl. Environ. Microbiol. 69, 2284-2291.

Cho, M., Chung, H, Choi, W., Yoon, J., 2004. Linear correlation between inactivation of E. coli and OH radical concentration in TiO_2 photocatalytic disinfection. Wat. Res. 38, 1069-1077.

Cho, I.H., Zoh, K.D., 2007. Photocatalytic degradation of azo dye (*Reactive Red 120*) in TiO_2/UV system: Optimization and modelling using a response surface methodology (RSM) based on the central composite design. Dyes. Pigments. 75, 533-543.

Cho, M., Yoon, J., 2008. Measurement of OH radical CT for inactivating Cryptosporidium parvum using photo/ferrioxalate and photo/TiO_2 systems. J. Appl. Microbiol. 104, 759-766.

Choi, W., Termin, A., Hoffman, M.R., 1994. The role of metal ion dopants in quantum-sized TiO_2: Correlation between photoreactivity and charge carrier recombination dynamics. J. Phys. Chem. 98, 13669-13679.

Choi, H., Stathatos, E., Dionysiou, D.D., 2005. Sol–gel preparation of mesoporous photocatalytic TiO_2 films and TiO_2/Al_2O_3 composite membranes for environmental applications. Appl. Catal. B: Environ. 63, 60–67.

Choi, H., Stathatos, E., Dionysiou, D.D., 2007. Photocatalytic TiO_2 films and membranes for the development of efficient wastewater treatment and reuse systems. Desalination 202, 199–206.

Chong, M.N., Vimonses, V., Lei, S., Jin, B., Chow, C., Saint, C., 2009a. Synthesis and characterisation of novel titania impregnated kaolinite nano-photocatalyst. Micro. Meso. Mater. 117, 233-242.

Chong, M.N., Lei, S., Jin, B., Saint, C., Chow, C.W.K., 2009b. Optimisation of an annular photoreactor process for degradation of Congo red using a newly synthesized titania impregnated kaolinite nano-photocatalyst. Sep. Purif. Technol. 67, 355-363.

Chong, M.N., Jin, B., Zhu, H.Y., Chow, C.W.K., Saint, C., 2009c. Application of H-titanate nanofibers for degradation of Congo red in an annular slurry photoreactor. Chem. Eng. J. 150, 49-54.

Chong, M.N., Jin, B., Chow, C.W.K., Saint, C.P., 2009d. A new approach to optimise an annular slurry photoreactor system for the degradation of Congo red: Statistical analysis and modelling. Chem. Eng. J. 152, 158-166.

Coleman, H.M., Marquis, C.P., Scott, J.A., Chin, S.S., Amal, R., 2005. Bactericidal effects of titanium dioxide-based photocatalysts. Chem. Eng. J. 113, 55-63.

Consoli, F., Allen, D., Boustead, I., de Oude, N., Fava, J., Franklin, W., Quay, B., Parrish, R., Perriman, R., Postlethwaite, D., Seguin, J., Vigon, B., 1993. Guidelines for Life-Cycle Assessment: A Code of Practice. Society of Environmental Toxicology and Chemistry, Brussels, Belgium.

Crittenden, J.C., Zhang, Y., Hand, D.W., Perram, D.L., Marchand, E.G., 1996. Solar detoxification of fuel-contaminated groundwater using fixed-bed photocatalysts. Wat. Environ. Res. 68, 270-278.

Cunningham, J., Sedlak, P., 1996. Kinetic studies of depollution process in TiO_2 slurries: Interdependences of adsorption and UV-intensity. Catal. Today 29, 209-315.

Curcó, D., Giménez, J., Addarak, A., Cervera-March, S., Esplugas, S., 2002. Effects of radiation absorption and catalyst concentration on the photocatalytic degradation of pollutants. Catal. Today 76, 177-188.

De Laat, J., Le, G.T., Legube, B., 2004. A comparative study of the effects of chloride, sulphate and nitrate ions on the rates of decomposition of H_2O_2 and organic compounds by Fe(II)/H_2O_2 and Fe(III)/H_2O_2. Chemosphere 55, 715-723.

Doll, T.E., Frimmel, F.H., 2005. Cross-flow microfiltration with periodical back-washing for photocatalytic degradation of pharmaceutical and diagnostic residues-evaluation of the long-term stability of the photocatalytic activity of TiO_2. Wat. Res. 39, 847-854.

Domínguez, C., García, J., Pedraz, M.A., Torres, A., Galán, M.A., 1998. Photocatalytic oxidation of organic pollutants in water. Catal. Today 40, 85-101.

Diebold, U., 2003. The surface science of titanium dioxide. Surf. Sci. Reports 48, 53-229.

Esplugas, S., Giménez, J., Conteras, S., Pascual, E., Rodríguez, M., 2002. Comparison of different advanced oxidation processes for phenol degradation. Wat. Res. 36, 1034-1042.

Evgenidou, E., Fytianos, K., Poulios, I., 2005. Semiconductor-sensitized photodegradation of dichlorvos in water using TiO_2 and ZnO as catalysts. Appl. Catal. B: Environ. 59, 81-89.

Fallmann, H., Krutzler, T., Bauer, R., Malato, S., Blanco, J., 1999. Applicability of the photo-Fenton method for treating water containing pesticides. Catal. Today 54, 309-319.

Fernández-Ibáñez, P., Blanco, J., Malato, S., de las Nieves, F.J., 2003. Application of the colloidal stability of TiO_2 particles for recovery and reuse in solar photocatalysis. Wat. Res. 37, 3180-3188.

Fernándezs-Ibáñez, P., Sichel, C., Polo-López, M.I., de Cara-García, M., Tello, J.C., 2009. Photocatalytic disinfection of natural well water contaminated by Fusarium solani using TiO_2 slurry in solar CPC photo-reactors. Catal. Today 144, 62-68.

Finch, G.R., Black, E.K., Labatiuk, C.W., Gyürék, L., Belosevic, M., 1993. Comparison of Giardia lamblia and Giardia muris cyst inactivation by ozone. Appl. Environ. Microbial. 59, 3674-3680.

Fogler, H.S., 1999. Elements of chemical reaction engineering: Chapter 10: Catalysis and catalytic reactors. Prentice-Hall PTR Inc., 581-685.

Fu, X., Clark, L.A., Zeltner, W.A., Anderson, M.A., 1996. Effects of reaction temperature and water vapour content on the heterogeneous photocatalytic oxidation of ethylene. J. Photochem. Photobiol. A: Chem. 97, 181-186.

Fu, J., Ji, M., Wang, Z., Jin, L., An, D., 2006. A new submerged membrane photocatalysis reactor (SMPR) for fulvic acid removal using a nano-structured photocatalyst. J. Hazard. Mater. 131, 238-242.

Fu, J., Zhao, Y., Wu, Q., 2007. Optimising photoelectrocatalytic oxidation of fulvic acid using response surface methodology. J. Hazard. Mater. 144, 499-505.

Fujishima, A., Honda, K., 1972. Electrochemical photolysis of water at a semiconductor electrode. Nature 238, 37-38.

Fujishima, A., Rao, T.N., Tryk, D.A., 2000. Titanium dioxide photocatalysis. J. Photochem. Photobiol. C: Photochem. Rev. 1, 1-21.

Fujishima, A., Zhang, X., Tryk, D.A., 2008. TiO_2 photocatalysis and related surface phenomena. Surf. Sci. Reports 63, 515-582.

Fukahori, S., Ichiura, H., Kitaoka, T., Tanaka, H., 2003. Capturing of bisphenol A photodecomposition intermediates by composite TiO_2–zeolite sheets. Appl. Catal. B: Environ. 46, 453-462.

Furube, A., Asahi, T., Masuhara, H., Yamashita, H., Anpo, M., 2001. Direct observation of a picosecond charge separation process in photoexcited platinum-loaded TiO_2 particlees by femtosecond diffuse reflectance spectroscopy. Chem. Phys. Lett. 336, 424-430.

Gaya, U.I., Abdullah, A.H., 2008. Heterogeneous photocatalytic degradation of organic contaminants over titanium dioxide: A review of fundamentals, progress and problems. J Photochem. Photobiol. C: Photochem. Rev. 9, 1-12.

Gelover, S., Gómez, L.A., Reyes, K., Teresa Leal, M., 2006. A practical demonstration of water disinfection using TiO_2 films and sunlight. Wat. Res. 40, 3274-3280.

Gernjak, W., Maldonado, M.I., Malato, S., Cáceres, J., Krutzler, T., Glaser, A., Bauer, R., 2004. Pilot-plant treatment of olive mill wastewater (OMW) by solar TiO_2 photocatalysis and solar photo-Fenton. Solar Energy 77, 567-572.

Gernjak, W., Fuerhacker, M., Fernández-Ibáñez, P., Blanco, J., Malato, S., 2006. Solar photo-Fenton treatment—process parameters and process control. Appl. Catal. B: Environ. 64, 121–130.

Gernjak, W., Krutzler, T., Malato, S., 2007. Photo-Fenton treatment of olive mill wastewater applying a combined Fenton/flocculation pretreatment. J. Solar Energy Eng. 129, 53-59.

Glatzmaier, G.C., Nix, R.G., Mehos, M.S., 1990. Solar destruction of hazardous chemicals. J. Environ. Sci. Health A 25, 571-581.

Glatzmaier, G.C., 1991. Innovative solar technologies for treatment of concentrated organic wastes. Sol. Energy Mater. 24, 672.

Gogate, P.R., Pandit, A.B., 2004. A review of imperative technologies for wastewater treatment II: Hybrid methods. Adv. Environ. Res. 8, 553-597.

Gogniat, G., Thyssen, M., Denis, M., Pulgarin, C., Dukan, S., 2006. The bactericidal effect of TiO_2 photocatalysis involves adsorption onto catalyst and the loss of membrane integrity. FEMS Microbiol. Lett. 258, 18-24.

Gryta, M., Tomaszewska, M., Grzechulska, J., Morawski, A.W., 2001. Membrane distillation of NaCl solution containing natural organic matter. J. Membr. Sci. 181, 279-287.

Guillard, C., Lachheb, H., Houas, A., Ksibi, M., Elaloui, E., Hermann, J.M., 2003. Influence of chemical structure of dyes, of pH and of inorganic salts on their photocatalytic degradation by TiO_2 comparison of the efficiency of powder and supported TiO_2. J. Photochem. Photobiol. A: Chem. 158, 27-36.

Gyürék, L.L., Finch, G.R., 1998. Modelling water treatment chemical disinfection kinetics. J. Environ. Eng. 124, 783–792.

Habibi, M.H., Hassanzadeh, A., Mahdavi, S., 2005. The effect of operational parameters on the photocatalytic degradation of three textile azo dyes in aqueous TiO_2 suspensions. J. Photochem. Photobiol. A: Chem. 172, 89-96.

Herrera Melián, J.A., Doña Rodríguez, J.M., Viera Suárez, A., Valdés do Campo, C., Arana, J., Pérez Peña, J., 2000. The photocatalytic disinfection of urban waste waters. Chemosphere 41, 323-327.

Herrmann, J.M., Disdier, J., Pichat, P., 1988. Photocatalytic deposition of silver on powder titania: Consequences for the recovery of silver. J. Catal. 113, 72-81.

Herrmann, J.M., 1999. Heterogeneous photocatalysis: fundamentals and applications to the removal of various types of aqueous pollutants. Catal. Today. 53, 115-129.

Herrmann, J.G., 2005. Research to protect water infrastructure: EPA's water security research program. Proc. SPIE 5781, 48.

Heyde, M., Portalier, R., 1990. Acid shock proteins of Escherichia coli. FEMS Microbiol. Lett. 69, 19-26.

Hom, L.W., 1972. Kinetics of chlorine disinfection in an ecosystem. J. Sanitary Eng. Div. 98, 183-194.

Hosono, E., Fujihara, S., Kakiuchi, K., Imai, H., 2004. Growth of submicrometer-scale reactangular parallelepiped rutile TiO_2 films in aqueous $TiCl_3$ solutions under hydrothermal conditions. J. Am. Chem. Soc. 126, 7790-7791.

Huang, M., Tso, E., Datye, A.K., 1996. Removal of silver in photographic processing waste by TiO_2-based photocatalysis. Environ. Sci. tech. 30, 3084-3088.

Huang, X., Meng, Y., Liang, P., Qian, Y., 2007. Operational conditions of a membrane filtration reactor coupled with photocatalytic oxidation. Sep. Purif. Technol. 55, 165-172.

Huston, P.L., Pignatello, J.J., 1999. Degradation of selected pesticide active ingredients and commercial formulations in water by the photo-assisted Fenton reaction. Wat. Res. 33, 1238-1246.

Ibáñez, J.A., Litter, M.I, Pizarro, R.A., 2003. Photocatalytic bactericidal effect of TiO_2 on Enterobacter cloacae: Comparative study with other Gram (-) bacteria. J. Photochem. Photobiol. A: Chem. 157, 81-85.

Ihara, T., Miyoshi, M., Iriyama, Y., Matsumoto, O., Sugihara, S., 2003. Visible-light-active titanium dioxide photocatalyst realized by an oxygen-deficient structure and by nitrogen doping. Appl. Catal. B: Environ. 42, 403-409.

Irie, H., Watanabe, Y., Hashimoto, K., 2003. Nitrogen-concentration dependence on photocatalytic activity of $TiO_{2-x}N_x$ powders. J. Phys. Chem. B 107, 5483-5486.

Ishibai, Y., Sato, J., Nishikawa, T., Miyagishi, S., 2008. Synthesis of visible-light active TiO_2 photocatalyst with Pt-modification: Role of TiO_2 substrate for high photocatalytic activity. Appl. Catal. B: Environ. 79, 117-121.

Jaworski, R., Pawlowski, L., Roudet, F., Kozerski, S., Petit, F., 2008. Characterization of mechanical properties of suspension plasma sprayed TiO_2 coatings using scratch test. Surf. Coatings. Technol. 202, 2644-2653.

Johnston, M.D., Simons, E.A., Lambert, R.J.W., 2000. One explanation for the variability of the bacterial suspension test. J. Appl. Microbiol. 88, 237-242.

Joo, J., Kwon, S.G., Yu, T., Cho, M., Lee, J., Yoon, J., Hyeon, T., 2005. Large-scale synthesis of TiO_2 nanorods via nonhydrolytic sol-gel ester elimination reaction and their

application to photocatalytic inactivation of E.coli. J. Phys. Chem. B. 109, 15297-15302.

Jung, J.T., Kim, J.O., Choi, W.Y., 2007. Performance of photocatalytic microfiltration with hollow fiber membrane. Mater. Sci. Forum 544, 95-98.

Kabra, K., Chaudhary, R., Sawhney, R.L., 2004. Treatment of hazardous organic and inorganic compounds through aqueous-phase photocatalysis: A review. Ind. Eng. Chem. Res. 43, 7683-7696.

Karunakaran, C., Senthilvelan, S., 2005. Photooxidation of aniline on alumina with sunlight and artificial UV light. Catal. Comm. 6, 159-165.

Kehoe, S.C., Barer, M.R., Devlin, L.O., McGuigan, K.G., 2004. Batch process solar disinfection is an efficient means of disinfecting drinking water contaminated with Shigella dysenteriae type I. Lett. Appl. Microbiol. 38, 410-414.

Kerzhentsev, M., Guillard, C., Herrmann, J.M., Pichat, P., 1996. Photocatalytic pollutant removal in water at room temperature: case study of the total degradation of the insecticide fenitrothion (phosphorothioic acid O,O-dimethyl-O-(3-methyl-4-nitro-phenyl) ester). Catal Today 27, 215-220.

Kim, S.H., Kwak, S.Y., Sohn, B.H., Park, T.H., 2003. Design of TiO_2 nanoparticle self-assembled aromatic polyamide thin-film-composite (TFC) membrane as an approach to solve biofouling problem. J. Membr. Sci. 211, 157–165.

Kleine, J., Peinemann, K.V., Schuster, C., Warnecke, H.J., 2002. Multifunctional system for treatment of wastewaters from adhesive-producing industries: Separation of solids and oxidation of dissolved pollutants using doted microfiltration membranes. Chem. Eng. Sci. 57, 1661–1664.

Kondo, Y., Yoshikawa, H., Awaga, K., Murayama, M., Mori, T., Sunada, K., Bandow, S., Iijima, S., 2008. Preparation, photocatalytic activities, and dye-sensitized solar-cell performance of submicron-scale TiO_2 hollow spheres. Langmuir 24, 547-550.

K□rbahti, B.K., Rauf, M.A., 2008. Application of response surface analysis to the photolytic degradation of Basic Red 2 dye. Chem. Eng. J. 138, 166-171.

Kormann, C., Bahnemann, D.W., Hoffman, M.R., 1991. Photolysis of chloroform and other organic molecules in aqueous titanium dioxide suspensions. Environ. Sci. Technol. 25, 494-500.

Kun, R., Mogyorósi, K., Dékány, I., 2006. Synthesis and structural and photocatalytic properties of TiO_2/montmorillonite nanocomposites. Appl. Clay Sci. 32, 99-110.

Kwak, S.Y., Kim, S.H., 2001. Hybrid organic/inorganic reverse osmosis (RO) membrane for bactericidal anti-fouling. 1. Preparation and characterization of TiO_2 nanoparticle self-assembled aromatic polyamide thin-film-composite (TFC) membrane. Environ. Sci. Tech. 35, 2388-2394.

Lambert, R.J.W., Johnston, M.D., 2000. The effect of interfering substances on the disinfection process: A mathematical model. J. Appl. Microbiol. 91, 548-555.

Lapeña, L., Cerezo, M., García-Augustin, P., 1995. Possible reuse of treated municipal wastewater for Citrus spp. plant irrigation. Bulletin Environ. Contamination Toxicol. 55, 697-703.

Lapertot, M., Pulgarín, C., Fernández-Ibáñez, P., Maldonado, M.I., Pérez-Estrada, L., Oller, I., Gernjak, W., Malato, S., 2006. Enhancing biodegradability of priority substances (pesticides) by solar photo-Fenton. Wat. Res. 40, 1086–1094.

Lawson, K.W., Lloyd, D.R., 1997. Membrane distillation. J. Membr. Sci. 124, 1-25.

Lee, S.A., Choo, K.H., Lee, C.H., Lee, H.I., Hyeon, T., Choi, W., Kwon, H.H., 2001. Use of ultrafiltration membranes for the separation of TiO_2 photocatalysts in drinking water treatment. Ind. Eng. Chem. Res. 40, 1712-1719.

Lee, D.K., Kim, S.C., Cho, I.C., Kim, S.J., Kim, S.W., 2004. Photocatalytic oxidation of microcystin-LR in a fluidized bed reactor having TiO_2-coated activated carbon. Sep. Purif. Technol. 34, 59-66.

Lee, H.S., Im, S.J., Kim, J.H., Kim, H.J., Kim, J.P., Min, B.R., 2008. Polyamide thin-film nanofiltration membranes containing TiO_2 nanoparticles. Desalination 219, 48-56.

Leng, W., Liu, H., Cheng, S., Zhang, J., Cao, C., 2000. Kinetics of photocatalytic degradation of aniline in water over TiO_2 supported on porous nickel. J. Photochem. Photobiol. A: Chem. 131, 125-132.

Li, H., Li, J., Huo, Y., 2006. Highly active TiO_2N photocatalysts prepared by treating TiO_2 precursors in NH_3/ethanol fluid under supercritical conditions. J. Phys. Chem. B 110, 1559-1565.

Lindner, M., Bahnemann, D.W., Hirthe, B., Griebler, W.D., 1995. Novel TiO_2 powders as highly active photocatalysts. In: Stine, W.R, Tanaka, T., Claridge, D.E., Editors, Solar water detoxification; Solar Eng., ASME, New York, 339.

Litter, M.I., 1999. Heterogeneous photocatalysis: Transition metal ions in photocatalytic systems. Appl. Catal. B: Environ. 23, 89-114.

Liu, H.L., Chiou, Y.R., 2005. Optimal decolorization efficiency of Reactive Red 239 by UV/TiO_2 photocatalytic process coupled with response surface methodology. Chem. Eng. J. 112, 173-179.

Lizama, C., Freer, J., Baeza, J., Mansilla, H.D., 2002. Optimized photodegradation of Reactive Blue 19 on TiO_2 and ZnO suspensions. Catal. Today 76, 235-246.

Lonnen, J., Kilvington, S., Kehoe, S.C., Al-Touati, F., McGuigan, K.G., 2005. Solar and photocatalytic disinfection of protozoan, fungal and bacterial microbes in drinking water. Wat. Res. 39, 877-883.

Lu, J., Zhang, T., Ma, J., Chen, Z., 2009. Evaluation of disinfection by-products formation during chlorination and chloramination of dissolved natural organic matter fractions isolated from a filtered river water. J. Hazar. Mater. 162 (2009) 140-145.

Machulek Jr., A., Moraes, J.E.F., Vautier-Giongo, C., Silverio, C.A., Friedrich, L.C., Nascimento, C.A.O., Gonzalez, M.C., Quina, F.H., 2007. Abatement of the inhibitory effect of chloride anions on the photo-Fenton process. Environ. Sci. Technol. 41, 8549-8463.

Maness, P.C., Smolinski, S., Blake, D.M., Huang, Z., Wolfrum, E.J., Jacoby, W.A., 1999. Bactericidal activity of photocatalytic TiO_2 reaction: Toward an understanding of its killing mechanism. Appl. Environ. Microbiol. 65, 4094-4098.

Magrini, K.A., Webb, J.D., 1990. Decomposition of aqueous organic compounds as a function of solar irradiation intensity. 12th ASME Int. Sol. Energy Conference, in Beard, M.A., Ebadian, Eds.; ASME: New York; 159-162.

Malato-Rodríguez, S., Richter, C., Gálvez, J.B., Vincent, M., 1996. Photocatalytic degradation of industrial residual waters. Sol. Energy 56, 401-410.

Malato, S., Blanco, J., Campos, A., Cáceres, J., Guillard, C., Herrmann, J.M., Fernández-Alba, A.R., 2003. Effect of operating parameters on the testing of new industrial titania catalysts at solar pilot plant scale. Appl. Catal. B: Environ. 42, 349-357.

Malato, S., Fernández-Ibáñez, P. Maldonado, M.I. Blanco, J., Gernjak, W., 2009. Decontamination and disinfection of water by solar photocatalysis: Recent overview and trends. Catal. Today 147, 1-59.

Martin, S.T., Lee, A.T., Hoffmann, M.R., 1995. Chemical mechanism of inorganic oxidants in the TiO_2/UV process: Increased rates of degradation of chlorinated hydrocarbons. Environ. Sci. Technol. 29, 2567-2573.

Marugán, J., Aguado, J., Gernjak, W., Malato, S., 2007. Solar photocatalytic degradation of dichloroacetic acid with silica-supported titania at pilot-plant scale. Catal. Today 129, 59-68.

Marugán, J., Lopez-Muñoz, M.J., Gernjak, W., Malato, S., 2006. Fe/TiO_2/pH interactions in solar degradation of Imidacloprid with TiO_2/SiO_2 photocatalysts at pilot-plant scale. Ind. Eng. Chem. Res. 45, 8900-8908.

Marugán, J, van Grieken, R., Sordo, C., Cruz, C., 2008. Kinetics of the photocatalytic disinfection of Escherichia coli suspensions. Appl. Catal. B: Environ. 82, 27–36.

Matsunaga, T., Tomoda, R., Nakajima, T., Wake, H., 1985. Photoelectrochemical sterilization of microbial cells by semiconductor powders. FEMS Microbiol. Lett. 29, 211-214.

Matthews, R.W., McEnvoy, S.R., 1992. Photocatalytic degradation of phenol in the presence of near-UV illuminated titanium dioxide. J. Photochem. Photobiol. A: Chem. 64, 231.

McGuigan, K.G., Méndez-Hermida, F., Castro-Hermida, J.A., Ares-Mazás, E., Kehoe, S.C., Boyle, M., Sichel, C., Fernández-Ibáñez, P., Meyer, B.P., Ramalingham, S., Meyer, E.A., 2006. Batch solar disinfection inactivates oocysts of Cryptosporidium parvum and cysts of Giardia muris in drinking water. J. Appl. Microbiol. 101, 453-463.

Meares, P., 1986. Synthetic membranes: Science, engineering and applications, Peidel, Dordrecht Netherlands.

Meng, Y., Huang, X., Yang, Q., Qian, Y., Kubota, N., Fukunaga, S., 2005. Treatment of polluted river water with a photocatalytic slurry reactor using low-pressure mercury lamps coupled with a membrane. Desalination 181, 121-133.

Minero, C., Pelizetti, E., Malato, S., Blanco, J., 1996b. Large solar plant photocatalytic water decontamination: Effect of operational parameters. Sol. Energy 56, 421-428.

Minero, C., 1999. Kinetic analysis of photoinduced reactions at the water semiconductor interface. Catal. Today 54, 205-216.

Molinari, R., Grande, C., Drioli, E., Palmisano, L., Schiavello, M., 2001. Photocatalytic membrane reactors for degradation of organic pollutants in water. Catal. Today 67, 273-279.

Molinari, R., Palmisano, L., Drioli, E., Schiavello, M., 2002. Studies on various reactor configurations for coupling photocatalysis and membrane processes in water purification. J. Membr. Sci. 206, 399-415.

Molinari, R., Pirillo, F., Falco, M., Loddo, V., Palmisano, L., 2004. Photocatalytic degradation of dyes by using a membrane reactor. Chem. Eng. Process. 43, 1103–1114.

Molinari, R., Pirilla, F., Loddo, V., Palmisano, L., 2006. Heterogeneous photocatalytic degradation of pharmaceuticals in water by using polycrystalline TiO_2 and a nanofiltration membrane reactor. Catal. Today 118, 205-213.

Molinari, R., Caruso, A., Argurio, P., Poerio, T., 2008. Degradation of the drugs Gemfibrozil and Tamoxifen in pressurized and de-pressurized membrane photoreactors using suspended polycrystalline TiO_2 as catalyst. J. Membr. Sci. 319, 54-63.

Monllor-Satoca, D., Gómez, R., González-Hidalgo, M., Salvador, P., 2007. The "Direct–Indirect" model: An alternative kinetic approach in heterogeneous photocatalysis based on the degree of interaction of dissolved pollutant species with the semiconductor surface. Catal. Today 129, 247-255.

Mozia, S., Morawski, A.W., Toyoda, M., Tsumura, T., 2009. Effect of process parameters on photodegradation of Acid Yellow 36 in a hybrid photocatalysis-membrane distillation system. Chem. Eng. J. 150, 152-159.

Mu, Y., Yu, H.Q., Zheng, J.C., Zhang, S.J., 2004. TiO_2-mediated photocatalytic degradation of Orange II with the presence of Mn^{2+} in solution. J. Photochem. Photobiol. A: Chem. 163, 311-316.

Muñoz, I., Peral, J., Ayllón, J.A., Malato, S., Passarinho, P., Domènech, X., 2006. Life cycle assessment of a coupled solar photocatalytic–biological process for wastewater treatment. Wat. Res., 40, 3533-3540.

Muradov, N.Z., Raissi, A.T., Muzzey, D., Painter, C.R., Kemme, M.R., 1996. Selective photocatalytic degradation of airborne VOCs. Sol. Energy 56, 445-453.

Najm, I., 2006. An alternative interpretation of disinfection kinetics. J. Am. Wat. Works Assoc. 98, 93-101.

Nagaveni, K., Sivalingam, G., Hegde, M.S., Madras, G., 2004a. Solar photocatalytic degradation of dyes. High activity of combustion synthesized nano TiO_2. Appl. Catal. B: Environ. 48, 83-93.

Nagaveni, K., Sivalingam, G., Hegde, M.S., Madras, G., 2004b. Photocatalytic degradation of organic compounds over combustion synthesized nano-TiO_2. Environ. Sci. Tech. 38, 1600-1604.

Ni, M., Leung, M.K.H., Leung, D.Y.C., Sumathy, K., 2007. A review and recent developments in photocatalytic water-splitting using TiO_2 for hydrogen production. Renew. Sust. Energy Rev. 11, 401-425.

Neyens, E., Baeyens, J., 2003. A review of classic Fenton's peroxidation as an advanced oxidation technique. Wat. Res. 98, 33-50.

Ochuma, I.J., Fishwick, R.P., Wood, J., Winterbottom, J.M., 2007. Optimisation of degradation conditions of 1,8-diazabicyclo[5.4.0]undec-7-ene in water and reaction kinetics analysis using a cocurrent downflow contactor photocatalytic reactor. Appl. Catal. B: Environ. 73, 259-268.

Okonomoto, K., Yamamoto, Y., Tanaka, H., Tanaka, M., Itaya, A., 1985. Heterogeneous photocatalytic decomposition of phenol over TiO_2 powder. Bull. Chem. Soc. Jpn. 58, 2015-2022.

Oliveros, E., Legrini, O., Hohl, M., Müller, T., Braun, A.M., 1997. Industrial wastewater treatment: Large scale development of a light-enhanced Fenton reaction. Chem. Eng. Proc. 36, 397-405.

□zkan, A., □zkan, M.H., Gürkan, R., Akçay, M., S□kmen, M., 2004. Photocatalytic degradation of a textile azo dye, Sirius Gelb GC on TiO_2 or Ag-TiO_2 particles in the absence and presence of UV irradiation: the effects of some inorganic anions on the photocatalysis. J. Photochem. Photobiol. A: Chem. 163, 29-35.

Padmanabhan, P.V.A., Sreekumar, K.P., Thiyagarajan, T.K., Satpute, R.U., Bhanumurthy, K., Sengupta, P., Dey, G.K., Warrier, K.G.K., 2006. Nano-crystalline titanium dioxide formed by reactive plasma synthesis. Vacuum 80, 11-12.

Pareek, V., Chong, S., Tadé, M., Adesina, A.A., 2008. Light intensity distribution in heterogeneous photocatalytic reactors. Asia-Pacific J. Chem. Eng. 3, 171-201.

Parra, S., Malato, S., Pulgarin, C., 2002. New integrated photocatalytic-biological flow system using supported TiO_2 and fixed bacteria for the mineralization of isoproturon. Appl. Catal. B: Environ. 36, 131-144.

Pera-Titus, M., García-Molina, V., Baños, M.A., Giménez, J., Esplugas, S., 2004. Degradation of chlorophenols by means of advanced oxidation processes: a general review. Appl. Catal. B: Environ. 47, 219-256.

Pignatello, J.J., 1992. Dark and photoassisted iron(3+)-catalyzed degradation of chlorophenoxy herbicides by hydrogen peroxide. Environ. Sci. Tech. 26, 944-951.

Pignatello, J.J., Liu, D., Huston, P., 1999. Evidence of an additional oxidant in the photoassisted Fenton reaction. Environ. Sci. Tech. 33, 1832-1839.

Pignatello, J.J., Oliveros, E., MacKay, A., 2006. Advanced oxidation processes for organic contaminant destruction based on the Fenton reaction and related chemistry. Crit. Rev. Environ. Sci. Technol. 36, 1- 84.

Pozzo, R.L., Baltanás, M.A., Cassano, A.E., 1997. Supported titanium dioxide as photocatalyst in water decontamination: State of the art. Catal. Today 39, 219-231.

Pozzo, R.L., Giombi, J.L., Baltanas, M.A., Cassano, A.E., 2000. The performance in a fluidized bed reactor of photocatalysts immobilized onto inert supports. Catal. Today 62, 175-187.

Prairie, M.R., Evans, L.R., Martinez, S.L., 1994. Destruction of organics and removal of heavy metals in water via TiO_2 photocatalysis. In: Eckenfelder, W.W., Roth, J.A., Bowers, A.R., Editors, Chemical oxidation: Technologies for the nineties, Technomic Publishing Company Inc., Pennsylvania US. Vol. 2, 428-441.

Qamar, M., Muneer, M., Bahnemann, D., 2006. Heterogeneous photocatalysed degradation of two selected pesticide derivatives, triclopyr and daminozid in aqueous suspensions of titanium dioxide. J. Environ. Management 80, 99-106.

Radjenovíc, J., Sirtori, C., Petrovíc, M., Barceló, D., Malato, S., 2009. Solar photocatalytic degradation of persistent pharmaceuticals at pilot-scale: Kinetics and characterization of major intermediate products. Appl. Catal. B: Environ. 89, 255-264.

Richardson, S.D., 2008. Environmental mass spectrometry: Emerging contaminants and current issues. Anal. Chem. 80, 4373-4402.

Riga, A., Soutsas, K., Ntampegliotis, K., Karayannis, V., Papapolymerou, G., 2007. Effect of system parameters and of inorganic salts on the decolorization and degradation of

Procion H-exl dyes. Comparison of H_2O_2/UV, Fenton, UV/Fenton, TiO_2/UV and TiO_2/UV/H_2O_2 processes. Desalination 211, 72-86.

Rincón, A.G., Pulgarin, C., 2003. Photocatalytical inactivation of E.coli: Effect of (continuous-intermittent) light intensity and of (suspended-fixed) TiO_2 concentration. Appl. Catal. B: Environ. 44, 263-284.

Rincón, A.G., Pulgarin, C., 2004. Effect of pH, inorganic ions, organic matter and H_2O_2 on E.coli K12 photocatalytic inactivation by TiO_2-Implications in solar water disinfection. Appl. Catal. B: Environ. 51, 283-302.

Rincón, A.G., Pulgarin, C., 2005. Use of coaxial photocatalytic reactor (CAPHORE) in the TiO_2 photo-assisted treatment of mixed E.coli and Bacillus sp. and bacterial community present in wastewater. Catal. Today 101, 331-344.

Rincón, A.G., Pulgarin, C., 2006. Comparative evaluation of Fe^{3+} and TiO_2 photoassisted processes in solar photocatalytic disinfection of water. Appl. Catal. B: Environ. 63, 222-231.

Rivero, M.J., Parsons, S.A., Jeffrey, P., Pidou, M., Jefferson, B., 2006. Membrane chemical reactor (MCR) combining photocatalysis and microfiltration for grey water treatment. Wat. Sci. Technol. 53, 173-180.

Rizzo, L., Koch, J., Belgiorno, V., Anderson, M.A., 2007. Removal of methylene blue in a photocatalytic reactor using polymethylmethacrylate supported TiO_2 nanofilm. Desalination 211, 1-9.

Ryu, J., Choi, W., Choo, K.H., 2005. A pilot-scale photocatalyst-membrane hybrid reactor: Performance and characterization, Wat. Sci. Technol. 51, 491-497.

Saquib, M., Muneer, M., 2003. TiO_2-mediated photocatalytic degradation of a triphenylmethane dye (gentian violet), in aqueous suspensions. Dyes. Pigments 56, 37-49.

Schmelling, D.C., Gray, K.A., Vamat, P.V., 1997. The influence of solution matrix on the photocatalytic degradation of TNT in TiO_2 slurries**.** Wat. Res. 31, 1439-1447.

Seffaj, N., Persin, M., Alami Younssi, S., Albizane, A., Bouhria, M., Loukili, H., Larbot, A., 2005. Removal of salts and dyes by low $ZnAl_2O_4$-TiO_2 ultrafiltration membrane deposited on support made from raw clay. Sep. Purif. Technol. 47, 36-42.

Serpone, N., Sauvé, G., Koch, R., Tahiri, H., Pichat, P., Piccinini, P., Pelizetti, E., Hidaka, H., 1996. Standardization protocol of process efficiencies and activation parameters in

heterogeneous photocatalysis: Relative photonic efficiencies ζ_r. J. Photochem. Photobiol. A: Chem. 94, 191-203.

Seven, O., Dindar, B., Aydenir, S., Metin, D., Ozinel, M.A., Icli, S., 2004. Solar photocatalytic disinfection of a group of bacteria and fungi aqueous suspensions with TiO_2, ZnO and Sahara desert dust. J. Photochem. Photobiol. A: Chem. 165, 103-107.

Severin, B.F., Suidan, M.T., Engelbrecht, R.S., 1984. Series-event kinetic model for chemical disinfection. J. Environ. Eng. ASCE 110, 430-439.

Shaban, Y.A., Khan, S.U.M., 2008. Visible light active carbon modified n-TiO_2 for efficient hydrogen production by photoelectrochemical splitting of water. Int. J. Hydrogen Energy 33, 1118-1126.

Shang, C., Cheung, L.M., Ho, C.M., Zeng, M., 2009. Repression of photoreactivation and dark repair of coliform bacteria by TiO_2-modified UV-C disinfection. Appl. Catal. B: Environ. 89, 536-542.

Shirayama, H., Tohezo, Y., Taguchi, S., 2001. Photodegradation of chlorinated hydrocarbons in the presence and absence of dis-solved oxygen in water. Wat. Res. 35, 1941-1950.

Sichel, C., Tello, J., de Cara, M., Fernández-Ibáñez, P., 2007. Effect of UV solar intensity and dose on the photocatalytic disinfection of bacteria and fungi. Catal. Today 129, 152-160.

Siddiquey, I.A., Furusawa, T., Sato, M., Honda, K., Suzuki, N., 2008. Control of the photocatalytic activity of TiO_2 nanoparticles by silica coating with polydiethoxysiloxane. Dyes. Pigments. 76, 754-759.

Sopajaree, K., Qasim, S.A., Basak, S., Rajeshwar, K., 1999a. An integrated flow reactor-membrane filtration system for heterogeneous photocatalysis. Part I. Experiments and modelling of a batch-recirculated photoreactor. J. Appl. Electrochem. 29, 533-539.

Sopajaree, K., Qasim, S.A., Basak, S., Rajeshwar, K., 1999b. An integrated flow-reactor membrane filtration system for heterogeneous photocatalysis. Part II. Experiments on the ultrafiltration unit and combined operation. J. Appl. Electrochem. 29, 1111-1118.

Stylidi, M., Kondarides, D.I., Verykios, X.E., 2003. Pathways of solar light-induced photocatalytic degradation of azo dyes in aqueous TiO2 suspensions. Appl. Catal. B: Environ. 40, 271-286.

Suárez, S., Carballa, M., Omil, F., Lema, J.M., 2008. How are pharmaceutical and personal care products (PPCPs) removed from urban wastewaters? Rev. Environ. Sci. Biotechnol. 7, 125-138.

Sun, Z., Chen, Y., Ke, Q., Yang, Y., Yuan, J., 2002. Photocatalytic degradation of a cationic azo dye by TiO_2/bentonite nanocomposite. J. Photochem. Photobiol. A: Chemistry 149, 169-174.

Sun, D., Meng, T.T., Loong, T.H., Hwa, T.J., 2004. Removal of natural organic matter from water using a nano-structured photocatalyst coupled with filtration membrane. Wat. Sci. Technol. 49, 103–110.

Tang, C., Chen, V., 2004. The photocatalytic degradation of reactive black 5 using TiO_2/UV in an annular photoreactor. Wat. Res. 38, 2775-2781.

Tomaszewska, M., Gryta, M., Morawski, A.W., 1998. The influence of salt in solution on hydrochloric acid recovery by membrane distillation. Sep. Purif. Technol. 14, 183-188.

Toor, A.P., Verma, A., Jotshi, C.K., Bajpai, P.K., Singh, V., 2006. Photocatalytic degradation of Direct Yellow 12 dye using UV/TiO_2 in a shallow pond slurry reactor. Dyes. Pigments. 68, 53-60.

Torrades, F., Pérez, M., Mansilla, H.D., Peral, J., 2003. Experimental design of Fenton and photo-Fenton reactions for the treatment of cellulose bleaching effluents. Chemosphere 53, 1211-1220.

Torres, R.A., Nieto, J.I., Combet, E., Pétrier, C., Pulgarin, C., 2008. Influence of TiO_2 concentration on the synergistic effect between photocatalysis and high-frequency ultrasound for organic pollutant mineralization in water. Appl. Catal. B: Environ. 80, 168-175.

Tsarenko, S.A., Kochkodan, V.M., Samsoni-Todorov, A.O., Goncharuk, V.V., 2006. Removal of humic substances from aqueous solutions with a photocatalytic membrane reactor. Colloid J. 68, 341-344.

Tyrrell, R.M., Keyse, S.M., 1990. New trends in photobiology the interaction of UVA radiation with cultured cells. J. Photochem. Photobiol. B: Biol. 4, 349-361.

Viessman Jr., W., Hammer, M.J., 1998. Water supply and pollution control. Addison Wesley Longman Inc. 6th Edition, California USA.

Vilar, V.J.P., Maldonado, M.I., Oller, I., Malato, S., Boaventura, R.A.R., 2009. Solar treatment of cork boiling and bleaching wastewaters in a pilot plant. Wat. Res, In Press: doi:10.1016/j.watres.2009.06.019

Vinodgopal, K., Kamat, P.V., 1992. Photochemistry on surfaces: photodegradation of 1, 3-diphenylisobenzofuran over metal oxide particles. J. Phys. Chem. 96, 5053-5059.

Vinodgopal, K., Wynkoop, D.E., Kamat, P.V., 1996. Environmental photochemistry on semiconductor surfaces: Photosensitized degradation of a textile azo dye, Acid Orange 7, on TiO_2 particles using visible light. Environ. Sci. Technol. 30, 1660-1666.

Wang, R., Hashimoto, K., Fujishima, A., Chikuni, M., Kojima, E., Kitamura, A., Shimohigoshi, M., Watanabe, T., 1999. Photogeneration of highly amphiphilic TiO_2 surfaces. Adv. Mater. 10, 135-138.

Wang, Y., Hong, C.S., 2000. TiO_2-mediated photomineralization of 2-chlorobiphenyl: The role of O_2. Wat. Res. 34, 2791-2797.

Wang, K., Zhang, J., Lou, L., Yang, S., Chen, Y., 2004. UV or visible light induced photodegradation of AO7 on TiO_2 particles: the influence of inorganic anions. J. Photochem. Photobiol. A: Chem. 165, 201-207.

WHO, Guidelines for drinking-water quality first addendum to third edition 1 recommendations. WHO Library Cataloguing-in-Publication Data, 2006.

Wintgens, T., Salehi, F., Hochstrat, R., Melin, T., 2008. Emerging contaminants and treatment options in water recycling for indirect potable use. Wat. Sci. Tech. 57, 99-107.

Wong, C.C., Chu, W., 2003. The direct photolysis and photocatalytic degradation of alachlor at different TiO_2 and UV sources. Chemosphere 50, 981-987.

Wu, C.H., Huang, K.S., Chern, J.M., 2006. Decomposition of acid dye by TiO_2 thin films prepared by the sol-gel method. Ind. Eng. Chem. Res. 45, 2040-2045.

Xi, W., Geissen, S., 2001. Separation of titanium dioxide from photocatalytically treated water by cross-flow microfiltration. Wat. Res. 35, 1256-1262.

Xie, Z.M., Chen, Z., Dai, Y.Z., 2009. Preparation of TiO_2/sepiolite photocatalyst and its application to printing and dyeing wastewater treatment. Environ. Sci. Tech. 32, 123-127.

Xu, Y., Langford, C.H., 2000. Variation of Langmuir adsorption constant determined for TiO_2-photocatalyzed degradation if acetophenone under different light intensity. J. Photochem and Photobiol. A: Chem. 133, 67-71.

Yang, Y., Wang, P., 2006. Preparation and characterizations of a new PS/TiO_2 hybrid membrane by sol-gel process. Polymer 47, 2683-2688.

Yang, H., Cheng, H., 2007a. Controlling nitrite level in drinking water by chlorination and chloramination. Sep. Purif. Technol. 56, 392-396.

Yang, G.C.C., Li, C.J., 2007b. Electrofiltration of silica nanoparticle-containing wastewater using tubular ceramic membranes. Sep. Purif. Technol. 58, 159-165.

Yu, J.C., Yu, J., Zhao, J., 2002. Enhanced photocatalytic activity of mesoporous and ordinary TiO_2 thin films by sulphuric acid treatment. Appl. Catal. B: Environ. 36, 31-43.

Yu, Y., Yu, J.C., Yu, J.G., Kwok, Y.C., Che, Y.K., Zhao, J.C., Ding, L., Ge, W.K., Wong, P.K., 2005. Enhancement of photocatalytic activity of mesoporous TiO_2 by using carbon nanotubes. Appl. Catal. A: General 289, 186-196.

Zhang, H., Quan, X., Chen, S., Zhao, H., Zhao, Y., 2006a. Fabrication of photocatalytic membrane and evaluation its efficiency in removal of organic pollutants from water. Sep. Purif. Technol. 50, 147–155.

Zhang, H., Quan, X., Chen, S., Zhao, H., Zhao, Y., 2006b. The removal of sodium dodecylbenzene sulfonate surfactant from water using silica/titania nanorods/nanotubes composite membrane with photocatalytic capability. Appl. Surf. Sci. 252, 8598–8604.

Zhang, X., Du, A.J., Lee, P., Sun, D.D., Leckie, J.O., 2008a. TiO_2 nanowire membrane for concurrent filtration and photocatalytic oxidation of humic acid in water. J. Membr. Sci. 313, 44-51.

Zhang, X., Du, A.J., Lee, P., Sun, D.D., Leckie, J.O., 2008b. Grafted multifunctional titanium dioxide nanotube membrane: Separation and photodegradation of aquatic pollutant. Appl. Catal. B: Environment 84, 262-267.

Zhang, X., Pan, J.H., Du, A.J., Fu, W., Sun, D.D., Leckie, J.O., 2009. Combination of one-dimensional TiO_2 nanowire photocatalytic oxidation with microfiltration for water treatment. Wat. Res. 43, 1179-1186.

Zhao, Y., Zhong, J., Li, H., Xu, N., Shi, J., 2002. Fouling and regeneration of ceramic microfiltration membranes in processing acid wastewater containing fine TiO_2 particles. J. Membr. Sci. 208, 331-341.

Zhu, H., Zhang, M., Xia, Z., Low, G.K.C., 1995. Titanium dioxide mediated photocatalytic degradation of monocrotophos. Wat. Res. 29, 2681-2688.

Zhu, H., Gao, X., Lan, Y., Song, D., Xi, Y., Zhao, J., 2004. Hydrogen titanate nanofibers covered with anatase nanocrystals: A delicate structure achieved by the wet chemistry reaction of the titanate nanofibers. J. Am. Chem. Soc. 126, 8380-8381.

CHAPTER 3

EXPERIMENTAL MATERIALS AND METHODS

1. Synthesis and Characterisation of Photocatalysts

1.1. Titania Impregnated Kaolinite Nano-Photocatalyst

The TiO_2-K catalyst particles were synthesized in accordance to our developed method (Chong et al., 2009). A modified two step sol–gel method was used, where 25 mL titanium precursor was hydrolysed by 30 mL absolute ethanol. The resultant hydrolysed solution was then acid-catalysed under controlled acidic conditions. This was followed by the heterocoagulation of the catalysed product with 10% (w/v) kaolinite suspension at 37^{o}C under constant overhead stirring. The kaolinite clays were pre-treated in a series of alkalization and thermal treatments at 750^{o}C for 1 h prior to use. The kaolinite particles were used as the inert carriers for the deposition of TiO_2 sol, enabling ease of catalyst particles separation after water treatment. The heterocoagulated catalyst products were filtered and washed repeatedly with distilled water (MilliQ water from Barnstead Nanopure Diamond Water ion exchange system with 18.2 M-cm resistivity) up to three times to remove any excess chemical impurities. The filtrate cake was dried in a conventional oven at 65-70^{o}C for 3 h, before being fired at 600^{o}C. The final TiO_2-K catalysts were grinded to an appropriate particle size range prior to use. Further detailed synthesis and characterisation of the TiO_2-K catalyst can be found in Sub-Chapter 4.1. The complete experimental setup for the synthesis process is as shown in Fig. 1. Fig. 2 shows the TiO_2-K catalysts after being calcined in a muffle furnace.

Figure 1: Experimental setup for the synthesis of TiO_2-K catalyst particles.

Figure 2: Final TiO_2-K catalyst particles after calcination process.

1.2. Anatase Titanate Nanofiber Catalyst

The anatase titanate nanofiber catalyst (TNC) was synthesized in accordance to the method developed by Zhu et al. (2004). A hydrothermal reaction between the concentrated NaOH and TiO_2 was used to yield the nanofiber catalyst and followed by a post-synthesis ion exchange with HCl solution to remove the excess sodium ions. Specifically, 3 g of anatase particles (~ 325 meshes from Aldrich) were mixed with 80 mL of 10 M NaOH. The resultant suspension was sonicated for 0.5 h and transferred into a PTFE container for autoclaving. The autoclave was maintained at a hydrothermal temperature of 180 °C for 48 h. The precipitate (sodium titanate nanofibers) was recovered and washed with distilled water to remove excess NaOH. The sodium ions in the titanate nanofibers were exchanged with H^+ ions (using 0.1 M HCl) to produce hydrogen titanate nanofibers. These products were repeatedly washed with distilled water until pH ~7 was reached. The hydrogen titanate product was dried at 80 °C for 12 h and then calcined at 700 °C for 3 h to yield the TNC fibrils.

1.3. Characterisation of Synthesized Photocatalysts

Various microscopic characterisation techniques were used to understand both the physical and chemical properties of the synthesized photocatalysts at their nano-scale dimensions. The

following outlines the different characterisation methods used, together with a short explanation on their operating procedures and conditions.

1.3.1. Differential Thermal Analysis and Thermogravimetric Analysis

Differential thermal analysis was performed using a thermogravimetric analyser (DTA-TG) (TA Instruments) to obtain the weight loss as a function of temperature. During the analysis, the photocatalyst sample was heated from room temperature to 1200˚C at a ramping rate of 10˚C min^{-1} under highly nitrogenised conditions to avoid any possible oxidation.

1.3.2. Static Particle Size Measurement

Particle size of the photocatalysts was measured using a static light scattering laser diffraction particle sizer instrument (Malvern Mastersizer 2000), covering the detection range from 0.02 to 2000 μm. Prior to the measurement, the photocatalyst particles were dispersed in sodium pyrophosphate solution with constant agitation and sonication until a stable dispersion was attained.

1.3.3. Electron Microscopic Measurements

Morphological and surface characteristics of the photocatalysts were analysed using scanning electron microscopy (SEM) (Philips XL30 SEM) at an accelerating voltage of 10 kV. A thin platinum coating was applied to the sample prior to analysis, in order to prevent the accumulation of static electric charge on the surface of the particle.

Transmission electron microscopy (TEM) (Philips CM-100 TEM) was performed at an accelerating voltage of 100 kV. Prior to the analysis, minimal amount of the photocatalysts were suspended in ethanol solution, followed by ultrasonic dispersion and subsequent immobilisation onto the copper measurement grids of 2 mm diameter.

1.3.4. Physical Surface Area and Pore Size Measurements

Brunauer-Emmett-Teller (BET) specific surface area and pore size measurements were performed on the photocatalyst samples using a Micrometrics gas adsorption analyser (Gemini Type 2375) at 77 ± 0.5 K in liquid nitrogen. The sample vessels loaded with ca. 0.5–1.0 g of photocatalysts were vacuum-treated overnight at 105˚C and evacuation pressure of 50 mTorr.

During the analysis, nitrogen adsorption isotherms of the samples were then analysed for the specific surface area using the BET equation.

1.3.5. Powder X-ray Diffractionometric Measurement

X-ray diffraction (XRD) measurements were performed with a Philips PW Diffractometer (Co X-rays λ=1.7902Å) over the range of 5 to 90º 2θ for the solid kaolin powder samples. Samples were spiked with 10 wt% zinc oxide before analysis to facilitate the calculation for the weight percent of the amorphous to crystalline ratio. The basal distances, d_L, were calculated from the Bragg reflections using the automated powder diffraction software. The average crystallite diameters of the particles, D_{hkl}, were obtained by using the Debye-Scherrer equation [$D_{hkl} = k\alpha / \beta \cos\theta$], where β is the line broadening ($\beta = \beta_s - \beta_o$, where β_s and β_o are the half-widths of the XRD peak of the standard), k is related to the crystalline shape and taken to be 0.89 with Warren's correction for instrumental broadening, and α and θ are the radiation wavelength and Bragg angle respectively. A standard for this instrumental measurement based on single crystal anatase TiO_2 was used as a means for calibration.

1.3.6. UV-Vis Diffuse-Reflectance Analysis

Optical absorption characteristic of the photocatalysts was measured using UV–Vis diffuse-reflectance spectroscopy (UVDRS). The UVDRS spectra were measured using a Varian Cary 5000 UV–Vis spectrophotometer and scanned between the wavelengths of 250 to 600 nm.

2. Annular Slurry Photoreactor System

In this study, a self-designed annular slurry photoreactor (ASP) system was set up for the studies on photocatalytic water treatment of organic mineralization and disinfection. The ASP was constructed in the mechanical workshop at the University of South Australia (Mawson Lakes campus). This ASP has a total volume of 4.5 L and a standard working volume of 3.6 L. It was operated as a bubble column reactor, where the TiO_2 photocatalyst was suspended within the annulus zone via compressed air sparging. A 45-microns porous air sparger was fitted to the detached bottom of the ASP to provide homogeneous aeration for catalyst suspension and mixing. The UV light was fitted to the quartz thimble at the central axis of the

ASP to provide a uniform irradiation field for photonic activation of the catalysts during operation. Electronic probes and meters for in-situ data logging of pH, dissolved oxygen and temperature (TPS, Australia) were also connected to the ASP. Fig. 3 shows an image of the ASP used in this study. The following subsections outline the schematic and operation of the ASP via batch or sequential-batch reactor mode.

Figure 3: Image of the self-designed ASP column.

2.1. Batch Operation Mode

The ASP system was operated in a batch photo-reactor process mode, where the catalyst-water suspension was pumped into the ASP after 0.5 h mixing. Depending on the application, low intensity UVC and UVA light of 11W and 8W respectively, was fitted to the ASP for the photonic activation of the catalyst during operation. For the photo-disinfection experiments, a UVA light of 8W (NEC, Holland) was used instead of the UVC light in order to study the photo-inactivation efficiency as mediated by the synthesized photocatalysts.

Once the ASP had been recharged with the suspension mixture, the UV light was turned on. Samples were collected from the four-descended level sampling ports under the designated reaction time to yield the concentration-time profile of the specific surrogate water indicator. The reaction temperature was monitored and controlled using a relay-feedback system, where the pump was activated to recirculate the cooling water through the external jacket. The detailed design of the batch ASP system and setup are shown in Fig. 4.

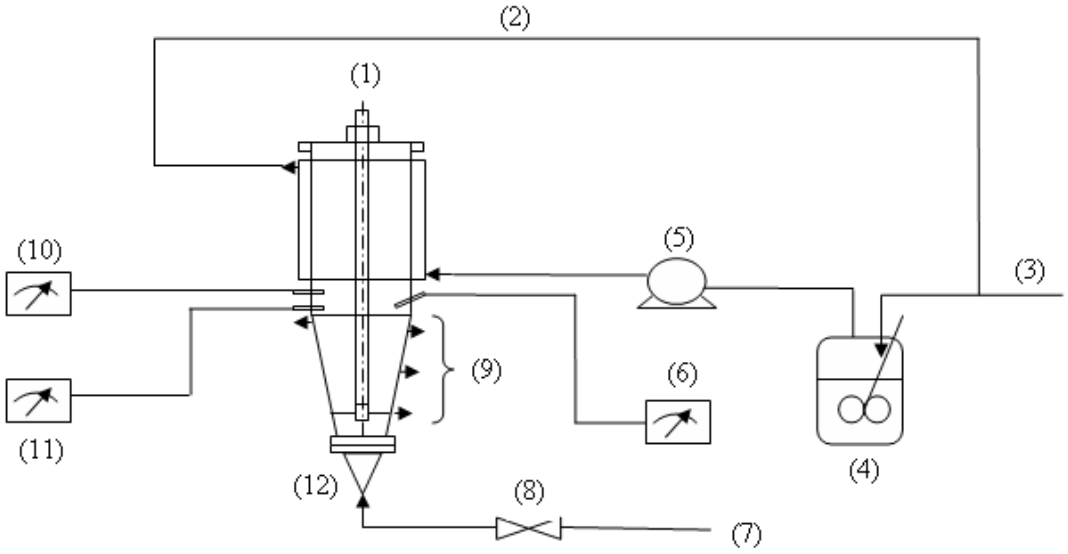

Figure 4: Schematic for the annular batch slurry photoreactor system. (1) UV light, (2) recirculation water line, (3) fresh cool water line, (4) cooling water vessel, (5) cooling water pump, (6) temperature meter, (7) compressed air supply line, (8) compressed air regulation valve, (9) sampling ports, (10) pH meter, (11) dissolved oxygen meter, (12) photoreactor.

2.2. Sequential Batch Reactor Operation Mode

The sequential batch annular slurry photoreactor (SB-ASP) system was operated semi-continuously with the aid of a microfiltration module of 0.2 μm (Varian Inc, Australia) that retains the photocatalyst particles. A low-intensity (11W) UVC lamp (Davis Ultraviolet, Australia) was fitted within the quartz thimble at the central axis of the column, to prevent direct fluid contact between the lamp and reaction water-catalyst suspension. Sampling was done at the mixing tank before pumping into the ASP and in the collecting tank after the reaction. All the fluid connection lines were fitted with appropriate sized Tygon tubes.

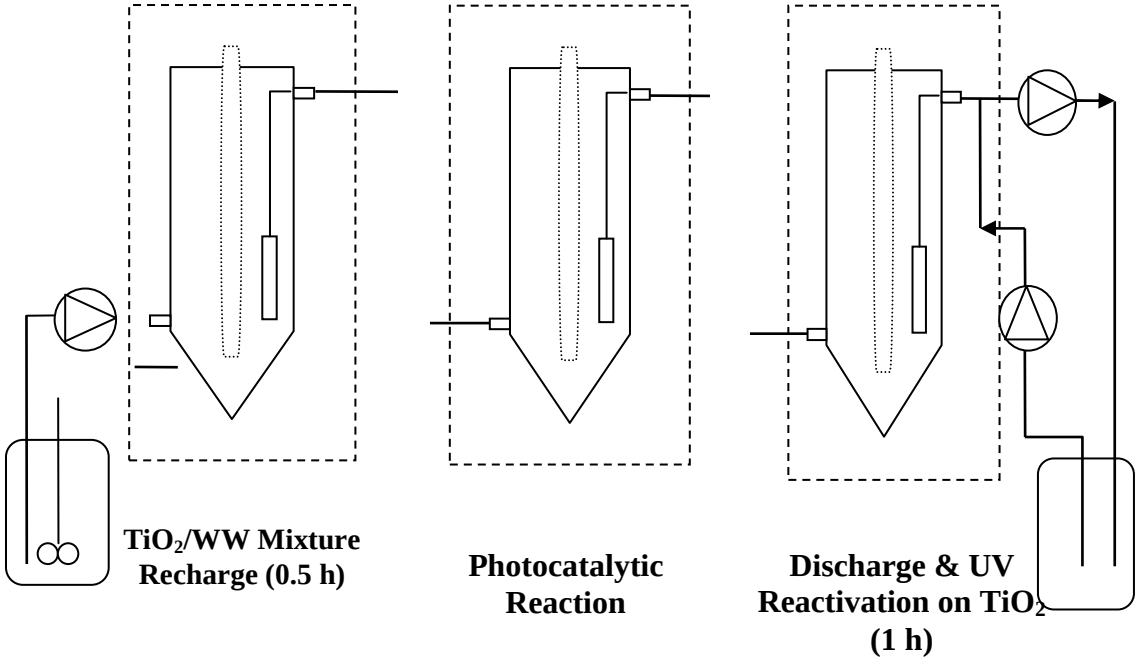

Figure 5: Schematic for the sequential operation mode of the annular slurry photoreactor. Schematic for a sequencing batch reaction cycle with three different phases in a cycle. (1) TiO_2/Wastewater (WW) recharges; (2) Batch photocatalytic reaction and (3) Discharge of 2/3 of original and UV reactivation on catalyst.

To operate the SB-ASP mode, three pumps were connected at the reactor inlet and outlet respectively with the proper electronic timer adjustment. Two pumps were allocated in the reactor outlet to withdraw the reaction water after the reaction and backwash the microfiltration module. During the wastewater discharge, the microfiltration module was back-washed intermittently (10 s every 10 min) to prevent a decline in filtration flux. In the setup of SB-ASP system, three different reaction phases were proposed in one SBR cycle where initially (1) 3L of the catalyst-water mixture was recharged into the ASP in 0.5 h; followed by (2) the UVC photocatalytic reaction and finally (3) the discharge of 2L of the reacted water and co-catalyst reactivated by UVC within the same 1 h duration. With these three phases, a SBR cycle is completed. In the following SBR cycle, 2L of the fresh water-

catalyst suspension was recharged and reacted with the aged suspension, before discharging. The experimental setup of the SB-ASP is shown in Fig. 5.

3. Experimental Procedures

3.1. Photomineralization Experiments

3.1.1. Congo Red

Congo Red (CR) ($C_{32}H_{22}N_6Na_2O_6S_2$, Colour Index 22120, Labchem Ajax Finechem, Australia), a secondary diazo dye was used as a surrogate indicator to simulate industrial wastewater and to evaluate the photoactivity of the photocatalysts used in this study. CR is a recalcitrant secondary diazo dye that is commonly found in industrial wastewater and thus considered suitable as an effectiveness measure, in terms of its chemical structure, molecular weight and diazo bonding. The chemical structure of CR is as shown in Fig. 6.

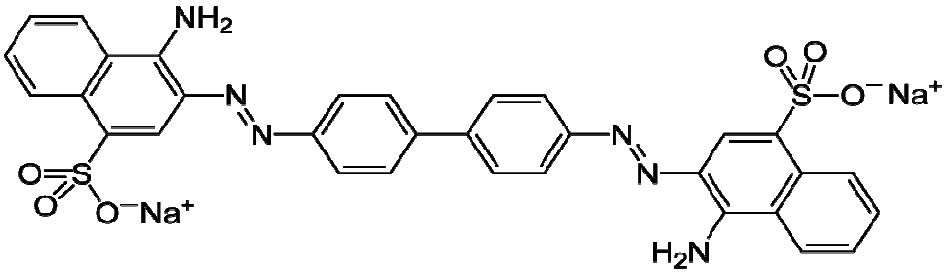

Figure 6: Chemical structure of Congo Red.

The solid CR dye powders are readily dissolved in distilled water. To begin the experiment, a known amount of the dye powder was dissolved in the water to bring the solution up to a required concentration. The pH of the CR solution was measured using a pH meter (TPS, Australia). To alter the pH of the CR solution, hydrochloric acid (HCl) and sodium hydroxide (NaOH) were titrated accordingly (as per experimental requirement) with pH meter verification. Once the appropriate CR solution was made, it was added to the mixing tank for stabilisation with the specific amount of photocatalysts used. Prior to recharging the solution

mixture into the ASP, the compressed air flow was turned on to prevent the deposition of the catalyst on the surface of the bottom air sparger. The catalyst-solution mixture was usually dark-stabilized for 0.5 h before the UV light was turned on. Sampling of the CR concentration was done using the four-descending ports. The collected samples were immediately centrifuged (Eppendorf Centrifuge 5415R, Germany) at 5000 rpm for 10 min. The supernatant was decanted after the centrifugation and subsequently filtered using the Millex VX filter (Millipore 0.45 μm) to ensure complete removal of catalyst particles. The filtered solution was then subjected to spectroscopic concentration measurement for the CR concentration using a UV-Vis spectrophotometer (Helios Gamma, England).

3.1.2. Carbamazepine

Carbamazepine (CBZ) is an antiepileptic drug that is used as sedative. From a toxicological point of view, this drug can produce serious toxic effects on the liver and emopoietic system (Molinari et al., 2006). CBZ was used as a reaction surrogate pharmaceutical indicator to observe the effects of complexity in wastewater effluents on its removal efficiency. The chemical structure of CBZ is given in Fig. 7.

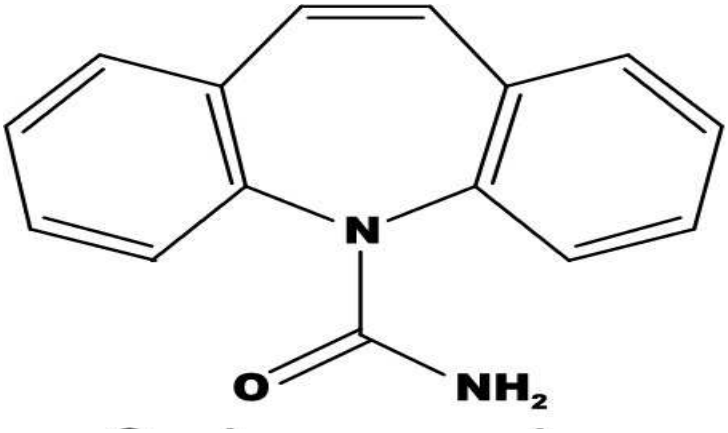

Figure 7: The chemical structure of Carbamazepine (an antiepileptic drug).

CBZ has a low solubility in water as indicated from its octanol-water coefficients. To prepare the CBZ solution in secondary municipal wastewater, a known amount of the CBZ powder (Sigma-Aldrich, Australia) was magnetically stirred for 5 min in the wastewater, followed by a rapid sonication of 5 min. This stirring-sonication procedure was repeated twice to ensure

the complete dissolution of CBZ in the effluent. Similarly, after CBZ-spiked effluent was prepared, a given amount of catalyst was added and mixed in a stirring tank. Prior to recharging the solution mixture into the ASP, the compressed air flow was turned on to prevent the deposition of the catalysts on the surface of the bottom air sparger. Sampling was conducted prior to addition of CBZ and photocatalyst, and during the reaction. The collected samples were filtered using the Millex VX filter (Millipore 0.45 μm) to ensure complete removal of catalyst particles. The concentration of filtered CBZ samples were measured using the HPLC method as outlined in Section 4.4.

3.2 Photo-Disinfection Experiments

A sewage-isolated *E.coli* strain (ATCC 11775) was used as an indicator microorganism for faecal contamination and microbial standard to evaluate the photoactivity of the new photocatalysts used in this study.

To prepare the bacterial suspension for the batch photo-disinfection experiments, a 50 mL fresh liquid culture of tryptone soy broth media (TSB) (Oxoid, England) was inoculated, followed by incubation at 35^{o}C for 19 h in a rotary shaker at 150 rpm. The final bacterial count after 19 h incubation was determined. An aliquot of the final liquid culture was directly inoculated into phosphate buffered saline (PBS) solution, in order to prepare the final bacterial suspensions for each batch experiment. The use of PBS is to prevent sudden osmotic shock to the bacteria, so as to maintain the bacterial numbers for accurate dilution purposes. The bacterial cell density in the prepared bacterial suspension was determined using heterotrophic plate count (HPC) procedures (APHA, 2005).

Once the bacterial suspension of the required density was prepared, a dark homogenization period of 0.5 h with photocatalysts was allowed for enhanced surface interaction. The UVA light was then turned on, and the samples were collected via the descending sampling ports. The reduction in the bacterial density over the irradiation period was then determined using HPC method.

4. Analysis Procedures

4.1 Monochromatic Spectroscopy Measurement of Congo Red Concentration

A monochromatic spectroscopy method to correlate the concentration of the CR at the characteristic peak of 496.5 nm was developed (Vimonses et al., 2009). To establish this absorbance-concentration correlation, a stock solution of the CR was prepared. This stock solution was then diluted in series to obtain different CR concentrations. Subsequently, the absorbance for each of these diluted CR solutions was measured at 496.5 nm with a cell pathlength of 1 cm. A plot of the absorbance against concentration was then obtained. By adding the linear trend line and setting the line through the origin, a calibration factor could then be obtained from the slope. This calibration factor could be used to convert the measured absorbance value for the collected samples at 496.5 nm, to the corresponding CR concentration. It should be noted that the CR will has a shift in characteristic peak when the pH is lower than 3. A calibration factor is then applied to prevent the mis-interpretation of the measured absorbance.

4.2. LC-MS Analysis of the Intermediate Oxidation By-Products

Photooxidation intermediates from the CR degradation were determined using the liquid chromatography/mass spectrometry (LC/MS) method. The LC separation was provided by a Waters liquid chromatograph (Waters, Milford USA), which was equipped with a 2695 Separation Module and 2487 dual wavelength UV detector. The operating conditions were set up as follows: HPLC column (SGE Wakosil 2mm X 150 mm C18); ammonium acetate-acetonitrile mobile eluent phase; flow rate of 0.2 mL/min; injection volume of 20 μL; UV detector at 235 nm and 350 nm. The entire flow from the LC was then directed into a Micromass Quattro micro tandem quadrupole MS (Waters, Manchester UK). Data were acquired using the Masslynx data system for both the MS and UV data. The MS analysis was operated in both positive and negative ion electrospray mass spectrometry (ESI). The operating conditions for one of the negative ion ESI was set up as follows; capillary of 3.5 kV; source temperature of 80^{o}C; desolvation temperature and gas flow of 350^{o}C and 500 L/h respectively; scan duration of 1 s; mass range scanned of 80 – 800; cone of 30-70 V. The

results were then compared to the MS library to determine the intermediate photo-oxidation products that evolve during the irradiation period.

4.3. Chemical Oxygen Demand Measurement

Chemical oxygen demand (COD) was measured to analyse the extent of mineralization during the photocatalytic treatment. COD is a sum measurement of the amount of oxygen (mg) consumed per litre of the sample. To determine the COD, an open reflux method was used where 2 mL of the sample was added into the low range 0-150 mg L^{-1} COD reagent (Hach Lange GmbH, Germany) containing potassium dichromate ($K_2Cr_2O_7$) and subsequently heated for 2 h at 150°C in a digestion reactor DRB 200 (Hach Lange GmbH, Germany) (Ihara et al., 2006). The oxidizable organic compounds present in the solution react with the $K_2Cr_2O_7$, reducing the dichromate ion to green chromic ion. Furthermore the digestion reagent contains silver and mercury ions. Silver is used as a catalyst and mercury is used to complex the chloride interferences. By this method, the total oxidizable organic compounds (COD) was correlated to the spectroscopic measurement (DR4000, Hach Lange GmbH, Germany) of the amount of Cr^{3+} formed at the wavelength of 620 nm.

4.4. HPLC Analysis

4.4.1 Glucose Concentration

The glucose concentration during the study of the residual disinfecting effect of TiO_2 photocatalytic reaction was determined using the HPLC. Specifically, one hundred μL of the sample supernatant were filtered through a 0.22 μm membrane. The HPLC was equipped with a ROA Organic Acid Column (Phenomenex, 300 × 7.8, Varian, CA, USA) and a refractive index detector (Model 350, Varian), as shown in Fig 5. The mobile eluent phase was 4 mM H_2SO_4 at a flow rate of 0.6 mL min^{-1} and the column temperature was 50 °C.

4.4.2. Carbamazepine Concentration

The CBZ concentrations were analysed by HPLC [Varian Pro-star, Varian Microsorb-MW 100-5 C18 column (4.6 x 150 mm, 5 μm)] at a flowrate of 1.0 mL min^{-1} and UV absorbance detection at 254 nm. The mobile phase was methanol 60% plus ammonium acetate (10mM)

and acetic acid (5mM). The injection volume was 20 μL. Fig. 8 shows the HPLC system that was used for both the glucose and CBZ analyses.

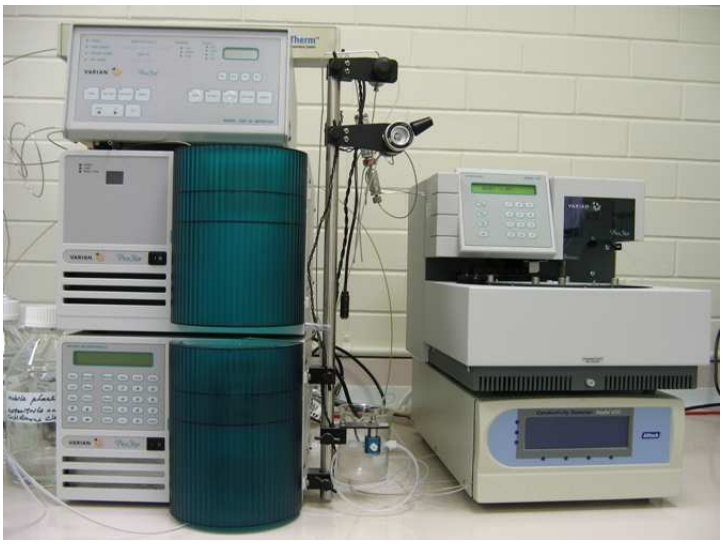

Figure 8: High performance liquid chromatography system.

4.5. High Performance Size Exclusion Chromatography Analysis

To investigate the changes in apparent molecular weight (AMW) profile of the samples during photocatalysis, the samples were analysed using a coupling method of high-performance size exclusion chromatography (HPSEC) and UV detection (Liu et al., 2008). Sample injection and separation were conducted with a Waters 2690 Alliance system with a temperature-controlled oven (30 °C) and a Shodex KW802.5 glycol functionalized silica gel column (Chow et al., 1999). Elution was monitored with a Waters 996 photodiode array detector (260 nm). The samples were filtered through a 0.22 μm membrane filter prior to analysis and 100 μL sample was injected. The mobile phase was 0.02 M phosphate buffer at pH 6.8 adjusted to an ionic strength of 0.1 M with sodium chloride. The system was operated at isocratic conditions with an eluent flow rate of 1.0 mL min^{-1}. Polystyrene sulfonate standards (Polysciences, USA) with MW 4.6, 8, 18, and 35 kDa were used to calibrate the retention time response to AMW.

4.6. Inorganic Ions Measurement

4.6.1. Nitrate

To measure the concentration of the NO_3^- ions, a reagent kit was purchased from Hach Lange GmbH, Germany. In this instance, the NO_3^- concentration was measured using the persulfate

digestion method using the kit, which comprises of 0-25 mg L^{-1} N reagents, spectrophotometer DR4000 and digestion reactor DRB 200 (Kima et al., 2008). All nitrogen atoms that present in the samples are converted into NO_3^- through an alkaline persulfate digestion reagent and further heated at 105°C for 30 min. Sodium metabisulfite is added after the digestion to eliminate the interference of halogen oxide during the measurement. A final yellow complex is formed when the nitrate in the sample has reacted with chromotropic acid under acid conditions. The final NO_3^- measurements were obtained from the absorbance characteristic peak of 410 nm using the DRB 200 spectrophotometer.

4.6.2. Phosphate

A vanadium molybdate spectrometry method was used to determine the PO_4^{3-} concentration in the Hach kit (Hach Lange GmbH, Germany) which comprises spectrophotometer DR4000, reagents and cuvette tubes (total phosphorous, 0-100 mg L^{-1} PO_4^{3-}) (Hosni et al., 2008). Within this method, the orthophosphate in the sample reacts with molybdate in an acid medium to produce a phosphomolybdate complex. When further reacted with vanadium, a yellow vanadomolybdophosphoric acid is formed. The intensity of the yellow color is used to correlate the phosphate concentration in the wastewater sample. To hydrolyze the condensed inorganic forms of phosphorus, the samples were pretreated with acid and heated to 105°C for 30 min in the DRB 200 reactor. The final PO_4^{3-} concentration was determined using the yellow colour correlation that gives the total phosphorus concentration, and subsequent conversion to PO_4^{3-} using their corresponding molecular weights.

4.7. Heterotrophic Plate Count of Bacterial *Escherichia Coli* (ATCC 11775)

To measure the colony forming units (CFU) of the treated sample, the collected samples were added to the prepared plate count agar (PCA) (Merck, Germany). Owing to the variability in the bacterial cell density, a standard serial dilution procedure of the samples using PBS solution was done to find the best dilution factor. The knowledge of this dilution factor is important, in particular to enable the ease of bacterial count using the HPC. Once the dilution factor was known, 100 μL of the samples were analysed in duplicate and the PCA plates were incubated at 35^{o}C for 24 h before final cell counting. The normalised fraction of bacterial survivor against irradiation time curves was plotted to compare the disinfection kinetic profiles under different operating conditions.

5. References

APHA., 2005. Standard methods for the examination of water and wastewater, 21st edition, Joint Publication of the American Public Health Association, the American Water Works Association and the Water Environment Federation.

Chong, M.N., Vimonses, V., Lei, S., Jin, B., Chow, C., Saint, C., 2009a. Synthesis and characterisation of novel titania impregnated kaolinite nano-photocatalyst. Micro. Meso. Mater. 117, 233-242.

Chow, C.W.K., van Leeuwen, J.A., Drikas, M., Fabris, R., Spark, K.M. and Page, D.W., 1999. The Impact of the Character of Natural Organic Matter in Conventional Treatment with Alum**.** Wat. Sci. Tech. 40(9) 97-104.

Hosni, K., Moussa, S.B., Chachi, A., Amor, M.B., 2008. The removal of PO_4^{3-} by calcium hydroxide from synthetic wastewater: optimisation of the operating conditions. Desalination 223, 337-343.

Ihara, I., Umetsu, K., Kanamura, K., Watanabe, T., 2006. Electrochemical oxidation of the effluent from anaerobic digestion of dairy manure. Bioresource Technol. 97, 1360-1364.

Kima, D., Kima, T.S., Ryua, H.D., Le, S.I., 2008. Treatment of low carbon-to-nitrogen wastewater using two-stage sequencing batch reactor with independent nitrification. Proc. Biochem. 43, 406-413.

Liu, S., Lim, M., Fabris, R., Chow, C., Drikas, M., Amal, R., 2008. TiO_2 photocatalysis of natural organic matter in surface water: Impact on trihalomethanes and haloacetic acid formation potential. Environ. Sci. Technol. 42, 6218-6223.

Molinari, R., Pirillo, F., Loddo, V., Palmisano, L., 2006. Heterogeneous photocatalytic degradation of pharmaceuticals in water by using polycrystalline TiO_2 and a nanofiltration membrane reactor. Catal. Today 118, 205-213.

Vimonses, V., Jin, B., Chow, C.W.K., Saint, C., 2009. Enhancing removal efficiency of anionic dye by combination and calcination of clay materials and calcium hydroxide. J. Hazard. Mater. 171, 941-947.

Zhu, H., Gao, X., Lan, Y., Song, D., Xi, Y., Zhao, J., 2004. Hydrogen titanate nanofibers covered with anatase nanocrystals: A delicate structure achieved by the wet chemistry reaction of the titanate nanofibers. J. Am. Chem. Soc. 126, 8380-8381.

CHAPTER 4

SYNTHESIS AND CHARACTERISATION OF NOVEL TITANIA IMPREGNATED KAOLINITE AND ITS PHYSICAL PROPERTIES AND PHOTOOXIDATION ABILITY

SUB-CHAPTER 4.1

SYNTHESIS AND CHARACTERISATION OF NOVEL TITANIA IMPREGNATED KAOLINITE NANO-PHOTOCATALYST

M.N. Chong [a], V. Vimonses [a], S. Lei [c], B. Jin [a,b,d], C. Chow [d], C. Saint [b,d]

[a] School of Chemical Engineering, The University of Adelaide, Adelaide, SA 5005, Australia

[b] School of Earth and Environmental Sciences, The University of Adelaide, Adelaide, SA 5005, Australia

[c] School of Resource and Environment Engineering, Wuhan University of Technology, Wuhan 430070, China

[d] Australian Water Quality Centre, SA Water Corporation, Bolivar 5110, Australia

Microporous and Mesoporous Materials 2009; 117: 233-242.

STATEMENT OF AUTHORSHIP

SYNTHESIS AND CHARACTERISATION OF NOVEL TITANIA IMPREGNATED KAOLINITE NANO-PHOTOCATALYST

Microporous and Mesoporous Materials 2009; 117: 233-242.

Chong, M.N. (Candidate)

Performed experiment design; analysis of samples; interpreted data; manuscript evaluation; wrote manuscript.

Signed……*Date*……..

Vimonses, V.

Performed experiment design; analysis of samples; interpreted data.

I give consent for M. N. Chong to present this paper for examination towards the Doctor of Philosophy

Signed……*Date*……..

Lei, S.

Performed experiment design; interpreted data.

I give consent for M. N. Chong to present this paper for examination towards the Doctor of Philosophy

Signed……*Date*……..

Jin, B.

Manuscript evaluation; acted as corresponding author.

I give consent for M. N. Chong to present this paper for examination towards the Doctor of Philosophy

Signed……*Date*……..

Chow, C.

Manuscript evaluation.

I give consent for M. N. Chong to present this paper for examination towards the Doctor of Philosophy

Signed……*Date*……..

Saint, C.

Manuscript evaluation.

I give consent for M. N. Chong to present this paper for examination towards the Doctor of Philosophy

Signed……*Date*……..

Chong, M.N., Vimonses, V, Lei, S., Jin, B., Chow, C. and Saint, C. (2009) Synthesis and characterisation of novel titania impregnated kaolinite nano-photocatalyst. *Microporous and Mesoporous Materials, v.117 (1-2), pp. 233-242, January 2009*

SUB-CHAPTER 4.2

EVALUATION OF THE PHYSICAL PROPERTIES AND PHOTODEGRADATION ABILITY OF TITANIA NANOCRYSTALLINE IMPREGNATED ONTO MODIFIED KAOLIN

V. Vimonses [a, b], M. N. Chong [a, b], B. Jin [a,b,c]

[a] School of Chemical Engineering, The University of Adelaide, Adelaide, SA 5005, Australia

[b] School of Earth and Environmental Sciences, The University of Adelaide, Adelaide, SA 5005, Australia

[c] Australian Water Quality Centre, SA Water Corporation, Bolivar 5110, Australia

Submitted manuscript to Microporous and Mesoporous Materials.

STATEMENT OF AUTHORSHIP

EVALUATION OF THE PHYSICAL PROPERTIES AND PHOTODEGRADATION ABILITY OF TITANIA NANOCRYSTALLINE IMPREGNATED ONTO MODIFIED KAOLIN

Submitted manuscript to Microporous and Mesoporous Materials.

Vimonses, V.

Performed experiment design, analysis of samples; interpreted data; manuscript evaluation; wrote manuscript.

I give consent for M. N. Chong to present this paper for examination towards the Doctor of Philosophy

Signed……*Date*……..…

Chong, M. N. (Candidate)

Performed experiment design; interpreted data; manuscript evaluation.

Signed……*Date*……..…

Jin, B.

Manuscript evaluation; acted as corresponding author.

I give consent for M. N. Chong to present this paper for examination towards the Doctor of Philosophy

Signed……*Date*……..……

Evaluation of the Physical Properties and Photodegradation Ability of Titania Nanocrystalline Impregnated onto Modified Kaolin

Vipasiri Vimonses [a, b], Meng Nan Chong [a,b], Bo Jin [a,b,c,*]

[a] School of Chemical Engineering, The University of Adelaide, Adelaide, SA 5005, Australia

[b] School of Earth and Environmental Sciences, The University of Adelaide, Adelaide, SA 5005, Australia

[c] Australian Water Quality Centre, SA Water Corporation, Adelaide, SA 5000, Australia

[*] To whom correspondence should be addressed.

Tel.: +61 8 8303 7056. Fax: +61 8 8303 6222. Email: bo.jin@adelaide.edu.au

Abstract

In this study, a microporous layer photocatalyst of titania nano-crystallites heterocoagulated with structurally modified kaolin (TiO_2-K) was synthesised via a modified sol-gel method. Physical properties (particle size, morphology, stability and settleability) and photodegradation capacity of the TiO_2-K catalyst subject to its synthesis, regeneration and use for water treatment were studied. The modified kaolin, as a support for the titania nano-crystallites had a delaminated sandwich silica structure that minimises chemical intercalation within the nanocomposite structure. Microscopic examination revealed that the TiO_2 nano-crystallites were uniformly deposited on the kaolin external surface, resulting in a high degree of photon activation. Compared to the commercial TiO_2 P25, the TiO_2-K demonstrated a superior photocatalytic degradation capacity to remove an anionic Congo red dye. Its removal efficiency and photoreaction performance were improved when the TiO_2-K was regenerated by thermal treatment. The TiO_2-K particles can be easily separated from the water system for further reuse. This unique nanocomposite photocatalyst shows promising technical advantages for a continuous industrial process of water treatment.

Keywords: TiO_2; Photocatalysis; Sol-gel; Kaolin; Thermal regeneration.

1. Introduction

The multi-faceted properties and photocatalytic performance of titanium dioxide (TiO_2) for water purifications have received an increasing interest in recent decades owing to its high photostability, non-toxicity and cost effectiveness [1]. Many successes in TiO_2–assisted photodegradation of recalcitrant organic contaminants in water, including different complexes endocrine disrupting compounds and dyes has been well-documented [2-4]. In reality, however, such heterogeneous photocatalysis processes for water purification utilising commercial TiO_2 are still facing a number of constraints that annihilate its feasibility for an industrial application.

Since the main photo-induced charged separation occurs on the surface of the photocatalysts, a larger specific area would promote a higher photocatalytic reaction rate. Herrmann [5] suggested that adsorption is a pre-dominant step in ensuring rapid photocatalytic surface reaction on the water contaminants. Owing to the large surface area to volume ratio, nano-sized photocatalysts (i.e. Degussa P25) present a significant physical advantage that compromises the organic adsorption. These nano-sized TiO_2 photocatalysts can lead to a latent difficulty for a downstream process to separate and recover the TiO_2 particles before reaching the consumer-end. Such ultra-fine particle separation usually incurs high operation and capital costs, and thus has seriously impeded the large scale applications of TiO_2 photocatalysts for an industrial treatment process.

Immobilisation of the nano-sized TiO_2 photocatalysts can avoid the technical problem associated with the post downstream process required to separate the TiO_2 catalysts. Such a deposition method is usually technically-subjective, and requires significant experimental efforts to optimise between the surface areas to volume ratio of the supported-photocatalysts with its photoactivity. The exploitation of various titania-supported photocatalysts to achieve desirable physicochemical properties, photoactivity and stability for water treatment has received a great attention [6]. Deposition of TiO_2 thin films onto a larger catalyst support, such as ferromagnetic cores or silica materials considerably improved both the particle recovery and adsorptive capacity [7]. Different layer silicate materials such as clay minerals were investigated as a possible supporting platform for the TiO_2 nanocrystals. A few studies have

explored the possibility of clays-supported TiO_2 nanocrystals, with frequent emphasis on the natural montmorillonite subclass. So far, a little attention has been paid how the physicochemical properties and photoactivity of the TiO_2 nanocrystals could be varied during the photocatalytic process, especially if the catalysts are repeatedly recovered and reused in a water purification system. .

In this study, we synthesized a thin-layer TiO_2 nanocrystalline impregnated onto physiochemically modified kaolin as the immobiliser platform. Natural kaolin, $Al_2Si_2O_5(OH)_4$, is a phyllosilicate (sheet silicates) mineral with a tetrahedral silica sheet alternating with an octahedral alumina sheet. The ideas of exploiting kaolin is owing to its relatively low isomorphous substitution within its lattice structure, that limits the molecular interaction in water system, in which the clay structure can be possibly altered as found in montmorillonite. Such an ordered structure of kaolin, however, can restrict its functional active site to the plane and edge of kaolin particles. To improve the physical surface properties of kaolin as the catalyst platform, we investigated for the first time a series of pre-treatment methods of the kaolin prior to the sol-gel deposition of TiO_2 thin film, including acid dissolution, alkaline treatment and thermal activation. This was followed by controlled heterocoagulation of the TiO_2 sol with the treated kaolin particles, as previously reported by this team. [8]. The resultant physicochemical properties of the TiO_2-impregnated kaolin (TiO_2-K) nanocomposites were characterized using X-ray diffractionometry (XRD), Brunauer-Emmett-Teller (BET), and electroscopic techniques of scanning electron microscopy (SEM) and transmission electron microscopy (TEM). Such techniques were also used to unveil the variation in physicochemical properties during different thermal regeneration cycles. Photoactivity of the TiO_2-K catalyst was evaluated against the degradation of anionic Congo red dye as a model surrogate compound. The settleability of the photocatalyst particles were also analyzed using Kynch's hindered settling conditions, in terms of the single photocatalyst particle terminal settling velocity.

2. Materials and Methods

2.1. Materials

Physicochemical properties of kaolin may be varied, depending upon the geographic source of origin. Natural white dry-milled kaolin obtained from Unimin, Australia was used in this study. The kaolin consisted of SiO_2 (48.7%), Al_2O_3 (34.6%), TiO_2 (1.3%), Fe_2O_3 (0.9%) and other trace compositions of K_2O, CaO, MgO and Na_2O. The details of the physical and chemical properties of the kaolin materials were reported in our previous work [9]. Commercial TiO_2 P25 (Degussa, Germany) was used as received for comparison study. The Degussa P25 has a surface area of 50 ± 5 m^2g^{-1} and composes of 80% anatase and 20% rutile with elementary particle sizes of 25-85 nm respectively.

Titanium (IV) butoxide (tetrabutyl orthotitanate AR grade ≥ 97% gravimetric, Sigma-Aldrich), absolute ethanol (AR grade, Labserv Pronalys, Australia), and sodium pyrophosphate (AR grade, BDH VWR, England) were used as received. Congo red (CR) ($C_{32}H_{22}N_6Na_2O_6S_2$, Labchem Ajax Finechem Australia), sulphuric acid (AR grade, 98 wt%, BDH VWR, England), nitric acid (AR grade, 69 wt%, BDH VWR, England), sodium hydroxide (AR grade, BDH VWR, England) were prepared using double-deionised water with 18.2 M-ΩM, resistivity.

2.2. Pre-treatment on Natural Kaolin Clay

Natural kaolin was first pre-treated, in order to purify and augment the surface availability prior to the subsequent heterocoagulation process with TiO_2 sol. A series of acid-alkaline-thermal treatment was performed to alter the surface properties of the clay. Kaolin suspensions (ca. 20 g L^{-1}) were magnetically suspended in a 20 cm high jar that fills with deionised water for particle size screening. At a certain stirring extent, the suspension was allowed for settling within 0.5 h. Supernatant from the jar containing particles with a size range <10 μm was decanted and filtered. The filtrate cake was then resuspended in 1M sulphuric acid solution with continuous stirring up to 10 h before being filtered and washed repeatedly with deionised water. Following this, the kaolin particles were treated by 2 M sodium hydroxide at pH 10 for 0.5 h. The final kaolin filtrate cake was washed and dried at 70 ^oC for 4 h before firing at 750^oC for 1 h.

2.3. Synthesis of TiO_2-Kaolin Catalysts

Deposition of TiO_2 thin film onto surface-augmented kaolin was prepared according to our previously reported method [8]. Twenty five mL titanium (IV) butoxide was vigorously mixed with 30 mL of absolute ethanol for 0.5 h. The mixture was then acid catalysed via backdrop into a controlled-molar nitric acid solution. After the acid catalysed reaction a transparent homogeneous TiO_2 sol was then attained under continuous stirring for 0.5 h. Following this, the homogeneous TiO_2 sol was carefully heterocoagulated with the treated kaolin (ca. 10 % w/v) via slow addition of the sol into the vigorously-stirred kaolin suspension. The stirring flask was kept at 37 ºC in a water bath. Heterocoagulated TiO_2-kaolin was continually stirred for 4 h, before aging for 14 – 16 h at room temperature. The aged nanocomposites were then filtered and washed repeatedly with deionised water to remove any excess chemical impurities. Then, the nanocomposites were dried at 70±2˚C for 2-4 h to remove any surface-bound water molecules before calcination at 600˚C at a heat ramping rate of 4-5 ˚C min^{-1} for 3 h. The final product of TiO_2-K particles was readily used as photocatalysts for the following experiments.

2.4. Characterisation of Kaolin and TiO_2-K Catalysts

The following analytical methods were conducted to characterise both the raw kaolin and TiO_2–K particles. This information is useful to gain insight into the physical, chemical and photochemical characteristics of the TiO_2-K particles using surface augmented kaolin as a support platform.

Differential temperature analysis coupled with thermogravimetric analysis (DTA-TG) (TA Instruments) was performed on the raw kaolin to obtain the weight loss of kaolin as a function of temperature. During the analysis, the raw kaolin sample was heat-treated from room temperature to 1200˚C at a ramping rate of 10˚C min^{-1} under highly nitrogenised condition to avoid any possible oxidation.

Particle size of pre-treated kaolin was then measured using a static light scattering laser diffraction particle sizer instrument (Malvern Mastersizer 2000), covering the detection range from 0.02 to 2000 microns. The kaolin particles were first dispersed in sodium pyrophosphate solution, with constant agitation and sonication until a stable dispersion was attained. The

particle size distribution of the pre-treated kaolin particles from the particle size screening are shown in Fig. 1.

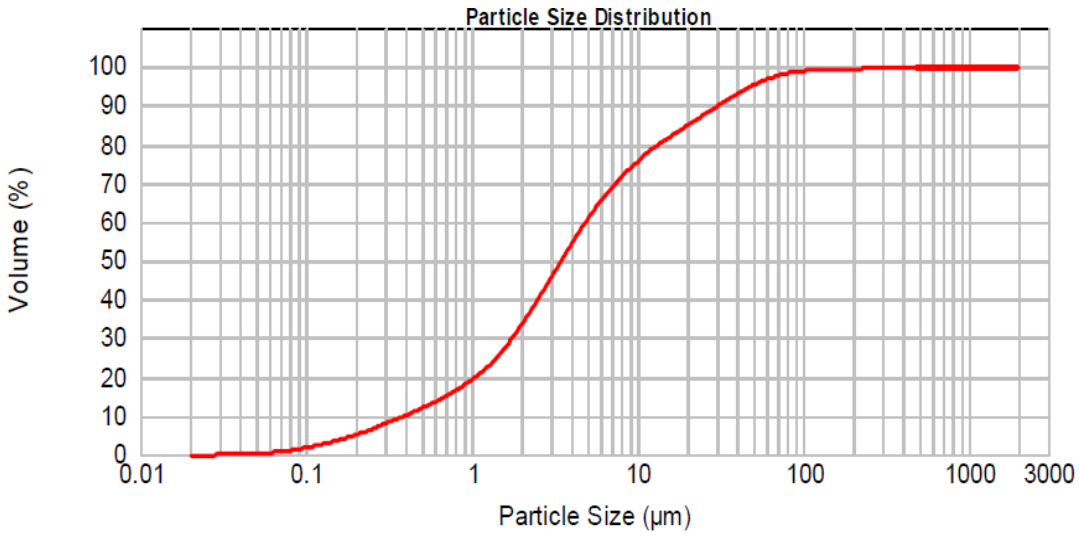

Figure 1: The particle size distribution of natural kaolin ($d_{0.1}$=0.396 µm, $d_{0.5}$=3.471 µm and $d_{0.9}$=30.558 µm.)

Morphological and surface characteristics of the resultant TiO_2-K particles were analysed using SEM (Philips XL30 SEM) at an accelerating voltage of 10 kV. Thin platinum coating was applied on the particle sample prior to analysis. TEM was also performed using Philips CM-100 TEM at an accelerating voltage of 100 kV. Before the analysis, the TiO_2-K particles were minimally suspended in ethanol solution (ca. 0.01% w/v), followed by ultrasonic dispersion and subsequent immobilisation on the copper measurement grids of 2 mm diameter.

BET specific surface area and pore size measurements on the resultant nanocomposites were performed using a Micrometrics gas adsorption analyser (Gemini Type 2375) at 77 ± 0.5 K in liquid nitrogen. Prior to the surface analysis, the sample vessels loaded with ca. 0.5–1.0 g were vacuum treated overnight at 105˚C and evacuation pressure of 50 mTorr. Nitrogen adsorption isotherms of the samples were then analysed for the specific surface area using the BET equation.

XRD measurements were performed using a Philips PW Diffractometer (Cu X-rays λ = 1.54 Å) over the range of 5–75° 2θ for all the samples. Samples were spiked with 10 wt% of zinc oxide before the diffractionometric analysis to facilitate the determination of amorphous phase TiO_2 to the amount of TiO_2 nanocrystals formed. The average crystallite diameter of the TiO_2 nanocrystals, D_{hkl}, was obtained using the Debye–Scherrer equation [$D_{hkl} = k\alpha/\beta \cos\theta$], where β is the line broadening, k is the crystalline shape with Warren's correction value for instrumental broadening of 0.89, and α and θ are the radiation wavelength and Bragg angle, respectively. A standard for the line broadening width based on a single anatase crystal of TiO_2 was used for calibration.

Optical absorption characteristic of the resultant TiO_2-K composites was measured using a UV–Vis diffuse-reflectance spectroscopy. The diffuse-reflectance spectra were measured using a Varian Cary 5000 UV–vis spectrophotometer between the wavelengths of 250 to 600 nm.

2.5 Photoactivity Assessment of TiO_2-Kaolin Catalysts

Photoactivity of the resultant TiO_2-K was probed using CR as a standard photo-oxidation rate. Initially, an aqueous solution with concentration of 57.4 μmol L^{-1} CR was photochemically reacted with TiO_2-K catalyst. An 11W UV-C light (Davis Ultraviolet, Australia) was positioned centrally to a magnetically-stirred beaker that contained the reaction solution. The linear attenuation of the UV intensity at the reaction solution surface was determined to be 300 μW cm^{-2} using a UV radiometer. Prior to the photochemical reaction, the TiO_2-K was remained in dark homogenisation for 0.5 h allowed to ensure constant dispersion and mixing. Sampling was conducted every 1 h, and the supernatant was obtained for calorimetric measurement via centrifugation at 5000 rpm for 10 min. Single maximum wavelength of 496.5 nm was used with a path cell length of 1 cm in a UV-Vis spectrophotometer for analysing CR concentration. The CR concentrations were measured in triplicate and were evaluated as the average photo-oxidation rate.

3. Results and Discussions

3.1. Surface Augmentation of Kaolin Clay as Nanocrystals Support

Raw kaolin was initially subjected to acid treatment to purify the clay through dissolving the undesired chemical impurities that may be present naturally or during the manufacturing process. The presence of a high level of impurities in the raw kaolin might severely affect the interlayer pore space and thus, the total effective surface area. Komadel and Madejová [10] stated that the acidification of clay mineral under controlled acid conditions might also induce partial dissolution of other undesired elements (i.e. Fe and Mg) within the clay structure. Such acid attack is known to preferentially occur at the octahedral alumina sheet, while the tetrahedral sheet (i.e. SiO_4 and SiO_3OH) remain largely intact [11].

In this instance, reaction time for the kaolin acidification remains a crucial factor for effective surface augmentation while maintaining a stable alumina structure for immobilising the TiO_2 nanocrystals. We found that at an acidification time shorter than 10 h, the leaching rate of both the Fe and Mg cations to the Al cations were able to be suppressed from the clay structure (data not shown). Such a retention time was found to be relatively shorter than those previously reported by Steudel et al [11]. The partial dissolution of kaolin during the acidification process, however, induces delamination of kaolin structure, in which the remaining tetrahedral sheets are connected to the residual octahedral sheet. The acidification of the kaolin resulted in formation of micropores within the kaolin structure, and consequently an increase in both the specific surface area and porosity. The BET adsorption isotherms calculation indicated that the specific surface area of the acidified kaolin increased from 20.3 m^2g^{-1} to 26.1 m^2g^{-1}. The acidification of the kaolin can also be proven from the apparent color change of the kaolin from yellowish to white, as a result of the low level of chemical impurities present.

To counterbalance the net positive surface of the acidified kaolin, a subsequent alkalization treatment step was carried out to shift the surface charge to be slightly negative. The extent of such alkalization treatment is important, in order to promote the latter heterocoagulation between the positively charged TiO_2 sol and the kaolin particles. Such an alkalization treatment, however, is quite complicated to implement across kaolin particles of different

point of zero charge (PZC); kaolin (ca. 4 – 4.7) and its edges (ca. 6 – 7) [12-13]. In our study, we adjusted the kaolin suspension with sodium hydroxide to pH 10 to ensure the conversion of surface charge. In contrast to acidification, tetrahedral silica compounds are more soluble in alkaline media than the Al, Fe and Mg cations. Jozefaciuk et al [14] reported that alkalization is beneficial in purifying kaolin of the most irregular amorphous mineral structures.

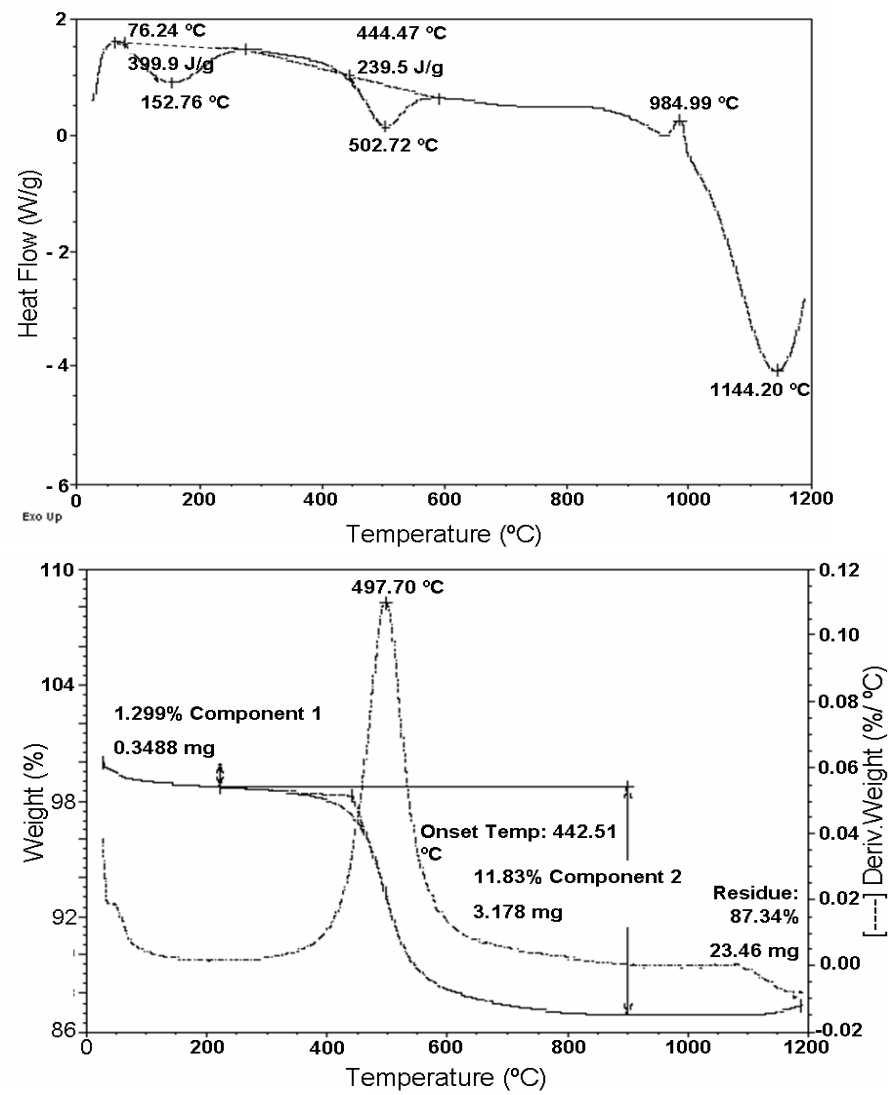

Figure 2: Differential thermal analysis (DTA- Heat flow against temperature profile) and thermogravimetric (TG- Weight loss against temperature profile) of natural kaolin

Thermoanalytical measurement of the kaolin was eventually performed to understand the stability of the kaolin structure against elevated temperature gradient (Fig. 2). From the DTA-TG plots of the acidified-alkalized treated kaolin, the initial peak of weight loss was found to

correspond to the removal of surface-bounded water and other attached foreign molecules on the kaolin surface. This dehydration stage was manifested by the onset of endothermic process at 153°C. The second weight loss peak that appears at 503ºC was related to the water dehydroxylation between each silicate pair sheets within the skeleton kaolin structure. The following exothermic peak at 985°C was an indicative of the maximum applicable firing temperature before the collapse of kaolin structure. Thus, in order to maintain the skeleton kaolin structure, the treated kaolin particles heated up to 750°C at a heating rate of 10°C min^{-1}.

Changes in the surface morphology of the fired kaolin structure were subsequently compared with the raw kaolin via SEM imaging. Fig. 3a shows the morphological surface of the raw kaolin particles, where the scattering of hexagonal flakes were piled up on top of one another along with consistent distribution of micropores. The SEM image presented in Fig. 3b shows that the surface structure of the treated kaolin particles was changed to rather flat surface with a low porosity. Such surface augmentation, as a result of the series of acidification-alkalization-thermal treatment, provides an increased surface area for ease of light accessibility and TiO_2 sol deposition. Eventual BET measurements revealed that the treated kaolin particles had significantly enlarged specific surface area of 31.3 m^2 g^{-1} compared with the raw kaolin particles of 20.3 m^2g^{-1}.

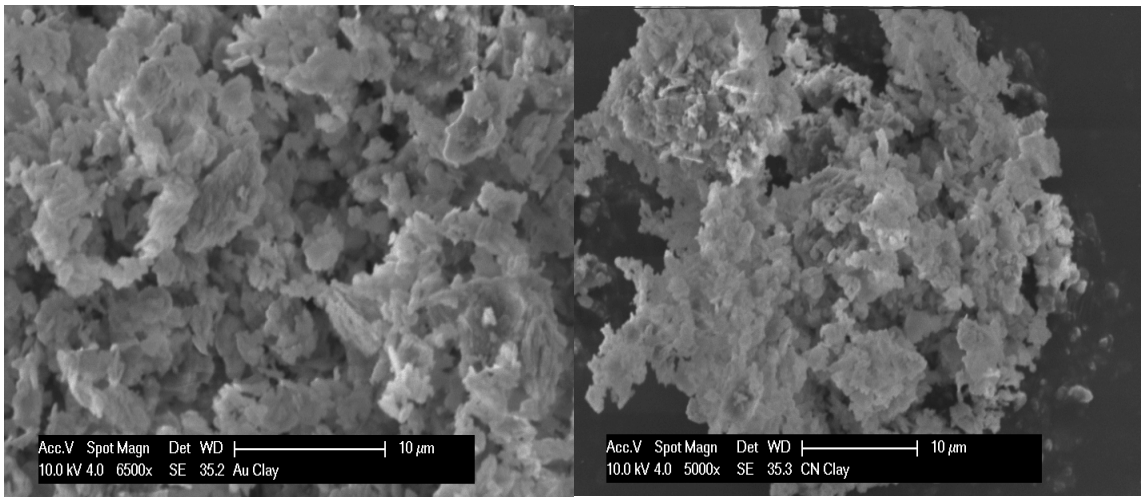

Figure 3: SEM images of kaolin a) without pre-treatment and b) with treatment

3.2. Physicochemical Properties of TiO_2-Kaolin

It is well known that the photo-oxidation capacity of a photocatalyst can be strongly influenced by its physicochemical properties, which include size and morphology, crystalline phase, specific surface area and porosity. In this section, we report the physicochemical properties of the TiO_2-K particles.

Since the prepared TiO_2-K particles consist of single layer of TiO_2 nanocrystals with the kaolin, the thickness of the nanocrystals growth was carefully monitored using TEM. A consistent TiO_2 nanocrystals layer with an average size distribution of 7 - 9 nm was observed (Fig. 4a). Such layered TiO_2 nanocrystals can significantly alter the surface morphology of the core kaolin particles. It can be observed that a highly porous structure (Fig. 4b) was attained after the controlled deposition of TiO_2 nanocrystals, as this is relative to the flat sheet prototype of pre-treated kaolin particles. Presence of such deposited TiO_2 nanocrystals remarkably increased the specific surface area of the kaolin. This was evidenced from the specific surface area and average pore size of the nanocomposites, as determined using nitrogen adsorption measurements. These results show that the specific surface area increased from 31.3 to 57.6 m^2 g^{-1}, and the average pore diameter was estimated to be 8.3 nm, suggesting the prominent existence of microporous TiO_2 structure on the surface of core kaolin particle.

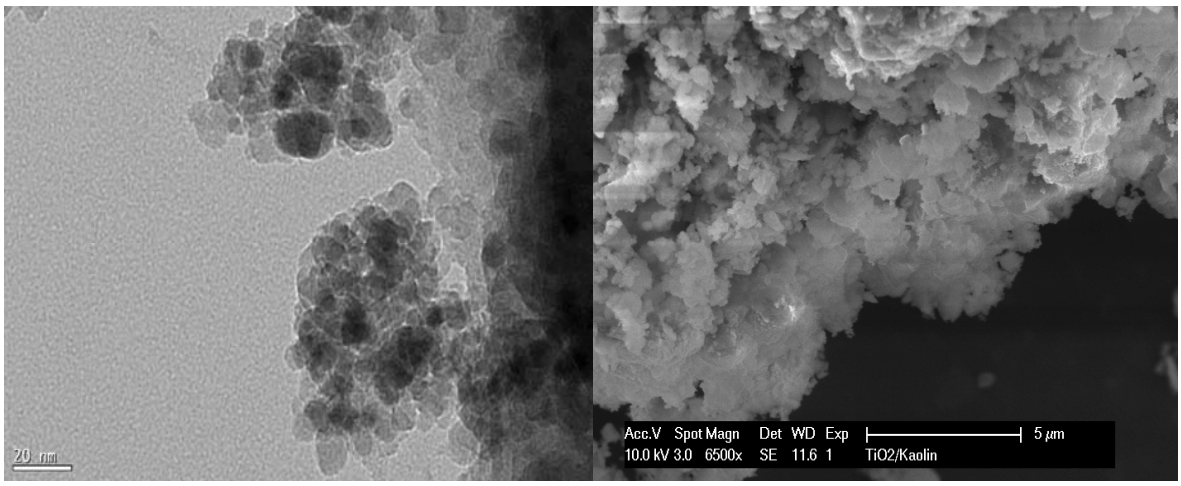

Figure 4: Electron microscopy images of TiO_2-K a) TEM and b) SEM

XRD measurement on the TiO_2-K particles revealed that the layered microporous TiO_2 constitutes by anatase TiO_2 phase alone. Fig. 5 suggests that the layered TiO2 is made up of anatase structure as evidenced by the 25.3º (2Θ) for anatase (101), with no significant 27.5º (2Θ) for appearance of rutile (110) [15]. Nishimoto et al [16] reported that the anatase TiO_2 performed a more prominent photoactivity than the rutile TiO_2. Using the zinc oxide spiking method, it was estimated that the weight of anatase TiO_2 formed on the core kaolin only accounted for approximately 9 wt% of total TiO_2-K particles. Further verification of the nanocrystals size was calculated base on the Scherrer equation, and was found to be consistent with those obtained from TEM of approximately 7.6 nm in diameter.

Subsequent UV-Vis diffuse reflectance was performed on the TiO_2-K particles, in order to determine its light absorption capability. A strong shift in the light absorption degree in relative to the bare kaolin was apparently observed at wavelengths lower than 400 nm. This indicated the photo-reaction using the layered TiO_2 nanocrystals can take place using a light source in the UV region. It was observed, however, that the tail of the absorption spectrum in longer wavelengths of the samples may attribute to the presence of large TiO_2 nanocrystals at the edges of clay platelets [17].

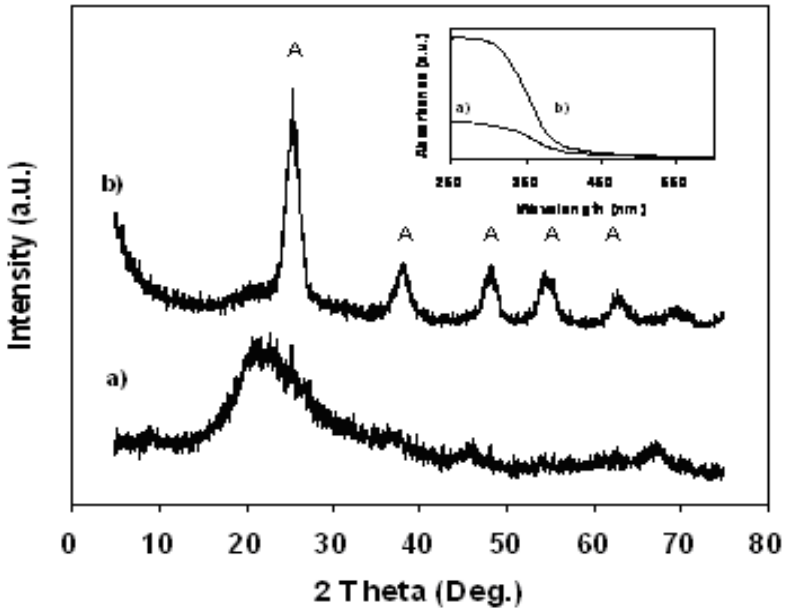

Figure 5: X-ray diffraction (XRD) and UV-Vis diffuse reflectance spectra of a) TiO_2-K and b) bared kaolin. A: Anatase.

3.3. Variation in the Physicochemical Properties of TiO_2-K Catalysts during Repetitive Thermal Regeneration

In a water treatment system, the photocatalyst particles are usually subjected to hydrodynamic and operating conditions in the semiconductor system, resulting in a possible change of their physicochemical properties. These changes might affect significantly on the photoactivity of the catalysts. Although immobilisation of TiO_2, on separable catalyst support was reported in a number of studies, no study has been found to investigate the possible changes of the physicochemical properties of the photocatalysts under a thermal regeneration. In our study, the TiO_2-K catalysts were recovered and regenerated by a simple thermo-treatment. We investigated the change in the physicochemical properties of the TiO_2-K particles which were experienced a recycling and regeneration cycle at $550^{\circ}C$ for 0.5 h. The impact of thermal regeneration cycles on the photoactivity of the catalysts was evaluated by the CR photodegradation experiments.

Table 1 shows the variation in physicochemical properties of the TiO_2-K particles associated with the number of regeneration cycles. The specific surface area of the catalysts decreased slightly after each thermal regeneration cycle. This might be that the thermal treatment may result in partial collapse of the structural bonding within the layered TiO_2 nanocrystals, therefore, leading to its densification (i.e. decrease in internal pore size. Imai et al [18] observed that such densification in deposited layered TiO_2 might also be induced by the UV irradiation during photocatalysis. Irradiation with photons which have higher energy than the bandgap can induce the densification through the bond cleavage via electronic excitation from the TiO_2 valence band to the conduction band [18].

Another postulation for the decline in specific surface area of the catalysts after repetitive reuse may be due to possible re-growth of the TiO_2 nanocrystals during the thermal regeneration treatment. This postulation was evidenced from the XRD measurement (Fig. 6). Whilst the number of regeneration cycle increases, the intensities of the diffraction peak for the anatase (101) at 2Θ equal to 25.3^{o} increased with intensely narrower peak signals. Such incident may be explained by possible aggregation of the TiO_2 nanocrystals during the course of regeneration. This was proven by the increase in the average TiO_2 nanocrystals size. From

Table 1 and Fig. 6, we found that the average nanocrystals size increased from 7.6 nm to 10.1 nm after six regeneration cycles.

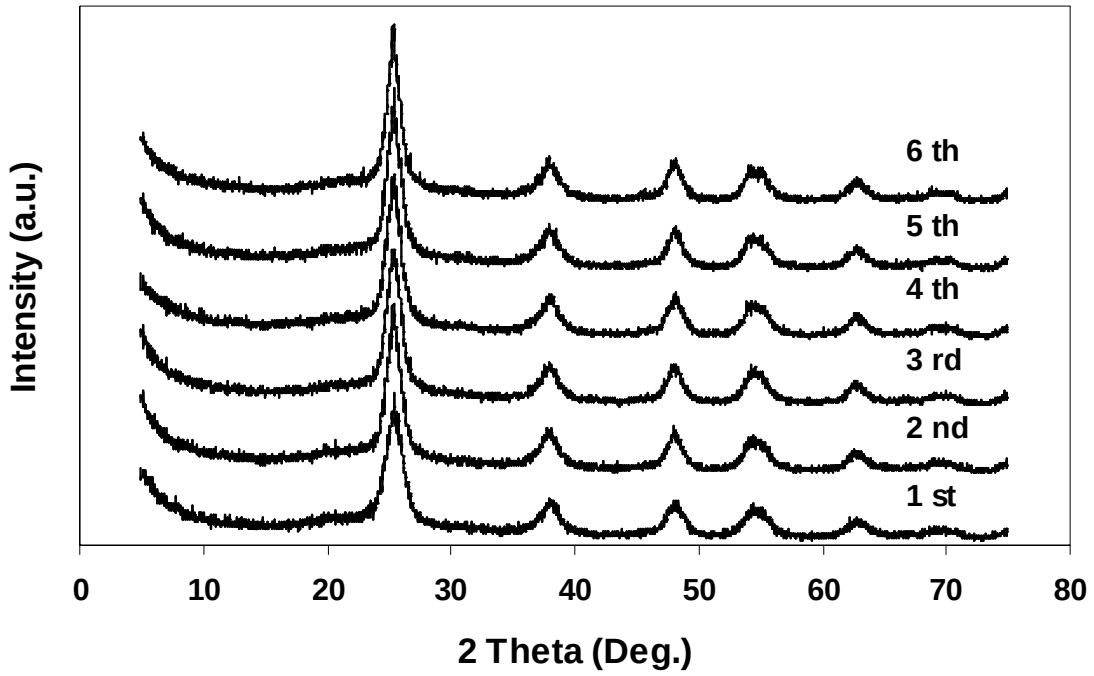

Figure 6: X-ray diffraction (XRD) of recycled TiO_2 -K photocatalysts after cycles of thermal treatment.

Table 1: The characteristic of the recycled titania impregnated kaolin photocatalysts after thermal treatment

Recycled catalyst	BET specific surface area (m^2g^{-1})	Particle diameter (nm)	Pore diameter (nm)
1 st	57.66	7.63	8.31
2 nd	54.90	8.27	8.62
3 rd	52.65	8.71	8.84
4 th	49.65	9.38	9.03
5 th	47.93	9.72	9.17
6 th	44.98	10.13	9.80

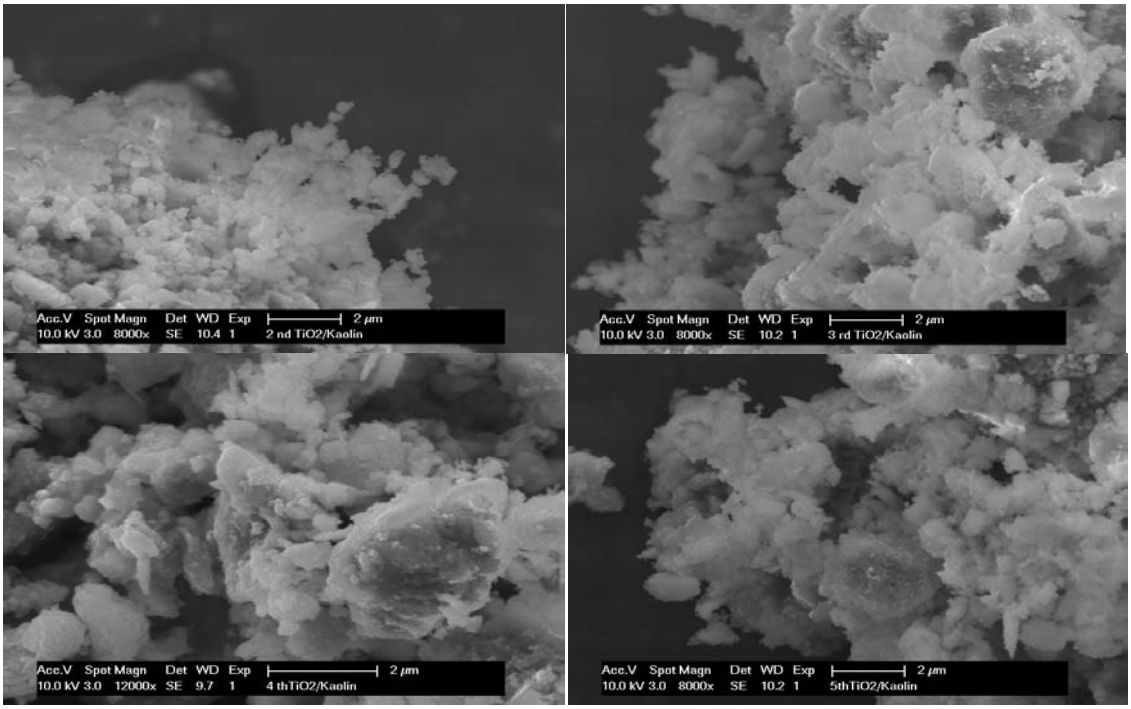

Figure 7: SEM images of recycled TiO_2-K photocatalyst cycles of thermal treatment a) 2nd run, b) 3rd run, c) 4th run, and d) 5th run

One of the prominent findings as indicated by the XRD measurements is that the studied thermal regeneration conditions did not significantly alter the stability of the TiO_2 nanocrystals. Beydoun and Amal [19] reported that the transformation from the anatase to rutile resulted in significant rupture of the Ti-O bonds. We found that, however, after six thermal regeneration cycles, the layered TiO_2 nanocrystals on the kaolin remained in anatase TiO_2 forms. This finding shows that our previous postulation on the nanocrystals re-growth is valid, where the decline in specific surface area is not owed to the photoactive phase transformation. The stability in the layered TiO_2 nanocrystals structure can be related to the formation of Ti-O-Si bonds between the TiO_2 network and siliceous side of kaolin particles during the course of synthesis. It was also known that the presence of Ti-O-Si bonds could suppress the TiO_2 phase transformation from anatase to rutile, and thus directly influenced its stability [19-20]. We used SEM imaging to further confirm the stability of the attached layered TiO_2 on the kaolin surface. Fig. 7 shows that the porous structure of the regenerated catalysts remains with the TiO_2 nanocrystals distributed consistently on the kaolin surface. In overall, we only found that a slight increase in TiO_2 nanocrystals size and its pore diameter is a direct result of the thermal

regeneration. No remarkable change on surface morphology was observed after each regeneration cycle.

3.4. Photodegradation of Congo Red using TiO_2-K Catalysts

Here, we investigated the photocatalytic performances of the TiO_2-K catalysts prepared by treated kaolin clay and the TiO_2-K catalysts regenerated by thermal regeneration cycles. Commercial Degussa P25 TiO_2, which has been commonly used in the many studies, was tested to compare the photo-degradation ability with the TiO_2-K photocatalysts.

The photoactivity of the TiO_2-K was tested against 57.4 μmol L^{-1} CR. Control experiments were carried out in the CR solution with UV irradiation and no TiO_2-K. Only 6% CR removal was found in the control experiment under UV irradiation for 7 h. The photoactivity of the TiO_2-K was subsequently tested against bare TiO_2 nanocrystals (i.e. without a kaolin core) and Degussa P25 TiO_2. Results in Fig. 8 show that the predominant decolourisation of approximately 70% CR by the TiO_2-K was achieved in the first hour, and subsequent 90% CR removal was obtained in 2 h irradiation, while approximately 80% CR removal by the P25 TiO_2 was found in 2 h. The rapid CR removal by the TiO_2-K was attributed to the enhanced adsorption of dye molecules on the microporous layered TiO_2 nanocrystals, and importantly on the surface of the kaolin particles. Several studies evidenced that the photocatalytic reaction is likely restricted to the adsorbed phase of the catalyst particles [21-22].

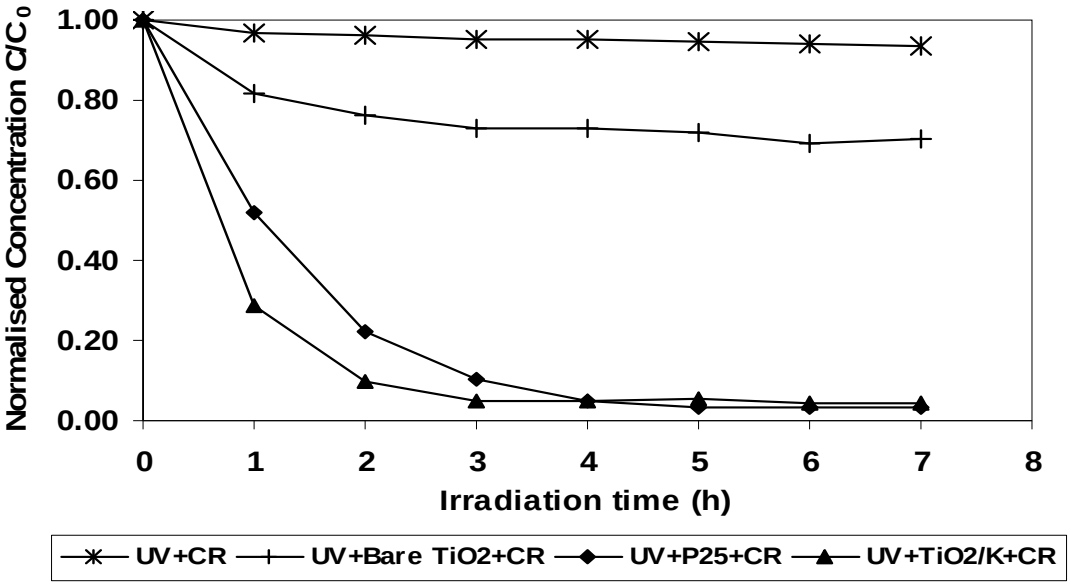

Figure 8: The photocatalytic degradation of 40 ppm of Congo red by different catalysts. The concentration for P-25 TiO_2 is 1 g/L, while TiO_2/K is 10 g/L.

The mechanisms of the enhanced photodegradation rate of the TiO_2-K catalysts can be explained that the porous clay support can constantly replenish the CR molecules to the "dynamic equilibrated" surface for surface reaction. When the photoactivity of the TiO_2-K was compared to the P25 TiO_2, it could be observed that both photocatalysts undertake different degradation mechanisms. Titania impregnated kaolin was found to be more adsorption dominant than the P25 TiO_2 and the bare TiO_2 nanocrystals. These can conclude that the rigid porous structure of the kaolin can enhance the adsorption capacity and hence, its photoactivity. Kun et al [15] proposed that such catalyst improvement via immobilisation might be owed to the force field between the nanocrystals supports with particles that inhibit the recombination of electron-hole pairs in the interlamellar clay structure. All these can prove the synergistic effect of core kaolin on its photoactivity, apart as the rigid catalyst support platform.

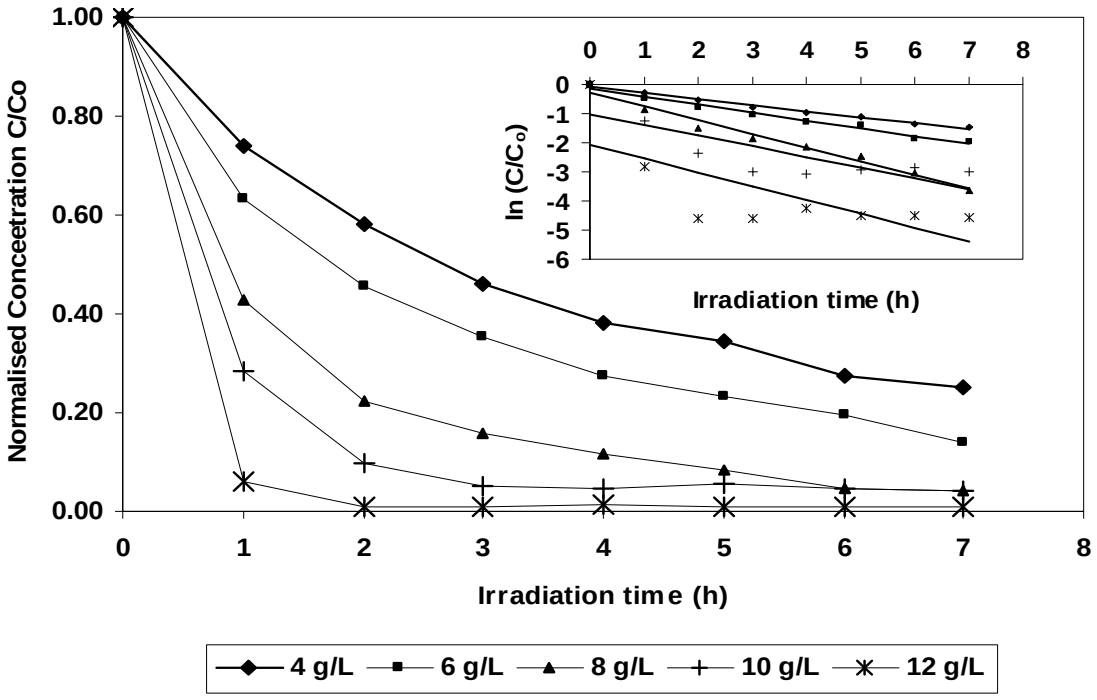

Figure 9: The photocatalytic degradation of 40 ppm of Congo red by different photocatalyst concentrations.

Photoactivity of the catalysts, however, is known to be highly dependent on its loading in the reaction system [23]. Fig. 9 shows the effects of different photocatalyst loading on the degradation of 57.4 μmol L^{-1} CR. It is expected that the photodegradation rate increases when the catalyst loading varies from 4 g L^{-1} to 12 g L^{-1}, as a direct result of more availability of catalyst active sites. In general, the kinetic of photocatalytic degradation is often referred to the Langmuir-Hinshelwood model, [3,24]. At a low concentration of the reactant (C<<1 mM), this model can be simplified to an apparent first rate order equation [2, 25].

$$\ln\frac{C_0}{C} = kKt = K_{app}t \qquad \text{(Eq. 1)}$$

K_{appt} is the apparent first order rate constant (h^{-1}) estimated from the plot of ln C_0/C versus t. (Fig. 9). Table 2 presents the estimated K_{appt} values from the different photocatalyst loadings. Results show that the CR degradation kinetic was well-fitted with the apparent first rate order

equation model, up to catalysts concentration of 8 g L^{-1}. The maximum rate of 0.470 h^{-1} was attained at the catalyst concentration of 8 g L^{-1}. Such fittingness to the kinetic model agreed on the prerequisite adsorption mechanism on the photocatalyst surface prior to surface oxidation reaction.

Table 2: The photocatalytic degradation rate of TiO_2-K at different catalyst concentration

Catalyst loading (g L^{-1})	Photocatalytic degradation rate (K_{appt}) (h^{-1})	R^2
4	0.208	0.9891
6	0.272	0.9787
8	0.470	0.9759
10	0.368	0.6544
12	0.473	0.5095

Estimation in the photoactivity during the repetitive use of the spent photocatalysts was performed to correlate the variation in physicochemical properties of the catalyst with its photoactivity. Fig. 10 shows that the adsorption capacity of the catalysts increases with the thermal regeneration cycles. As stated in earlier sections, such improvements may be well-correlated to the increase in the average pore sizes (i.e. formation of macroporous anatase TiO_2) of the spent catalysts, as evidenced in Table 1. Sasaki et al [26] proposed that the increase in the number of macropores was associated with the degree of unevenness on the TiO_2 flake surface with the increasing number of thermal regeneration cycle. Similar reaction conditions were tested on the photoactivity of the spent photocatalysts. The K_{app} values given in Fig. 10 show the competency of the regenerated photocatalysts to the fresh photocatalysts on CR removal in 7h irradiation. It can be thus, concluded that the TiO_2-K has the potential application in the wastewater treatment owing to its proven economical catalyst lifespan.

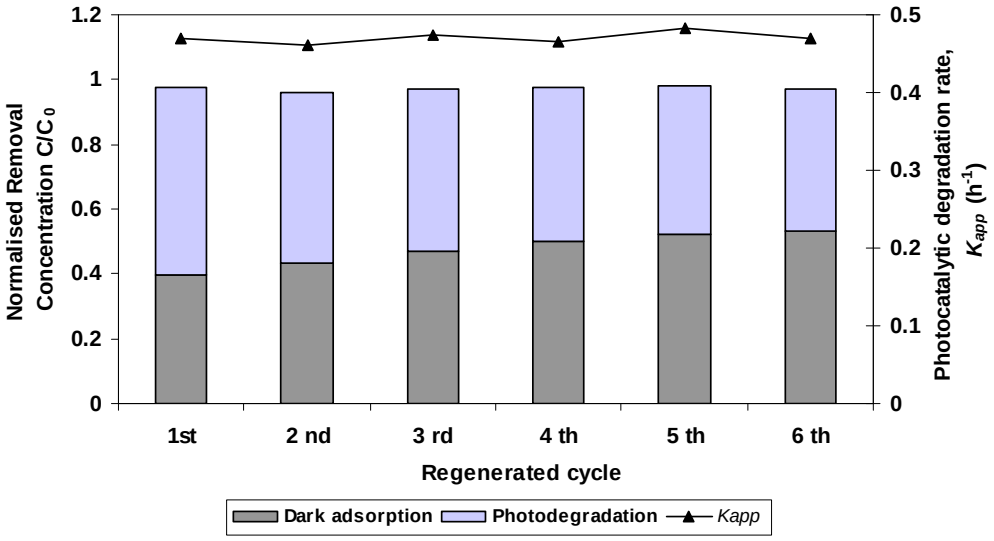

Figure 10: The photocatalytic degradation performance of recycled TiO_2-K photocatalyst cycles of thermal treatment

3.5. Settleability of the TiO_2-K Particles

Since the kaolin particles were made up of the TiO_2-K particle size in the micron range, the feasible application in the slurry semiconductor photoreactor system was examined. The settleability of particles in a liquid phase is an important physical property in relative to its separation performance. In this study, we examined the settling ability of the TiO_2-K particles by the hindered settling velocity of the photocatalyst particles, which was estimated based on Kynch's theory. Batch settling test was carried out, in which different amount of the photocatalyst (0.05, 0.1, 0.15 and 0.2g.) were simulated with 25 mL of deionised water.

During the analysis, the TiO_2-K particles were allowed to settle under gravitation, during which the decline of particle interface level with time was recorded. The interface height measured at different time intervals for each sample was used to plot the catalyst particle settling curve. The batch settling velocity (v) was estimated from the initial slope of the settling curve. Fig. 11 shows that the batch settling velocity was inversely proportional to the amount of the TiO_2-K particles in suspension. Such a correlation might be attributed to the overall upward flux of the fluid that arises when the settling photocatalyst displaces the water into the sediment zone [27-28]. By fitting the settling kinetics into the linearized Richardson

and Zaki correlation (Eq. 2), the single particle terminal velocity (v_t) was found to be 5.28 x 10^{-3} m s^{-1}.

$$\log(v_t) = \log(v_{t0}) + (N)\log(1-c) \quad \text{(Eq. 2)}$$

We repeated such batch settling test on the regenerated TiO_2-K particles after each thermal regeneration cycle, and found that the regeneration process did not significantly affect the settling ability of the TiO_2-K particles. It was foreseen that the TiO_2-K catalyst particles performed a higher settling ability than the P25 TiO_2. The high settling ability of the TiO_2-K catalyst makes its application technically promising in a slurry sequential batch reactor system for water/wastewater treatment.

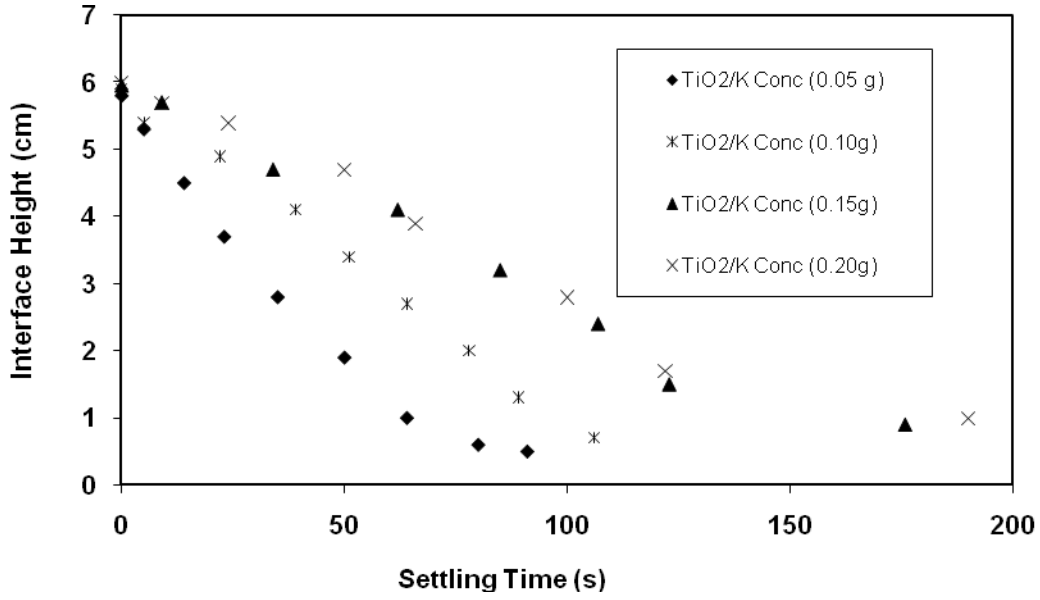

Figure 11: Settling curves for different TiO_2-K concentration in 25 mL of water.

4. Conclusion

The TiO_2 nanocrystals impregnated on the treated kaolin particles were synthesized using the modified two step sol-gel/surface heterocoagulation process. The delaminated flat surface of the treated kaolin prepared under consecutive series of acidification-alkalization-thermal treatment enables homogeneous partition of TiO_2 nanocrystals growth. Furthermore, the

chemical interaction between the deposited TiO_2 networks with the siliceous side of the kaolin via Ti-O-Si bonding endorsed the photostability of the prepared photocatalysts. Homogeneous distribution of the TiO_2 nanocrystals on kaolin surface enhances the photo-oxidation performance of the light photon activation process. During repetitive thermal regeneration, the surface-deposited microporous anatase TiO_2 was observed to meld into macroporous TiO_2 structure without any significant phase transformation to rutile. These were found to be accompanied by a slight reduction in specific surface area of the catalyst particles and increase in the average nanocrystals sizes. Parallel photoactivity probing with model CR indicates that the removal efficiency of TiO_2-K was comparable over the six thermal regenerative cycles. Additionally, the TiO_2-K nanocomposites showed a favourable settling ability for separation and recovery of the catalysts in the water treatment system. The high degradation efficiency, physical stability and high settling ability of the TiO_2-K could make the photocatalytic water treatment technology technically feasible and economically possible for an industrial application.

Acknowledgment

The authors are grateful to the technique advice given by Professor Shaomin Lei from Wuhan University of Technology, China, Associate Professor Huaiyong Zhu from Queensland University of Technology Australia, for in-kind sample analysis, and Unimin Australia Ltd. for kindly supplying clay mineral. This work was financially supported by the Australian Research Council Linkage Grant (LP0562076) and Australian Water Quality Centre through the Water Environmental Biotechnology Laboratory (WEBL) at the University of Adelaide.

Reference

[1] U.I Gaya, A.H. Abdullah, J. Photochem. Photobiol., C. 9 (2008) 1-12.

[2] I.K. Konstantinou, T. A. Albanis, Appl. Catal. B: Environ. 49 (2004), 1-14.

[3] N.T. Dung, N.V. Khoa, J-M. Herrmann, Int. J. Photoenergy. 7(2005), 11-15.

[4] O.K. Dalrymple, D.H. Yeh, M.A. Trotz, J. Chem. Technol. Biotechnol. 82 (2007) 121-134.

[5] J-M. Hermann, Catal. Today. 53 (1999) 115-129.

[6] Y. Gao, H. Liu, Mater. Chem. Phys. 92 (2005), 604-608.

[7] R.K. Wahi, W.W. Yu, Y. Liu, M.L. Mejia, J.C. Falkner, W. Nolte, V.L. Colvin, J. Mol. Catal. A: Chem. 242 (2005) 48-56.

[8] M.N. Chong, V. Vimonses, S. Lei, B. Jin, C. Chow, C. Saint, Microporous Mesoporous Mater. 117 (2009) 233-242.

[9] V. Vimonses, S. Lei, B. Jin, C.W.K. Chow, C. Saint, Appl. Clay Sci. 43 (2009) 465-472.

[10] P. Komadel, J. Madejová, in: F. Bergaya, B.K.G. Theng, G. Lagaly, (Eds.), Handbook of Clay Science, Development in Clay science, vol.1, Elsevier, The Netherlands, 2006, pp. 263-287.

[11] A. Steudel, L.F. Batenburg, H.R. Fischer, P.G. Weidler, K. Emmerich, Appl. Clay Sci. 44 (2009) 95-104.

[12] D.J.A. Williams, K.P. Williams, J. Colloid Interface Sci.. 65 (1978) 79-87.

[13] G. Lagaly, in: F. Bergaya, B.K.G. Theng, G. Lagaly, (Eds.), Handbook of Clay Science, Development in Clay science, vol.1, Elsevier, The Netherlands, 2006, pp.141-245.

[14] G. Jozefaciuk, G. Bowanko, Clays Clay Miner. 50 (2002) 771-783.

[15] R. Kun, K. Mogyorósi, I. Dékány, Appl. Clay Sci. 32 (2006) 99-110.

[16] S.I. Nishimoto, B. Ohtani, H. Kajiwara, T. Kagiya, J. Chem. Soc., Faraday Trans. 181 (1985) 61-68.

[17] H. Yoneyama, S. Haga, S. Yamanaka, J. Phys. Chem. 93 (1989) 4833-4837.

[18] H. Imai, K. Awazu, M. Yasumori, H. Onuki, H. Hirashima, J. Sol-Gel Sci. Technol. 8 (1997) 365-369.

[19] D. Beydoun, R. Amal, Mater. Sci. Eng., B. 94 (2002) 71-81.

[20] B.C. Gates, H. Knozinger, Advances in Catalysis, Elsevier Science Book Edition, 2004.

[21] K. Vinodgopal, P.V. Kamat, J. Phys. Chem. 96 (1992) 5053–5059.

[22] K. Kogo, H. Yoneyama, H.Tamaru, J. Phys. Chem. 84 (1980) 1705-1710.

[23] J. Krýsa, M. Keppert, J. Jirkovský, V. Štengl, J. Šubrt, Mater. Chem. Phys. 86 (2004) 333-339.

[24] A. Mills, S. Le Hunte, . 1997. J. Photochem. Photobiol., A. 108 (1997) 1-35.

[25] K. Kabra, R. Chaudhary, R.L. Sawhney, Ind. Eng. Chem. Res. 43 (2004) 7683–7696.

[26] T. Sasaki, S. Nakano, S. Yamauchi, M. Watanabe, Chem. Mater. 9 (1997) 602-608.

[27] R.H. Perry, D.W. Green, Perry's Chemical Engineering Handbook 7th Edition, McGraw-Hill, 1997.

[28] J.F. Richardson, J.H. Harker, J.R. Backhurst, Coulson & Richardso's Chemical Engineering Vol. 2, Particle Technology and Separation Processes, Butterworth-Heinemann,2003.

Brief Summaryof Chapter 4

The following important findings were generated in the researches associated with Chapter 4:

- A reproducible two step sol-gel method was developed for the synthesis of TiO_2 nanocrystals immobilized on the modified kaolinite clay substrate (TiO_2-K).
- During the synthesis process, the concentration of nitric acid used was found not only to have a profound effect on the gelation rate and behaviours but also on the final porosity of the TiO_2 nanocrystals formed on the external surface of the kaolinite.
- Chemical and thermal pre-treatments on the kaolinite clay enabled a highly delaminated flat surface for homogenous immobilization of TiO_2 sol.
- The thickness of the TiO_2 nanocrystals formed on the kaolinite clay was found to be highly dependent on the amount of kaolinite in suspension during the heterocoagulation process. The optimum kaolinite suspension was found to be 10% (w/v), resulting in a TiO_2 nanocrystal layer with a thickness of 7 nm.
- When the prepared TiO_2-K catalysts were subjected to heat treatment, the catalyst particles exhibited different physical properties (i.e. particle size, specific surface area and photoactive phase) under elevated temperature. The optimum calcination temperature for the conversion of amorphous-to-crystalline TiO_2 was 600^oC, which suppresses the appearance of rutile TiO_2 phase (i.e. has lower surface area due to the rupture of Ti-O bonds).
- The resultant heat-treated TiO_2-K catalyst particles were highly photostable, as attributed to the chemical Ti-O-Si bonding between the TiO_2 nanocrystals and the siliceous side of the kaolinite clay.
- During the regeneration process of the TiO_2-K catalysts, the initial microporous TiO_2 nanocrystals on the surface of the kaolinite clay was melded into a macroporous structure without any significant phase transformation. Such structure transition of the surface TiO_2 was accompanied by a reduction in specific surface area and an increase in the average nanocrystals sizes.
- Photoactivity study with the recycled TiO_2-K catalysts revealed that its photoactivity was retained high even after six thermal regeneration cycles.

- Furthermore, the TiO_2-K catalyst particles could be separated easily by means of sedimentation with a single particle terminal velocity of 5.28 x 10^{-3} ms^{-1}.

CHAPTER 5

OPTIMISATION OF AN ANNULAR PHOTOREACTOR PROCESS FOR DEGRADATION OF CONGO RED USING A TITANIA IMPREGNATED KAOLINITE AND H-TITANATE NANOFIBERS

SUB-CHAPTER 5.1

OPTIMISATION OF AN ANNULAR PHOTOREACTOR PROCESS FOR DEGRADATION OF CONGO RED USING A NEWLY SYNTHESIZED TITANIA IMPREGNATED KAOLINITE NANO-PHOTOCATALYST

M.N. Chong [a, b], S. Lei [c], B. Jin [a, b, d], C. Saint [b, d], C. W. K. Chow [d]

[a] School of Chemical Engineering, The University of Adelaide, Adelaide, SA 5000, Australia

[b] School of Earth and Environmental Sciences, The University of Adelaide, Adelaide, SA 5000, Australia

[c] School of Resource and Environmental Engineering, Wuhan University of Technology, Wuhan 430070, China

[d] Australian Water Quality Centre, SA Water Corporation, Bolivar, SA 5110, Australia

Separation and Purification Technology 2009; 67: 355-363.

STATEMENT OF AUTHORSHIP

OPTIMISATION OF AN ANNULAR PHOTOREACTOR PROCESS FOR DEGRADATION OF CONGO RED USING A NEWLY SYNTHESIZED TITANIA IMPREGNATED KAOLINITE NANO-PHOTOCATALYST

Separation and Purification Technology 2009; 67: 355-363.

Chong, M.N. (Candidate)

Performed experiment design; analysis of samples; interpreted data; manuscript evaluation; wrote manuscript.

Signed……*Date*……..……

Lei, S.

Performed experiment design; interpreted data.

I give consent for M. N. Chong to present this paper for examination towards the Doctor of Philosophy

Signed……*Date*……..……

Jin, B.

Manuscript evaluation; acted as corresponding author.

I give consent for M. N. Chong to present this paper for examination towards the Doctor of Philosophy

Signed……*Date*……..……

Saint, C.

Manuscript evaluation.

I give consent for M. N. Chong to present this paper for examination towards the Doctor of Philosophy

Signed……*Date*……..……

Chow, C. W. K.

Manuscript evaluation.

I give consent for M. N. Chong to present this paper for examination towards the Doctor of Philosophy

Signed……*Date*……..……

Chong, M.N., Lei, S., Jin, B., Saint, C. and Chow, C. (2009) Optimisation of an annular photoreactor process for degradation of congo-red using a newly synthesized titania impregnated kaolinite nano-photocatalyst.
Separation and Purification Technology, v. 67 (3), pp. 355-363, June 2009

SUB-CHAPTER 5.2

APPLICATION OF H-TITANATE NANOFIBERS FOR DEGRADATION OF CONGO RED IN AN ANNULAR SLURRY PHOTOREACTOR

M.N. Chong [a, b], B. Jin [a, b, c], H. Y. Zhu [d], C. W. K. Chow [c], C. Saint [b, c]

[a] School of Chemical Engineering, The University of Adelaide, Adelaide, SA 5000, Australia

[b] School of Earth and Environmental Sciences, The University of Adelaide, Adelaide, SA 5000, Australia

[c] Australian Water Quality Centre, SA Water Corporation, Bolivar, SA 5110, Australia

[d] School of Physical and Chemical Sciences, Queensland University of Technology, Brisbane, QLD 4001, Australia

Chemical Engineering Journal 2009; 150: 49-54.

STATEMENT OF AUTHORSHIP

APPLICATION OF H-TITANATE NANOFIBERS FOR DEGRADATION OF CONGO RED IN AN ANNULAR SLURRY PHOTOREACTOR

Chemical Engineering Journal 2009; 150: 49-54.

Chong, M.N. (Candidate)

Performed experiment design, analysis of samples; interpreted data; manuscript evaluation; wrote manuscript.

Signed……*Date*……..……

Jin, B.

Manuscript evaluation; acted as corresponding author.

I give consent for M. N. Chong to present this paper for examination towards the Doctor of Philosophy

Signed……*Date*……..……

Zhu, H. Y.

Manuscript evaluation.

I give consent for M. N. Chong to present this paper for examination towards the Doctor of Philosophy

Signed……*Date*……..……

Chow, C. W. K.

Manuscript evaluation.

I give consent for M. N. Chong to present this paper for examination towards the Doctor of Philosophy

Signed……*Date*……..……

Saint, C.

Manuscript evaluation.

I give consent for M. N. Chong to present this paper for examination towards the Doctor of Philosophy

Signed……*Date*……..……

Chong, M.N., Jin, B., Zhu, H.Y., Chow, C. and Saint, C. (2009) Application of H-Titanate nanobibers for degradation of Congo Red in an annular slurry photoreactor. *Chemical Engineering Journal, v. 150 (1), pp. 49 - 54, July 2009*

Brief Summary for Chapter 5

Specific research findings associated with Chapter 5 include:

- The application of two novel photocatalysts, namely titania impregnated kaolinite (TiO_2-K) catalyst and H-titanate nanofibers (TNC) for the degradation of Congo Red (CR) in an annular slurry photoreactor (ASP) system were demonstrated.
- The mechanism of photocatalysis in TiO_2-K catalyst was of adsorption predominated, where significant amount of CR was adsorbed on the external surface prior to the subsequent surface photocatalytic reaction.
- The two photocatalysts used exhibited distinct isoelectric property, where the point of zero charge (PZC) for the TiO_2-K catalysts was of slightly basic of 9.5 to a slightly acidic characteristic of 4.6 in TNC fibrils.
- TiO_2-K performed a higher PZC than the TNC catalyst. Photocatalytic reaction is functional at a wider pH range. The initial pH of the CR solution was the most determining factor in the feasible application of photocatalysts in the ASP system.
- The optimum operating conditions for the degradation of 40 mg L^{-1} CR in the ASP using (1) TiO_2-K catalysts were determined to be 6 g L^{-1} TiO_2-K, pH 7 and 7.5 L min^{-1} aeration; (2) TNC fibrils were determined to be 4 g L^{-1} TNC, pH 3 and 5.0 L min^{-1} aeration.
- The external mass transfer resistance in the TiO_2-K catalyst diminished with step increases in the aeration rate.
- Under the similar optimum operating conditions, the TiO_2-K catalyst was found to be capable to reduce the initial COD by 80% while the TNC fibrils showed a 90 % reduction after 4 h of irradiation.
- The LC-MS analysis revealed that eight possible oxidation intermediates were formed during the 7 h degradation period of CR. The resultant MS intermediate peaks were identified by matching them with both the NIST and NISTREP library data.
- The TNC fibrils can be easily separated with single particle terminal velocity of 8.38 x 10^{-4} ms^{-1}.

CHAPTER 6

STATISTICAL OPTIMISATION AND MODELLING OF PHOTOCATALYTIC PROCESS FOR MINERALIZATION OF CONGO RED

SUB-CHAPTER 6.1

A NEW APPROACH TO OPTIMISE AN ANNULAR SLURRY PHOTOREACTOR SYSTEM FOR DEGRADATION OF CONGO RED: STATISTICAL ANALYSIS AND MODELLING

M.N. Chong [a, b], B. Jin [a, b, c], C. W. K. Chow [c], C. P. Saint [c]

[a] School of Chemical Engineering, The University of Adelaide, Adelaide, SA 5000, Australia

[b] School of Earth and Environmental Sciences, The University of Adelaide, Adelaide, SA 5000, Australia

[c] Australian Water Quality Centre, SA Water Corporation, Bolivar, SA 5110, Australia

Chemical Engineering Journal 2009; 152: 158-166.

STATEMENT OF AUTHORSHIP

A NEW APPROACH TO OPTIMISE AN ANNULAR SLURRY PHOTOREACTOR SYSTEM FOR DEGRADATION OF CONGO RED: STATISTICAL ANALYSIS AND MODELLING

Chemical Engineering Journal 2009; 152: 158-166.

Chong, M.N. (Candidate)

Performed experiment design; analysis of samples; interpreted data; manuscript evaluation; wrote manuscript.

Signed……*Date*……..……

Jin, B.

Manuscript evaluation; acted as corresponding author.

I give consent for M. N. Chong to present this paper for examination towards the Doctor of Philosophy

Signed……*Date*……..……

Chow, C. W. K.

Manuscript evaluation.

I give consent for M. N. Chong to present this paper for examination towards the Doctor of Philosophy

Signed……*Date*……..……

Saint, C.

Manuscript evaluation.

I give consent for M. N. Chong to present this paper for examination towards the Doctor of Philosophy

Signed……*Date*……..……

Chong, M.N., Jin, B., Chow, C. and Saint, C. (2009) A new approach to optimise an annular slurry photoreactor system for degradation of Congo Red: statistical analysis and modelling.
Chemical Engineering Journal, v. 152 (1), pp. 158 - 166, October 2009

SUB-CHAPTER 6.2

RESPONSE SURFACE OPTIMIZATION OF PHOTOCATALYTIC PROCESS FOR DEGRADATION OF CONGO RED USING H-TITANATE NANOFIBER CATALYST

M.N. Chong [a, b], H. Y. Zhu [c], B. Jin [a, b, d]

[a] School of Chemical Engineering, The University of Adelaide, Adelaide, SA 5005, Australia

[b] School of Earth and Environmental Sciences, The University of Adelaide, Adelaide, SA 5005, Australia

[c] School of Physical and Chemical Sciences, Queensland University of Technology, Brisbane, QLD 4001, Australia

[d] Australian Water Quality Centre, SA Water Corporation, Bolivar, SA 5000, Australia

Chemical Engineering Journal 2010; 156: 278-285.

STATEMENT OF AUTHORSHIP

RESPONSE SURFACE OPTIMIZATION OF PHOTOCATALYTIC PROCESS FOR DEGRADATION OF CONGO RED USING H-TITANATE NANOFIBER CATALYST

Chemical Engineering Journal 2010; 156: 278-285.

Chong, M.N. (Candidate)

Performed experiment design; analysis of samples; interpreted data; manuscript evaluation; wrote manuscript.

Signed……*Date*……..……

Zhu, H. Y.

Manuscript evaluation.

I give consent for M. N. Chong to present this paper for examination towards the Doctor of Philosophy

Signed……*Date*……..……

Jin, B.

Manuscript evaluation; acted as corresponding author.

I give consent for M. N. Chong to present this paper for examination towards the Doctor of Philosophy

Signed……*Date*……..……

Chong, M.N., Zhu, H.Y. and Jin, B. (2010) Response surface optimization of photocatalytic process for degradation of Congo Red using H-Titanate nanofiber catalyst.
Chemical Engineering Journal, v. 156 (2), pp. 278 - 285, January 2010

Brief Summary of Chapter 6

Key research activities and important results in Chapter 6 are summarised as follow:

- This chapter demonstrated a new approach to optimize the photodegradation of CR in the ASP system. The Taguchi design of experiments (orthogonal array) approach was combined with the statistical analysis for determining the optimum operating factor combinations and the relevant factor interactions, if exist.

- With a combined DOE-statistical approach, the optimum factor combination using TiO_2-K catalyst was determined to be 8 g L^{-1} TiO_2-K, pH 5.0, 7.5 L min^{-1} aeration and 40 mg L^{-1} CR. Kinetics study resulted in a Langmuir-Hinshelwood apparent rate constant of 3.46 x 10^{-2} min^{-1}. Results from the statistical optimization using the TNC fibrils revealed that a factor combination of 4.0 g L^{-1} TNC, pH 3.0, 5 L min^{-1} aeration and 60 mg L^{-1} CR, leading to a reaction rate of 3.47 x 10^{-2} mol L^{-1} min^{-1}.

- Analysis of variance (ANOVA) revealed that (1) the initial CR concentration is the most significant factor that affects the CR photodegradation using TiO_2-K, while pH appeared to be the least significant factor; (2) pH is the most significant factor that affects the CR photodegradation using TNC fibrils, while TNC loading is the least significant one.

- The response surface analysis plots showed that (1) the aeration rate has a synergistic effect with the photocatalysts loading when TiO_2-K catalyst was used; (2) the pH has profound effect on the synergistic interaction with the TNC photocatalyst.

- The resultant regression equations from the analysis provided a system-specific correlation that can be used to predict the subsequent photocatalytic performance of the catalysts in the ASP system.

CHAPTER 7

DISINFECTION PERFORMANCE OF THE PHOTOCATALYTIC PROCESS: INACTIVATION ACTIVITY, KINETICS AND MODELLING

SUB-CHAPTER 7.1

PHOTO-DISINFECTION ACTIVITY AND KINETICS OF ESCHERICHIA COLI USING NOVEL TITANIA IMPREGNATED KAOLINITE CATALYST

M.N. Chong [a, b], B. Jin [a, b, c]

[a] School of Chemical Engineering, The University of Adelaide 5005 Adelaide Australia

[b] Schools of Earth and Environmental Sciences, The University of Adelaide 5005 Adelaide Australia

[c] Australian Water Quality Centre, South Australian Water Corporation, 5000 Adelaide South Australia

Submitted manuscript to Chemical Engineering Journal.

STATEMENT OF AUTHORSHIP

PHOTO-DISINFECTION ACTIVITY AND KINETICS OF ESCHERICHIA COLI USING NOVEL TITANIA IMPREGNATED KAOLINITE CATALYST

Submitted manuscript to Chemical Engineering Journal.

Chong, M.N. (Candidate)

Performed experiment design; analysis of samples; interpreted data; manuscript evaluation; wrote manuscript.

Signed……*Date*……..…

Jin, B.

Manuscript evaluation; acted as corresponding author.

I give consent for M. N. Chong to present this paper for examination towards the Doctor of Philosophy

Signed……*Date*……..

Photo-Disinfection Activity and Kinetics of *Escherichia coli* using Novel Titania Impregnated Kaolinite Catalyst

Meng Nan Chong [a, b], Bo Jin [a, b, c*]

[a] School of Chemical Engineering, The University of Adelaide 5005 Adelaide Australia

[b] Schools of Earth and Environmental Sciences, The University of Adelaide 5005 Adelaide Australia

[c] Australian Water Quality Centre, South Australian Water Corporation, 5000 Adelaide South Australia

[*] To whom correspondence should be addressed.

Tel.: +61 8 8303 7056. Fax: +61 8 8303 6222. Email: bo.jin@adelaide.edu.au

Abstract

We have recently developed a novel titania impregnated kaolinite (TiO_2-K) catalyst and an annular slurry photoreactor (ASP). The present study was to determine its optimal operational factors: TiO_2-K loading, pH, aeration rate, bacterial population and irradiation time, and their impact on disinfection activity and kinetics of a sewage isolate of *Escherichia coli sp.* (ATCC 11775). The disinfection kinetics was evaluated with experimental data and three Hom series empirical models, namely; Hom model, modified-Hom model and Hom-Power model. The bacterial inactivation rate in the ASP-TiO_2-K system was pH-independent up to pH 7.0. At the optimum conditions, 120 min irradiation time was required to achieve 5 bacterial log-reduction units for an average bacterial inoculum size of 8.0×10^6 CFU mL^{-1}. A sigmoid-shape bacterial inactivation profile with strong shoulder and prolonged tailing characteristics was proved. The inactivation kinetic studies revealed that among the Hom series models the modified Hom model appeared to be the best empirical model that represents the disinfection kinetics with three different inactivation characteristic regions in the ASP-TiO_2-K system.

Keywords: TiO_2; Kaolinite Clay; Annular Reactor; Disinfection; Empirical Kinetics Modelling; *E.Coli;* Photocatalysis.

1. Introduction

Water disinfection is one of the most important final treatment stages to ensure the water is free of pathogenic microbes that might convey severe waterborne diseases [1]. To date, various chemical disinfection methods such as chlorination and chloramination have been widely practiced. However, it has been widely concerned that these disinfection methods have serious environmental drawbacks as chlorine can react with many natural organic matters or dissolved organic carbons to form recalcitrant disinfection by-products (DBPs) [2 - 5]. Coleman et al. [5] have reported that low concentration of common DBPs in water such as haloacetic acid (60 ppb) and trihalomethanes (80 ppb) might cause serious congenital cardiac defects in human beings when consumed. In addition, poor maintenance of ammonia during chloramination might result in direct nitrification in water which directly promotes algal bloom and treatment costs [6]. Considering preventing the use of the chemical disinfection methods, various chemical-free water disinfection technologies without the formation of DBPs are highly soughed in recent years.

Among the chemical-free disinfection methods, heterogeneous photocatalysis employing titanium dioxide (TiO_2) has been investigated [7 – 9]. Photocatalytic water disinfection operates in a semiconductor system, where the TiO_2 particles are mixed with the targeted water being subjected to UV irradiation. When the TiO_2 particles are irradiated by UV light, the photon energy excites the lone electron from its conduction band to valance band to form electron-hole pairs [10 – 12]. In the presence of electron scavengers, the availability of the valence band is prolonged with surface adsorbed hydroxyl groups being oxidized to radicals [13]. These hydroxyl radicals ($OH^{\cdot}$) are primarily responsible for the inactivation and destruction of microorganisms [13]. In the absence electron scavengers, no photocatalytic reaction occurs due to the rapid recombination of electron-hole pairs. The detailed photochemical reactions on the TiO_2 surface during photocatalysis have been discussed in numerous literatures [14, 15].

Since the pioneering work by Matsunaga and the co-workers, a number of preliminary photocatalytic disinfection studies have been shown to inactivate successfully various

coliforms, viruses, bacteria, cysts, fungi, algae and protozoa [16 – 19]. Commercial Degussa P25 TiO_2 has been used in most previous studies. Except for those studies of Pulgarin and co-workers [11, 20, 21], very few other case studies of pilot and large scale processes of such photocatalytic disinfection technologies for water treatment have been reported. A bottle-neck technical and economical issue associated with photocatalytic treatment process using P25 TiO_2 is the difficulty and high cost of separating the fine P25 TiO_2 particles (10–30 nm) [22]. Numerous material engineering solutions have been investigated in order to resolve this problem. One of the more prominent solutions is to immobilise the TiO_2 nanoparticles onto an inert carrier to retain its quantum effects, while allowing ease of separation from the treated water stream [23 – 27]. Different materials have been successfully demonstrated as potential carriers for TiO_2 nanoparticles, including optical fibers, clay materials and magnetic core [28 – 30].

We synthesized a novel titania impregnated kaolinite (TiO_2-K) catalyst, in which nanocrystals TiO_2 (7.0 nm) particles are immobilised onto layered kaolinite clays (3.5 microns). Due to its high photo-oxidation capacity and recoverable characteristics, the TiO_2-K catalyst has been proven to be a promising catalyst for the photocatalytic water treatment. Previously, we have examined the photocatalytic activity of the TiO_2-K particles against the degradation of dye molecules in an annular slurry photoreactor (ASP) [11, 31, 32]. In this study, the photo-disinfection performance of the TiO_2-K catalyst was tested against a sewage isolated *Escherichia coli* (ATCC 11775). *E.coli* is a common surrogate for measure against treatment efficacy. The use of a strain isolated from sewage allows the measurement of disinfection ability of the treatment process in a natural environment. The effects of operation factors of the ASP system on the irradiation time required to inactivate 5 bacterial log-reduction units were investigated. These included the TiO_2-K loading, pH, aeration rate and bacterial inoculum size. Subsequently, we evaluated the inactivation kinetics using the empirical Hom series models for comparison and modelling of the disinfection system. The Hom series models used were Hom model, modified Hom model and Hom-Power model.

2. Materials and Methods

2.1. Materials

Chemicals employed for the synthesis of TiO_2-K included titanium (IV) butoxide (tetrabutyl orthotitanate, purum grade ≥97% gravimetric, Sigma–Aldrich), absolute ethanol (AR grade, Labserv Pronalys Australia), nitric acid (AR grade 69 wt%, BDH VWR, England), and raw kaolinite clays (Unimin, South Australia). Hydrochloric acid (Labserv Pronalys, Australia), sodium hydroxide (Analar grade, BDH Chemicals, England), tryptone soy broth media (TSB) (Oxoid, England) and plate count agar (PCA) (Merck, Germany) were prepared to a desired concentration by the addition of Milli-Q water obtained from Barnstead Nanopure ion exchange water system with 18.2 MΩ-cm resistivity.

2.2. Preparation of Titania Impregnated Kaolinite Catalyst

The TiO_2-K catalyst particles were synthesized in accordance with our previously developed method [30]. A modified two step sol–gel method was used, where 25 mL titanium precursor was hydrolysed by 30 mL absolute ethanol. The resultant hydrolysed mixture was then acid-catalysed under controlled nitric acid conditions. In the following step, this catalysed product was heterocoagulated with 10% (w/v) kaolinite suspension at 37^oC under constant stirring. Prior to the heterocoagulation, the kaolinite clays were pre-treated in a series of alkalization and thermal treatments at 750^oC for 1 h. The kaolinite particles were used as the inert carriers for the deposition of titania sol, enabling ease of catalyst particles separation during the water disinfection application. The heterocoagulated products were filtered and washed repeatedly with distilled water up to three times to remove any excess chemical impurities. The filtrate cake was dried in a conventional oven at 65-70^oC for 3 h, before being fired at 600^oC. Fig. 1 shows the scanning electron microscopic images of the TiO_2-K catalyst at different magnifications.

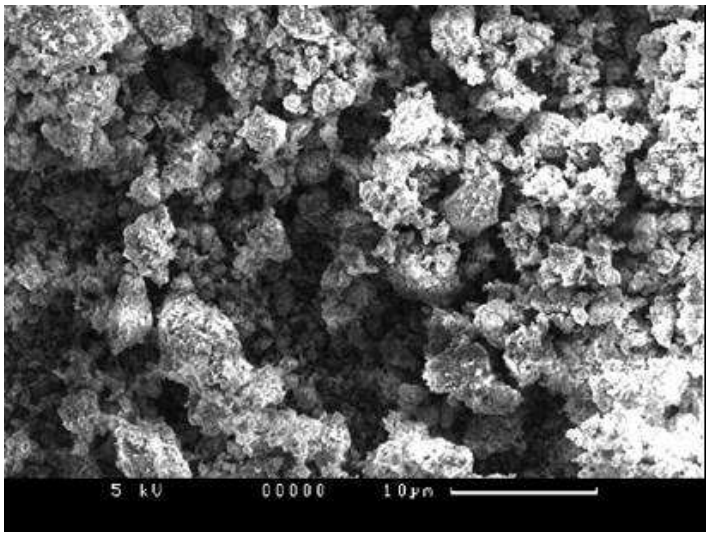

(a)

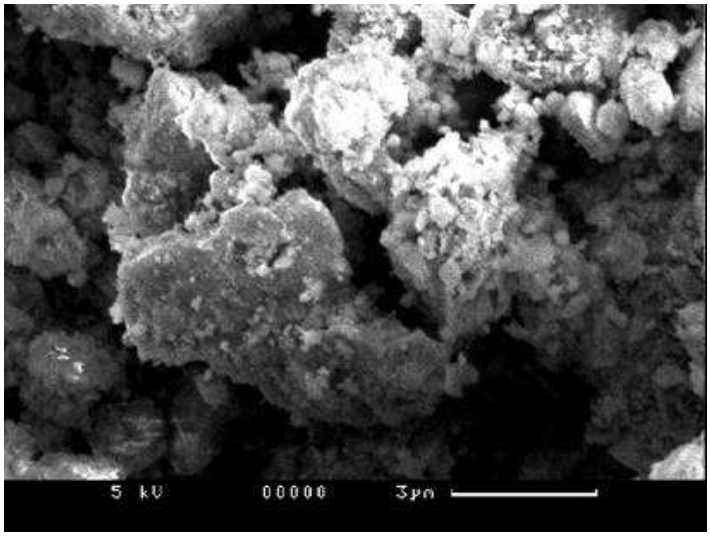

(b)

Figure 1: Scanning electron microscopic images of the TiO_2-K catalyst (a) 10 μm resolution; (b) 3 μm resolution.

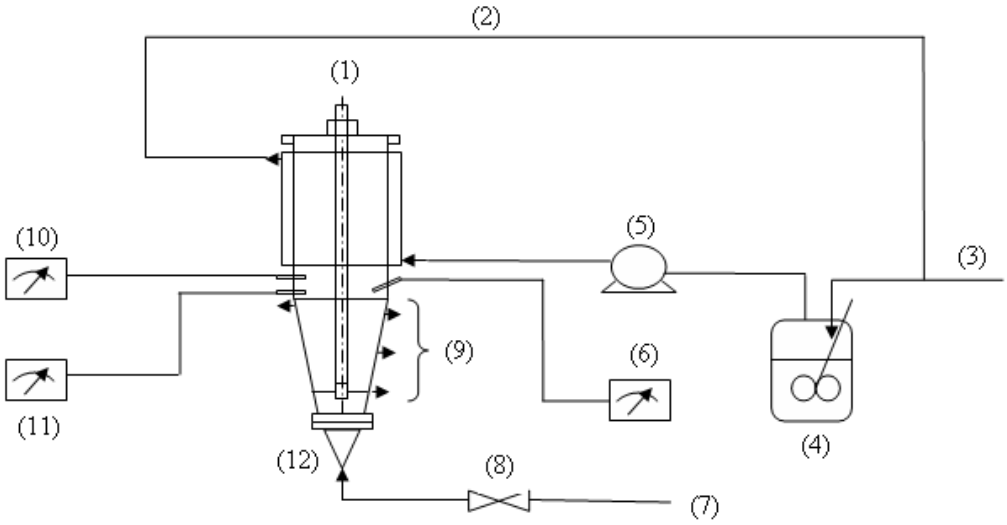

Figure 2: Experimental set-up for the annular slurry photoreactor system: (1) UV light, (2) Recirculation water line, (3) Fresh cool water line, (4) Cooling water vessel, (5) Cooling water pump, (6) Temperature meter, (7) Compressed air supply line, (8) Compressed air regulation valve, (9) Sampling ports, (10) pH meter, (11) Dissolved oxygen meter, (12) Photoreactor.

2.3. Annular Slurry Photoreactor

In this study, a stainless steel ASP was used as a photo-disinfection reactor [11, 31, 32]. The ASP was a three-phase bubble column reactor, where the TiO_2-K particles were dispersed in the targeted water by bubble aeration. A detachable conical bottom was made to the ASP to prevent reaction dead zone for the TiO_2-K catalyst, as well as promoting ease of cleaning and maintenance. At the lower end, a 45 μm air sparger was fitted to provide homogeneous aeration for catalyst suspension and mixing. An UV-A black light of 8W (NEC, Holland) light was positioned annularly within a quartz thimble to prevent direct contact with the reaction fluid, while allowing optimal UV transmission into the annulus reaction zone. An UV-A light was used for photonic excitation of the TiO_2-K catalyst alone. Unlike the germicidal UV-C light with high-end UV electromagnetic spectrum, the associated UV energy for UV-A is significantly lower and does not cause substantial direct bacterial inactivation. The wavelength range of UV-A light lies between 315 – 400 nm, which is close to solar irradiation. Samples were collected from the four-descended level sampling ports. Electronic probes and meters for in-situ data logging of pH, dissolved oxygen and temperature (TPS, Australia) were connected

to the reactor. The operating temperature for the ASP system was kept at 25^{o}C. The detailed design of the ASP and experimental setup are shown in Fig. 2.

2.4. Cell Culture, Medium Preparation and Bacterial Counting

To prepare the bacterial suspension, 50 mL fresh liquid culture prepared in TSB was inoculated with *E.coli* strain ATCC 11775. The cell culture was incubated in a rotary shaker at 150 rpm and 35^{o}C for 19 h until the late exponential phase. The cell density during the incubation was determined by heterotrophic plate counted (HPC), and found to be 9x10^{9} CFU mL^{-1} after 19 h. An aliquot of the incubated liquid culture was directly inoculated into 1.5 L of phosphate buffered saline (PBS) solution for bacterial suspension. The use of PBS is to prevent sudden osmotic shock to the bacteria, so as to maintain the bacterial numbers for accurate dilution purposes. The initial bacterial density was HPC similarly using standard procedures [33].

Prior to the photo-disinfection experiment, a known amount of TiO_2-K catalyst was mixed with the bacterial suspension and further dark homogenized for 30 min. The UVA light was turned on after the homogenisation period and the bubble aeration was run continuously for up to 300 min. Samples were collected every 10 min up to 40 min, thereafter every 20 min up to 120 min, and finally every 60 min up to 300 min. The enumeration of the *E.coli* was carried out following a standard serial dilution procedure and every sample was determined by HPC in the prepared PCA in duplicate. With the duplicate of 2.5 mL samples collected from the different sampling ports, a 0.1 mL was then diluted in serial of 0.9 mL PBS. After that, the diluted 0.1 mL of samples was HPC in triplicate in PCA to determine the eventual bacterial cell density. The PCA plates were then incubated at 35^{o}C for 24 h before final cell counting. The bacterial log-reduction against irradiation time curve was plotted for kinetic analysis. Each photo-disinfection experiments were then repeated for standard experimental verification and error analysis.

3. Results and Discussion

3.1. Effect of TiO_2-K Loading

Optimisation of the photocatalyst loading used in a photoreactor system is particularly important, affecting the overall treatment costs and process efficacy. Previous studies on photocatalyst loadings of the Degussa P-25 TiO_2 on microbial inactivation were reported to be in the range of 0.5–2.0 gL^{-1}, depending on the configuration of the photoreactor used [8, 17]. In this study, TiO_2-K dosing experiments were studied over a range of 4.0–10.0 gL^{-1}. The use of such catalyst weigh amplitude is owing to the weigh contribution by the kaolinite carrier. As previously determined using a zinc oxide spiking method in X-ray diffractionometry, the fractional weigh ratio of TiO_2:K is approximately 8 % (w/w) [30]. This indicates that the real TiO_2 loading used in this study is approximately 0.30–0.80 gL^{-1}.

Photolysis and dark control experiments were also conducted to measure the net bacterial inactivation level as mediated by different TiO_2-K catalyst loadings. In the UV-A photolytic experiment without TiO_2-K added, it was observed that less than a log bacterial reduction unit was achieved after 300 min of irradiation. This was owing to the UV-A light emits the least energetic fraction of UV spectra (3.10 – 3.94 eV) that usually cause least damage to the bacterial cell [21]. Rincon et al. [21] reported that the photo-killing by UV-A should be well-mediated by sensitizers, such as TiO_2 catalyst, to achieve greater bacterial cell damage. No inactivation activity was found in the control experiments using TiO_2-K without UV-A irradiation

When 4.0 gL^{-1} TiO_2-K was added (Fig. 3), it can be seen that the photo-killing in the ASP was significantly enhanced by approximately thirteen-folds. Such enhancement in bacterial inactivation was due to the formation of reactive oxygen species (ROS) such as $OH^{\bullet}$, $O_2^{\bullet-}$ and H_2O_2. Gyurek et al. [34] discussed that the activity of the ROS on the cytoplasmic membrane is rather cumulative than instantly lethal. This can be justified from the strong shoulder characteristic in the bacterial inactivation curve, where log-linear bacterial reduction started after 20 min UVA irradiation. Others view that such prolonged inactivation at the beginning of photocatalyst-mediated disinfection is owing to the slow permeation rate of the ROS (i.e. short

half-life) through the cell wall [35]. The irradiation time required to achieve approximately 5 log-reduction units was 300 min.

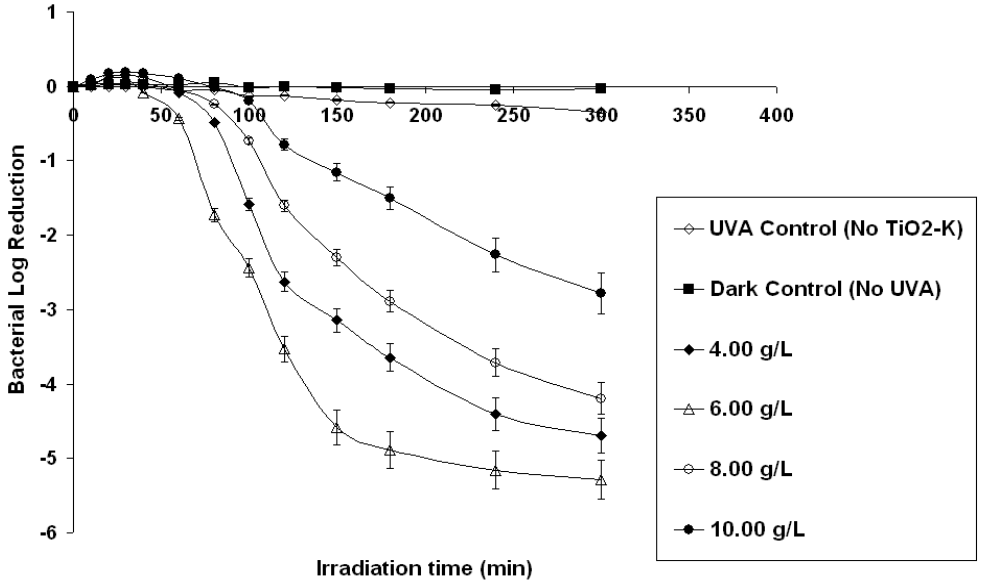

Figure 3: Effects of TiO_2-K catalyst loadings on the photocatalytic inactivation kinetics of *E.coli* at pH 7.0, 5.0 $Lmin^{-1}$ aeration and average initial bacterial population of $8.0x10^6$ CFU mL^{-1}.

At a high TiO_2-K loading of 6.0 gL^{-1}, however, the strong shoulder characteristics during bacterial inactivation was found to be depleted. A shorter UV-A irradiation time of 180 min was required to achieve a 5 log bacterial reduction units. At an increased TiO_2-K loading of 8.0 gL^{-1}, the bacterial inactivation kinetics become more sluggish than the 6.0 gL^{-1} loading. Similar attenuation in photo-disinfection efficacy was observed when 10.0 gL^{-1} of TiO_2-K loading was applied. It is worth noting that a further increased TiO_2-K loadings of 8.0 and 10.0 gL^{-1} resulted in little increasing disinfection efficiency. At a TiO_2-K loading 10.0 gL^{-1}, for instance, it was impossible to achieve a 5 log bacterial reduction unit even at an extended irradiation time. The highest bacterial inactivation levels using 8.0 and 10.0 gL^{-1} TiO_2-K at pH 7.0 were approximately 4 and 3 log reduction units, respectively. Such attenuations in photo-disinfection efficacy with increasing TiO_2-K loading indicate an increase in the overall light extinction coefficient. At a TiO_2-K particle concentration higher than 6.0 gL^{-1}, the radial light intensity across the annulus width (50 mm) was reduced as a direct result of rapid absorption and scattering by the TiO_2-K particles [12]. As a consequence, the TiO_2-K particles close to

the external cell wall were shielded from UV-A excitation and reduced the overall active TiO_2-K in suspension. In this ASP configuration, the overall reaction efficacy is a function of the catalyst loading, annulus width and light intensity used. If the light intensity remains unchanged, a smaller annulus width can tolerate higher TiO_2-K and vice versa. Considering the ASP operation, it can be concluded that the saturated TiO_2-K loading in the current experimental setup was 6.0 gL^{-1}. All the subsequent investigations were carried out at this TiO_2-K loading.

3.2. Effect of pH

In a semiconductor photocatalytic system, pH plays a key role in driving the oxidation reaction and efficiency. The pH can affect the surface charge of the photocatalyst used, and subsequently the rate of photooxidation [36 – 38]. When the pH is higher than the point of zero charge (PZC) of the TiO_2 catalyst, i.e. pH<PZC (TiO_2), the surface of the photocatalystsis positively charged, otherwise is oppositely charged at pH>PZC(TiO_2). For nominal TiO_2 catalysts, such as the P-25, their PZC usually lies in the range of 5.6-6.8 [37]. However, the PZC of the TiO_2-K particles used was determined to be 9.5 [11]. To investigate the effects of pH in the photo-disinfection of *E.coli* by the TiO_2-K catalyst, a variation of pH 4.0-10.0 was simulated in the ASP system.

E.coli is a Gram-negative bacterium with the outer cell membrane covered by a lipopolysaccharide layer of 1 – 3 microns thickness [39]. With the slightly negatively charged outer *E.coli* surface, it is expected that this bacterium could have an enhanced photo-disinfection rate with TiO_2-K catalyst at pH<PZC(TiO_2-K). This is owing to the nature of heterogeneous TiO_2 photocatalytic reaction, where the microbial contaminants transfer to the vicinity of TiO_2 surface for subsequent cyclic ROS penetration. The pH can affect the surface charge density of the TiO_2-K catalyst, according to the following equilibrium equations (Eq. 1-2) [9];

At pH<PZC: $TiOH + H^+ \leftrightarrow TiOH_2^+$ (Eq. 1)

At pH > PZC : $TiOH + OH^- \leftrightarrow TiO^- + H_2O$ (Eq. 2)

Fig. 4 illustrates the effect of pH 4.0-10.0 in the ASP on the photo-disinfection of *E.coli*. In this instance, the initial pH was adjusted using 0.1 M of sodium hydroxide and hydrochloric acid. Three control experiments on the direct UV-A photolysis and dark adsorption at both pH 4.0 and 7.0, were carried out to ensure that bacterial disinfection was mediated by the TiO_2-K photo-disinfection. Similar results of less than 1 log bacterial reduction unit were obtained in the UV-A direct photolysis, even when the pH was adjusted to 4.0. These agreed with the findings by Pulgarin and co-workers [9]. They found that the photolytic inactivation of *E.coli* was independent of initial pH between 4.0 and 9.0. Low degrees of bacterial reduction were also observed for the dark adsorption at both pH 4.0 and 7.0 without UVA irradiation. In this instance, pH 4.0 was observed to be optimal value to achieve a maximum disinfection levels for the TiO_2-K photocatalysis. Heyde et al. [40] explained that the negligible *E.coli* reaction to acid conditions was due to the presence of an acid tolerance response in the bacterium itself, which secreted the acid-induced proteins for bacterial acid-shock protection.

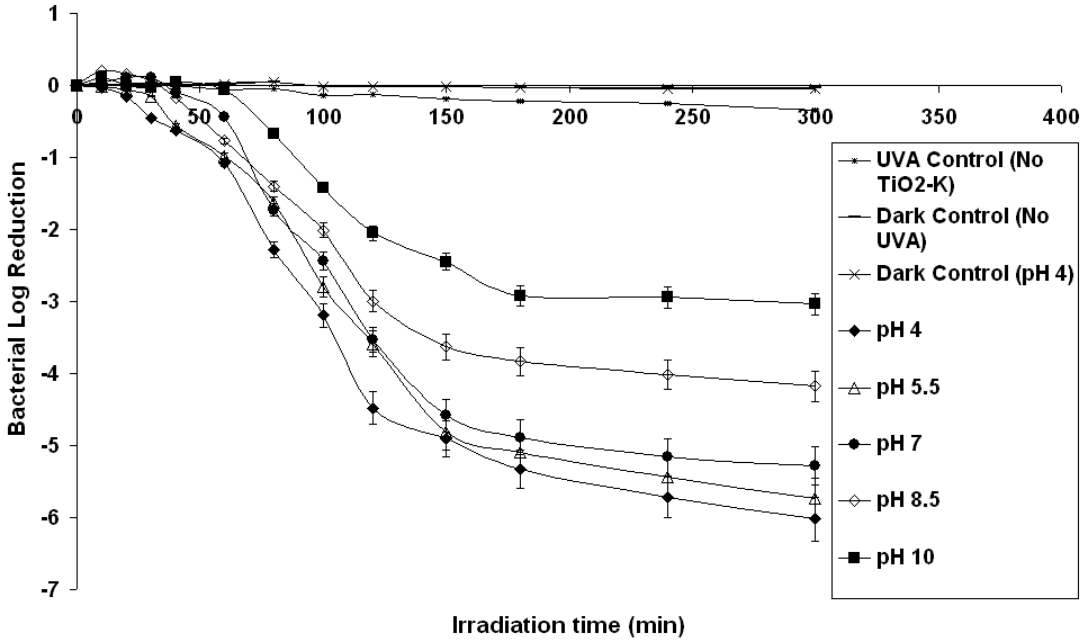

Figure 4: Effects of pH on the photocatalytic inactivation kinetics of *E.coli* at 6.0 gL^{-1} TiO_2-K, 5.0 $Lmin^{-1}$ aeration and average initial bacterial population of $8.0x10^6$ CFU mL^{-1}.

Fig. 4 indicates that a high photo-disinfection rate of *E.coli* was associated with a low pH. This may be attributed to the high proportion of dense $TiOH_2^+$ groups formed that draw the *E.coli* to the TiO_2-K surface for cell destruction. The total irradiation time required to achieve

5 log-reduction units was shortened to 150 min compared to pH 7.0. A declining trend in the photo-disinfection activity of the TiO_2-K was observed at pH up to 10.0. Similarly, the total irradiation time taken to achieve 5 log-reduction units at a pH over 8.5 was prolonged. It was however, interesting to note that bacterial inactivation during the tailing region was enhanced at a low pH. This was owing to more $TiOH_2^+$ groups generated and thus, increases in the electrostatic attraction force between the $TiOH_2^+$ groups and *E.coli*. The photo-disinfection activity was significantly reduced at pH 8.5 and 10, which was very close to PZC (TiO_2-K) = pH 9.5. Completely sluggish photo-disinfection kinetics of *E.coli* was observed at pH 10.0, in particular bacterial inactivation during the tailing region, as both TiO_2-K and *E.coli* surfaces become repellent of each other. It was however, noteworthy to find that the TiO_2-K catalyst with high PZC is highly functional over a wide pH range. Unlike conventional TiO_2 catalyst with low PZC, it can be concluded that disinfection using the TiO_2-K can be conducted at a wide pH range and a low pH can lead to a high disinfection rate due to the high electrostatic interaction. Thus, all the subsequent experiments were carried out at pH 4.0 in order to investigate the maximal photo-disinfection activity that could be attained.

3.3. Effect of Aeration

In the three phase ASP system, compressed air was used to disperse and keep the TiO_2 catalyst in suspension and in providing sufficient dissolved oxygen (DO) for electron-hole pair formation [11, 31, 32]. The extent of aeration, however, can affect the suspension states of the TiO_2-K particles in the ASP. Two different TiO_2-K suspension states can exist: homogeneous suspension where TiO_2-K particles are uniformly distributed throughout the ASP; and heterogeneous suspension where the TiO_2-K particles are non-uniformly distributed but in complete suspension [11].

To investigate the effect of aeration rate on the photo-disinfection activity of TiO_2-K-ASP system, a step change in aeration rate from 2.5 $Lmin^{-1}$ to 10.0 $Lmin^{-1}$ were evaluated (Fig. 5). Previously, the effect of aeration rate on the photodegradation of Congo red dye molecules was investigated [11]. At 2.5 $Lmin^{-1}$, we found large sediments of TiO_2-K particles on the sparger plate. This was because a low aeration pressure cannot remain the TiO_2-K particles suspended in the reactor. The photo-disinfection kinetic profile associated with 2.5 $Lmin^{-1}$, was found to exhibit strong shoulder characteristics. Marugan et al. [4] proposed that the

appearance of such shoulder characteristics was due to the low volumetric generation rate of ROS. This means that the amount of active TiO_2-K in suspension is low, resulting in strong bacterial growth inhibition on the photo-disinfection activity of TiO_2-K catalyst.

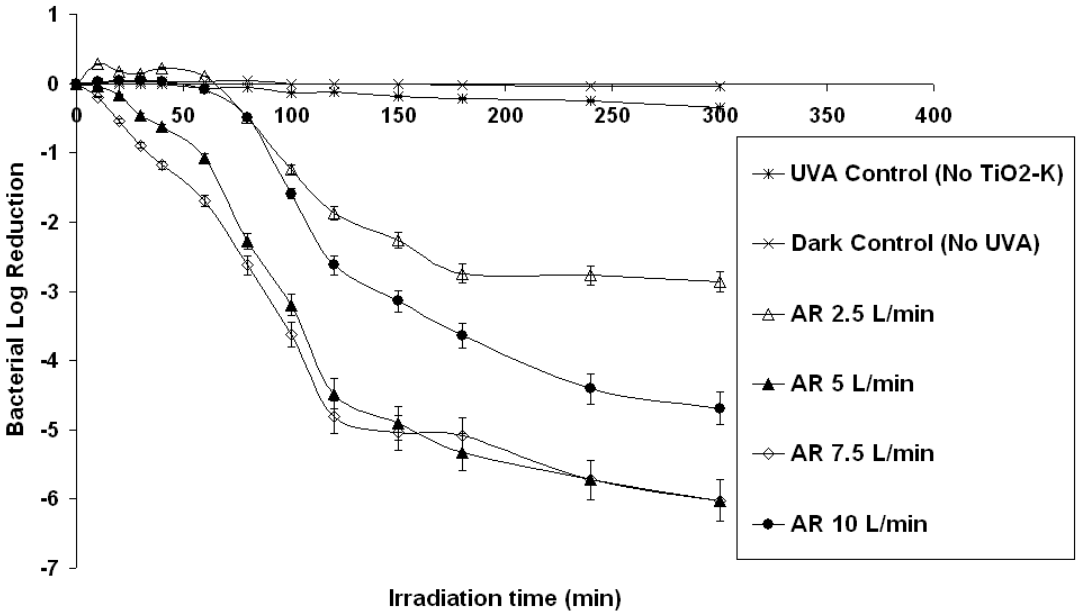

Figure 5: Effects of delivered aeration rate on the photocatalytic inactivation kinetics of *E.coli* at 6.0 gL^{-1} TiO_2-K, pH 4.0 and average initial bacterial population of $8.0x10^6$ CFU mL^{-1}.

The overall photo-disinfection rate was lower at 2.5 $Lmin^{-1}$ than at 5.0 $Lmin^{-1}$. This was evidenced from the prolonged irradiation time required to achieve only 3 log-reduction units after 300 min. Our previous experiments shown that TiO_2-K particles could remain in homogeneous suspension in the ASP at 7.5 $Lmin^{-1}$. Similarly, the optimal rate obtained in this photo-disinfection study was 7.5 $Lmin^{-1}$, where only 120 min was required to achieve 5 log bacterial reduction units. It was interesting to note that the shoulder characteristic was disappeared when the ROS volumetric generation rate is high. Thus, it can be verified that shoulder characteristic in the disinfection kinetics is a strong function of ROS volumetric generation rate, which is dependent on the state of catalyst suspension. A further increase in the aeration rate (10 $Lmin^{-1}$) resulted in a low disinfection rate compared with those at 5.0 and 7.5 $Lmin^{-1}$, respectively. Chin et al. [41] reported that a high aeration rate can create turbulence in the reaction water mixture, resulting in a "shadow" effect that attenuates light

distribution within the reactor. It can be thus, concluded that the optimum aeration was 7.5 $Lmin^{-1}$. All the subsequent experiments will be aerated at 7.5 $Lmin^{-1}$.

3.4. Effect of Bacterial Population

The number of viable bacteria in different water sources may vary. It is thus practicable to investigate the effect of bacterial population size on the photo-disinfection kinetics in the ASP. Dunlop et al. [42] found that inactivation rate was proportional to the initial bacterial loading present in water. At a high loading, the probability of collision between the *E.coli* and catalyst used increases and directly reduces the mass transfer rates at the catalyst surface. Similar observation was reported by Pham et al. [43] in their study on *Bacillus pumilus* spores in a slurry reactor.

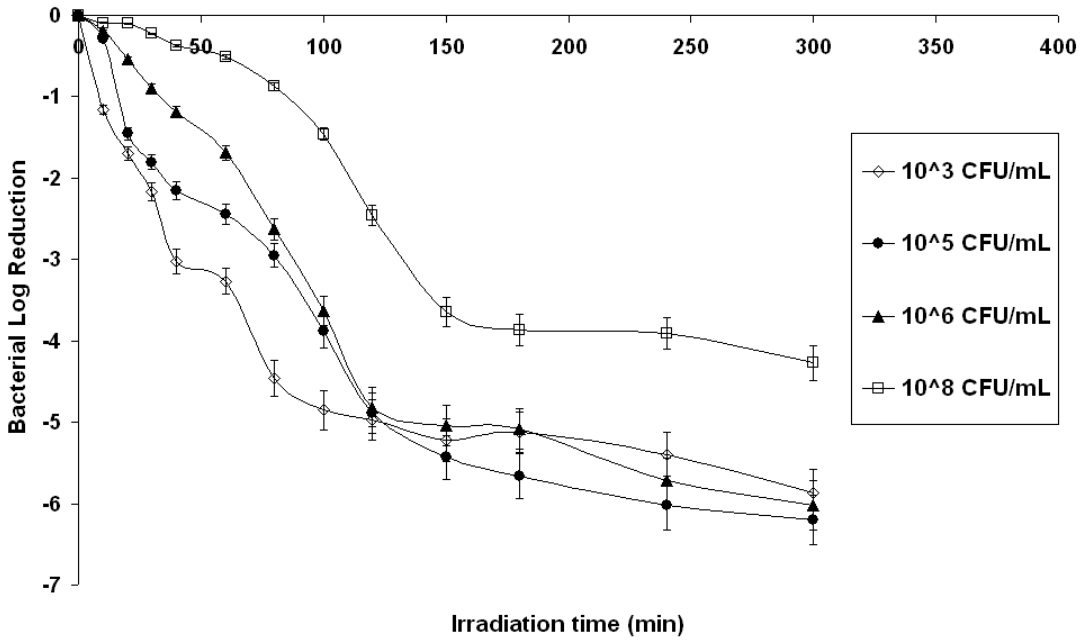

Figure 6: Effect of bacterial population on the photocatalytic inactivation kinetics of E.coli under operating conditions of ASP: TNC loading of 6.0 gL^{-1}, pH 4.0 and aeration rate of 7.5 $Lmin^{-1}$.

Fig. 6 shows the effect of the initial bacterial population on the photocatalytic inactivation rate of *E.coli*. The inactivation rate increased with the bacterial cell loadings from 10^5 to 10^6 CFU mL^{-1}, and thereafter decreased significantly owing to the effect of increasing bacterial population on the light extinction coefficient. A longer irradiation time was seen to be required

at the higher bacterial cell loading. Such observations might be due to the annulus width of the ASP, where any increase in turbidity (bacterial cell loading) might attenuate the radial light intensity. This was associated with the current annulus width of 50 mm, where the ASP system posses a limitation to a certain range of bacterial loading. From Fig. 6, it was determined that the most viable bacterial loading was 10^3–10^6 CFU mL^{-1}. A direct quantification on the photo-disinfection rate was evaluated (Section 3.5) using the Hom model series.

3.5. Evaluation of Empirical Models for the Photo-Disinfection in ASP System

Since the first application of TiO_2 catalyst by Matsunaga and the co-workers [16] for microbial inactivation, most photo-disinfection kinetic modelling works were based on the Chick-Watson (CW) model [7, 35]. In this CW model, the enumerated bacteria were proportional to the contact time. This correlation, however, can not be applicable for every instance as factors such as the reactor configuration. Inactivation mode and the bacterial resistance to disinfectant used might also cause severe non-linearity characteristics. From the previous sections, we found that the photo-disinfection kinetics of *E.coli* by UVA/TiO_2-K yielded non-linear profiles with both shoulders and tailing characteristics. The use of CT-design concept in CW model in this instance could "over-simplify" the photo-disinfection rate, resulting in generating inaccurate information for design of a photocatalytic disinfection system.

In this section, the applicability of Hom series models was evaluated for the representation of photo-disinfection kinetics of *E.coli* in the ASP system with three different inactivation characteristics. Mostly, the TiO_2-K inactivation profile begins with (i) a lag or initial smooth decay, known as the "shoulder", followed by (ii) a typical log-linear inactivation region, and ends with (iii) a long deceleration process at the end of the disinfection, which is known as the "tail" [4]. Within the Hom series models, three different Hom-based empirical models, namely; Hom model, modified-Hom model and Hom-Power model were compared and evaluated. The differences in the empirical modes are the number of empirical parameters, which directly correspond to the number of non-linearity that occurs within a disinfection profile. In all instances, the photo-disinfection kinetics is assumed to be demand-free where the photocatalyst loading is constant with contact time.

Hom [44] proposed the empirical Hom model after observing that the survivor plots of natural algal-bacterial systems were curvilinear, rather than typical log-linear type (Eq. 3);

$$\log\frac{N}{N_O} = -kC^nT^m \qquad \text{(Eq. 3)}$$

where log N/N_o = log bacterial reduction unit; N is the bacterial population at time, t; N_o is the initial bacterial population; k = experimental reaction rate; C = concentration of photocatalyst used; T is the applied irradiation time and m, n = empirical parameters. This two-parameter empirical model predicts the bacterial inactivation in a non-linear function for both C and T and is directly dependent on the model parameters n and m, respectively. Owing to the two-parameter nature of the model, it can only account for either shoulder or tailing characteristics but not both. A modification (Eq. 4) to incorporate an additional empirical parameter was made to accurately account for the three different inactivation characteristics [4, 35];

$$\log\frac{N}{N_O} = -k_1\left[1-\exp(-k_2t\right]^{k_3} \qquad \text{(Eq.4)}$$

where k_1, k_2 and k_3 is the empirical constants for the modified Hom model. Similarly, a further modification was modified and integrated according to the Rational Model with the introduction of parameter x to yield the Hom-Power model (Eq. 5) [45];

$$\log\frac{N}{N_O} = -\frac{\log\left[1+N_O^{x-1}(x-1)kC^nT^m\right]}{(x-1)} \qquad \text{(Eq. 5)}$$

where x is the additional empirical parameter for the Hom-Power model. Table 1 shows the evaluation and comparison of the Hom model series for modelling the photo-disinfection activity using TiO_2-K under optimum condition. All these models were then fitted to the experimental data via a non-linear approach, where the Excel® solver function was used together with the correlation coefficient as an indicator for the degree of fittingness. The outcomes revealed that both the Hom and modified Hom models show a high degree of fittingness, while the Hom-Power model was over-parameterization. These were evidenced

from the high correlation to unity by the Pearson correlation coefficient values (R^2). The Hom model has a limited application under optimum condition only, where the shoulder characteristic becomes less subtle. The *m*-value for the Hom model was then estimated to be 0.8792, which only accounted for the tailing region of the *E.coli* inactivation curves. This *m*–value actually suggested the presence of strong tailing during the disinfection in the ASP system. Similar tailing observation with m-value less than unity was observed by Roy and co-workers [46] during their ozone inactivation study on poliovirus type I.

Table 1: Estimated values for the empirical Hom series parameters during the photocatalytic inactivation kinetics of *E.coli* under optimum operational conditions.

Empirical Model	***k***	***k_1***	***k_2***	***k_3***	***m***	***n***	***x***	***N_o***	***Correlation coefficient R^2***
Hom	0.0622	-	-	-	0.8792	0.4288	-	-	0.9821
Modified Hom	-	5.7561	0.0288	6.2582	-	-	-	-	0.9904
Hom-Power	3.9687	-	-	-	0.2945	0.9008	1.0009	8.00E+06	0.8117

A better fittingness was observed with the modified Hom model under the optimum condition. This modified Hom model gives a more realistic mathematical expression as it takes into account the three different inactivation characteristics in the kinetic profiles. Marugan et al. [4] have used a similar modified Hom model for the photo-disinfection kinetic modelling of *E.coli* with standard P-25 TiO_2. From comparison, we found that the TiO_2-K used in this study has a comparable photo-disinfection activity but possesses an additional separation edge for possible large-scale operation. Fig. 7 shows the fitting of the modified Hom model for different bacterial loadings along with its empirically-estimated parameters. Low degree of fittingness, however, was observed with the Hom-Power model when comparing its R^2 value with the other Hom series models. This four-parameter empirical model was found to have logarithmic-constrained inflexion on the bacterial inactivation modelling, to simultaneously represent shoulder and tailing behaviours. A comparison plot on the fitting of different Hom

series model under optimum condition is shown in Fig. 8. Thus, it can be concluded that the modified Hom model provides a more realistic empirical model to account for the non-linear photo-disinfection profiles of *E.coli* in the ASP system.

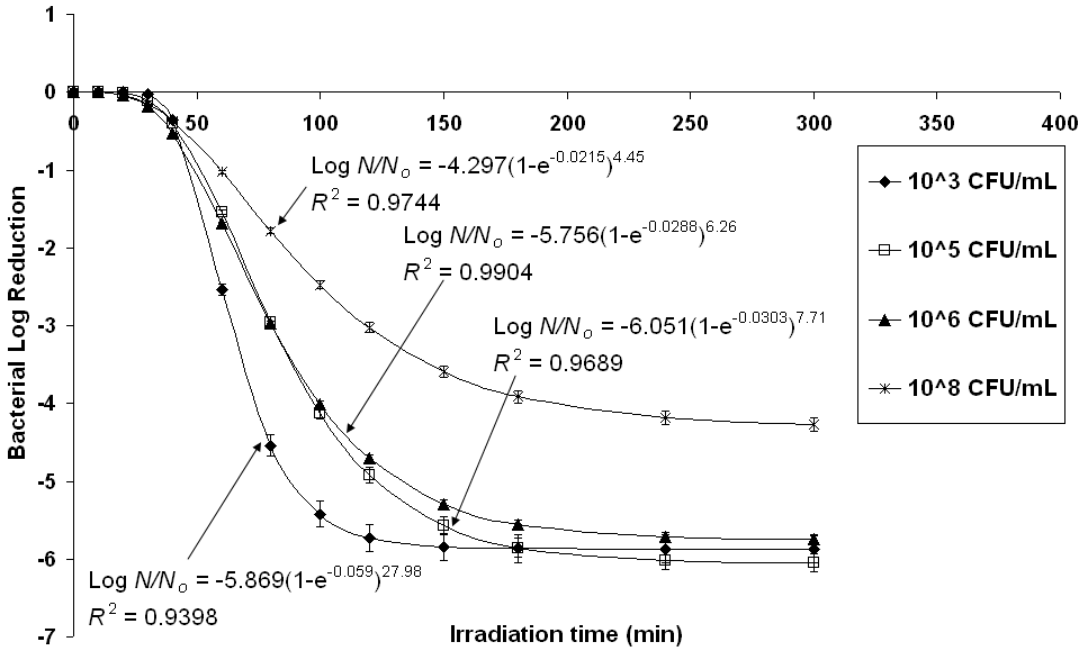

Figure 7: Fitting of modified Hom model to the photocatalytic inactivation kinetics of *E.coli* for different initial bacterial populations under optimum treatment conditions.

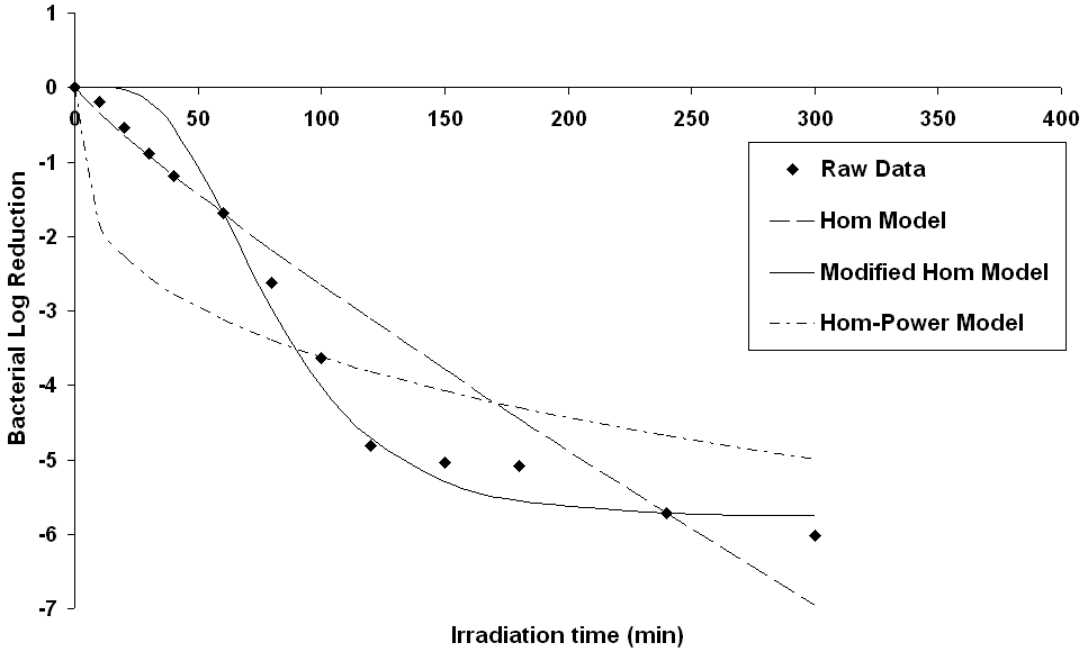

Figure 8: Comparison of the Hom series model for the fitting of photocatalytic inactivation kinetics of *E.coli* at optimum treatment conditions.

4. Conclusion

The photo-disinfection kinetics of *E.coli* strain (ATCC 11775) using TiO_2-K particles as an alternative photocatalyst was demonstrated successfully in this study. Under the illumination by UV-A light, a 5-log bacterial reduction unit was achieved after 70 min at the optimal operation conditions. The optimal operating conditions for the ASP system were experimentally determined as 6 gL^{-1} TiO_2-K loading, pH 4.0 and 7.5 $Lmin^{-1}$ aeration rate. It was found that the TiO_2-K catalyst was operable under wider span of pH conditions of up to pH 7.0 compared to other conventional photocatalysts. A very low photo-disinfection rate was achieved at pH 10.0, which is related to the surface charge alteration of PZC (TiO_2-K) that weakens the *E.coli* interaction link. All disinfection experiments demonstrated a highly non-linear bacterial inactivation kinetic profile, which started with shoulder lag, log-linear bacterial deactivation and prolonged tailing. The shoulder characteristic was strongly influenced by both the optimal TiO_2-K dosing and homogeneous dispersion. Subsequent evaluation on the aptness of Hom series model in representing the photo-disinfection of TiO_2-K catalyst in the ASP found that the modified Hom model is the best empirical model. Both the Hom and Hom-Power model were seen to be under and over-parameterized the kinetic profiles with three different inactivation regions. From this study, it is anticipated that the ASP-TiO_2-K system could be applied as an alternative disinfection method to replace the current chemical disinfectant methods in the water industry.

Acknowledgement

The authors would like to thank Ms Vipasiri Vimonses for her assistance during the study. This work was funded by the Australian Research Council Linkage Grant (LP0562153) and the Australian Water Quality Centre, SA Water Corporation through the Water Environmental Biotechnology Laboratory (WEBL) at the University of Adelaide, Australia.

References

[1] D.D. Sun, J.H. Tay, K.M. Tan, Water Research 37 (2003) 3452-3462.

[2] H. Yang, H. Cheng, Separation and Purification Technology 56 (2007) 392-396.

[3] J. Lu, T. Zhang, J. Ma, Z. Chen, Journal of Hazardous Materials 162 (2009) 140-145.

[4] J. Marugán, R.V. Grieken, C. Sordo, C. Cruz, Applied Catalysis B: Environmental 82 (2008) 27-36.

[5] H.M. Coleman, C.P. Marquis, J.A. Scott, S.S. Chin, R. Amal, Chemical Engineering Journal 113 (2005) 55-63.

[6] A. Sathasivan, I. Fisher, T. Tam, Water Research 42 (2008) 3623-3632.

[7] M. Cho, H. Chung, W. Choi, J. Yoon, Water Research 38 (2004) 1069-1077.

[8] A.G. Rincón, C. Pulgarin, Applied Catalysis B: Environmental 44 (2003) 263-284.

[9] A.G. Rincón, C. Pulgarin, Applied Catalysis B: Environmental 51 (2004) 283-302.

[10] L. Rizzo, J. Koch, V. Belgiorno, M.A. Anderson, Desalination 211 (2007) 1 – 9.

[11] M.N. Chong, S. Lei, B. Jin, C. Saint, C.W.K. Chow, Separation and Purification Technology 67 (2009) 355 – 363.

[12] I.J. Ochuma, R.P. Fishwick, J. Wood, J.M. Winterbottom, Applied Catalysis B: Environmental 73 (2007) 259 – 268.

[13] J.M. Herrmann, Catalysis Today 53 (1999) 115 – 129.

[14] I.K. Konstantinou, T.A. Albanis, Applied Catalysis B: Environmental 49 (2004) 1 – 14.

[15] R.J. Watts, S. Kong, W. Lee, Journal of Environmental Engineering 121 (1995) 730 – 735.

[16] T. Matsunaga, R. Tomodam, T. Nakajima, H. Wake, FEMS Microbiology Letter 29 (1985) 211-214.

[17] E.J. Wolfrum, J. Huang, D.M. Blake, P.C. Maness, Z. Huang, J. Fiest, Environmental Science and Technology 36 (2002) 3412-3419.

[18] J. Hong, M. Otaki, Journal of Bioscience and Bioengineering 96 (2003) 298-303.

[19] J.A. Ibánez, M.I. Litter, R.A. Pizarro, Journal of Photochemistry and Photobiology A: Chemistry 157 (2003) 81-85.

[20] A.G. Rincón, C. Pulgarin, Catalysis Today 101 (2005) 331 – 344.

[21] A.G. Rincón, C. Pulgarin, Applied Catalysis B: Environmental 63 (2006) 222 – 231.

[22] Z. Ding, H.Y. Zhu, G.Q. Lu, P.F. Greenfield, Journal of Colloids and Interface Science 209 (1998) 193 – 199.

[23] J. Fernandez, J. Kiwi, J. Baeza, J. Freer, C. Lizama, H.D. Mansilla, Applied Catalysis B: Environmental 48 (2004) 205 - 211.

[24] K. Mogyorosi, I. Dekany, J.H. Fendler, Langmuir 19 (2003) 2938 - 2946.

[25] R. Molinari, F. Pirillo, M. Falco, V. Loddo, L. Palmisano, Chemical Engineering and Processing 43 (2004) 1103 - 1114.

[26] Z. Xiong, Y. Xu, L. Zhu, J. Zhao, Langmuir 21 (2005) 10602 - 10607.

[27] W. Yan, B. Chen, S.M. Mahurin, E.W. Hagaman, S. Dai, H. Overbury, Journal of Physical Chemistry B 108 (2004) 2793 - 2796.

[28] D. Beydoun, R. Amal, Material Science and Engineering B 94 (2002) 71 - 81.

[29] S. Takeda, S. Suzuki, H. Odaka, H. Hosono, Thin Solid Films 392 (2001) 338 - 344.

[30] M.N. Chong, V. Vimonses, S. Lei, B. Jin, C. Chow, C. Saint, Microporous and Mesoporous Materials 117 (2009) 233 – 242.

[31] M.N. Chong, B. Jin, C. Chow, C. Saint, Chemical Engineering Journal 152 (2009) 158 – 166.

[32] M.N. Chong, B. Jin, H.Y. Zhu, C. Chow, C. Saint, Chemical Engineering Journal 150 (2009) 49-54.

[33] APAH (2005) Standard methods for the examination of water and wastewater, 21st edition.

[34] L.L. Gyürék, G.R. Finch, Journal of Environmental Engineering 124 (1998) 783 – 792.

[35] M. Cho, H. Chung, J. Yoon, Applied Environmental Microbiology 69 (2003) 2284-2291.

[36] C.S. Zalazar, C.A. Martin, A.E. Cassano, Chemical Engineering Science 60 (2005) 4311 – 4322.

[37] A.P. Toor, A. Verma, C.K. Jotshi, P.K. Bajpai, V. Singh, Dyes and Pigments 68 (2006) 53 – 60.

[38] Q. Chang, H. He, Z. Ma, Journal of Inorganic Biochemistry 102 (2008) 1736 – 1742.

[39] R. Sonohara, N. Muramatsu, H. Ohshima, T. Kondo, Biophysical Chemistry 55 (1995) 273 – 277.

[40] M. Heyde, R. Portalier, FEMS Microbiology Letter 69 (1990) 19.

[41] S.S. Chin, T.M. Lim, K. Chiang, A.G. Fane, Chemical Engineering Journal 130

(2007) 53-63.

[42] P.S.M. Dunlop, J.A. Byrne, N. Manga, B.R. Eggins, Journal of Photochemistry and Photobiology A: Chemistry 148 (2002) 355-363.

[43] H.N. Pham, T. McDowell, E. Wilkins, Journal of Environmental Science and Health A 30 (1995) 627 – 636.

[44] L.W. Hom, Journal of Sanitary Engineering Division 98 (1972) 183-194.

[45] J. Anotai, Effect of calcium ions on chemistry and disinfection efficiency of free chlorine at pH 10, PhD dissertation, Drexel University, Philadelphia, Pa (1996).

[46] D. Roy, E.S.K. Chian, R.S. Engelbrecht, Journal of Environmental Engineering Division ASCE 107 (1981) 887-901.

SUB-CHAPTER 7.2

BACTERIAL INACTIVATION KINETICS, REGROWTH AND SYNERGISTIC COMPETITION IN A PHOTOCATALYTIC DISINFECTION SYSTEM USING ANATASE TITANATE NANOFIBER CATALYST

M.N. Chong [a, b], B. Jin [a, b, c], H. Y. Zhu [d], C. Saint [b, c]

a School of Chemical Engineering, The University of Adelaide 5005 Adelaide Australia

b Schools of Earth and Environmental Sciences, The University of Adelaide 5005 Adelaide Australia

c Australian Water Quality Centre, South Australian Water Corporation, 5000 Adelaide South Australia

[d] School of Physical and Chemical Sciences, Queensland University of Technology, Brisbane, QLD 4001, Australia

Submitted manuscript to Journal of Photochemistry and Photobiology A: Chemistry.

STATEMENT OF AUTHORSHIP

BACTERIAL INACTIVATION KINETICS, REGROWTH AND SYNERGISTIC COMPETITION IN A PHOTOCATALYTIC DISINFECTION SYSTEM USING ANATASE TITANATE NANOFIBER CATALYST

Submitted manuscript to Journal of Photochemistry and Photobiology A: Chemistry.

Chong, M.N. (Candidate)

Performed experiment design; analysis of samples; interpreted data; manuscript evaluation; wrote manuscript.

Signed……*Date*……..…

Jin, B.

Manuscript evaluation; acted as corresponding author.

I give consent for M. N. Chong to present this paper for examination towards the Doctor of Philosophy

Signed……*Date*……..

Zhu, H. Y.

Manuscript evaluation.

I give consent for M. N. Chong to present this paper for examination towards the Doctor of Philosophy

Signed……*Date*……..……

Saint, C.

Manuscript evaluation.

I give consent for M. N. Chong to present this paper for examination towards the Doctor of Philosophy

Signed……*Date*……..……

Bacterial Inactivation Kinetics, Regrowth and Synergistic Competition in a Photocatalytic Disinfection System using Anatase Titanate Nanofiber Catalyst

Meng Nan Chong [a, b], Bo Jin [a, b, c*], Huaiyong Zhu [d], Chris Saint [b, c]

[a] School of Chemical Engineering, The University of Adelaide 5005 Adelaide Australia

[b] Schools of Earth and Environmental Sciences, The University of Adelaide 5005 Adelaide Australia

[c] Australian Water Quality Centre, South Australian Water Corporation, 5000 Adelaide South Australia

[d] School of Physical and Chemical Sciences, Queensland University of Technology, Brisbane, QLD 4001, Australia

[*] To whom correspondence should be addressed.

Tel.: +61 8 8303 7056. Fax: +61 8 8303 6222. Email: bo.jin@adelaide.edu.au

Abstract

This work studied the inactivation kinetics, bacterial regrowth and synergistic competition in the photocatalytic disinfection of a sewage isolated *Escherichia coli* (ATCC 11775) in an annular slurry photoreactor (ASP) system using anatase titanate nanofibers catalyst (TNC). The inactivation performance and disinfection kinetics of the TNC-ASP system were investigated with respect to operation conditions: TNC loading, pH, aeration rate and inoculum size. At optimum conditions, a 99.999% inactivation of 7 x 10^6 CFU mL^{-1} *E.coli* was achieved in 60 min. The modified Hom model was used to perfectly-fit the sigmoid-shaped disinfection kinetic profile. The residual disinfecting effect was evaluated by post-irradiation Fenton reaction. It was found that the 1.0 mg L^{-1} Fe^{2+} in conjunction with low chemical oxygen demand (COD) was able to initiate the post-photocatalytic Fenton reaction, where substantial bacterial regrowth was suppressed after 24 h treatment. Studies on the synergistic effect of COD concentration on the inactivation and the bacterial regrowth potential revealed that the *E. coli* could regrow at a COD concentration over 16 mg L^{-1}. Thus,

significant removal of COD has to be ensured in a photocatalytic disinfection process to successfully maintain the biostability of the treated water.

Keywords: TiO_2; Nanofibers; Annular Reactor; Photocatalysis; Bacterial Inactivation; *E.Coli*; Post-disinfection; Fenton Reaction; Synergistic Competition.

1. Introduction

The use of photocatalytic technology to eliminate trace organic pollutants in water treatment process has been well-documented [1-11]. When semiconductor titanium dioxide (TiO_2) is excited with photon energy greater or equal to its bandgap energy E_b (< 385 nm), electron-hole pairs will be generated in TiO_2. It was reported that the presence of surface adsorbed hydroxyl groups is indispensable in the generation of reactive hydroxyl radicals ($OH^{\bullet}$) from the direct valence band (VB) hole oxidation [1-8]. To ensure the prolonged availability of VB holes, oxygen is required to capture the excited conduction band electrons through the formation of superoxide ions ($O_2^{\bullet -}$) and thus, further prevent the recombination of electron-hole pairs [9]. The presence of other reactive oxygen species (ROS) during the photocatalytic reaction in an aqueous environment, such as hydrogen peroxide (H_2O_2) and singlet oxygen, has also been reported [9]. In the absence of oxygen or other electron acceptors, no photocatalytic reaction occurs due to the rapid recombination of electron-hole pairs. The detailed photochemical reactions on the TiO_2 surface during photocatalysis have been discussed in numerous literatures [9-11].

In recent years, the emergence of toxic disinfection by-products (DBPs) from water chlorination has been of major environmental and public health concern [12-14]. Prominent DBPs such as haloacetic acids and trihalomethanes can cause congenital cardiac defects in human beings, if their concentrations are higher than 60 or 80 ppb, respectively [14]. Removal of such DBPs in a cost-effective and sustainable manner is keenly sought, owing to their persistent nature that might penetrate through to the end-user. Considering the growth in treatment of recycled wastewater for domestic utilisation, there is a need to find a sustainable water disinfection technology to replace chlorination, so as to avoid the formation of DBPs.

To date, chlorination is still the preferred disinfection method owing to its cost-effective removal of microorganisms and the ability to maintain residual free-chlorine that prevents further bacterial regrowth [15, 16].

Since the first application of TiO_2 photocatalyst under UV irradiation for microbial inactivation by Matsunaga and co-workers in 1985, many preliminary investigations were performed to examine the possibility of using photocatalytic technology for water disinfection [17]. A wide range of microbial types, from coliforms, viruses, bacteria, cysts, fungi, algae and protozoa have been successfully inactivated using photocatalytic disinfection [18-20]. Surprisingly, very few cases were reported for a pilot or large scale photocatalytic disinfection process except those reported by Pulgarin and co-workers [16]. This was largely attributed to the difficulty in downstream processes for the recovery of the powder photocatalysts, such as commercial Degussa P-25 TiO_2, and thus limiting its industrial application [21-23]. Numerous engineering solutions have been adopted to enhance the feasibility of photocatalytic disinfection technology. One of the prominent solutions is to utilise an inert carrier for the immobilisation of TiO_2 particles. Different inert carriers, such as optical fibers, clay materials and magnetic core TiO_2 particles have been investigated [24-31].

The use of photocatalytic disinfection technology for water treatment has been reported to exhibit a lesser extent of residual disinfecting effect (RDE) against chlorination [32-34]. The RDE was restricted by the nature of the $OH^{\bullet}$ radicals, which usually have a short half-life in the water environment. Wist et al. [15] reported that there was a drastic increase in culturable *E.coli* cells in a crude river water sample in the subsequent 24 h after UV irradiation. Similar bacterial regrowth problems were observed by Rincon and Pulgarin [32] after 48 h of UV irradiation. To enhance the RDE of photocatalytic disinfection, consecutive illuminated TiO_2 photocatalysis and post-irradiation Fenton reaction was proposed [33]. The ROS of H_2O_2 was the primary species that is responsible for initiating the dark Fenton reaction, together with the presence of trace transition metals (i.e. Fe, Mn or Cu). The residual H_2O_2 from the illuminated TiO_2 reaction phase will be periodically reverted into $OH^{\bullet}$ with the aid of such transition metals, preventing any bacterial regrowth [33]. In this instance, it is important to stress that the targeted water quality constitutes one of the major suppressant to diminish the RDE of the

photocatalytic disinfection. It is thus, imperative to understand the extent of the dark Fenton reaction for enhanced RDE on photocatalytic water disinfection.

In this study, we reveal the superiority of a recently developed anatase titanate nanofiber catalyst (TNC) for the photocatalytic disinfection of a sewage isolated *E.coli* (ATCC 11775) strain under UVA irradiation ($\lambda < 380$ nm). We have reported the photocatalytic degradation of organics over the TNC surface and its particle recovery [35]. The TNC was found to have a competitive separation edge over the commercial Degussa P-25 TiO_2 with enhanced surface mass transfer for both the adsorbed reactants and desorbed photocatalyzed products [35]. The influence of operation parameters of the ASP system on bacterial inactivation and irradiation time was investigated. These parameters include the TNC loading, pH, aeration rate and bacterial inoculum size. The sewage-isolated *E.coli* strain was used as an indicator microorganism for faecal contamination and microbiological standard to measure against the photocatalytic treatment efficiency. So far, *E.coli* is the most widely used microbial standard for studying water disinfection and thus, considered appropriate for comparison with other studies. Currently, it is also utilised as a key indicator organism for the effective disinfection of wastewater. We used the experimental data and disinfection kinetic model for comparison of photocatalytic disinfection efficiency. Subsequently, the RDE of the TNC-ASP system was evaluated by the post-irradiation Fenton reaction against different Fe^{2+} concentrations, with the presence of glucose as the organic carbon source. The synergistic effect of the chemical oxygen demand (COD) on the photocatalytic inactivation of *E.coli* and its bacterial regrowth potential (BRP) were investigated.

2. Experimental

2.1. Materials

Ferrous sulphate ($FeSO_4.7H_2O$, Analar grade, BDH Chemicals, England), D(+)-glucose ($C_6H_{12}O_6$, BDH VWR, England) and digestion solution for COD 0-150 ppm range (Hach, USA) were used as received. Hydrochloric acid (HCl) (Labserv Pronalys, Australia) and sodium hydroxide (NaOH) (Analar grade, BDH Chemicals, England) were prepared to a

desired concentration by the addition of Milli-Q water obtained from Barnstead Nanopure Barnstead ion exchange water system with 18.2 MΩ-cm resistivity.

The *anatase titanate nanofiber catalyst* (TNC) was synthesized through a hydrothermal reaction between concentrated NaOH and TiO_2 and a post-synthesis ion exchange with HCl solution [36, 37]. Specifically, 3 g of anatase particles (~325 mesh from Aldrich) was mixed with 80 mL of 10 M NaOH. The resultant suspension was sonicated for 30 min and transferred into a PTFE container for autoclaving. The autoclave was maintained at a hydrothermal temperature of 180 °C for 48 h. The precipitate (sodium titanate nanofiber) was recovered, washed with distilled water (to remove excess NaOH) and finally sodium ions in the titanate nanofibers were exchanged with H^+ ions (using a 0.1 M HCl solution) to produce hydrogen titanate nanofibers. These products were repeatedly washed with distilled water until pH ~7 was reached. The hydrogen titanate product was dried at 80 °C for 12 h and then calcined at 700 °C for 3 h to yield anatase nanofibers.

2.2. Annular Slurry Photoreactor System

A previously developed stainless steel-lined ASP column was used as a photo-disinfection reactor in this study [5, 35]. The ASP was operated as a three-phase bubble column reactor, where the TNC fibrils were dispersed in the targeted water. The lower-end of the ASP was fabricated with a detachable conical bottom free of a reaction dead zone, making it easy for cleaning and maintenance. A 45-μm air sparger was fitted to the detachable conical bottom to provide homogeneous bubble distribution for agitation, mixing and aeration for the photocatalytic reaction. The light configuration in the ASP was designed in such a way, where additional light could be placed within the central quartz core. In this study, an UVA black light of 8W (NEC, Holland) was fitted annularly within the quartz thimble to prevent direct contact with the reaction fluid, while allowing optimal UV transmission for excitation of the suspended TNC fibrils. It should be stressed that the UVA light used in this study was for the photonic excitation of the TNC alone. Unlike the germicidal UVC light with high-end UV electromagnetic spectrum (i.e. 4.43 – 12.4 eV), the associated UV energy for such UVA is significantly lower (i.e. 3.10 – 3.94 eV) and will not cause substantial bacterial inactivation [16]. The wavelength range of UVA light lies in the range of 315 – 400 nm, which is close to solar irradiation. Samples were collected from the four-descended level sampling ports.

Electronic probes and meters for in-situ data logging of pH, dissolved oxygen (DO) and temperature (TPS, Australia) were connected to the reactor. The operating temperature for the ASP system was kept at room temperature of 25^{o}C during the experiments. A detailed design of the ASP and the whole experimental set up are shown in Fig. 1.

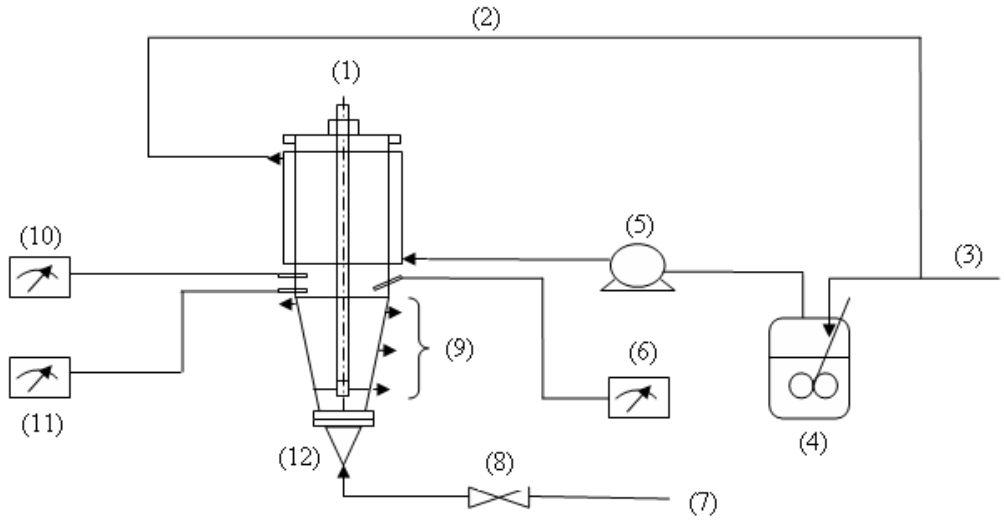

Figure 1: Experimental set-up for the annular slurry photoreactor system: (1) UV light, (2) Recirculation water line, (3) Fresh cool water line, (4) Cooling water vessel, (5) Cooling water pump, (6) Temperature meter, (7) Compressed air supply line, (8) Compressed air regulation valve, (9) Sampling ports, (10) pH meter, (11) Dissolved oxygen meter, (12) Photoreactor.

2.3. Preparation of Bacterial Strain and Water Samples

A sewage-isolated *E.coli* strain (ATCC 11775) was used as an indicator microorganism for faecal contamination and microbial standard to evaluate the inactivation performance and disinfection efficiency. The use of this isolated *E.coli* strain rather than a common laboratory strain allows the measurement of the disinfection ability of the treatment process in a natural environment.

The ASP was first filled with 1.5 L of bacterial suspension of known cell number for each batch run. A 50 mL fresh liquid culture was prepared by inoculation in a tryptone soy broth media (TSB) (Oxoid, England) followed by incubation at 35^{o}C for 19 h in a rotary shaker at 50 rpm. The final bacterial count after 19 h incubation was determined to be 9 x 10^{9} CFU mL^{-1}.

To prepare the bacterial suspensions for each batch experiment, an aliquot of the incubated liquid culture was directly inoculated into 1.5 L of phosphate buffered saline (PBS) solution, prepared using Nanopure Water of 18.2 MΩ cm resistivity. The use of PBS is to prevent sudden osmotic shock to the bacteria, so as to maintain the bacterial numbers for accurate dilution purposes. Subsequently, the initial bacterial density was heterotrophic plate counted (HPC) using standard procedures [38].

Prior to the batch disinfection trial, TNC at a given concentration was added to the bacterial suspension in the ASP and further homogenized in the dark for 30 min under constant aeration. The UVA light was turned on after the homogenisation period at t = 0 min and the aeration were allowed to run continuously for up to 120 min. Sampling was conducted every 10 min up to 40 min, and thereafter every 20 min up to 120 min. The determination of *E.coli* was carried out following a standard serial dilution procedure and every sample was HPC duplicately in the prepared plate count agar (PCA) (Merck, Germany). The PCA plates were incubated at 35^{o}C for 24 h before final cell counting. The normalised fraction of bacterial survivor against irradiation time curves was plotted for disinfection kinetic analysis. Each photo-disinfection experiments were then repeated for standard experimental verification and error analysis.

For the RDE experiments, we added a fixed amount of glucose to the pure water and adjusted the pH. A specific amount of Fe^{2+} was also added to the ASP before the experiment. The bacterial suspension was prepared in the same procedures as described previously. After UV irradiation for 120 min, 150 mL of the treated water sample were charged into a 250 mL flask. The flask was incubated at 35^{o}C in the orbital shaker incubator at 150 rpm for 24 h. The treated water sample was subjected to HPC to monitor the efficacy of post-irradiation Fenton reaction. Similarly, each analysis was repeated for standard experimental replication and error analysis.

2.4. Water Sample Analysis

Organic carbon, referred to as COD, during the entire illuminated TNC reaction phase in the TNC-ASP was monitored using a COD measurement kit (Hach, United States), which comprises of COD digestion solution, Hach DRB 200 digestion chamber and Hach DR890 COD calorimeter. Two mL of the treated water sample after the UVA irradiation was added to

the digestion solution. The digestion solution was then subjected to the digestion chamber at 150^{o}C for 120 min. After digestion, the solution was allowed to cool down prior to the COD measurements using the calorimeter. In addition, one hundred μL of the supernatant was then filtered through a 0.22 μm membrane for glucose analysis by HPLC. The HPLC analysis used a ROA Organic Acid Column (Phenomenex, 300 × 7.8, Varian, CA, USA) and a refractive index detector (Model 350, Varian). The mobile phase was 4 mM H_2SO_4 at a flow rate of 0.6 mL min^{-1} and the column temperature was 50 °C.

3. Results and Discussion

3.1. Effect of TNC Loading

The influence of photocatalyst loadings on microbial inactivation in different photocatalytic systems has been reported [39]. Experiments were carried out in the TNC-ASP system using TNC at a loading range of 0.25 – 2.0 g L^{-1}. Two control experiments without either TNC or UVA irradiation were also tested. Fig. 2 shows the normalised plot of enumerated *E.coli* cells against UVA irradiation time. The TNC showed no inactivation activity on the *E.coli* in the dark control experiment. A small fraction of the *E.coli* was inactivated under the UVA irradiation without TNC. Since the UVA radiation (320 – 400 nm) is the least energetic fraction of the UV spectra, the radiation-induced cell damage to the bacterial cell is usually insignificant owing to the absence of direct absorption by the sensitive cell components [16]. It was reported that the photokilling by UVA irradiation should be well-mediated by sensitizers, such as TiO_2, to achieve greater bacterial cell damage [16].

When 0.25 g L^{-1} TNC was added (Fig. 2) as the sensitizer in inducing the formation of chemical intermediates during the irradiation period, such as $OH^{\bullet}$, $O_2^{\bullet-}$ and H_2O_2, significant enhancement in *E.coli* inactivation was observed. An inactivation level of 99.999% was easily attained within 120 min irradiation, resulting in a significant 5-fold enhancement in *E.coli* inactivation higher than the control experiment with UVA irradiation alone. Using 0.5 g L^{-1} TNC, the irradiation time taken to achieve 99.999% of bacterial inactivation was reduced to 100 min, while a shorter irradiation time of 80 min was needed as the TNC loading increased to 1.0 g L^{-1}. However, a further increase in TNC loadings to 2.0 g L^{-1} resulted in a significant

prolongation of irradiation time required to achieve similar bacterial inactivation levels. We found that longer irradiation time, such as 360 min had limited impact on the bacterial inactivation level.

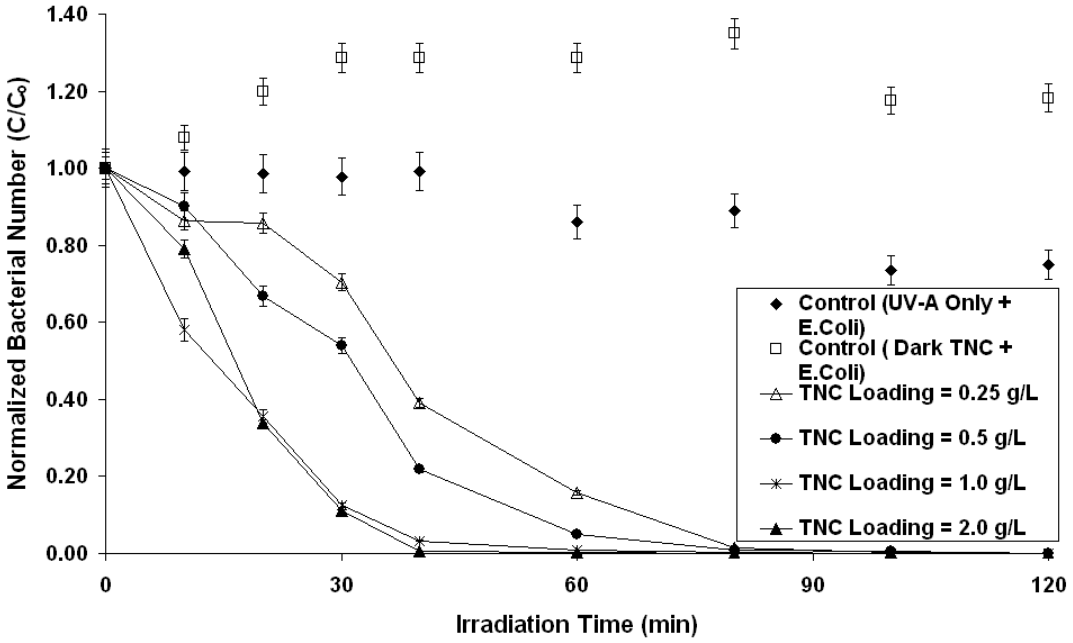

Figures 2: Effect of TNC loading on the photocatalytic inactivation of *E.Coli* at average initial bacterial population of $7x10^6$ CFU mL^{-1}.

Ochuma et al. [8] found that an increase in the catalyst particle concentration in a photoreactor results in increasing the light source extinction coefficient, and subsequently reducing the reaction efficiency. This arises from the attenuation of light intensity across the annulus zone and rapid increase in light absorption and scattering phenomena that hinder the photocatalytic inactivation to proceed at a high rate. As a consequence of such TNC saturation within the annulus reaction zone, a non-linear inactivation profile with strong tailing characteristics was observed with increasing TNC loadings. This was strongly evidenced from the long irradiation time required to achieve 99.999% inactivation if the TNC loading was doubled from 1.0 to 2.0 g L^{-1}. We believe that the efficiency of the photocatalytic disinfection in the ASP is a strong function of the annulus width, where a significant reduction in the annulus results in greater disinfection efficiency and less bacterial tailing characteristic. Wider annulus gap, together with low light intensity and high TNC loadings can affect extinction co-efficiency and result

in decreasing photon contact with *E.coli* adhered to the reactor wall. Thus, it can be concluded that the saturation TNC loading in the ASP system is at 1.0 g L^{-1} for the effective disinfection. The subsequent investigations were carried out at the saturated TNC loading of 1.0 g L^{-1}.

3.2. Effect of pH

The impact of pH on TiO_2 surface charge and its photo-oxidation performance for effective surface adsorption and reaction with organics and bacteria has been well-documented [5-8, 40-41]. In our previous study, we found that the point of zero charge (PZC) of TNC is 4.6, which is slightly lower than the Degussa P25 TiO_2 of 5.6 – 6.8 [35]. To elucidate the effects of pH in the photocatalytic inactivation of *E.coli* by TNC, the variation in pH 4.0 - 9.0 in the TNC-ASP was investigated in this study.

E.coli is a Gram-negative bacterium with the outer cell membrane covered by a lipopolysaccharide layer of 1 – 3 μm thickness [42]. With the slightly negatively-charged surface of the *E.coli*, it is expected that the bacterial cell could induce an electrostatic attraction with TNC fibrils of surface charge lower than its PZC value. The water pH affects the surface charge density of the TNC according to the following equilibrium equations (Eq. 1 – 2) [40];

$$pH < PZC : TiOH + H^+ \leftrightarrow TiOH_2^+ \quad \text{(Eq. 1)}$$

$$pH > PZC : TiOH + OH^- \leftrightarrow TiO^- + H_2O \quad \text{(Eq. 2)}$$

Fig. 3 shows the effect of pH on the photocatalytic inactivation of *E.coli*. Initial pH was adjusted by dropwise addition of 0.1M HCl and NaOH. Control experiments under UVA irradiation and pH 4.0 were conducted to measure the extent of bacterial cell lysis, as induced by the pure photolytic and cell acidification reaction respectively. Results show that the control UVA photolytic reaction on *E.coli* contributes to an approximate 25% inactivation, while no significant destruction was observed via cell acidification at pH 4.0. Rincon and Pulgarin [40] reported similar findings where the photolytic inactivation of *E.coli* was independent of initial pH between 4.0 and 9.0.

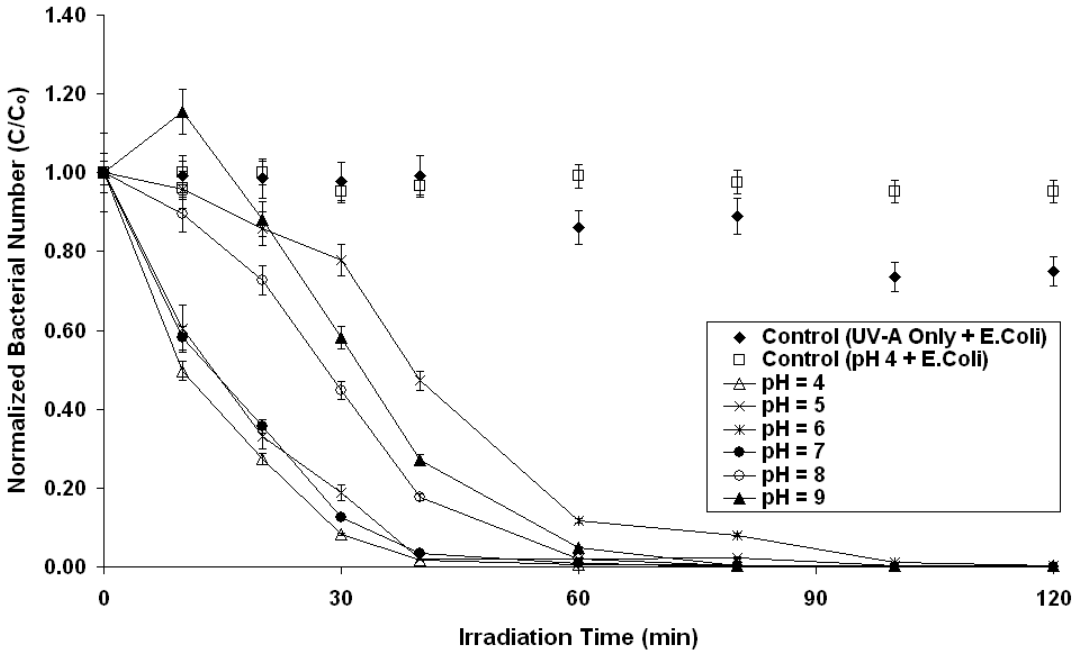

Figure 3: Effect of pH on the photocatalytic inactivation of *E.Coli* at average initial bacterial population of $7x10^6$ CFU mL^{-1} and TNC loading of 1.0 g dm^{-3}.

At pH 4.0 < PZC (TNC), we found that the photocatalytic inactivation was enhanced. This may be that more *E.coli* were attracted to the positively-charged TNC surface, resulting in forming dense $TiOH_2^+$ groups (Eq. 1) that attract the bacterial cell to the TNC surface for subsequent photo-oxidation reaction. The irradiation time required to achieve 99.999% inactivation was reduced to 70 min. A similar enhancement in the inactivation was observed at pH 5.0. We found that such enhancement was contributed by the TNC action alone, where slight bacterial resistance (i.e. tailing/regrowth) to TNC was not observed during the controlled acidification experiment (pH 4). Heyde and Portalier [43] found that such negligible *E.coli* reaction to acid conditions was due to the presence of an acid tolerance response in the bacterium itself, which secreted the acid-induced proteins for bacterial acid-shock protection.

It is however, interesting to note that the inactivation of *E.coli* at a slight acidic pH of 6.0 was slowed down compared to the experiment with other pH conditions. One of the possibilities is linked to the growth nature of *E.coli* at pH 6.0 that overcomes the photocatalytic activity of TNC [40]. The tendency of bacterial growth at this pH range might partially reduce the rate of

photocatalytic destruction on the bacterial cell. Together with the inception of electrostatic repulsion forces that avert the *E.coli* from the TNC surface at pH 6.0, this prevents the *E.coli* from the TNC surface interaction for effective photo-destruction. In short, it can be concluded that the photocatalytic inactivation by the TNC fibrils was best performed at pH 4.0 – 5.0. Operating the photocatalytic inactivation system at a high pH would result in prolonged photo-destruction of *E.coli* to achieve a high inactivation level. Although much justifications have been discussed in link of the *E.coli* sensibility to both low and high pH conditions, other operating issue might be neglected such as the TNC aggregation as a function of pH. All the subsequent experiments were performed at pH 4.0 – 5.0.

3.3. Effect of Aeration Rate

In this study, compressed air was used to keep the TNC fibrils in suspension within the annulus core of the ASP column. Previously, we examined the effect of aeration rate on the photodegradation of anionic Congo red dye [35]. We found that aeration rate was a key operation parameter, which can significantly affect the mixing, dispersion or aggregation state of the catalyst particles within the ASP column.

To understand the effect of aeration rate on the inactivation performance of the TNC-ASP system, a control experiment was performed at an aeration rate of 5 L min^{-1} without photocatalyst. Results indicate that there was no net aeration effect on the bacterial cell numbers. With this, we can conclude that there is minimal effect of aeration on bacteria and its subsequent inactivation was dependent on the combined effect of UVA photolytic mediated with TNC photocatalytic activity. Fig. 4 shows the effect of the aeration rate on the inactivation of *E.coli* in the ASP column. It shows that at a low aeration rate (2.5 L min^{-1}), the photocatalytic inactivation yields sluggish kinetics with strong shoulder phenomena up to 30 min before cell destruction takes place. Such shoulder characteristics might be owing to the low volumetric generation rate of the ROS as a direct result of poor dispersion for the TNC fibrils [13, 44]. We previously found that at a similar aeration rate, large amounts of TNC fibrils were sediment on the sparger plate. This indirectly reduces the amount of TNC fibrils in suspension for photon excitation, and thus the amount of active TNC for bacterial inactivation. A further increase (up to 10 L min^{-1}) in aeration rate resulted in a reduction of the photocatalytic inactivation rates. We found that the optimal aeration rate for the ASP column

was 5.0 L min^{-1} with 99.999% inactivation in 60 min. A higher aeration rate (i.e. >5.0 L min^{-1}) might induce the TNC fibril aggregation, and thus reduce the total available TNC active sites for inactivation.

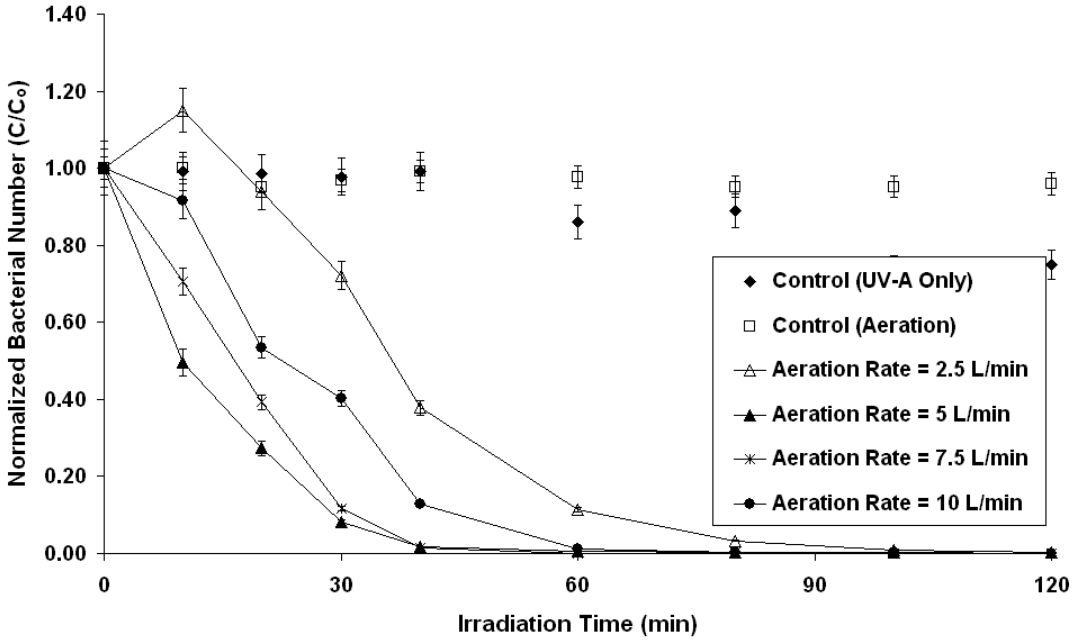

Figure 4: Effect of delivered aeration rate in the ASP column on the photocatalytic inactivation of *E.Coli* at average initial bacterial population of $7x10^6$ CFU mL^{-1}, TNC loading of 1.0 g dm^{-3} and pH 4 – 5.

In addition, we performed DO probing for its variation throughout the irradiation period. It should be noted that the correlation between the aeration rate and DO is not proportionate, with restriction from the ASP column gas hold-up and oxygen-air equilibrium. We observed that the DO profile (data not shown) was rapidly revived to a higher value after a slight drop within the initial 10 min at the saturation TNC loading of 1.0 g L^{-1}. This can be explained that the photo-destruction taking place before any microbial respiration may result in generating high concentration of the ROS. The rapid revival of the DO to its saturation level might due to the performance of the ASP system, where it was operated as an open system. Also we believe that the morphology of the thin TNC fibrils (i.e. 40 – 100 nm) does not trap any DO within its physical structure and thus, present a promising physical structure for an efficient photocatalytic disinfection process.

3.4. Effect of Bacterial Population

The bacterial cell numbers may vary in a water treatment plant and thus, it is necessary to investigate the impact of initial *E.coli* numbers on the photocatalytic inactivation kinetics. Dunlop et al. [12] suggested that an increase in the initial bacterial loading enhances the interaction with the photocatalyst used and reduces the overall mass transfer limitations, resulting in a higher inactivation rate. Similar observation was reported by Pham et al. [44] during the inactivation of *Bacillus pumilus* spores in a slurry reactor.

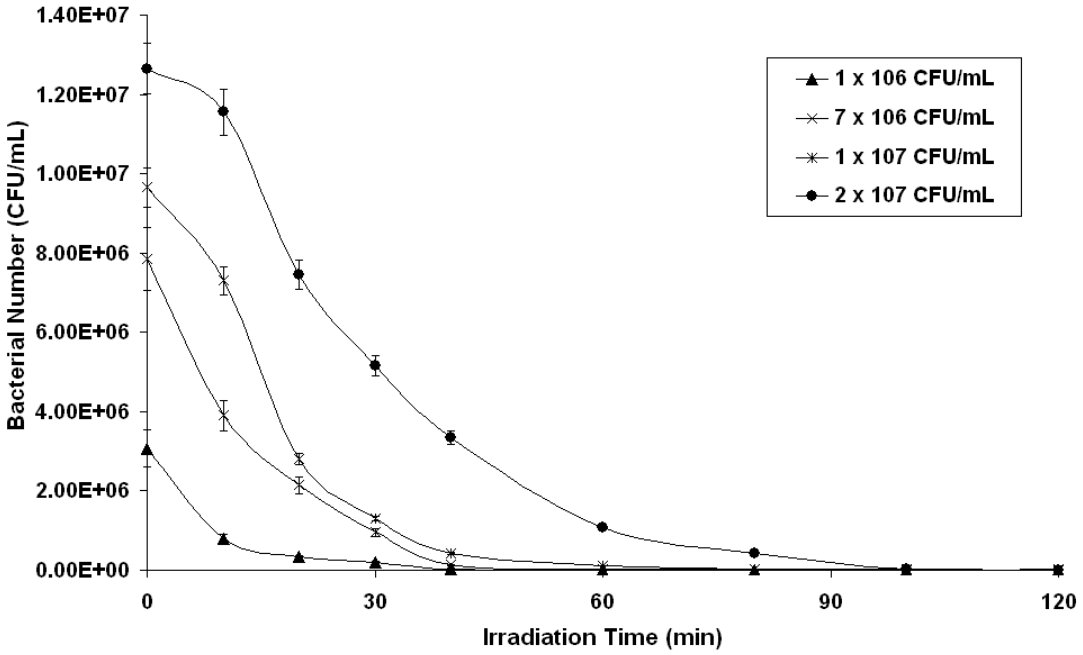

Figure 5: Effect of bacterial population on the photocatalytic inactivation of *E.Coli* under operating conditions of ASP: TNC loading of 1.0 g dm^{-3}, pH 4 – 5 and aeration rate of 5 dm^3min^{-1}.

Fig. 5 shows the effect of initial bacterial numbers on the rate of photocatalytic inactivation in the TNC-ASP system. We found that an increase in *E.coli* numbers improves the inactivation rate, as evidenced from the steeper log-linear inactivation region of the kinetics profile. Although a steeper inactivation curve was attained, the inactivation level was slightly reduced owing to the increase in water turbidity across the annulus radii. Such an improved disinfection rate was attributed to the increased collision probability between the surface-generated ROS and *E.coli* cells [12]. Due to the appearance of strong shoulder and tailing

characteristics of the inactivation profiles, a direct comparison of the inactivation rate could not be easily made. We have compared the *E.coli* inactivation kinetics empirically by fitting with the modified Hom model and this is further discussed in the following section 3.5.

3.5. Empirical Modelling of the TNC-ASP System

Bacterial inactivation modelling was attempted with the classical Chick-Watson model that conformed to a first-order relationship between the photocatalyst loading and enumerated *E.coli* [45-48]. In this study however, we found that such a linear relationship was inadequate to represent the three different regions of the photocatalytic inactivation curves in the TNC-ASP system, as shown in Fig. 5. The inactivation curve starts with (i) a lag or initial smooth decay, which is known as a "shoulder", followed by (ii) a typical log-linear inactivation region and ends with (iii) a long deceleration process at the end of the disinfection, which is known as a "tail" [13]. Cho et al. [48] attempted to use a delayed CW model with empirical lag time to represent the shoulder characteristic, but not the tailing region simultaneously.

To fit the inactivation kinetics in the TNC-ASP system, the empirical model might require three different kinetic parameters for each characteristic region. The shoulder region was justified by the cumulative damage nature of the photocatalytic treatment on the cytoplasmic membrane rather than instantly lethal [49]. This can also be viewed in terms of the slow permeation rate of the ROS, which are bounded by their short half-life, through the cell wall before inducing any irreversible damage to the bacterial cell. The tailing region was related to the competition for photocatalysis between the organic products released from constant cell lyses [50]. Here, we used the modified Hom model for kinetic evaluation as previously used by Marugán et al. [13]. They utilised this modified Hom model to represent the photocatalytic inactivation of *E.coli* using commercial Degussa P25 TiO_2. Thus, a direct comparison could be made between the TNC fibril photocatalyst and the commercial one. Fig 6 shows the modified Hom model fitted kinetics at the variable initial *E.coli* population. The log-linear inactivation rate constant (k_2) varied in the range of 0.053 – 0.098 min^{-1}. From this, we can conclude that the inactivation activity of TNC is comparable to Degussa P-25 TiO_2. Given that the TNC was found to have a competitive separation edge over the commercial Degussa P-25 TiO_2, which is difficult to recover for reuse, the anatase nanofibers should be considered as a potential photocatalyst for water treatment.

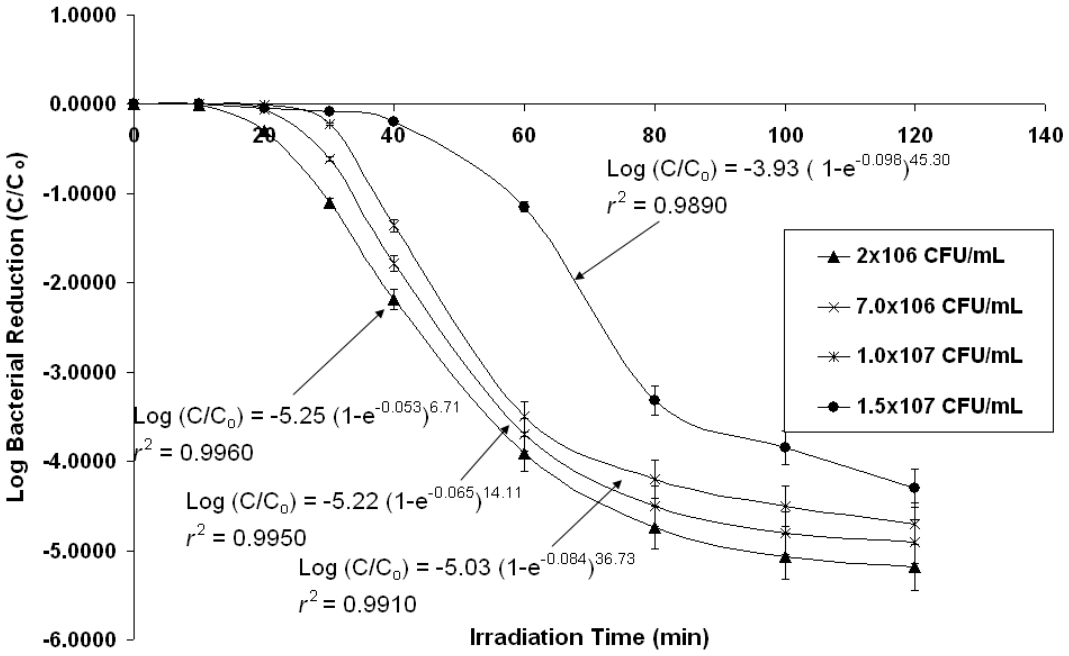

Figure 6: Fitting of modified Hom empirical model to experimental data with different initial bacterial concentrations.

3.6. Influence of Fe^{2+} on the Residual Disinfecting Effect

Previous works on photocatalytic inactivation of different microbes mostly focused on the bacterial reduction, without further monitoring the BRP of the water after photocatalytic treatment. Dunlop et al. [12] and Rincon et al. [16] investigated the dark repair mechanisms associated with the remaining bacteria during the post-irradiation period. Farr et al. [51] proposed that the bacterial cells may enter a viable but non-culturable (VBNC) state when they are exposed to oxidative stress, but will revert to a viable state when growth conditions become favourable. To verify these propositions, we investigated the bacterial lethality of *E.coli* induced by the TNC fibrils after 120 min irradiation and the BRP in the subsequent 24 h period. Glucose (0.1 g L^{-1}) was added to the reaction water as the baseline organic carbon source, in order to prevent bacterial cell lyses from limiting nutrient conditions during the 24 h dark period. The Fe^{2+} at different concentrations was supplemented at the beginning of the experiment, in order to observe the RDE during the post-irradiation Fenton reaction. It is known that Fe^{2+} can exist in different hydrolysed forms in water, and the Fe^{2+} can dissociate H_2O_2 molecules into $OH^{\bullet}$ radicals [16]. The followings represent the chemical equilibrium of

Fe^{2+} and its ferric aquacomplexes on the continuous evolution of $OH^{\bullet}$ radicals during the post-irradiation period [16];

$$Fe^{2+} + H_2O_2 \rightarrow Fe^{3+} + OH^- + OH^{\bullet} \quad (4)$$

$$Fe^{3+} + H_2O_2 \rightarrow Fe^{2+} + HO_2^{\bullet} + H^+ \quad (5)$$

$$Fe(OH)^{2+} + h\upsilon \rightarrow Fe^{2+} + OH^{\bullet} + H^+ \quad (6)$$

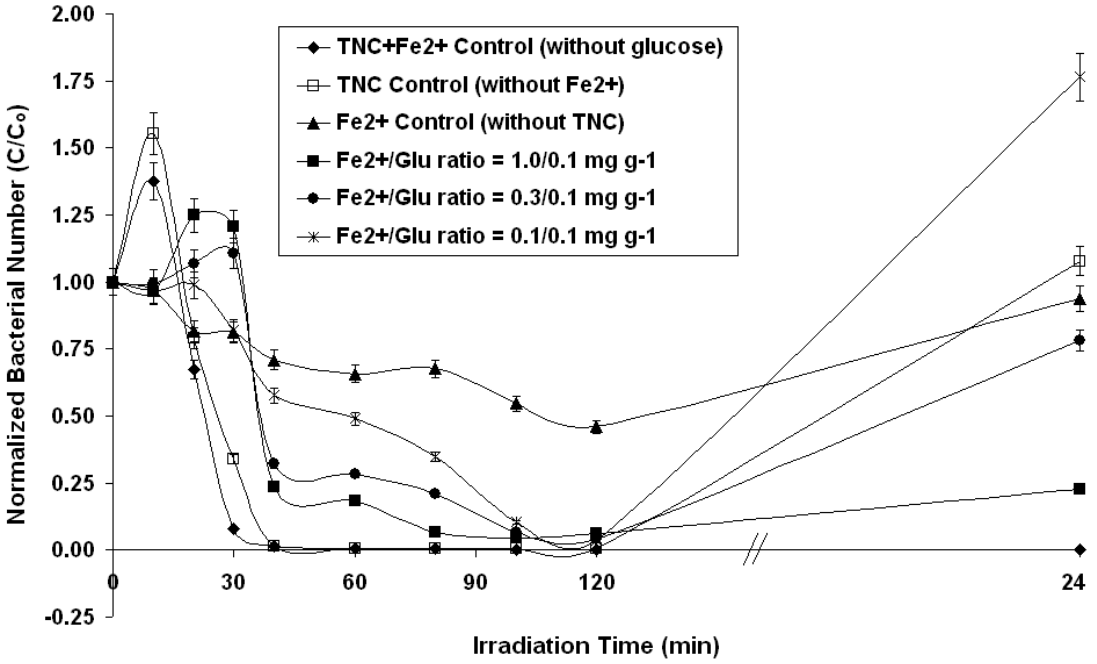

Figure 7: Evaluation of the residual disinfecting effect of combined TNC/Fenton treatment during the subsequent 24 h under different Fe^{2+} ion concentrations. Initial glucose concentration is 100 mg.

Fig 7. shows the tendency of bacterial regrowth under different experimental conditions (i.e. with/without Fe^{2+} and without glucose/TNC). Control experiments without glucose show that the *E.coli* numbers remain low during the post-irradiation period, indicating no bacterial regrowth occurs. In the control experiment with 1.0 mg L^{-1} Fe^{2+} , there was a 55% inactivation of *E.coli* over 120 min. After the latent period of photo-Fenton reaction, the population of *E.coli* further increased 10% from the initial culturable cell numbers. This increase in *E.coli*

numbers is due to the presence of glucose and parallel absence of the BRP-inhabitant H_2O_2 species (i.e. TNC absent) from the preceding photocatalytic reaction.

In the TNC control experiment with no Fe^{2+} added, the bacterial lethality was high in the first 120 min. There was a strong bacterial regrowth found in the subsequent 24 h dark period. In this instance, the absence of Fe^{2+} was seen to be more beneficial for bacterial regrowth than the absence of the TNC. When 0.1 mg L^{-1} Fe^{2+} was added, its inactivation kinetic profile was of more log-linear type (i.e. shoulder becomes more subtle) relative to standard TNC control experiment. A 99.995% reduction in *E.coli* was attained after 120 min irradiation. During a subsequent 24 h, the bacterial regrowth resulted in numbers equating to 93% of the initial *E.coli* numbers.

At higher Fe^{2+} concentrations of 0.3 and 1.0 mg L^{-1}, both the initial photo-killing rate and RDE effect becomes more prominent than the experiment using 0.1 mg L^{-1} Fe^{2+}. A more distinct sigmoid-type of inactivation profile was observed in the TNC-ASP system with more Fe^{2+} added. At a high concentration of Fe^{2+} (i.e. 1.0 mg L^{-1}), the sigmoidal profiles become prominent but a prolonged irradiation time is required to achieve a similar inactivation level. As for the RDE, we found that the Fe^{2+} at a high concentration could partially suppress the bacterial regrowth during the subsequent 24 h dark period. Under this 24 h period, use of 1.0 mg L^{-1} Fe^{2+} resulted in only 20% regrowth, while a significant high bacterial regrowth of 78% was associated with using 0.3 mg L^{-1} Fe^{2+}. A high Fe^{2+} concentration may cause water colorization. The maximum Fe^{2+} concentration allowed for recycled water is 1.0 mg L^{-1}. Thus, 1.0 mg L^{-1} Fe^{2+} was used in this study in order to simulate real water treatment conditions. One of the possibilities for such a weak RDE effect is owing to the low H_2O_2 generated during the irradiation and fast recombination with $OH^{\bullet}$ to form $HO_2^{\bullet}$. It was anticipated that the addition of supplementary H_2O_2 up to 0.3 mmol L^{-1} could enhance the BRP effect of TNC, as discussed by Rincon et al. [16]. Other possibilities might be due to the presence of organic carbon, whose synergistic effects on the bacterial regrowth will be discussed in Section 3.7.

3.7. Synergistic Interaction between COD and *E.coli* in the Photocatalytic Disinfection Process

The presence of organic compounds in either dissolved or particulate form in the treated water might provide sufficient carbon and energy sources for bacterial regrowth [52-55]. In considering reuse of treated wastewater, the BRP in the water sources should be suppressed and the microbial population needs to be lower than the standard level in the recycled water scheme. The concentrations of such organic compounds vary from different treatment plants, mainly depending on the efficiency of the water treatment process. It was reported that the COD level of treated wastewater might vary between 45 – 150 mg L^{-1}, depending on the seasonal activities of the local population [52].

We investigated the effect of organic carbon concentrations on the BRP of the treated water. Glucose at 0.01, 0.1 and 1.0 g L^{-1} was added, in order to make up different baseline COD conditions. The addition of glucose is also to verify its synergistic mineralisation during the photocatalytic treatment. With 1.0 mg L^{-1} Fe^{2+} added, the water was subjected to photocatalytic treatment for 120 min, followed by a dark incubation at 35^{o}C for 24 h. The glucose concentrations and the COD were monitored during the treatment period. The residual number of *E.coli* after the 24 h dark period was determined using HPC.

A control experiment was performed on the glucose degradation alone in a 120 min treatment. We found that at the optimised ASP conditions, 0.1 g L^{-1} glucose was completely degraded after 120 min of photocatalytic treatment. When the experiment was repeated with the co-existence of *E.coli* suspension, a slower degradation of glucose was observed after 120 min. The COD remained at a relatively high level of 87 mg L^{-1}. Parallel interpretation of the glucose and COD suggested that the glucose molecules were photocatalyzed into other intermediate organic carbons during 120 min of photo-oxidation. Such transition in organic carbon state indicates that the *E.coli* is more susceptible to the photo-oxidation than the simpler organic carbon molecules, which are more persistent and require longer irradiation time. The existence of such intermediate organic carbons, as a direct result of photocatalytic treatment was observed to synergistically affect the bacterial regrowth.

To verify the impact of organic carbon concentration on bacterial regrowth, experiments were performed using glucose at 0.01 g L^{-1} and 1.0 g L^{-1} respectively. Fig. 8 shows that glucose at 0.01 g L^{-1} (ca. COD 16 mg L^{-1}) was rapidly degraded and resulted in a significant COD reduction down to approximately 1 mg COD L^{-1} in 120 min. When *E.coli* was enumerated after a 24 h dark period, bacterial regrowth has been suppressed. Similar glucose degradation was observed after 120 min at an initial concentration of 1.0 g L^{-1}. A significant bacterial regrowth, however, was associated with this glucose concentration. Therefore, it could be concluded that COD content of the targeted water affected the inactivation activity and the BRP of the treated water. Ultimately, the irradiation time required for a successful operation of the photocatalytic treatment process need to be justified according to the chemical compositions and contents of the target water.

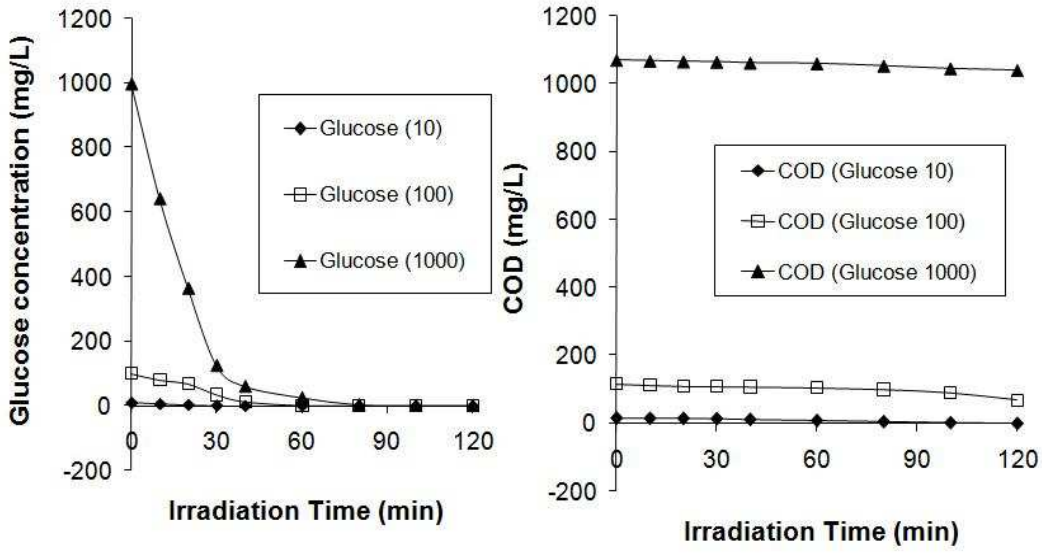

Figure 8: Correlation between the mineralization of glucose and its corresponding COD during the photocatalytic inactivation of *E.Coli* (as in Figure 7).

4. Conclusion

The photocatalytic inactivation of sewage isolated *E.coli* strain (ATCC 11775) using TNC was successfully achieved. Under UVA irradiation, the 99.999% inactivation level of 7 x 10^6 CFU mL^{-1} *E.coli* was well-attained within 60 min in the ASP system operated under the optimal

operating conditions: TNC of 1 g L^{-1}, pH 4.0 – 5.0 and aeration rate of 5 L min^{-1}. The log-linear rate constant, k_2, derived from the modified Hom model suggested that the photocatalytic inactivation activity using the TNC is comparable to the commercial Degussa P25 TiO_2. We found that the Fe^{2+} at 1.0 mg L^{-1} could induce RDE during the post-irradiation period, but will prolong the total irradiation time required. Simple organic carbon, such as glucose can be photocatalyzed into other intermediate forms, while *E.coli* was preferentially oxidized in the 120 min photocatalytic treatment. The persistent intermediate carbon forms were seen as the synergistic factor that affects the biostability of the treated water to bacterial regrowth. It is thus anticipated that the COD of the targeted water needs to be low, in order to functionalize the TNC-ASP system as a potential advanced wastewater treatment process.

Acknowledgement

The authors would like to thank Mr Philip Adcock for his valuable discussions and feedback during the initial planning stage of this study. This work was funded by the Australian Research Council Linkage Grant (LP0562153) and the Australian Water Quality Centre, SA Water Corporation through the Water Environmental Biotechnology Laboratory (WEBL) at the University of Adelaide.

References

[1] L. Rizzo, J. Koch, V. Belgiorno, M.A. Anderson, Desalination 211 (2007) 1 – 9.

[2] S.R. Couto, A. Dominguez, A. Sanroman, Chemosphere 46 (2002) 83 – 86.

[3] J.H. Jeon, S.D. Kim, T.H. Lim, D.H. Lee, Chemosphere 60 (2005) 1162 – 1168.

[4] W.L. Kostedt I.V., J. Drwiega, D.W. Mazyck, S.W. Lee, C.Y. Wu, P. Chadik, Environ. Sci. and Technol. 39 (2005) 8052 – 8056.

[5] M.N. Chong, S. Lei, B. Jin, C. Saint, C.W.K. Chow, Sep. Purif. Technol. 67 (2009) 355 – 363.

[6] C.S. Zalazar, C.A. Martin, A.E. Cassano, Chem. Eng. Sci. 60 (2005) 4311 – 4322.

[7] A.P. Toor, A. Verma, C.K. Jotshi, P.K. Bajpai, V. Singh, Dyes Pigments 68 (2006) 53 – 60.

[8] I.J. Ochuma, R.P. Fishwick, J. Wood, J.M. Winterbottom, Appl. Catal. B: Environ. 73 (2007) 259 – 268.

[9] J.M. Herrmann, Catal. Today 53 (1999) 115 – 129.

[10] I.K. Konstantinou, T.A. Albanis, Appl. Catal. B: Environ. 49 (2004) 1 – 14.

[11] R.J. Watts, S. Kong, W. Lee, J. Environ. Eng. 121 (1995) 730 – 735.

[12] P.S.M. Dunlop, J.A. Byrne, N. Manga, B.R. Eggins, J. Photochem. Photobiol A: Chem. 148 (2002) 355 – 363.

[13] J. Marugán, R. van Grieken, C. Sordo, C. Cruz, Appl. Catal. B: Environ. 82 (2008) 27 – 36.

[14] H.M. Coleman, C.P. Marquis, J.A. Scott, S.S. Chin, R. Amal, Chem. Eng. J. 113 (2005) 55 - 63.

[15] J. Wist, J. Sanabria, C. Dierolf, W. Torres, C. Pulgarin, J. Photochem. Photobiol A: Chem. 147 (2002) 241 – 246.

[16] A.G. Rincón, C. Pulgarin, Appl. Catal. B: Environ. 63 (2006) 222 – 231.

[17] T. Matsunaga, R. Tomodam, T. Nakajima, H. Wake, (1985) FEMS Microbiol. Lett. 29 (1985) 211 - 214.

[18] E.J. Wolfrum, J. Huang, D.M. Blake, P.C. Maness, Z. Huang, J. Fiest, Environ. Sci. Technol. 36 (2002) 3412 - 3419.

[19] J. Hong, M. Otaki, J. Biosci. Bioeng. 96 (2003) 298 - 303.

[20] J.A. Ibáñez, M.I. Litter, R.A. Pizarro, J. Photochem. Photobiol A: Chem. 157 (2003) 81 – 85.

[21] A. Arques, A.M. Amat, L.S. Juanes, R.F. Vercher, M.L. Marin, M.A. Miranda, J. Mol. Catal. A: Chem. 271 (2007) 221 - 226.

[22] D. Beydoun, R. Amal, Mater. Sci. Eng. B 94 (2002) 71 - 81.

[23] A. Bhattacharyya, S. Kawi, M.B. Ray, Catal. Today 98 (2004) 431 - 439.

[24] Z. Ding, H.Y. Zhu, G.Q. Lu, P.F. Greenfield, J. Col. Inter. Sci. 209 (1998) 193 – 199.

[25] J. Fernandez, J. Kiwi, J. Baeza, J. Freer, C. Lizama, H.D. Mansilla, Appl. Catal. B: Environ. 48 (2004) 205 - 211.

[26] K. Mogyorosi, I. Dekany, J.H. Fendler, Langmuir 19 (2003) 2938 - 2946.

[27] R. Molinari, F. Pirillo, M. Falco, V. Loddo, L. Palmisano, Chem. Eng. Proc. 43 (2004) 1103 - 1114.

[28] S. Takeda, S. Suzuki, H. Odaka, H. Hosono, Thin Solid Films 392 (2001) 338 - 344.

[29] Z. Xiong, Y. Xu, L. Zhu, J. Zhao, Langmuir 21 (2005) 10602 - 10607.

[30] W. Yan, B. Chen, S.M. Mahurin, E.W. Hagaman, S. Dai, H. Overbury, J. Phys. Chem. B 108 (2004) 2793 - 2796.

[31] M.N. Chong, V. Vimonses, S. Lei, B. Jin, C. Chow, C. Saint, Micro. Meso. Mater. 117 (2009) 233 – 242.

[32] A.G. Rincón, C. Pulgarin, Appl. Catal. B: Environ. 49 (2004) 99 – 112.

[33] A.G. Rincón, C. Pulgarin, Catal. Today 101 (2005) 331 – 344.

[34] J.A. Herrera Melián, J.M. Doña Rodríguez, A. Viera Suárez, E. Tello Rendón, C. Valdés do Campo, J. Arana, J. Pérez Peña, Chemosphere 41 (2000) 323 – 327.

[35] M.N. Chong, B. Jin, H.Y. Zhu, C.W.K. Chow, C. Saint, Chem. Eng. J. 150 (2009) 49 – 54.

[36] H. Zhu, X. Gao, Y. Lan, D. Song, Y. Xi, J. Zhao, J. Am. Chem. Soc. 126 (2004) 8380 – 8381.

[37] H.Y. Zhu, Y. Lan, X.P. Gao, S.P. Ringer, Z.F. Zheng, D.Y. Song, J.C. Zhao, J. Am. Chem. Soc. 127 (2005) 6730 – 6736.

[38] APAH (2005) Standard methods for the examination of water and wastewater, 21st edition.

[39] A.G. Rincón, C. Pulgarin, Appl. Catal. B: Environ. 44 (2003) 263 – 284.

[40] A.G. Rincón, C. Pulgarin, Appl. Catal. B: Environ. 51 (2004) 283 – 302.

[41] Q. Chang, H. He, Z. Ma, J. Inorg. Biochem. 102 (2008) 1736 – 1742.

[42] R. Sonohara, N. Muramatsu, H. Ohshima, T. Kondo, Biophys. Chem. 55 (1995) 273 – 277.

[43] M. Heyde, R. Portalier, FEMS Microbiol. Lett. 69 (1990) 19.

[44] H.N. Pham, T. McDowell, E. Wilkins, J. Environ. Sci. Health A 30 (1995) 627 – 636.

[45] R.J.W. Lambert, M.D. Johnston, E.A. Simons, J. Appl. Microbiol. 87 (1999) 782-786.

[46] R.J.W. Lambert, M.D. Johnston, J. Appl. Microbiol. 88 (2000) 907-913.

[47] M. Cho, H. Chung, W. Choi, J. Yoon, Water Res. 38 (2004) 1069 – 1077.

[48] M. Cho, H. Chung, J. Yoon, Appl. Environ. Microbiol 69 (2003) 2284-2291.

[49] L.L. Gyürék, G.R. Finch, J. Environ. Eng. 124 (1998) 783 – 792.

[50] A.K. Benabbou, Z. Derriche, C. Felix, P. Lejeune, C. Guillard, Appl. Catal. B: Environ. 76 (2007) 257-263.

[51] S.B. Farr, T. Kogoma, Microbiol. Rev. 55 (1991) 561 – 585.

[52] R. Dillert, U. Siemon, D. Bahnemann, Chem. Eng. Technol. 21 (1998) 356 – 358.

[53] I.C. Escobar, S. Hong, A.A. Randall, J. Membr. Sci. 175 (2000) 1 – 17.

[54] F. Ribas, J. Frías, J.M. Huguet, F. Lucena, Water Res. 31 (1997) 639 – 649.

[55] I.C. Escobar, A.A. Randall, Water Res. 35 (2001) 4444 – 4454.

SUB-CHAPTER 7.3

KINETIC AND MATHEMATICAL MODELLING FOR THE PHOTOCATALYTIC INACTIVATION OF ESCHERICHIA COLI IN AN ANNULAR SLURRY PHOTOREACTOR USING TITANATE NANOFIBER CATALYST

M.N. Chong [a, b], B. Jin [a, b, c], C. Saint [b, c]

[a] School of Chemical Engineering, The University of Adelaide 5005 Adelaide Australia

[b] Schools of Earth and Environmental Sciences, The University of Adelaide 5005 Adelaide Australia

[c] Australian Water Quality Centre, South Australian Water Corporation, 5000 Adelaide South Australia

Submitted manuscript to Chemical Engineering Journal.

STATEMENT OF AUTHORSHIP

KINETIC AND MATHEMATICAL MODELLING FOR THE PHOTOCATALYTIC INACTIVATION OF ESCHERICHIA COLI IN AN ANNULAR SLURRY PHOTOREACTOR USING TITANATE NANOFIBER CATALYST

Submitted manuscript to Chemical Engineering Journal.

Chong, M.N. (Candidate)

Performed experiment design; analysis of samples; interpreted data; manuscript evaluation; wrote manuscript.

Signed……*Date*……..…

Jin, B.

Manuscript evaluation; acted as corresponding author.

I give consent for M. N. Chong to present this paper for examination towards the Doctor of Philosophy

Signed……*Date*……..

Saint, C. P.

Manuscript evaluation.

I give consent for M. N. Chong to present this paper for examination towards the Doctor of Philosophy

Signed……*Date*……..……

Kinetic and Mathematical Modeling for the Photocatalytic Inactivation of *Escherichia Coli* in an Annular Slurry Photoreactor using Titanate Nanofiber Catalyst

Meng Nan Chong [a, b], Bo Jin [a, b, c*], Chris P. Saint [b, c]

[a] School of Chemical Engineering, The University of Adelaide 5005 Adelaide Australia

[b] Schools of Earth and Environmental Sciences, The University of Adelaide 5005 Adelaide Australia

[c] Australian Water Quality Centre, South Australian Water Corporation, 5000 Adelaide South Australia

[*] To whom correspondence should be addressed.

Tel.: +61 8 8303 7056. Fax: +61 8 8303 6222. Email: bo.jin@adelaide.edu.au

Abstract

Semiconductor titanium dioxide (TiO_2) has been intensively studied as a promising photocatalyst for oxidation processes in water treatment. Titanate nanofiber catalyst (TNC) was proven as a promising alternate carrier in this study for the photocatalytic inactivation of sewage isolated *Escherichia coli* (ATCC 11775) in an annular slurry photoreactor (ASP). We studied the effect of TNC loadings on the inactivation performance of the surrogate indicator *E.coli* in a bench-scale ASP system. We also investigated the impact of TNC loadings on the dissolved oxygen (DO) level change during the photocatalytic inactivation of *E.coli*. The optimum TNC loading was found to be 1.0 g L^{-1}, resulting in a 99.999 % inactivation level of $7x10^6$ CFU mL^{-1} *E.coli* within 80 min of UVA irradiation. The photocatalytic inactivation activity of TNC on *E.coli* was then compared to the commercial Degussa P25 TiO_2 by using different empirically-estimated kinetic parameters. Owing to the presence of shoulders and tailing behaviours that cause non-linearity in the bacterial survivor curves, the modified Hom model appeared to be the best empirical correlation to account for the sigmoid-type inactivation profiles. Further Langmuir-Hinshelwood (L-H) mechanistic models were developed to account for the photocatalytic inactivation performance, in relation to the observed change in DO levels. An additional $K_{O2}[DO/DO_o]^{\alpha}(C_{undam}{}^{\alpha}+C_{dam}{}^{\alpha})$ term was

integrated in the proposed model for sub-optimal TNC loading owing to the limiting DO condition. These L-H mechanistic models show a reasonably good fittingness for the experimental results, and its cross validations verified the necessity of such term for accurate kinetic interpretation.

Keywords: TiO_2; Photocatalysis; Nanofibers; Photocatalytic inactivation; Kinetic Modelling; *Escherichia Coli*.

1. Introduction

The presence of pathogenic microbial communities in water sources either for drinking or ecosystem applications (i.e. aquaculture, agriculture or irrigation) are of concern owing to the possible outbreak of severe waterborne diseases [1]. To date, chlorination has been widely used as the most effective disinfection method to remove microorganisms in water treatment plants, while maintaining a residual free-chlorine along the water distribution lines [2 – 5]. Recently, the use of chlorination has come under close scrutiny due to the formation of different disinfection by-products (DBPs) such as trihalomethanes (THMs) and haloacetic acids (HAAs) under certain conditions. These resulted DBPs from the reaction between chlorine and different organic matters (i.e. DOC or NOM), are of health concern owing to their promotion of congenital cardiac defects and carcinogenic properties [6, 7]. The current US EPA allowable limits for THMs are 80 ppb in the treated water and 60 ppb for the sum of different HAAs (i.e. chloro-, dichloro- and trichloro-acetic acid) [7].

In view of such increasing environmental and health concerns, alternative water treatment technologies for water disinfection without formation of DBPs are highly sought. Among the advanced oxidation processes, heterogeneous photocatalysis utilising semiconductor titanium dioxide (TiO_2) has been recognised as an attractive and promising candidate to replace the chlorination practice. Reactive oxygen species (ROS) (i.e. $OH^{\bullet}$, $O_2^{\bullet-}$ and H_2O_2) generated from the photo-induced TiO_2 surface charge separation have a high oxidising potential to break down the organic contaminants and microbial cells that are present in water [8 – 10]. These

ROS are usually short-lived, unselective and react instantaneously with both microbial and organic contaminants for their inactivation, oxidation and eventually lead to their complete removal from the treated water [11]. The photocatalytic process is thus, an ideal technology that should be commercialised for water treatment as it reduces the significant disinfectant costs and formation of various DBP compounds.

Currently, the practicality of photocatalytic water disinfection process is being impeded by the difficulty in post separation and recovery of the Degussa P25 TiO_2 photocatalyst particles after treatment [12]. The fine dimensions of photocatalyst particles means they can penetrate through the downstream process and consumed by the end stream user. Since the photocatalyst particles exhibit better photon-induced surface charge separation in the nano-dimensional size range, many have investigated conserving such quantum properties while presenting a macrostructure for particle recovery. This includes the immobilisation of nanoscale TiO_2 onto various inert substrates, such as clay minerals, fibre optics and magnetic cores [12]. Immobilised photocatalysts however, have reduced photoactivity due to their structurally-impeded light photon activation, increased tortuosity and mass transfer resistance for photocatalytic reaction [12, 13]. A titanate nanofibers catalyst (TNC) with thin and long fibril morphology was recently developed for application in photocatalytic water treatment [14, 15]. This TNC consists of small anatase TiO_2 crystals of 10 – 20 nm deposited on titanate fibrils of 40 – 100 nm thickness and length up to 30 µm. Its photoactivity for oxidation of organic compounds was investigated previously [13]. The advantages of TNC include low mass transfer resistance due to its thin fibril morphology, ease of dispersion and recovery by free photocatalyst settling [13].

Preliminary investigations of photocatalytic disinfection technology in water treatment has been previously demonstrated on a diverse range of coliforms, viruses, bacteria, cysts, fungi, algae and protozoa [16 – 18]. Surprisingly after Matsunaga and co-workers pioneering work on the bactericidal effect of semiconductor TiO_2 in 1985, few studies have emphasized on the detailed kinetic modelling of photocatalytic bacterial inactivation activity during water treatment [19]. The absence of such kinetic interpretation has seriously hindered the proper development of large-scale photocatalytic disinfection technology. To date, the most commonly reported photocatalytic disinfection kinetics has been centred on the commercial

Degussa P-25 TiO_2 that poses serious photocatalyst recovery issues. In this study, the TNC was assessed for its photocatalytic inactivation of an *E.coli* strain in an annular slurry photoreactor (ASP). A sewage-isolated *E.coli* strain (ATCC 11775) was used as an indicator microorganism for faecal contamination and microbiological standard to measure against the treatment efficiency. The purpose of using this isolated *E.coli* strain over common laboratory strains is that it permits measurement of disinfection ability against an environmental isolate rather than a possibly attenuated laboratory strain that may yield misleading results. So far, *E.coli* is the most widely used microbiological standard for photocatalytic water treatment and thus, considered appropriate for comparison with other studies [3, 7]. The influence of TNC loading on the inactivation kinetics of *E.coli* and its simultaneous dissolved oxygen (DO) change in the TNC-ASP coupling system was investigated. The resultant disinfection kinetic data were then compared with different empirical kinetic models. Two DO-correlated mechanistic models were proposed based on the observed inactivation kinetics to both DO level and TNC loading changed. Further cross validations on these DO-correlated models were investigated, in order to verify its fittingness in representing the TNC disinfection data.

2. Material and methods

2.1. Materials

The *H-titanate nanofiber catalyst* (TNC) was synthesized through a hydrothermal reaction between concentrated NaOH and TiO_2 and a post-synthesis ion exchange with HCl solution [14, 15]. Specifically, 3 g of anatase particles (~325 mesh from Aldrich) was mixed with 80 mL of 10 M NaOH. The resultant suspensions were sonicated for 30 min and transferred into a PTFE container for autoclaving. The autoclave was maintained at a hydrothermal temperature of 180 °C for 48 h. The precipitate (sodium titanate nanofibers) was recovered, washed with distilled water (to remove excess NaOH) and finally exchanged with H^+ (using a 0.1 M HCl solution) to produce hydrogen TNC. These products were repeatedly washed with distilled water until pH ~7 was reached. The hydrogen titanate product was dried at 80 °C for 12 h and then calcined at 700 °C for 3 h to yield anatase nanofibers. Further detailed synthesis and microscopic characterisations of the TNC can be obtained from Zhu and co-workers [14, 15].

2.2. Annular Photocatalytic Reactor System

A stainless steel-lined ASP was used in this study [13]. The ASP was operated as a three-phase continuous air-aerated open system, where TNC particles were dispersed in the targeted water by the bubbles formed. The lower-end of the ASP was fabricated with a detachable conical bottom free of reaction dead zone, making it easy for cleaning and maintenance. A 45-μm air sparger was fitted to the detachable conical bottom to provide homogeneous bubble distribution for agitation, mixing and aeration for the photocatalytic reaction. The light configuration in the ASP was designed where additional light could be placed within the central quartz core. In this study, an UVA black light of 8W (NEC, Holland) was fitted annularly within the quartz thimble to prevent direct contact with the reaction fluid, while allowing optimal UV transmission for surface activation of the suspended TNC fibrils. It should be stressed that the UVA light used in this study was purely for the photonic surface activation of the TNC alone. Unlike the germicidal UVC light with high-end UV electromagnetic spectrum (i.e. 4.43 – 12.4 eV), the associated lethal UV energy for such UVA is significantly lower (i.e. 3.10 – 3.94 eV) and will not cause substantial bacterial inactivation. The wavelength range of UVA light lies in the range of 315 – 400 nm, which is close to solar irradiation. Samples were collected from four-descended level sampling ports. Electronic probes and meters for in-situ data logging of pH, DO and temperature (TPS, Australia) were connected to the reactor. The operating temperature for the ASP system was kept at room temperature of 25^{o}C during the experiments. A detailed design of the ASP and the whole experimental set up are shown in Figure 1.

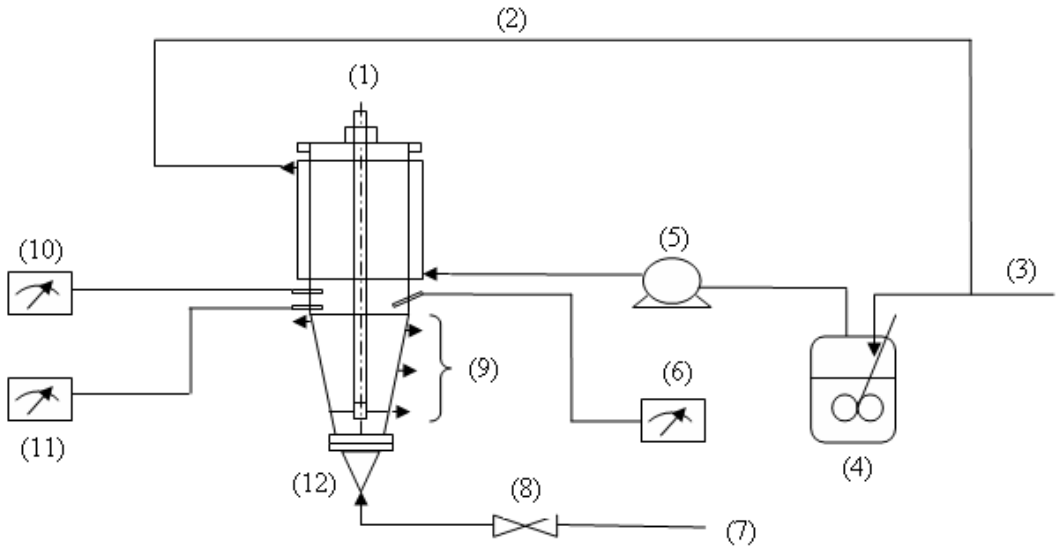

Figure 1: Experimental set-up for the annular slurry photoreactor system: (1) UV light, (2) Recirculation water line, (3) Fresh cool water line, (4) Cooling water vessel, (5) Cooling water pump, (6) Temperature meter, (7) Compressed air supply line, (8) Compressed air regulation valve, (9) Sampling ports, (10) pH meter, (11) Dissolved oxygen meter, (12) Photoreactor.

2.3. Photocatalytic Disinfection Experiments

The ASP column was filled with 1.5 L of bacterial suspension at a given cell density for each batch run. *E.coli* (ATCC 11775) was used as the microbiological standard in this study. Fifty-mL of fresh liquid culture was prepared in a tryptone soy broth medium (TSB) (Oxoid, England) and incubated in a rotary shaker at 150 rpm and 35^{o}C for 19 h. The final bacterial density was determined to be $9x10^{9}$ CFU mL^{-1}.

To prepare the bacterial suspensions for each batch experiment, an aliquot of the incubated liquid culture was directly inoculated into 1.5 L of phosphate buffered saline (PBS) solution, prepared using Nanopure Water of 18.2 MΩ cm resistivity. The use of PBS is to prevent sudden osmotic shock to the bacteria, so as to maintain the bacterial numbers for accurate dilution purposes. Subsequently, the initial bacterial density was determined via heterotrophic plate counting (HPC).

Prior to the disinfection experiment, a determined amount of TNC was added to the bacterial suspension in the ASP and further homogenized in the dark for 30 min under constant aeration. The UVA light was turned on after the homogenisation period at t = 0 min and the aeration were run continuously for 120 min. Samples were collected every 10 min up to 40 min, and thereafter every 20 min up to 120 min. The enumeration of the *E.coli* was carried out by following a standard serial dilution procedure and every sample was HPC in the prepared plate count agar (PCA) (Merck, Germany) in duplicate. The PCA plates were then incubated at 35^{o}C for 24 h before final cell counting. The normalised fraction of bacterial survivors against irradiation time curve was plotted for inactivation analysis. Each photo-disinfection experiments were then repeated for standard experimental verification and error analysis.

3. Results and Discussion

3.1. Impact of TNC Loading on Dissolved Oxygen Level

The effects of photocatalyst loading on the inactivation rate of *E.coli* had been investigated using different semiconductor photocatalysts, mostly Degussa P-25 TiO_2 [7, 8]. Figure 2a shows the photocatalytic inactivation of *E.coli* at TNC concentration ranges of 0.25 to 2.0 g L^{-1}. Since DO is an important reactant in the photocatalysis reaction and microbial respiration activity, a standard DO electrode was probed to verify which scenario is pre-dominant during the photocatalytic inactivation process in the ASP (i.e. Figure 2b) [20].

From Figure 2a, we observed that no substantial bacterial inactivation took place when TNC fibrils were added to the *E. coli* suspension under both UVA irradiated and dark conditions. The concentration of *E.coli* however, reduced dramatically within 40 min of UVA irradiation when TNC fibrils were added. The photocatalytic inactivation rate increased considerably when the TNC loading increased from 0.25g L^{-1} to 1.0g L^{-1}. A plateau in the inactivation rate was observed when the TNC loading was doubled from 1.0 g L^{-1} to 2.0 g L^{-1}. It was seen that under 0.25 g L^{-1} TNC loading, 120 min of irradiation time was required to achieve 99.999% inactivation level. The DO level change for 0.25 g L^{-1} TNC loading was found to be less significant than both the control experiments, but more significant than other TNC loadings.

This was owing to the open system nature of the ASP, where the reaction water was continuously aerated with compressed air.

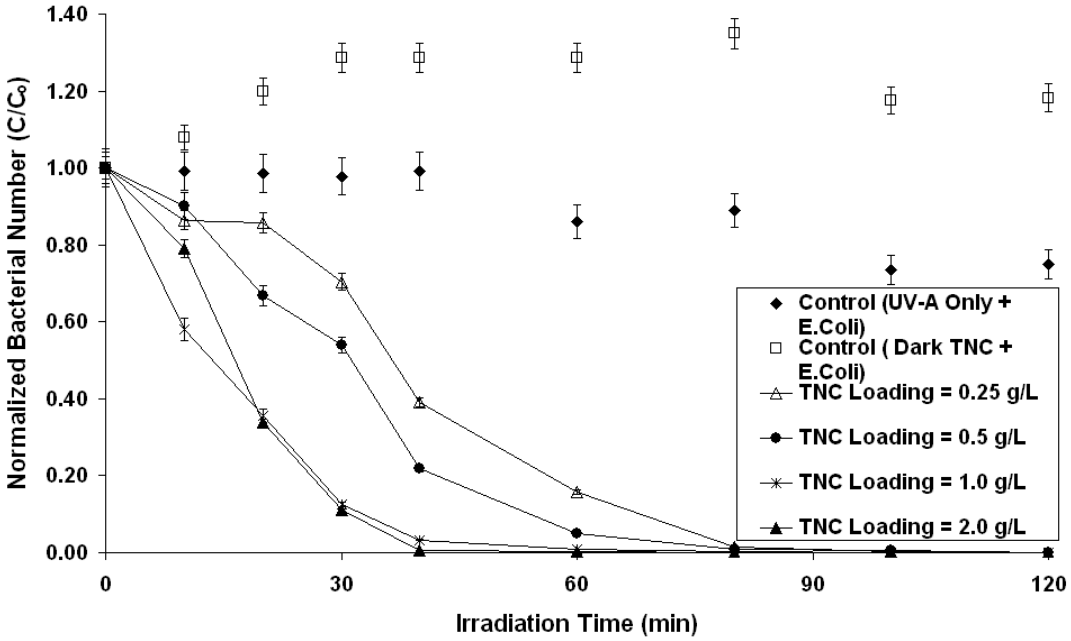

(a)

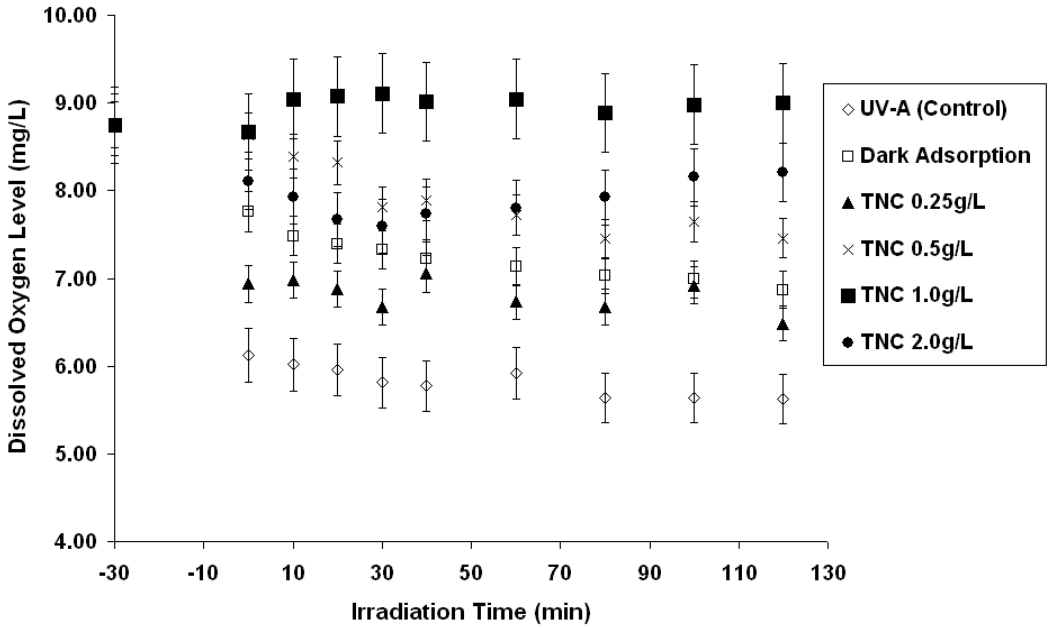

(b)

Figure 2: Photocatalytic inactivation of aqueous *E.Coli* (ATCC 11775) suspension of average initial density $7x10^6$ CFU mL^{-1}. (a) Bacterial reduction ratio (N/N_o) against irradiation time; (b) Measured DO profiles. UVA irradiation starts at t = 0 min.

The control experiment with UVA irradiation only consumed lower levels of DO for microbial respiration owing to the partial UVA photolysis, while substantial bacterial growth was enhanced in the dark control experiment. The direct absorption of UVA energy by the light sensitive cellular components of *E.coli* in this instance creates intermittent destructive effects on the *E.coli* itself without causing a complete bacterial cell inactivation [20]. When the UVA light was absent in the dark control experiment, a higher utilization rate of DO for bacterial growth was seen. Thus, the rate of photocatalytic inactivation of *E.coli* at 0.25 g L^{-1} TNC loading was seen to partially intercept the rapid DO utilization rate in the dark control experiment by low ROS generation rate.

When the TNC loading was increased to 0.5 g L^{-1}, it was observed that the irradiation time required to achieve 99.999% inactivation level for a similar bacterial density was reduced to 100 min. From Figure 2, it can be observed that the relative DO decay for TNC loading of 0.5 g L^{-1} is substantially smaller than the loading of 0.25 g L^{-1}. This indicated that doubling of the TNC loading will yield higher ROS generation rate and the subsequent photocatalytic reaction was rapidly onset before any microbial respiration could take place. Higher photocatalytic inactivation rate in this instance was seen to be proportionate to the doubling amount of TNC active sites used. It was interesting, however, to note that the DO decay profile was closer to the initial DO saturation value than the TNC loading of 0.25 g L^{-1}. The smaller DO decay was deduced to be offset by the simultaneous release of intracellular trapped oxygen and rapid DO replenishment from the air-water equilibrium within the open ASP system. Thus, it can be concluded that at TNC loading of 0.5 g L^{-1}, the variation in DO profiles were mainly dominated by the rapid ROS generation rate.

Doubling of the TNC loading from 1.0 to 2.0 g L^{-1} was found to result in a slight reduction in the photocatalytic inactivation rate required to achieve 99.999% of *E.coli* inactivation. This indicates that the optimum TNC loading in the ASP system for an effective disinfection process occurs at a concentration of 1.0 g L^{-1}. At TNC loading of 1.0g L^{-1}, it was interesting to note that the DO profile was quickly rejuvenated within the first 30 min of irradiation and remained at the highest level when compared to other TNC loadings. This maybe explained by the fact that at such optimum TNC loading, a well-dispersed number of illuminated active sites were achieved to generate maximum number of ROS for rapid photocatalytic inactivation.

This was further evident by the length of the shoulder region of each bacterial survivor curve in Figure 2a, where the inactivation curve at a TNC loading of 1.0 g L^{-1} appears to have the shortest shoulder and subsequently exhibited a rapid log-linear reduction in the subsequently enumerated *E.coli*. Marugán et al. [6] agreed that the length of such a shoulder region in the photocatalytic inactivation curves was due to the volumetric rate of ROS generation, which is a factor of photocatalyst concentration and incident radiation flow within the reactor. In this instance, the DO decay mechanism can be viewed as completely influenced by the volumetric ROS generation rate rather than the sluggish DO uptake for bacterial growth. A slightly saturated DO level (~ 8.75 mg L^{-1}) was observed for the optimum TNC loading after a slight initial decay at t = 0 min. The overall mass transfer limitation of DO to the thin TNC fibril for ROS generation was observed to be quite modest at TNC loading of 1.0 g L^{-1}. From Figure 2b, it can be concluded that the DO was a non-limiting reactant for the photocatalytic inactivation at optimum TNC loading. Thus, it can be concluded that different TNC loadings in the ASP have a direct impact on the DO decay profiles and the eventual photocatalytic inactivation rate of *E.coli*. It is likely that at an optimum TNC loading, the DO would be a non-limiting reactant in the photocatalytic inactivation mechanism under an open reactor system. This should be particularly noted for the exclusion of such non-limiting DO term during the development of a mechanistic disinfection model.

3.2. Comparison and Empirical Kinetics Evaluation for the Photocatalytic Inactivation Activity of *E.coli* in TNC-ASP System

Since the first application of semiconductor photocatalysts for disinfection by Matsunaga et al. [19], most studies found in the literature on the kinetics of photocatalytic inactivation of microorganisms during water treatment are of empirical-typed. To date, the most commonly used kinetic interpretation in photocatalytic disinfection is the classical Chick-Watson (CW) model with different *CT* values for the comparison of disinfection efficiency [21 – 23].

In this study, the classical CW model was found inadequate for simplifying such the TNC disinfection action. This was owing to the occurrence of three different regions in the photocatalytic inactivation curves (i.e. Figure 2a). The inactivation profile begins with (i) a lag or initial smooth decay, known as the “shoulder”, followed by (ii) a typical log-linear

inactivation region and ends with (iii) a long deceleration process at the end of the disinfection, which is known as the "tail". The presence of the shoulder region in the inactivation curve was justified by the nature of the cumulative damage of the photocatalytic treatment on the cytoplasmic membrane rather than an instantly lethal affect [24]. This can also be viewed in term of the slow permeation rate of the ROS species, which are bounded by their short half-life, through the cell wall before inducing any irreversible damage to the bacterial cell. The tail region for the photocatalytic inactivation in water treatment, however, is not well understood. Benabbou et al. [25] proposed that such a tail region, where the entire disinfection process was prolonged, is related to the competition for photocatalysis between the organic products released from the constant cell lyses and the remaining intact cells. Others proposed that the tailing deviations from the conventional log-linear reduction curves were due to the presence of variations in the bacterial population resistant to the disinfection method used [23].

During empirical model evaluation, a demand-free condition was usually assumed where the photocatalyst concentration generated during the irradiation period photocatalysis are considered to be constant. To compare the photocatalytic inactivation activity by the TNC on *E.coli*, different empirical models were fitted to obtain the kinetic parameters for comparison. Hom [26] reproduced a useful empirical integration of the CW model after having observed a curvilinear disinfection plots, rather than typical log-linear type (Eq. 1);

$$\log\frac{C}{C_O} = -kN^nT^m \qquad \text{(Eq. 1)}$$

where log C/C_o = bacterial log reduction; C = number of bacterial survivors at irradiation time t; k = experimental reaction rate; N = concentration of photocatalyst used; m and n are the empirical constants.

The resultant Hom model is a two-parameter empirical disinfection model and can either represent the shoulder or tail region. A further modification to this Hom model has been proposed to reproduce the different inactivation regions during TNC photocatalytic inactivation [6, 21];

$$\log\frac{C}{C_O} = -k_1\left[1-\exp(-k_2 t\right]^{k_3} \quad \text{(Eq. 2)}$$

This modified Hom model (Eq. 2) expands the applicability of the original Hom model for the simultaneous fitting of the initial shoulder, log-linear reduction and prolonged tailing behaviour. Another empirical model that can detail the different regions in the photocatalytic inactivation kinetics using the TNC is a power law expression [24];

$$\frac{dC}{dt} = -kC^x N^n \quad \text{(Eq. 3)}$$

Integration of this power rate law yields the Rational model (Eq. 4);

$$\log\frac{C}{C_O} = -\frac{\log\left[1+C_O^{x-1}(x-1)kN^n T\right]}{(x-1)} \quad \text{(Eq. 4)}$$

The resulting Rational model (Eq. 4) can describe both the shoulder and tailing-off characteristics for x less than and greater than unity respectively. Similarly, the Hom model (Eq. 1) can also be modified and integrated accordingly to yield the four-parameter Hom-Power law model (Eq. 5) [27];

$$\log\frac{C}{C_O} = -\frac{\log\left[1+C_O^{x-1}(x-1)kN^n T^m\right]}{(x-1)} \quad \text{(Eq. 5)}$$

The Selleck model (Eq. 6) reduces the number of null parameters in the empirical model; where S is the survival ratio = C/C_o at irradiation time t; k and K are the rate constants.

$$\frac{dS}{dt} = \frac{kCS}{1+KCT} \quad \text{(Eq. 6)}$$

Table 1 shows the evaluation outcomes for different empirical models on the photocatalytic inactivation kinetics of *E.coli* at 1.0 g L^{-1} of TNC loading. Results revealed that the application of the Hom model was limited to the condition where TNC loading was optimum. This is

owing to the occurrence of maximal ROS volumetric rate that deleted the long initial shoulder region, and thus the Hom model can selectively reproduce the tailing region of the inactivation curve. At the optimal TNC loading, the *m* value for the Hom model that accounted for the tailing of the inactivation curves was found to be $m = 0.21$. This *m*–value suggested the presence of strong tailing for disinfection in the TNC-ASP system [24]. It was also found that at $m > 1$, the Hom model could only reproduce the shoulder region. Owing to the empirical nature of the model, the *m*-value > 1 actually suggests increasing photocatalytic reactivity with irradiation time in the ASP. If the vitalistic assumption of bacterial population resistance distribution is valid, this actually signifies that the most resistant bacteria population are killed first prior to the least resistant one [23]. The empirical Hom model here was thus, considered as a pure correlation for experimental data analysis and comparison, rather than portraying any physical meaning for the disinfection action of TNC in the ASP system.

Table 1: Numerical evaluation for the fittingness of each empirical model on the inactivation kinetics of *E.coli* using TNC photocatalyst at a concentration of 1.0 g L^{-1}.

Empirical Model	***k***	***k_1***	***k_2***	***k_3***	***m***	***n***	***x***	***N_o***	***Correlation coefficient R^2***
Hom	1.9155	-	-	-	0.2084	1.1059	-	-	0.7531
Hom-Power	0.3568				0.9038	2.0300	0.9353	7.25E+06	0.9498
Modified Hom	-	5.6618	0.0578	10.5472	-	-	-	-	0.9976
Rational	0.9068	-	-	-	-	1.0800	1.4269	7.25E+06	0.9830
Selleck	0.6440	-	-	-	-	2.2782	-	-	0.7819

A better fittingness was observed with Hom-Power law, Rational model and modified Hom model at TNC loading of 1.0 g L^{-1}. It was observed that the Rational model could reproduce a partial shoulder and tailing region respectively, with certain logarithmic limitation at $x = 1.42$. However, this Rational model was found to provide a better fittingness over the Hom-Power

law as evidenced from the Pearson correlation coefficient R^2 values. Although the Hom-Power law involved four physical parameters, the logarithmic nature of its empirical expression has constrained the tendency for simultaneous representation of both shoulder and tailing behaviours. The inflexion of a smoothly fitted TNC inactivation curve with shoulder, log-linear and tailing region using the Hom-Power law was confined to the elementary logarithmic inactivation curve (i.e. no tailing representation). This over-parameterization model also provides a null physical meaning for each of its parameters in representing the disinfection action of TNC. In overall, the modified Hom model provides the best representation for the inactivation kinetics of *E.coli* using TNC in this study. It was found that the modified Hom model gives a more realistic mathematical expression as it takes into account all the different inactivation behaviours within its kinetics curve. Among all the empirical expressions, the Selleck model gives the least favourable representation for the TNC disinfection action in this study. Figure 3 compares the fittingness for the five different evaluated empirical models at TNC loadings of 0.25 g L^{-1} and 1.0 g L^{-1} respectively. The fitting of the modified Hom model for different TNC loadings is shown in Figure 4. With all these, the photocatalytic inactivation activity of the TNC could be compared with other photocatalysts via the estimated kinetic terms within each empirical model.

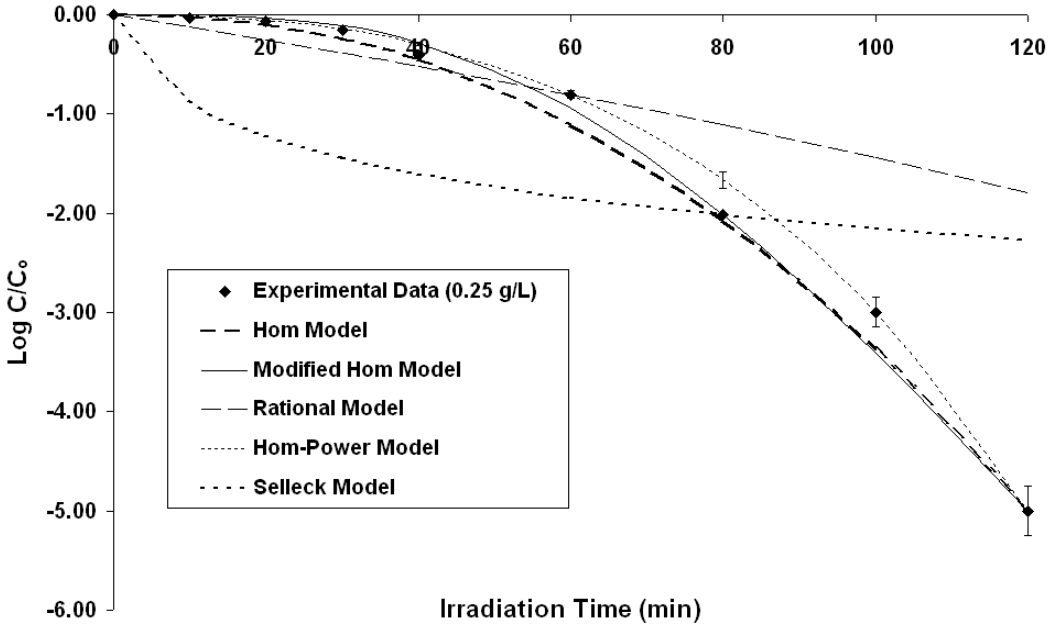

(a)

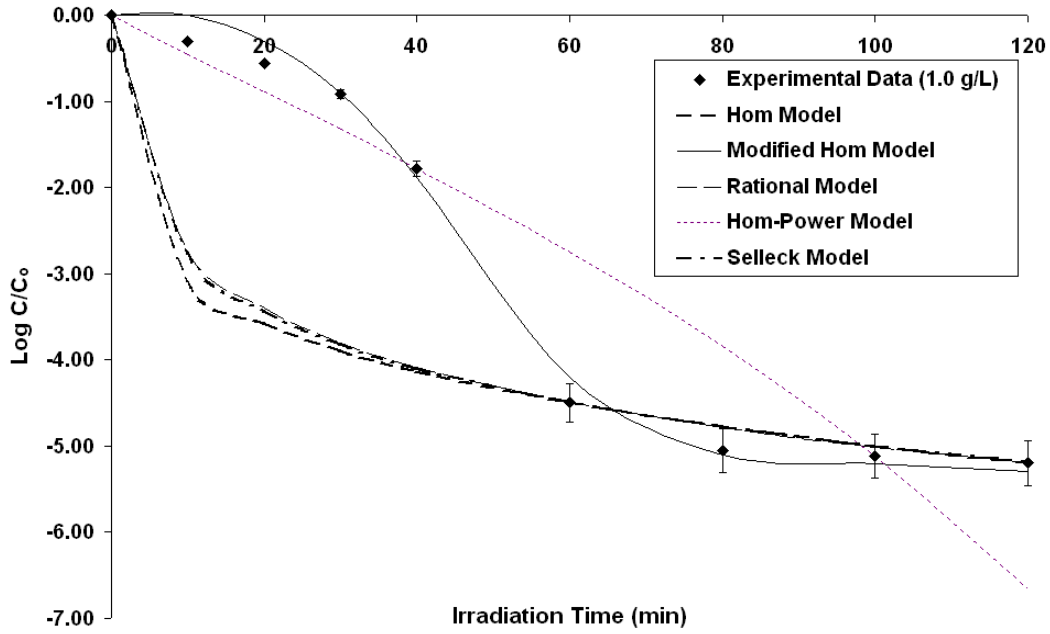

(b)

Figures 3: Fitting of different empirical disinfection kinetic models for TNC loading at (a) 0.25 g L^{-1} and (b) 1.0 g L^{-1} respectively. The average initial *E.Coli* concentration is $7x10^6$ CFU mL^{-1} and UVA irradiation starts at t = 0 min.

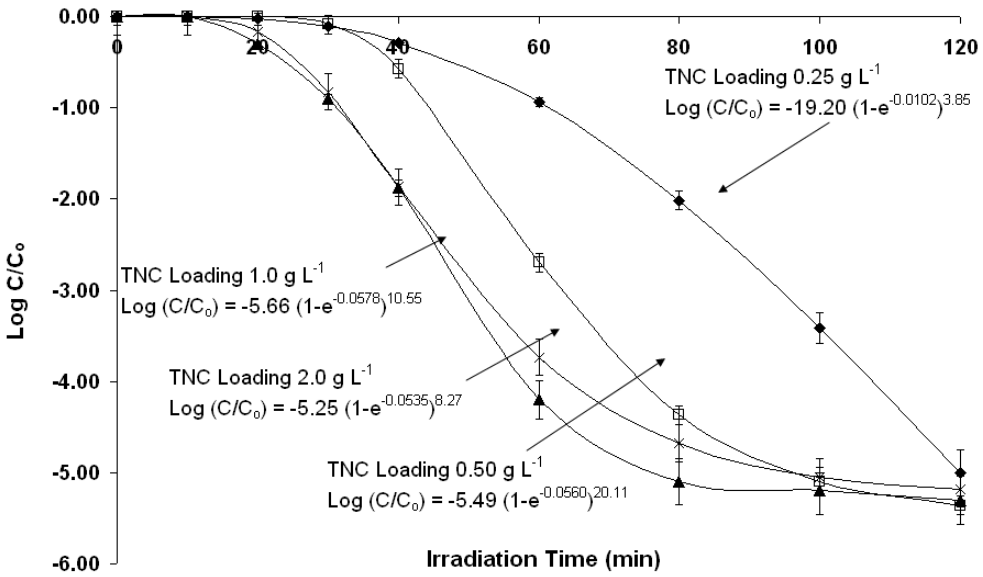

Figure 4: Fitting of modified Hom empirical model to experimental data with different TNC loadings. The average initial *E.Coli* density is $7x10^6$ CFU mL^{-1} and UVA irradiation starts at t = 0 min.

3.3. Development and Assessment of Mechanistic Modelling for *E.coli* Inactivation

Although the empirical models provide a better fit for the experimental data, the mathematical nature of their relevant terms usually yields null physical meaning in representing the photocatalytic inactivation behaviours. To elucidate the superiority of mechanistic model in expressing the disinfection action in the TNC-ASP coupling system, one was proposed here.

In the mechanistic hypothesis, the disinfection mechanism is a pure physicochemical phenomenon, and proceeded in a similar way as a chemical reaction [23]. The classical CW model (Eq. 7) is a typical example of the mechanistic disinfection kinetics model;

$$\frac{dC}{dt} = -k_o C \qquad \text{(Eq. 7)}$$

This basic CW equation dictates that the apparent exponential decay curves for the survival ratio against irradiation time follows similar decay mechanism of a chemical reaction, and is thus applicable under both phenomena. This can be visualised when (Eq. 7) is integrated

mathematically, where *C* assumes to be the number of moles of reactant to yield the log-linear curve of a first order chemical reaction.

To formulate a mechanistic model for the disinfection action of TNC in this study, however, one needs to have idealistic rationales to account for the shoulder and tailing region in the TNC inactivation curve (Fig. 2a). The presence of shoulder in the TNC inactivation curve can be justified mechanistically via the single-hit multiple targets or a series phenomenon event [24]. Under such a mechanistic assumption, the damage to the bacterial cell is viewed as cumulative rather than instantly lethal. This dictates that a large number of critical molecules need to be denatured prior to cell inactivation [24]. Severin et al. [28] proposed that the cumulative inactivation of a single organism can be collectively represented by a series of integer steps. These disinfection steps were thought to pass on an organism from one level to another in a first order reaction with respect to the TNC used until a finite number of damaged (*dam*) events was achieved. Microorganisms that accumulated less than the postulated number of damaged steps were considered to survive in the disinfection process. To comprehend this lethality concept, however, sufficient loading of TNC in the ASP had to be ensured where the volumetric ROS generation rate far exceeded the bacterial growth rate.

Many researchers have regarded that the tailing region was for the presence of a microbial subpopulation resistant to disinfection. Najm [29] supported a similar proposition that the tailing behaviour was due to the intrinsic distribution of bacterial resistance to the disinfection method that makes the bacteria more resistant, adapted and inaccessible. To date, no justifiable explanation has been proposed to account for the occurrence of tailing behaviour in water disinfection treatment with well-mixed conditions and equally resistant genetically cloned bacterial population in most of the studies. Some indicated that the tailing on the inactivation curves was a result of the gradual decline in the rate of inactivation, and total inactivation was achievable only after sufficient irradiation time.

In this study, we found that TNC loadings of higher than 1.0 g L^{-1} resulted in a significant prolongation of irradiation time to achieve 99.999% bacterial inactivation level. We found that even at an extended HRT of 360 min, the greatest bacterial inactivation level that could be achieved was only 99.995%. This observation not only conforms to the earlier hypothesis for

total inactivation after sufficient irradiation time, but is also deduced to be strongly affected by the TNC loading and annulus width of the ASP column [30]. At the current annulus width of 5 cm, the constant intensity of the UVA lamp used could easily penetrate through the low TNC suspension (0.25 g L^{-1}) to provide full illumination to the catalyst for ROS generation. This implies that even the *E.coli* adhered to the internal surface of the outer wall could be easily attacked by the generated ROS and thus, lead to lethality [17]. At higher TNC loadings, lower bacterial inactivation levels coupled with a strong photocatalytic inactivation tailing behaviour was observed. This was due to the high TNC loading that reduces the UVA light penetration, thus providing only partial illumination to the internal wall surface. A reduction in the current annulus width was expected to yield higher photocatalytic inactivation activity with no tailing characteristic. Although it is possible to increase the light intensity while retaining the current annulus width, it is foreseen to be unsuccessful owing to the mixing effects of catalyst particles, turbidity, ions and other water quality when real water/wastewater is used [9]. So far, there is no a single postulation that could ideally account for the tailing in water disinfection. All these propositions were acceptable under theoretical explanation of the observed tailing behaviour.

Lambert et al. [23] stated that in the formulation of mechanistic models that take into account the non-linearity inactivation behaviours, an intermediate population stage was usually suggested with different rates of disinfection for each microbial state. In this study, two different microbial states for the number of damaged bacterial and un-damaged bacteria (i.e. C_{dam} + C_{undam}) were introduced to account for the non-linearity in the survivor curves. As the interaction nature of the photocatalytic process in the ASP, a Langmuir-Hinshelwood (L-H) type of mechanistic kinetic model was proposed here (Eqs. 8 and 9) [6]. Since the TNC was earlier found to be non-limiting of DO at its optimal loading, two different kinetic expressions for each microbial state were extended from Marugan and co-workers findings [6] to take into account the impact change on DO level within the open ASP system.

$$\frac{dC_{undam}}{dt} = \frac{-k_{undam}K_{undam}C_{undam}^{\alpha}}{1+K_{undam}C_{undam}^{\alpha}+K_{dam}C_{dam}^{\alpha}+K_{O_2}[DO/DO_O]^{\alpha}(C_{undam}^{\alpha}+C_{dam}^{\alpha})} \quad \text{(Eq. 8a)}$$

$$\frac{dC_{undam}}{dt} = \frac{-k_{undam}K_{undam}C_{undam}^{\alpha}}{1+K_{undam}C_{undam}^{\alpha}+K_{dam}C_{dam}^{\alpha}} \quad \text{(Eq. 8b)}$$

$$\frac{dC_{dam}}{dt} = \frac{k_{undam}K_{undam}C_{undam}^{\alpha}-k_{dam}K_{dam}C_{dam}^{\alpha}}{1+K_{undam}C_{undam}^{\alpha}+K_{dam}C_{dam}^{\alpha}+K_{O_2}[DO/DO_O]^{\alpha}(C_{undam}^{\alpha}+C_{dam}^{\alpha})} \quad \text{(Eq. 9a)}$$

$$\frac{dC_{dam}}{dt} = \frac{k_{undam}K_{undam}C_{undam}^{\alpha}-k_{dam}K_{dam}C_{dam}^{\alpha}}{1+K_{undam}C_{undam}^{\alpha}+K_{dam}C_{dam}^{\alpha}} \quad \text{(Eq. 9b)}$$

where k_i is the true log-linear deactivation rate constant for the reaction between generated ROS and *E.coli*. The pseudo-interaction constant, K_i, represent the surface interaction between the TNC and *E.coli*. In the conventional L-H model of chemical reaction, K_i actually represents the strict interaction in terms of adsorption of the reactants onto the active sites of the catalyst. Due to the significant size differences between *E.coli* and the TNC particle, this term is better visualised as an interaction term that accounts for the shoulder appearance in the inactivation curve than the usual strict adsorption phenomenon. The inhibition coefficient, α, is a power-law expression that better accounts for the tailing behaviour in the inactivation curve. Although this inhibition coefficient can be fixed at α = 1, where the K_i could be expressed in terms of apparent K_i', such simplification should be avoided to represent the true tailing behaviours.

From the proposed mechanistic models, it can be seen that two different expressions were made for each microbial state (i.e. C_{dam} and C_{undam}). This was found to be in agreement with the earlier observation of DO profile at the optimal TNC loading. We found that when the TNC loading was optimum, the rapid ROS generation rate for disinfection can result in a non-limiting condition of DO reactant. It should be emphasized that DO is one of the basic reactants in photocatalysis, and insufficient DO will result in a limiting condition. Thus, two different expressions were tailored for each microbial state in order to visualise the importance of DO as a limiting reactant at TNC < $TNC_{optimal}$ (Eqs. 8a and 9a) and non-limiting at TNC = $TNC_{optimal}$ (Eqs. 8b and 9b). The K_{O2} term should be evaluated independently via the measured DO isotherms as presented in Figure 2b. So far, there have been no similar investigations that

correlate the effect of photocatalyst loading to its corresponding DO level. This correlation can be explained by the unique long fibril TNC morphology that is dissimilar to the commercial Degussa P25 TiO_2 photocatalyst. It was reported that the Degussa P25 TiO_2 experienced certain mass transfer limitations in terms of long diffusional paths for organic, microbial contaminants, light photon and DO respectively [31]. The thin titanate fibril of 40 – 100 nm with anatase TiO_2 crystals of 10 – 20 nm shorten the diffusional path, and thus promote rapid rates of DO evolution and surface reaction.

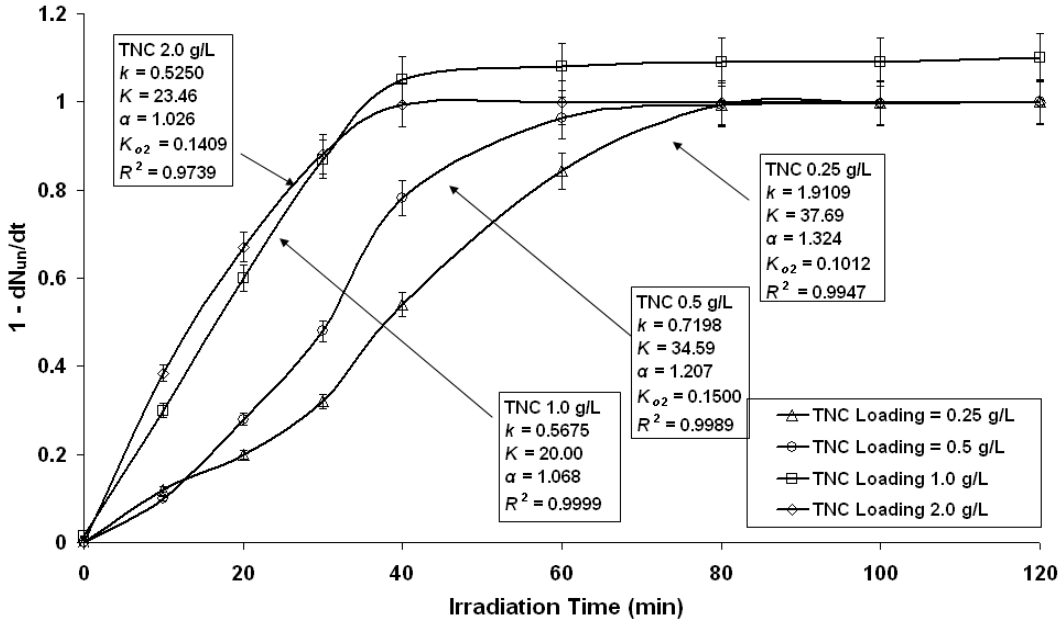

Figure 5: Fitting of a mechanistic kinetic model to experimental data of photocatalytic inactivation of average *E.Coli* density of $7x10^6$ CFU mL^{-1}. The UVA irradiation starts at t = 0 min.

One of the disadvantages of the proposed mechanistic models is that it requires prior knowledge on the optimal photocatalyst loading. To evaluate these models, some assumptions have to be made to prevent over-parameterization. Marugan et al. [6] proposed that the rate constant should equate to; $k_{dam} = k_{undam} = k$ and similarly the surface interaction constants, $K_{dam} = K_{undam} = K$. These reduce the proposed models to:

$$\frac{dC_{undam}}{dt} = \frac{-kKC_{undam}^{\alpha}}{1+K(C_{undam}^{\alpha}+C_{dam}^{\alpha})+K_{O_2}[DO/DO_O]^{\alpha}(C_{undam}^{\alpha}+C_{dam}^{\alpha})} \quad \text{(Eq. 10a)}$$

$$\frac{dC_{undam}}{dt} = \frac{-kKC_{undam}^{\alpha}}{1+K(C_{undam}^{\alpha}+C_{dam}^{\alpha})} \quad \text{(Eq. 10b)}$$

$$\frac{dC_{dam}}{dt} = \frac{kK(C_{undam}^{\alpha}-C_{dam}^{\alpha})}{1+K(C_{undam}^{\alpha}+C_{dam}^{\alpha})+K_{O_2}[DO/DO_O]^{\alpha}(C_{undam}^{\alpha}+C_{dam}^{\alpha})} \quad \text{(Eq. 11a)}$$

$$\frac{dC_{dam}}{dt} = \frac{kK(C_{undam}^{\alpha}-C_{dam}^{\alpha})}{1+K(C_{undam}^{\alpha}+C_{dam}^{\alpha})} \quad \text{(Eq. 11b)}$$

Fig. 5 shows the fitting of the experimental data using the proposed L-H mechanistic disinfection models. These models were found to give a high degree of fittingness. One problem which was encountered during the parameter estimation is that the oxygen-interaction term, K_{O2} needs to be first evaluated and the DO term was normalised [DO/DO_o] to achieve dimensional homogeneity with other denominator terms. The physical meaning of the DO limiting term, $K_{O2}[DO/DO_o]^{\alpha}(C_{undam}{}^{\alpha}+C_{dam}{}^{\alpha})$, actually signifies the presence of competition between the dissolved oxygen, un-damaged bacteria and the bacteria lysis products for surface active sites. At an increasing *K*-value, the length of the shoulder region was increased to enable interaction and longer reaction time for prime lethality events to occur. In addition, it should be noted from Fig. 5 that the tendency of tailing for the proposed mechanistic models was represented when α was greater than unity. This was observed in Fig. 5 where all the values for α is greater than unity, and this dictates that the reaction order with respect to the bacterial numbers is higher than unity. Fig. 6a shows the cross validation for the proposed models on the optimum TNC loading conditions, where its applicability and validity of Eq. 11a was tested. A lower R_2 value for the experimental data was observed using the DO limiting models. When the experimental data for non-$TNC_{optimal}$ conditions was tested on the DO non-limiting models (Eq. 11b), the surface-interaction constant (*K*) yields a significantly higher value than those reported in Fig. 5. It was understood that the surface-interaction constants take the $K_{O2}[DO/DO_o]^{\alpha}(C_{undam}{}^{\alpha}+C_{dam}{}^{\alpha})$ into account by integrating the effects into a

singular apparent constant of *K'* (i.e. $K' = K.\ K_{O2}[DO/DO_o]^{\alpha}(C_{undam}{}^{\alpha}+C_{dam}{}^{\alpha})$). All these have proven the rationale of correlating the effect of DO in the L-H mechanistic model for representing the disinfection action of TNC in the ASP system. The L-H models as presented were thus, considered as a more realistic approach to represent the inactivation activity of TNC in the ASP, in terms of its fittingness, physical meaning of each term and the practical integration of DO as a limiting reactant under non-optimal loading for the TNC used.

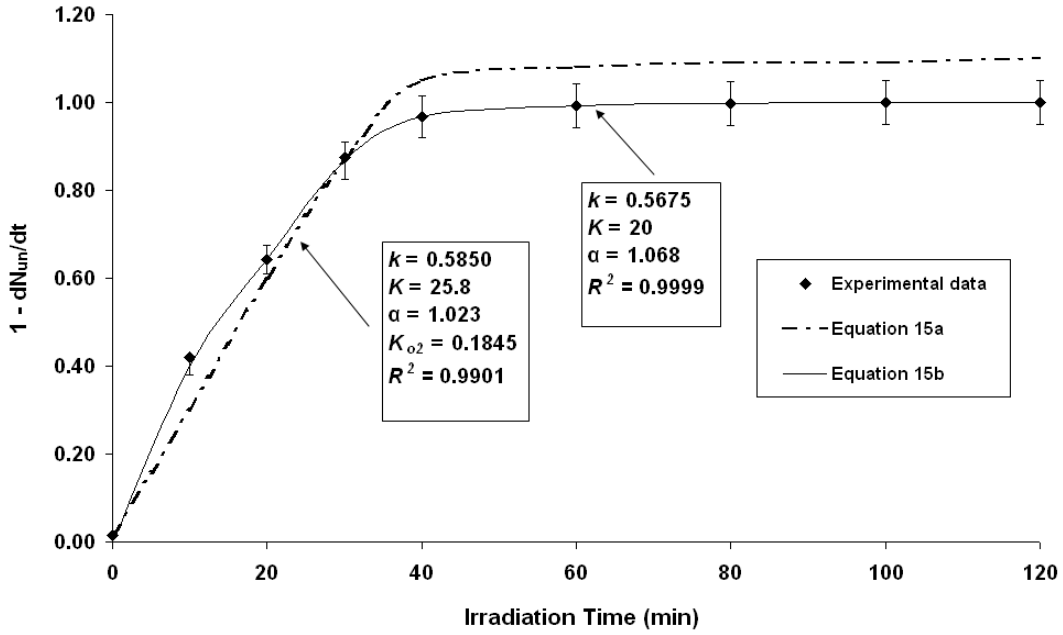

(a)

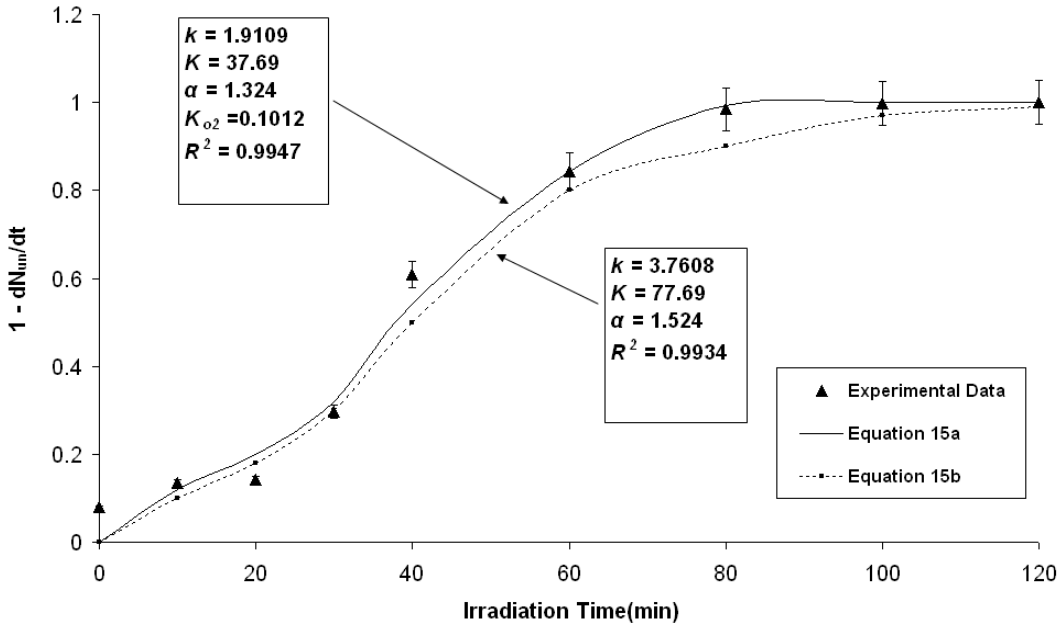

(b)

Figure 6: Cross validation for the proposed mechanistic models at TNC loadings of (a) 1.0 g L^{-1} and (b) 0.25 g L^{-1}.The average *E.Coli* density is$7x10^6$ CFU mL^{-1} and the UVA irradiation starts at t = 0 min.

4. Conclusion

The photocatalytic inactivation of sewage isolated *E.coli* strain (ATCC 11775) using UVA-TNC-photoreactor system was successfully implemented in this study. The optimum TNC loading was found to be 1.0 g L^{-1}, resulting in a 99.999 % inactivation level of $7x10^6$ CFU mL^{-1} *E.coli* within 80 min of UVA irradiation. It was found that the TNC loading in the ASP system also has a significant impact on the dissolved oxygen (DO) level. At the optimal TNC loading, the DO level was found to be a non-limiting reactant in the overall photocatalytic inactivation reaction. The rapid increase in the DO level at the $TNC_{optimal}$ condition was deduced to be owing to the thin titanate fibril morphology of TNC that shortens the DO diffusional path, and thus promotes a rapid rate of DO evolution and surface reaction. At other TNC loadings than the $TNC_{optimal}$, however, it was found that the DO levels appeared to be a limiting reactant in the photocatalytic inactivation reaction.

The photocatalytic inactivation activity of TNC was compared using the kinetic parameters estimated from the different empirical models. Since the inactivation profiles are highly non-linear, empirical models with at least 3 physical parameters were found to adequately represent the TNC inactivation data. The empirical expressions of the modified-Hom, Rational and Hom-Power models can adequately express the photocatalytic inactivation activity by TNC. In the case of Rational and Hom-Power models, however, it was found that both equations were of a logarithmic nature that restricts the curve inflexion for simultaneous representation of shoulder and tailing behaviours. The modified Hom model was found to be the best empirical expression for describing the bactericidal action of TNC on *E.coli* in the ASP system.

The L-H mechanistic models with three parameters; log-linear reaction rate (k), surface-interaction constant (K) and inhibition/tailing coefficient (α) were developed to simplify and give a better representation for the photocatalytic inactivation action. These models were further correlated with the effect of DO during inactivation in the ASP. Such DO-correlated models were built for which two different TNC loading states: sub-optimal and optimal were introduced. At the sub-optimal TNC loading condition, the DO acts as a limiting reactant and its absence may cause a pertinent effect to the disinfection rate; whereas DO level was found

as a non-limiting reactant at the optimal TNC loading. Cross validations on the proposed L-H models under both sub-optimal and optimal TNC loadings were examined to strengthen the observed DO correlation. It is anticipated that such models could be applicable to simulate the photocatalytic inactivation kinetics with different types of photocatalyst and water qualities.

Acknowledgement

The authors would like to thank Mr Philip Adcock for his valuable discussions and feedback during the initial planning stage of this study, and Associate Professor Huaiyong Zhu for providing the TNC samples. This work was funded by the Australian Research Council Linkage Grant (LP0562153) and the Australian Water Quality Centre, SA Water Corporation through the Water Environmental Biotechnology Laboratory (WEBL) at the University of Adelaide.

References

[1] Sun, D.D., Tay, J.H., Tan, K.M. (2003). Photocatalytic degradation of E.coliform in water. *Wat. Res.* 37: 3452-3462.

[2] Watts, R.J., Kong, S., Orr, M.P., Miller, G.C., Henry, B.E. (1994). Photocatalytic inactivation of coliform bacteria and viruses in secondary wastewater effluent. *Wat. Res.* 29(1): 95-100.

[3] Dunlop, P.S.M., Byrne, J.A., Manga, N., Eggins, B.R. (2002). The photocatalytic removal of bacterial pollutants from drinking water. *J. Photochem. Photobiol. A: Chem.* 148: 355-363.

[4] Wist, J., Sanabria, J., Dierolf, C., Torres, W., Pulgarin, C. (2002). Evaluation of photocatalytic disinfection of crude water for drinking-water production. *J. Photochem. Photobiol. A: Chem.* 147: 241-246.

[5] Rincón, A.G., Pulgarin, C. (2006). Comparative evaluation of Fe^{3+} and TiO_2 photoassisted processes in solar photocatalytic disinfection of water. *Appl. Catal. B: Environ.* 63: 222-231.

[6] Marugán, J., Grieken, R.V., Sordo, C., Cruz, C. (2008). Kinetics of the photocatalytic disinfection of Escherichia coli suspensions. *Appl. Catal. B: Environ.* 82: 27-36.

[7] Coleman, H.M., Marquis, C.P., Scott, J.A., Chin, S.S., Amal, R. (2005). Bactericidal effects of titanium dioxide-based photocatalysts. *Chem. Eng. J.* 113: 55-63.

[8] Cho, M., Chung, H., Choi, W., Yoon, J. (2004). Linear correlation between inactivation of E.coli and OH radical concentration in TiO_2 photocatalytic disinfection. *Wat. Res.* 38: 1069-1077.

[9] Rincón, A.G., Pulgarin, C. (2003). Photocatalytic inactivation of E.coli: effect of continuous-intermittent) light intensity and of (suspended-fixed) TiO_2 concentration. *Appl. Catal. B: Environ.* 44: 263-284.

[10] Rincón, A.G., Pulgarin, C. (2004). Effect of pH, inorganic ions, organic matter and H_2O_2 on E.coli K12 photocatalytic inactivation by TiO_2: Implications in solar water disinfection. *Appl. Catal. B: Environ.* 51: 283-302.

[11] Maness, P.C., Smolinski, S., Blake, D.M., Huang, Z., Wolfrum, E.J., Jacoby, W.A. (1999). Bactericidal activity of photocatalytic TiO_2 reaction: toward an understanding of its killing. *Appl. Environ. Microbiol.* 65(9): 4094-4098.

[12] Chong, M.N., Vimonses, V., Lei, S., Jin, B., Chow, C., Saint, C. (2009). Synthesis and characterisation of novel titania impregnated kaolinite nano-photocatalyst. *Micro. Meso. Mater*. 117(1): 233-242.

[13] Chong, M.N., Jin, B., Zhu, H.Y., Chow, C.W.K., Saint, C. (2008). Application of H-titanate nanofibers for degradation of Congo Red in an annular slurry photoreactor. *Chem. Eng. J* 150(1): 49-54.

[14] Zhu, H., Gao, X., Lan, Y., Song, D., Xi, Y., Zhao, J. (2004). Hydrogen titanate nanofibers covered with anatase nanocrystals: a delicate structure achieved by the wet chemistry reaction of the titanate nanofibers. *J. Am. Chem. Soc.* 126(27): 8380 – 8381.

[15] Zhu, H.Y., Lan, Y., Gao, X.P., Ringer, S.P., Zheng, Z.F., Song, D.Y., Zhao, J.C. (2005). Phase transition between nanostructures of titanate and titanium dioxides via simple wet-chemical reactions. *J. Am. Chem. Soc.* 127: 6730 – 6736.

[16] Wolfrum, E.J., Huang, J., Blake, D.M., Maness, P.C., Huang, Z., Fiest, J. (2002). Photocatalytic oxidation of bacteria, bacterial and fungal spores, and model biofilm components to carbon dioxide on titanium dioxide-coated surfaces. *Environ. Sci. Technol.* 36: 3412-3419.

[17] Hong, J., Otaki, M. (2003). Effects of photocatalysis on biological decolorization reactor and biological activity of isolated photosynthetic bacteria. *J. Biosci. Bioeng.* 96(3): 298-303.

[18] Ibánez, J.A., Litter, M.I., Pizarro, R.A. (2003). Photocatalytic bactericidal effect of TiO_2 on Enterobacter cloacae: Comparative study with other gram (-) bacteria. *J. Photochem. Photobiol. A: Chem.* 157: 81-85.

[19] Matsunaga, T., Tomodam, R., Nakajima, T., Wake, H. (1985). Photochemical sterilization of microbial cells by semiconductor powders. *FEMS Microbiol. Lett.* 29: 211-214.

[20] Rincón, A.G., Pulgarin, C. (2005). Use of coaxial photocatalytic reactor (CAPHORE) in the TiO_2 photo-assisted treatment of mixed E.coli and Bacillus sp. and bacterial community present in wastewater. *Catal. Today* 101: 331-344.

[21] Cho, M., Chung, H., Yoon, J. (2003). Disinfection of water containing natural organic matter by using ozone-initiated radical reactions. *Appl. Environ. Microbiol.* 69(4): 2284-2291.

[22] Lambert, R.J.W., Johnston, M.D., Simons, E.A. (1999). A kinetic study of the effect of hydrogen peroxide and peracetic acid against Staphylococcus aureus and Pseudomonas aeruginosa using the Bioscreen disinfection method. *J. Appl. Microbiol.* 87: 782-786.

[23] Lambert, R.J.W., Johnston, M.D. (2000). Disinfection kinetics: a new hypothesis and model for the tailing of log-survivor/time curves. *J. Appl. Microbiol.* 88: 907-913.

[24] Gyürék, L.L., Finch, G.R. (1998). Modelling water treatment chemical disinfection kinetics. *J. Environ. Eng.* 124(9): 783-793.

[25] Benabbou, A.K., Derriche, Z., Felix, C., Lejeune, P., Guillard, C. (2007). Photocatalytic inactivation of Escherichia coli: Effect of concentration of TiO_2 and microorganism, nature, and intensity of UV irradiation. *Appl. Catal. B: Environ.* 76: 257-263.

[26] Hom, L.W. (1972). Kinetics of chlorine disinfection in an ecosystem. *J. Sanitary Eng. Div.*, 98(1): 183-194.

[27] Anotai, J. (1996). Effect of calcium ions on chemistry and disinfection efficiency of free chlorine at pH 10. *PhD dissertation, Drexel University, Philadelphia, Pa.*

[28] Severin, B.F., Suidan, M.T., Engelbrecht, R.S. (1984). Series-event kinetic model for chemical disinfection. *J. Environ. Eng. ASCE* 110(2): 430-439.

[29] Najm, I. (2006). Formation of hydrazine as a chloraminse by-product. *J. Am. Wat. Works Assoc.* 98: 93-101.

[30] Shiraishi, F., Toyoda, K., Fukinbara, S., Obuchi, E., Nakano, K. (1999). Photolytic and photocatalytic treatment of an aqueous solution containing microbial cells and organic compounds in an annular-flow reactor. *Chem. Eng. Sci.* 54: 1547-1552.

[31] Chen, H.Y., Zahraa, O., Bouchy, M., Thomas, F., Bottero, J.Y. (1995). Adsorption properties of TiO_2 related to the photocatalytic degradation of organic contaminants in water. *J. Photochem. Photobiol. A: Chem.* 85: 179-186.

Brief Summary of Chapter 7

The main research tasks and findings in this Chapter 7 include:

- The photo-disinfection of a sewage isolated *E.coli* strain (ATCC 11775) using TiO_2-K and TNC in the ASP system was investigated.
- The optimum operating conditions of the ASP that contributes to 5-log bacterial reduction units of initial bacterial density of 7×10^6 CFU mL^{-1} were (1) 6.0 g L^{-1} TiO_2-K, pH 4.0 and 7.5 L min^{-1} aeration with an UVA illumination time of 70 min; (2) 1.0 g L^{-1} TNC, pH 4.0 – 5.0 and aeration rate of 5.0 L min^{-1} with an UVA illumination time of 60 min.
- The TiO_2-K catalyst was very active under wider span of pH conditions; up to pH 7.0 compared to the TNC fibrils. A very low photo-disinfection rate was examined at pH 10.0, which is related to the surface charge alteration that weakens the TiO_2-K-*E.coli* electrostatic interaction link.
- The photo-disinfection kinetics in the ASP system exhibited a highly non-linear bacterial inactivation profile, with shoulder lag, log-linear bacterial deactivation and prolonged tailing.
- The shoulder characteristic in the single particle terminal velocity of profile was strongly influenced by both the optimal photocatalyst loading and its homogeneous dispersion.
- Further empirical modelling of the non-linear photo-disinfection profile in the ASP system indicated that the modified Hom model was the best rate model for the bacterial inactivation profiles with three different regimes; shoulder, log-linear and tailing.
- The photo-disinfection kinetcs profiles using TiO_2-K and TNC confirmed that the empirical Rational and Hom-Power model equations showed a logarithmic nature and restricted the curve inflexion for simultaneous representation of shoulder and tailing behaviours.
- Coupled photocatalysis and dark Fenton study revealed that the residual disinfecting effect by the TNC could be initiated during the post-irradiation photocatalysis period, provided that the organic contents (COD) was sufficiently low (i.e. lower than 16 mg L^{-1}) at 1.0 mg L^{-1} Fe^{2+} concentration.

- The coupling photocatalysis study indicated that the bacterial *E.coli* is more susceptible to photocatalytic treatment than simple glucose compounds.
- The bacterial regrowth potential was highly dependent on the organic contents in the targeted water, and usually a longer UV irradiation was required to suppress the regrowth problem.
- The catalyst loading of TNC fibrils in the ASP system was examined to have a profound impact on the dissolved oxygen (DO) level. At the optimal TNC loading, the DO level was a non-limiting reactant in the overall photo-disinfection reaction.
- The rapid rejuvenation in the DO level at the optimal TNC loading was owed to its thin fibril morphology that shortens the DO diffusional path, and simultaneously promotes a rapid DO evolution rate and surface reaction. At other TNC loadings, the DO was a limiting reactant in the photo-disinfection reaction.
- Mechanistic Langmuir-Hinshelwood (L-H) photo-disinfection models were proposed, which take into account both the optimal and sub-optimal TNC loading. An additional DO term was introduced in the sub-optimal condition within the model, in order to elucidate its limiting role during the photo-disinfection reaction.
- The L-H mechanistic models were built with three main parameters, which are the log-linear reaction rate (k), surface-interaction constant (K) and inhibition/tailing coefficient (α) to simplify and give a better representation for the photo-disinfection reaction.

CHAPTER 8

ASSESSMENT OF SEQUENTIAL BATCH PHOTOREACTOR SYSTEM FOR THE REMOVAL OF CARBAMAZEPINE FROM SECONDARY MUNICIPAL WASTEWATER: IMPACTS OF EFFLUENT ORGANIC MATTER AND INORGANIC IONS

CHAPTER 8

ASSESSMENT OF SEQUENTIAL BATCH PHOTOREACTOR SYSTEM FOR THE REMOVAL OF CARBAMAZEPINE FROM SECONDARY MUNICIPAL WASTEWATER: IMPACTS OF EFFLUENT ORGANIC MATTER AND INORGANIC IONS

M.N. Chong [a, b], B. Jin [a, b, c], C. W. K. Chow [c], H. Zhu [d], C. P. Saint [b, c]

[a] School of Chemical Engineering, The University of Adelaide 5005 Adelaide Australia

[b] Schools of Earth and Environmental Sciences, The University of Adelaide 5005 Adelaide Australia

[c] Australian Water Quality Centre, South Australian Water Corporation, 5000 Adelaide South Australia

[d] School of Physical and Chemical Sciences, Queensland University of Technology, Brisbane, QLD 4001, Australia

Submitted to Water Research.

STATEMENT OF AUTHORSHIP

ASSESSMENT OF SEQUENTIAL BATCH PHOTOREACTOR SYSTEM FOR THE REMOVAL OF CARBAMAZEPINE FROM SECONDARY MUNICIPAL WASTEWATER: IMPACTS OF EFFLUENT ORGANIC MATTER AND INORGANIC IONS

Submitted to Water Research.

Chong, M.N. (Candidate)

Performed experiment design; analysis of samples; interpreted data; manuscript evaluation; wrote manuscript.

Signed……*Date*……..…

Jin, B.

Manuscript evaluation; acted as corresponding author.

I give consent for M. N. Chong to present this paper for examination towards the Doctor of Philosophy

Signed……*Date*……..

Chow, C. W. K.

Analysis of samples; manuscript evaluation.

I give consent for M. N. Chong to present this paper for examination towards the Doctor of Philosophy

Signed……*Date*……..……

Zhu, H.

Manuscript evaluation.

I give consent for M. N. Chong to present this paper for examination towards the Doctor of Philosophy

Signed……*Date*……..……

Saint, C. P.

Manuscript evaluation.

I give consent for M. N. Chong to present this paper for examination towards the Doctor of Philosophy

Signed……*Date*……..……

Assessment of Sequential Batch Photoreactor System for the Removal of Carbamazepine from Secondary Municipal Wastewater: Impacts of Effluent Organic Matter and Inorganic Ions

Meng Nan Chong [a, b], Bo Jin [a, b, c*], C. W. K. Chow [c], H. Zhu [d], Chris P. Saint [b, c]

[a] School of Chemical Engineering, The University of Adelaide 5005 Adelaide Australia

[b] Schools of Earth and Environmental Sciences, The University of Adelaide 5005 Adelaide Australia

[c] Australian Water Quality Centre, South Australian Water Corporation, 5000 Adelaide South Australia

[d] School of Physical and Chemical Sciences, Queensland University of Technology, Brisbane, QLD 4001, Australia

[*] To whom correspondence should be addressed.

Tel.: +61 8 8303 7056. Fax: +61 8 8303 6222. Email: bo.jin@adelaide.edu.au

Abstract

We assessed for the first time the photo-oxidation performance and operation mode of a sequential batch annular slurry photoreactor (SB-ASP) system for the removal of pharmaceutical Carbamazepine (CBZ) in secondary municipal wastewater. The SB-ASP system was operated in a sequential batch reactor (SBR) cycle. Two immobilized TiO_2 photocatalysts, namely anatase titanate nanofiber (TNC) and mesoporous TiO_2 impregnated kaolinite (TiO_2-K) catalyst were employed in the SB-ASP investigation. The influences of SBR cycles, effluent organic matter (EOM) and inorganic ions (nitrate and phosphate) on the SB-ASP performance were evaluated. It was found that the photocatalytic reaction preferentially attacks the high molecular weight EOM before the subsequent degradation of CBZ. The inorganic ions affected the surface fouling of the catalysts to a certain extent without completely retarding their photoactivity. This study revealed that the SBR operation of a photocatalytic reactor could be a useful operation mode in a semi-continuous treatment process to enhance the biodegradability of pharmaceuticals without constant catalyst

replacement. It is foreseeable that the combination of such SB-ASP operation with a biological treatment technology could be a cost-effective alternative treatment process for reclamation and reuse of municipal wastewater.

Keywords: TiO_2; Kaolinite Clay; Annular Reactor; Photocatalysis; Carbamazepine; Sequential Batch Reactor; Wastewater.

1. Introduction

In recent years, the presence of pharmaceutical residuals in wastewater has received increasing awareness from the research institutions and governmental organizations to public community worldwide owing to its potential deleterious impacts on both human beings and the natural ecosystems (Klavarioti et al., 2009; Kümmerer et al., 2009). When these pharmaceutical drugs are consumed, a proportion remains unchanged and passes through the human body as metabolites into the sewage system (Doll and Frimmel, 2005a, 2005b and 2005c). Muir et al. (1997) reported that 56-68% of a particular pharmaceutical compound can be excreted from the body during therapeutic use. Owing to the high chemical stability of these pharmaceutical drugs, their existence in the sewage system usually encompasses common chemical treatments and biotransformation processes with further possible contamination of the groundwater, surface water as well as drinking water sources (Heberer et al., 1997; Ternes, 1998; Putschew et al., 2000; Sacher et al., 2001; Anderson et al., 2004). These have created significant potential risks to the environment and public health. Thus, it is viable to search for a cost-effective treatment technology that could remove these substances from the wastewater effluents and altogether prevents its adverse effects from worsening in the natural environments.

Recently, the dependency on advanced wastewater treatment technologies are more elevated when the wastewater is to be treated for reuse. Radjenovic et al. (2009) found that the degree of biotransformation of 31 pharmaceuticals in an advanced membrane bioreactor (MBR) system was higher than in a conventional activated sludge treatment process. They found that, however, a few pharmaceuticals such as loratidine, carbamazepine and hydrochlorothiazide posses problematic, even with higher sludge retention times in MBR. Similarly, other

advanced treatment technologies such as ozonation, ultraviolet irradiation, photo-Fenton and filtration with granular activated carbon have been assessed for the effective removal of pharmaceuticals from the effluents (Zwiener and Frimmel, 2000; Ternes et al., 2002; Huber et al., 2003). Results showed that all these treatment methods experience a similar degree of partial removal of pharmaceuticals from the wastewater matrix. At the same time, some of these treatment methods incur high costs and create secondary pollution as the pharmaceutical residuals are transferred from one phase to another rather than being eliminated. To overcome the shortcomings of each of these technologies in pharmaceuticals removal, combinations of treatment technologies such as adsorption with ozonation or MBR with different advanced oxidation process (AOPs) have been proposed (Doll and Frimmel, 2004; Esplugas et al., 2007; Rosal et al., 2008).

Among the AOPs, heterogeneous photocatalysis employing semiconductor titanium dioxide (TiO_2) is an attractive candidate which can integrate with biological treatment processes and other AOPs (Doll and Frimmel, 2004; Belgiorno et al., 2007; Méndez-Arriaga et al., 2008). The mechanisms for the formation of electron-hole pairs on the surface of TiO_2 particles via a series of redox reactions are well-documented in the literature (Chong et al., 2009b). When the TiO_2 is photon-activated, the intermediary-formed hydroxyl radicals can react indiscriminately on the pharmaceuticals in order to degrade and even mineralize these environmentally persistent compounds. The TiO_2 photocatalysis in such a way could be integrated as a post-treatment process after the biological treatment. The treated water can be recycled back to biological process so as to enhance the biotransformation process. This biological-TiO_2 integrated process can improve treatment efficiency and water quality of the effluent, and can be cost-effective due to less foot-print land required. To date, however, the commercial application of TiO_2 photocatalysis is limited by the (1) low photocatalytic reaction turnover time and (2) photocatalysts deactivation, (3) post-separation of the solid photocatalyst particles and (4) the need of rapid reactivation of the TiO_2 particles in a separate unit operation (Chong et al., 2009a and 2009b; Benotti et al., 2009, Malato et al., 2009).

In this study, we operated and assessed for the first time a sequential batch annular slurry photoreactor (SB-ASP) system for the treatment of real secondary treated municipal wastewater spiked with antiepileptic drug of Carbamazepine (CBZ). A submerged

microfiltration module with porosity of 0.2 μm was integrated in a laboratory scale annular slurry photoreactor (ASP) in order to retain the TiO_2 photocatalysts for semi-continuous operation of the SB-ASP. Two self-made immobilized photocatalysts with microns size structure were used to facilitate the filtration, namely: anatase titanate nanofibers and mesoporous TiO_2-K catalysts. It was expected that the operation mode of SB-ASP could deliver a true engineering solution to resolve the technical problems in a commercial photoreactor system and further enhances the biodegrability of CBZ in the biological treatment. In addition, we also evaluated the influence of nitrate (NO_3^-) and phosphate (PO_4^{3-}) ions on the photocatalytic reaction. Further UV-Vis spectroscopic analysis via high performance size exclusion chromatography (HPSEC) at 260 nm and organic CBZ aromatic moieties at 280 nm was used to evaluate the change in the overall apparent molecular weight (AMW) profiles and the specific pharmaceutical indicator of CBZ. With these, the impacts of effluent organic matter (EOM) on the feasible photocatalytic degradation could be evaluated so as to determine the degree of organic mineralization.

2. Experimental

2.1. Chemicals

Anatase particles (~325 mesh from Aldrich), titanium (IV) butoxide (tetrabutyl orthotitanate, purum grade ≥ 97% gravimetric, Sigma-Aldrich) and absolute ethanol (AR grade, Labserv Pronalys Australia) were used as received. Raw kaolinite (K) clay materials were obtained from Unimin, Australia. Carbamazepine (CBZ) (Sigma-Aldrich) was dissolved accordingly in the secondary treated biological wastewater. Nitric acid HNO_3 (AR grade, Aldrich), hydrochloric acid HCl (Labserv Pronalys Australia) and sodium hydroxide NaOH (AR grade, Aldrich) were prepared to a designated concentration by the addition of Milli-Q water with 18.2 MΩcm resistivity.

Carbamazepine (CBZ) is an antiepileptic drug that is usually used as sedative. From a toxicological point of view, this drug can produce serious toxic effects on the liver and emopoietic system (Molinari et al., 2006). CBZ was used in this study, as a reaction surrogate

tracer to observe the effects of complexity in wastewater effluents on its removal. The complete chemical structure of CBZ is given as in Fig. 1.

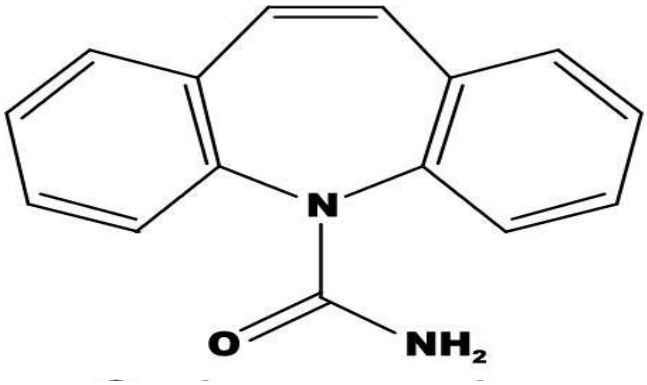

Figure 1: The chemical structure of Carbamazepine (an antiepileptic drug).

2.2. Preparation of Photocatalysts

Anatase titanate nanofibers catalyst (TNC) was synthesized through a hydrothermal reaction between concentrated NaOH and TiO_2 and a post-synthesis ion exchange with HCl solution (Zhu et al., 2004). Specifically, 3 g of anatase particles was mixed with 80 mL of 10 M NaOH. The resultant suspensions were sonicated for 30 min and transferred into a PTFE container for autoclaving. The autoclave was maintained at hydrothermal temperature of 180 °C for 48 h. The precipitate (sodium titanate nanofibers) was recovered, washed with distilled water (to remove excess NaOH) and finally exchanged with H^+ (using a 0.1 M HCl solution) to produce hydrogen TNC. These products were repeatedly washed with distilled water until pH ~7 was reached. The hydrogen titanate product was dried at 80 °C for 12 h and then calcined at 700 °C for 3 h to yield anatase nanofibers. The resultant TNC fibrils were measured with a thickness of 40 – 100 nm and length up to 30 µm. Such fibril structure of TNC is expected to be easily filtered and possesses high photocatalytic efficiency owing to its thin fibril morphology that removes mass transfer limitation.

The mesoporous TiO_2-K clay catalyst was synthesized by a modified two step sol-gel process (Chong et al., 2009a). Initially, 25 mL titanium n-butoxide precursor was hydrolysed by 30 mL of absolute ethanol. The hydrolysed mixture was then acid-catalysed with nitric acid of known molarity. In the following step, this acid-catalysed product was heterocoagulated with K-suspension of 10% (w/v) at 37^{o}C under constant stirring. The K clay particles in this

instance are to provide a mesoporous platform for the deposition of TiO_2 sol, enabling ease of post-separation of catalyst particles after water treatment and high surface area for enhanced adsorption. After the heterocoagulation process, the products were filtered and washed repeatedly with distilled water up to three times to remove any excess chemical impurities. The filtrate cake was dried in a conventional oven at 65-70^oC for 3 h, before being fired at 600^oC. The resultant TiO_2-K catalyst was measured to have particle size distribution spans from 0.03 to 600 μm, with median size of 3.5 μm.

2.3. Sample Preparation and Wastewater Collection

Primary wastewater sample was collected from the Glenelg Waste Water Treatment Plant (WWTP), South Australia. This effluent was treated in a laboratory scale MBR system of 4 L capacity. A Zenon® hollow membrane (surface area of 0.047 m^2 and nominal pore size of 0.1 μm) was used in the sequential batch MBR reactor, with a cycle of 15 min of wastewater recharge, 165 min of anoxic reaction, 60 min of aeration and followed by 240 min of combined aeration and filtration. The sludge retention time (SRT) used in the MBR was approximately 60 d. The treated effluents from the MBR were collected in a tank to ensure sufficient wastewater capacity for the subsequent photocatalytic integration treatment. Table 1 shows the wastewater quality of both the collected primary effluents from the WWTP and the secondary biological treated effluents from the MBR system.

Table 1: The average wastewater quality for the primary influent from the WWTP and the secondary biological MBR treated effluent.

Wastewater Parameters	Primary Influent to MBR	Secondary Treated Effluent from MBR
COD (mg L^{-1})	285 - 315	13.5 - 22.0
NO_3^- (mg L^{-1})	210 - 238	145.0 - 189.6
PO_4^{3-} (mg L^{-1})	21.7 - 23.8	19.9 - 20.3

The pharmaceutical CBZ compound was then dissolved in the effluents of MBR system at a concentration of 5 mg L^{-1}. Owing to the low solubility of CBZ, the mixture was magnetically stirred for 5 min followed by sonication of 5 min. This stirring-sonication procedure was repeated twice to ensure the complete dissolution of CBZ in the effluents. After this, 3 L of this spiked effluent was mixed with either TNC or TiO_2-K catalyst at 1 g L^{-1} for 30 min before being pumped through the SB-ASP system. Three different samplings were conducted both before the addition of CBZ and photocatalysts, and after 30 min mixing.

2.4. Setup of Sequential Batch Annular Slurry Photoreactor

The SB-ASP used in this study was a modified photoreactor system based on our previous studies (Chong et al., 2009b, 2009c and 2009d). This SB-ASP was fabricated from stainless steel with a capacity of approximately 4.5 L and working volume of 3.6 L. The SB-ASP was operated as a three phase bubble column reactor, where the photocatalyst particles were suspended in the aqueous solution with the aid of air sparging. An air sparger with porosity of 45 μm was fitted to the detachable conical base of the vertical column. A low-intensity (11W) UVC lamp was fitted annularly to the central axis of the column with the quartz thimble encapsulation to prevent direct fluid contact between the lamp and reaction mixture. Specific probes for in-situ measurement of pH and DO were also fitted to monitor the properties change during the reaction. All the fluid connection lines were fitted with appropriate sized Tygon tubes for a complete SB-ASP system. To operate the SB-ASP mode, three different pumps were connected at the reactor inlet and outlet with the proper electronic timer adjustment. In this study, three different reaction schemes was proposed in one SBR cycle where initially (1) 3L of the catalysts-water mixture will be recharged into column in a 0.5 h; follows by (2) the UVC photocatalytic reaction under certain post-determined time and finally (3) the discharge of 2L of the reacted medium and co-catalyst reactivation in 1 h. It should be noted that after 1 h, the UVC lamp was programmed to be turned-off regardless of the capacity of the discharged volume. During the wastewater discharge phase, the microfiltration module (Varian Inc, Australia) was back-washed intermittently (10 s in every 10 min) to prevent the decline in filtration flux. In the following SBR cycle, 2L of the fresh mixture will be recharged and mixed with the aged suspension. This procedure was repeated for three times to study of whether the catalysts were able to operate in such a mode or deactivated, requiring

the constant replacement of new photocatalysts. The experimental setup of the SB-ASP, together with the proposed SBR cycle is shown in Fig. 2.

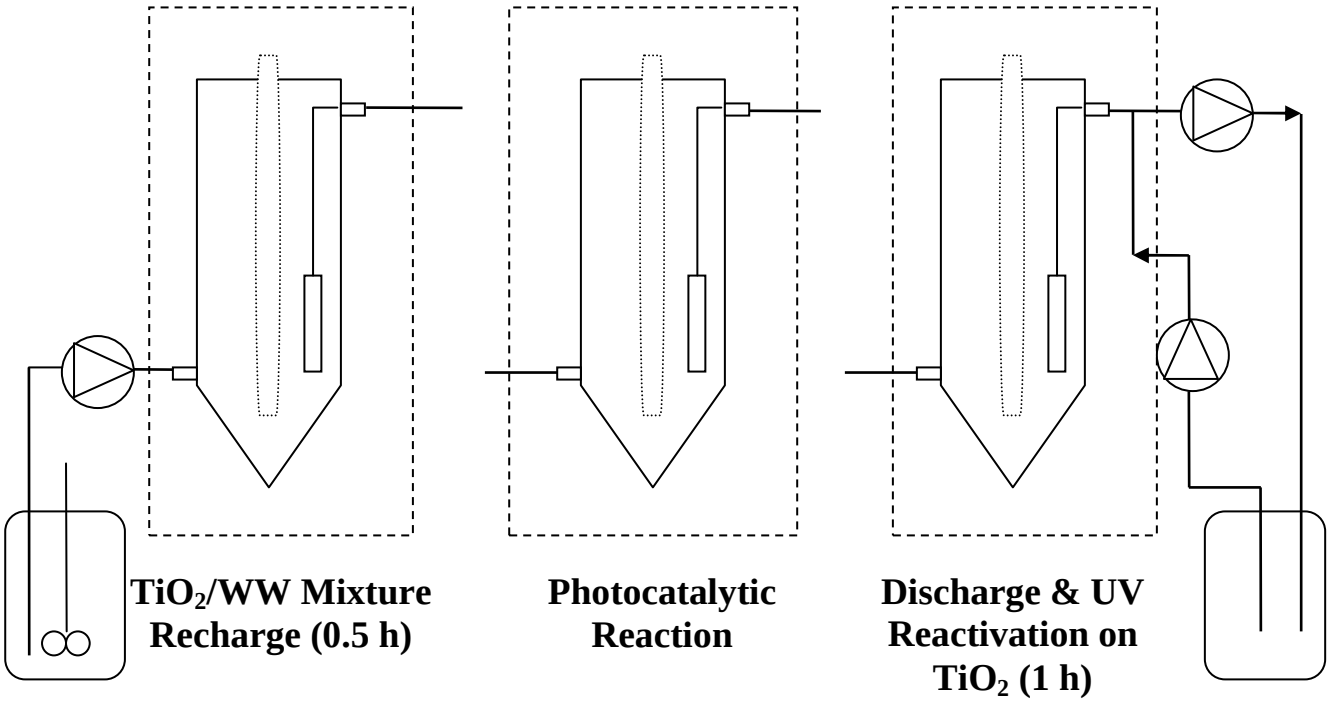

Figure 2: Schematic for a sequencing batch reaction cycle with three different phases in a cycle. (1) TiO_2/Wastewater (WW) recharges; (2) Batch photocatalytic reaction and (3) Discharge of 2/3 of original and UV reactivation on catalyst.

2.5. Analytical Procedures

Four separate analytical methodologies were employed to monitor the removal of pharmaceutical CBZ from the secondary treated effluents, to evaluate the subsequent effects of photocatalytic reaction on the CBZ intermediates and to determine the changes in the molecular weight profiles of the overall wastewater matrix.

The CBZ concentrations were analysed by a HPLC [Varian Pro-star, Varian Microsorb-MW 100-5 C18 column (4.6 x 150 mm, 5 μm)] at a flowrate of 1.0 mL min^{-1} and UV absorbance detection at 254 nm. The mobile phase was methanol 60% plus ammonium acetate (10mM) and acetic acid (5mM). The injection volume was 20 μL. The UV-Vis absorbance of the sample was measured using a UV-Visible spectrophotometer (LIUV-201, Lambda Scientific

Pty Ltd, Australia) equipped with a quartz cell having a path length of 1 cm. An absorbance at wavelength of 280 nm detected the presence of possible aromatic pharmaceutical intermediates.

To investigate the changes in the AMW profile of the wastewater samples during photocatalysis, the samples were analysed using a coupling method of high-performance size exclusion chromatography (HPSEC) and UV detection (Liu et al., 2008). Sample injection and separation were conducted with a Waters 2690 Alliance system with a temperature-controlled oven (30 °C) and a Shodex KW802.5 glycol functionalized silica gel column. Elution was monitored with a Waters 996 photodiode array detector (260 nm). Samples were filtered through a 0.22 μm membrane filter prior to analysis and a sample volume of 100 μL was injected. The mobile phase was 0.02 M phosphate buffer at pH 6.8 adjusted to an ionic strength of 0.1 M with sodium chloride. The system was operated at isocratic conditions with an eluent flow rate of 1.0 mL min^{-1}. Polystyrene sulfonate standards (Polysciences, USA) with MW 4.6, 8, 18, and 35 kDa were used to calibrate the retention time response to AMW.

Chemical oxygen demand (COD) was analysed to measure the extent of mineralization in the photocatalytic treatment of the wastewater samples. COD is a sum measurement of the amount of oxygen (mg) consumed per L of the wastewater sample. In order to determine the COD, an open reflux method was used where 2 mL of the sample was added into the low range 0-150 mg L^{-1} COD reagent (Hach Lange GmbH, Germany) containing potassium dichromate ($K_2Cr_2O_7$) and subsequently heated for 2 h at 150°C in a digestion reactor of DRB 200 (Hach Lange GmbH, Germany). The oxidizable organic compounds present will react with the $K_2Cr_2O_7$, and further reducing the dichromate ion to green chromic ion. Furthermore the digestion reagent contains silver and mercury ions. Silver is a catalyst and mercury is used to complex chloride interferences. Using this method, the amount of Cr^{3+} produced is measured at the wavelength of 620 nm using a spectrophotometer DR4000 (Hach Lange GmbH, Germany) and the color intensity was correlated to the total oxidizable organic compounds and thus, COD values.

As for the determination of inorganic NO_3^- and PO_4^{3-} in the wastewater matrix, similar manufactured reagents were purchased from Hach Lange GmbH, Germany. The total nitrogen

was measured using the persulfate digestion method by a Hach measurement kit (Hach Lange GmbH, Germany), which comprises of total nitrogen 0-25 mg L^{-1} N reagents, spectrophotometer DR4000 and digestion reactor DRB 200. All the nitrogen present in the samples is converted into NO_3^- through an alkaline persulfate digestion reagent and further heated at 105°C for 30 min in the DRB 200 reactor. To eliminate the interference of halogen oxide during the measurement, sodium metabisulfite is added after the digestion. Nitrate then reacts with chromotropic acid under acid conditions to yield the final yellow complex that has an absorbance maximum at 410 nm. The final NO_3^- values could be obtained from the molecular weights conversion.

A vanadium molybdate spectrometry method was used to determine the PO_4-P concentration in the Hach kit (Hach Lange GmbH, Germany) which comprises of spectrophotometer DR4000, reagents and cuvette tubes (total phosphorous, 0-100 mg L^{-1} PO_4^{3-}). In this method, the orthophosphate reacts with molybdate in an acid medium to produce a phosphomolybdate complex. When further reacted with vanadium, a yellow vanadomolybdophosphoric acid is formed. The intensity of the yellow color is used to correlate the phosphate concentration in the wastewater sample. To hydrolyze the condensed inorganic forms of phosphorous, the samples were pretreated with acid and heated at 105°C for 30 min in the DRB 200 reactor. Since the yellow color correlation gives the concentration in terms of total phosphorus, the final measurement in PO_4^{3-} must be converted using their corresponding molecular weights.

3. Results and Discussion

3.1. Preliminary Investigation on the Sequential Batch Reaction Time

In recent years, the application of photocatalytic processes for water treatment still encounters various technical challenges such as catalyst deactivation by complex water matrices and poor reaction turnover time to achieve complete mineralization (Lin and Lin, 2007). Doll and Frimmel (2004) proposed that instead of utilizing photocatalysis as a stand-alone treatment (requires long reaction time), it should be used as a pre- or post-treatment step to enhance the biodegrability of the persistent pollutants. Previous studies on the photocatalytic degradation of CBZ showed relatively good results in the distilled water matrices (Doll and Frimmel, 2004,

2005a and 2005b). It was found that there is a lack of information on the photocatalytic degradation of CBZ in real wastewater effluents. Thus, in this study the main aim is to investigate the optimal sequential batch reaction time (SBRT) for the semi-continuous treatment of secondary treated biological wastewater.

To achieve this, we first investigated the suitable range of SBRT to fit to the proposed scheme as in Section 2.4. Reaction times ranging from 0.5 to 4 h in 0.5 h increments were experimented, to find the optimum time between the COD, inorganic NO_3^- and PO_4^{3-} and AMW changes without CBZ spiked. The reason for not spiking CBZ is to serve as a control experiments, so that the direct synergistic effect of the CBZ can be differentiated in the following section. Fig. 3 shows the normalized experimental outcomes on the effects of different SBRT on the key water parameters for the two photocatalysts used. Fig. 3 shows that the two photocatalysts used have different mechanisms and reactivity towards N atoms in the wastewater effluent. Fig. 3a suggested that the TNC fibrils have higher affinity for the conversion of N atoms that present in the effluent, leading to an increase in NO_3^- concentration (24% increase) in a prolonged SBRT of 4 h. Low et al. (1991, 1992) explained that in the photocatalytic oxidation of nitrogen, N will be first converted to NH_4^+ and then to NO_3^-. The mesoporous TiO_2-K catalyst was found to have a lower conversion rate of N atoms to NO_3^- as we deduced that most of the NO_3^- was predominantly adsorbed (18% adsorbed at 4 h SBRT) onto the surface of the catalysts. Comparison of the two photocatalysts used suggested that such the gradual reduction in aqueous NO_3^- with TiO_2-K might be owing to the TiO_2 immobiliser platform of K that possess a larger surface area for adsorption and higher tendency for ion exchange phenomena.

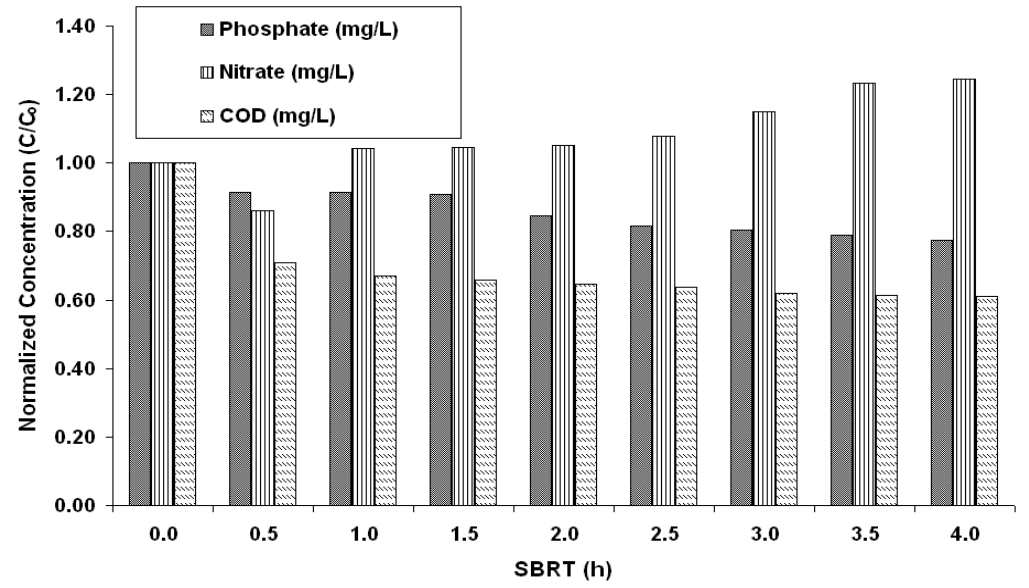

(a)

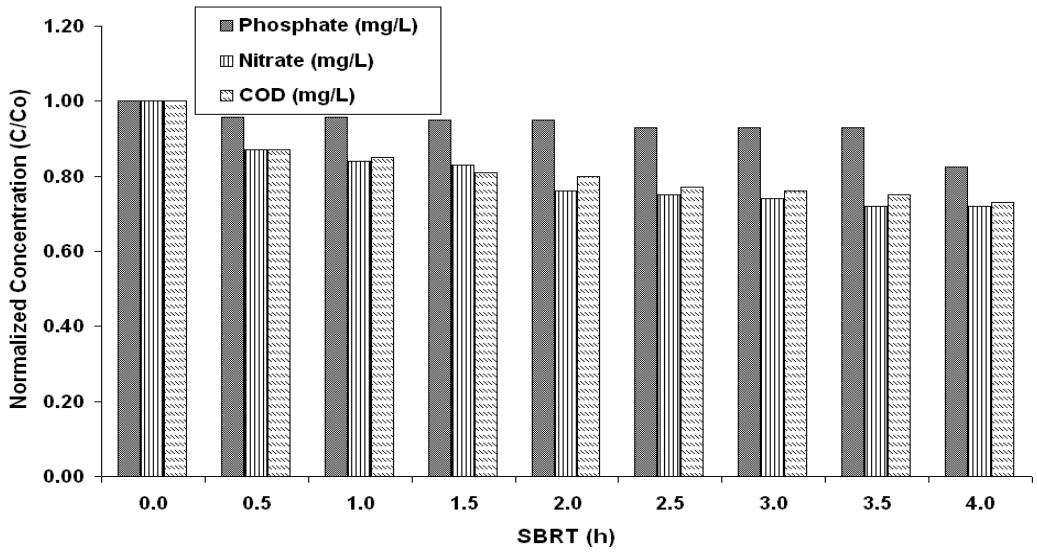

(b)

Figure 3: Normalized photocatalytic effects on the wastewater parameters at different SBRTs without CBZ spiked. (a) Using TNC fibrils; (b) Using mesoporous TiO_2-K catalyst. Initial reaction conditions: 1 g L^{-1} catalyst concentration and pH 7.40.

Similarly, Low et al. (1991, 1992) demonstrated that the P atoms in wastewater matrices will be converted to PO_4^{3-} during photocatalytic treatment. Connor and McQuillan (1999) found that PO_4^{3-} has a strong adsorption binds to the TiO_2 surface with further possibility to alter the surface chemistry of TiO_2 particles. The adsorption of PO_4^{3-}, however, is a strong function of

pH and usually is elevated at a low pH owing to the electrostatic interaction. Fig. 3 shows that the PO_4^{3-} was gradually reduced over prolonged SBRT by TNC photocatalysis, while PO_4^{3-} adsorption in TiO_2-K catalyst shows similar trend but to a lesser adsorption extent. The PO_4^{3-} concentration at 4 h SBRT using TiO_2-K only shows a 18% reduction, while 23% was observed in TNC fibrils. Two possible explanations for the higher PO_4^{3-} removal efficiency in TNC than TiO_2-K are that; (1) the PO_4^{3-} has a higher affinity for strong adsorption binds to the surface of the TNC and causing the lower PO_4^{3-} in the measured aqueous phase or (2) equilibration of PO_4^{3-} into different inorganic phosphate species in water such as HPO_4^{2-}, $H_2PO_4^-$, H_3PO_4 and others by TNC fibrils.

The COD measurements on the wastewater samples, accompanying with HPSEC UV 260 nm analysis (Fig. 4) shows that both photocatalyst able to mineralize the dissolved organic components to a different extent with varying SBRT. From Fig.3, it can be deduced that the TNC has a higher affinity for organic mineralization in the wastewater than the TiO_2-K. Over the 4 h SRBT, the TNC could reduce approximately 40% of dissolved organic content while TiO_2-K catalyst could only achieve a 27% COD reduction at a similar photocatalyst concentration of 1 gL^{-1}. As discussed in our previous communication, the low affinity for organic mineralization in TiO_2-K might be attributed to the low surface coverage of TiO_2 crystallites on the TiO_2-K catalyst (Chong et al., 2009b). In this study, however, we intend to keep both the photocatalysts loading at 1 gL^{-1} to facilitate the direct comparison with the standard Degussa P25 TiO_2 from other studies. The optimum aeration rates used in this study are different for both catalysts, and are highly dependent on prior studies (Chong et al., 2009b and 2009c). An aeration of 5.0 L min^{-1} and 7.5 L min^{-1} was used for TNC and TiO_2-K catalyst, respectively.

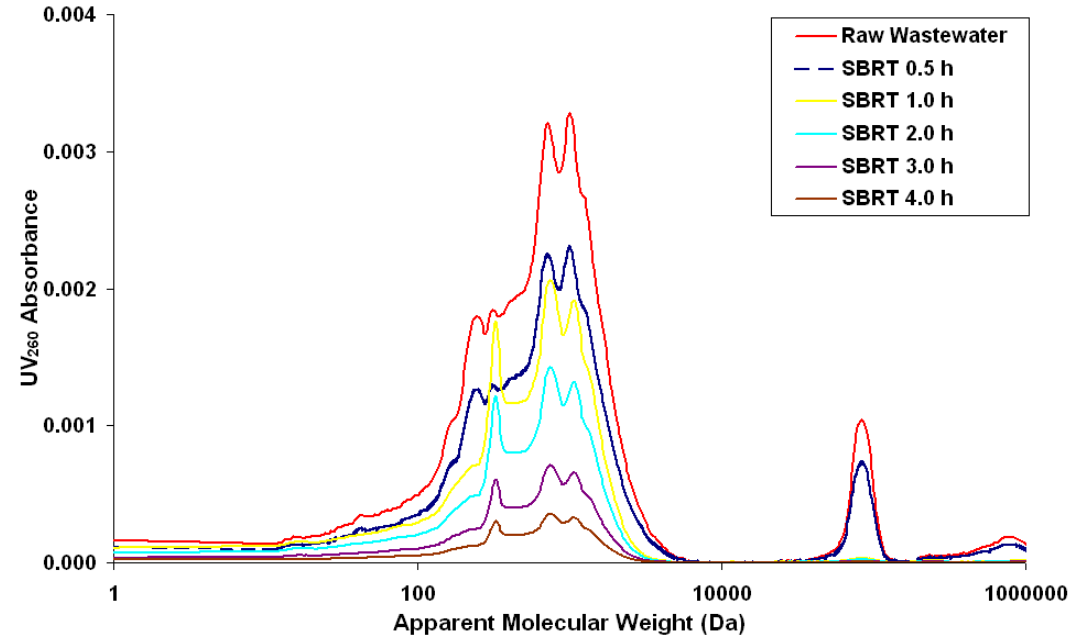

(a)

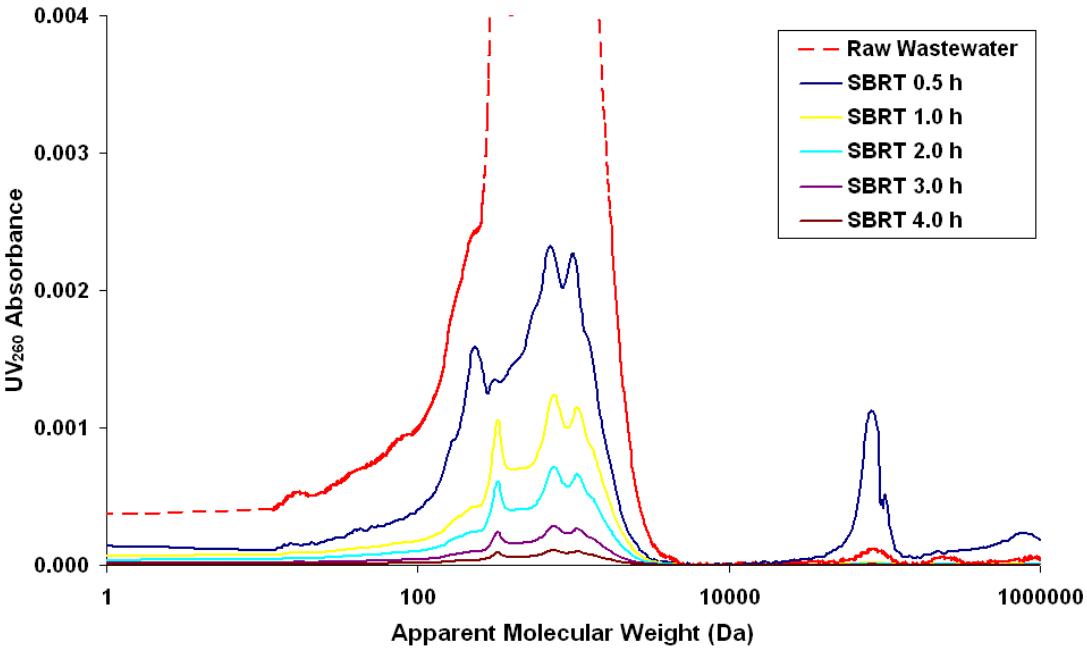

(b)

Figure 4: HPSEC chromatogram at different SBRTs without CBZ spiked. (a) Using TNC fibrils; (b) Using mesoporous TiO_2-K catalyst.

From the HPSEC analysis (Fig. 4), the EOM with AMW of >1–4 kDa in the wastewater samples was photocatalyzed to form organic compounds with lower AMW. The SBRT required to induce the changes in the physical and structural properties of the EOM at 1-4 kDa in wastewater appeared to be different for the two catalysts used and varied within 1 – 2 h. It was interesting to note that the higher AMW EOM could be more easily degraded by the photo-oxidation than the lower AMW ones. This would prevent the formation of disinfection by-products and membrane fouling in the subsequent wastewater treatment stages. Considering all these changes in water parameters, the 2 h SRBT was selected to complete the SB cycle of 0.5 h photocatalysts/wastewater mixture recharge, 2 h of photocatalytic reaction and followed by 1 h of wastewater discharge and simultaneous catalyst reactivation by means of UV irradiation.

3.2. Photocatalytic Degradation of Carbamazepine in the SB-ASP System

In this section, CBZ of 5 mg L^{-1} was spiked into the secondary biological treated wastewater as a collective representative of the pharmaceutical antiepileptic group that might present in wastewater. The extent of CBZ mineralization in the wastewater was measured using four complementary analytical techniques of HPSEC UV_{260nm}, UV_{280nm} and COD. The experimental data of the photocatalytic kinetics could be very useful to compare the controlled experiments in the previous section, and therefore could further contribute to knowledge of the degradation of CBZ in wastewater.

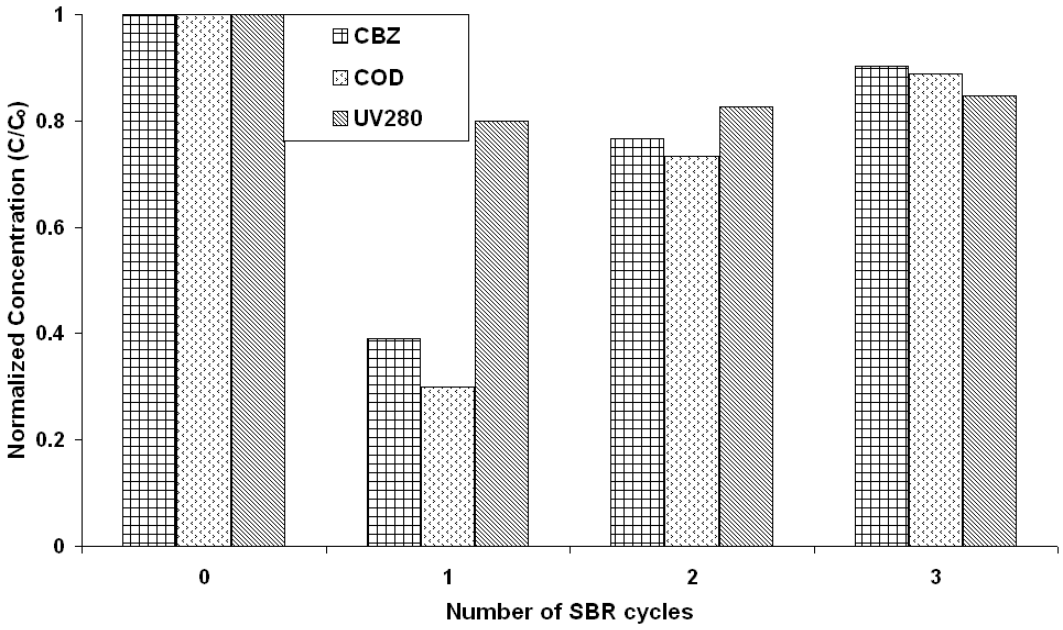

(a)

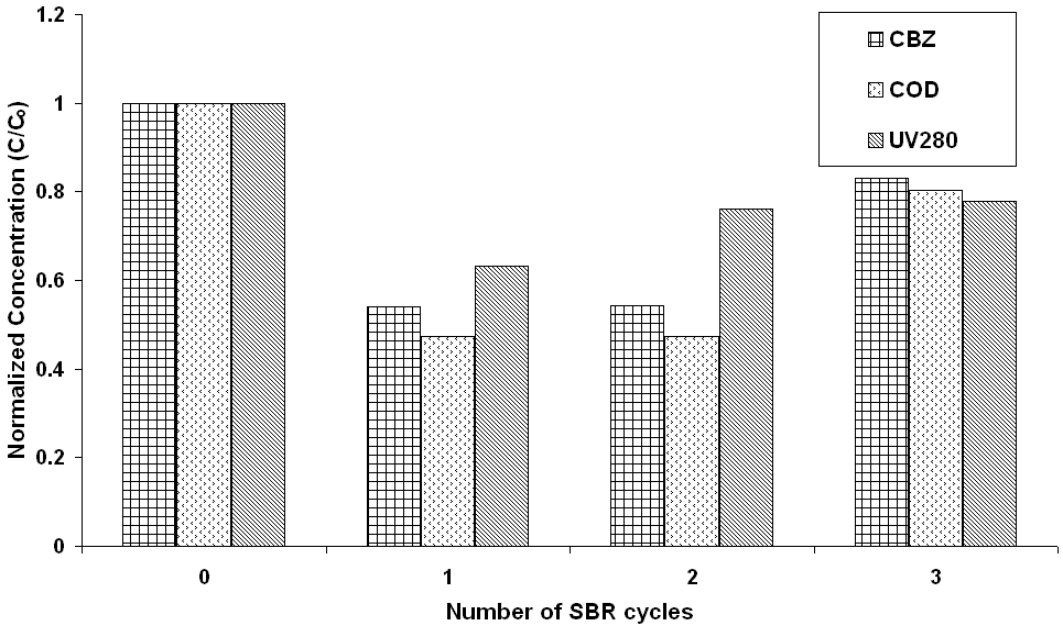

(b)

Figure 5: Normalized photocatalytic oxidation effects on the reduction of CBZ, COD and UV280 measurements in secondary wastewater over three SB reaction cycles. (a) Using TNC fibrils; (b) Using mesoporous TiO_2-K catalyst. Initial reaction conditions: 1 g L^{-1} catalyst concentration and pH 7.40.

Fig. 5 shows the photocatalytic oxidation of CBZ in secondary wastewater containing background EOM over three SBR cycles of 3.5 h each (10.5 h in total for 7 L treatment). From Fig. 5a, it can be seen that the TNC shows a high photoactivity in the first reaction cycle with a 70% COD reduction. When the concentration of CBZ was measured in parallel, it was found that the high COD reduction does not entirely correspond to the CBZ degradation. The COD reduction rate almost doubled when compared to the controlled experiment at 2 h SBRT without CBZ spiked. Such differences in COD might be attributed to the concurrent photocatalytic degradation of CBZ and its intermediates in the wastewater. This was further supported by the UV_{280} measurement, which shows reduction in the characteristics peak for the aromatic organic fraction of the pharmaceutical CBZ compound and its intermediates (Rizzo et al., 2009). Only a 20% reduction in the density of the aromatic organic fraction of the CBZ was obtained from the UV_{280} measurement. This means that a high COD reduction could originate from the background EOM of the wastewater. The HPSEC chromatogram in Fig. 6a shows that the high AMW peaks of the EOM at AMW > 100 kDa were degraded with TNC photocatalysis, resulting in smaller AMW peaks that arise at 750 and 1050 Da, respectively. At this UV absorbance, the peak for CBZ which should be between 200-1000 Da seems to be insignificant. Also the results from the HPSEC chromatogram (Fig. 6a) indicated that the photocatalytic treatment has slightly shifted the AMW peaks toward smaller AMW. From all these data, it can be deduced that the TNC photocatalysis preferentially degrades the high molecular weights fraction of the EOM, forming smaller organic by-products and these subsequently compete for the surface active sites with CBZ. High AMW fraction of the EOM is explained to be the preferential molecules to be attacked by the hydroxyl radicals, owing to the more reaction sites that promote TNC binding (Liu et al., 2008). Huang et al. (2008) also observed that the EOM has a very high adsorption affinity for TiO_2 particles with equilibrium reached in less than 5 min. Such preferential attack of high AMW fraction of the EOM rather than the CBZ has leaded to the partial oxidation of the CBZ compounds with 61% removal efficiency.

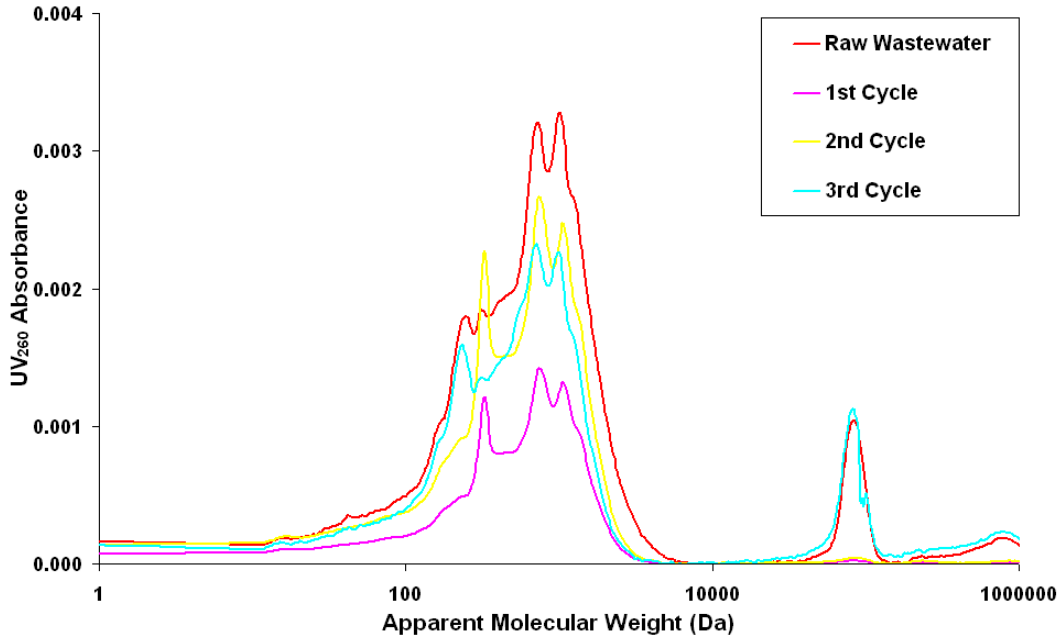

(a)

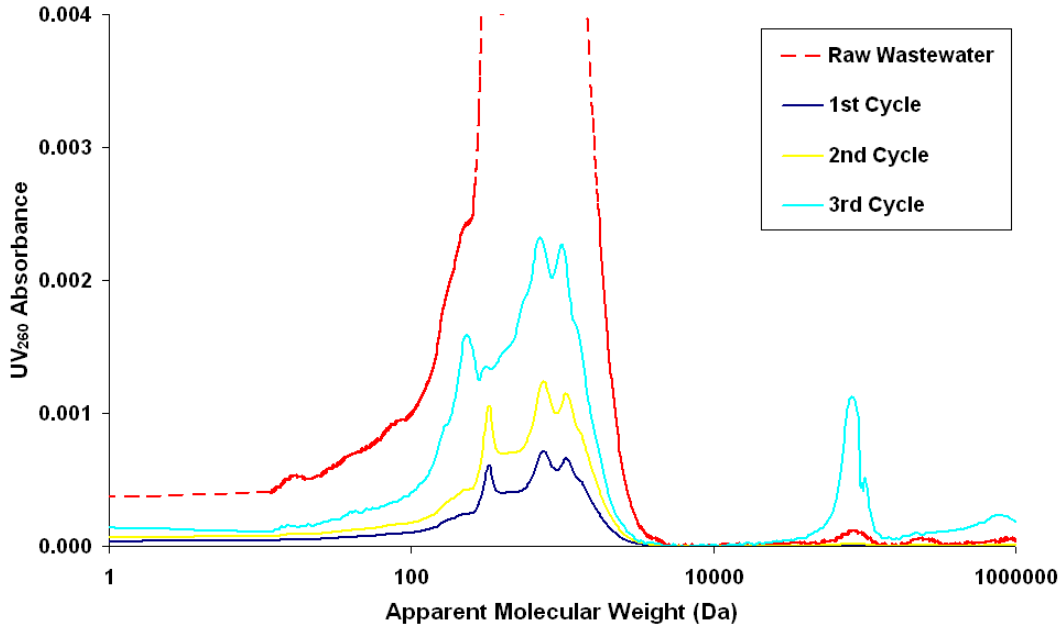

(b)

Figure 6: HPSEC chromatogram at different SBRTs with 5 mg L^{-1} CBZ spiked. (a) Using TNC fibrils; (b) Using mesoporous TiO_2-K catalyst.

In-situ pH measurement showed that there was a pH increase in the effluent from the average initial value of 7.41 to 7.75. This pH rise can be referred that the partially-oxidized CBZ intermediates were formed, due to its hydroxy- or chloro- nature. Doll and Frimmel (2005a) deducted on line the intermediates with CBZ degradation, and they found that 10,11-dihydro-CBZ-10,11-epoxide and 10,11-dihydro-CBZ were the main degradation products. When the same TNC catalysts were retained for the following two reaction cycles with fresh wastewater of 2 L added, it was observed that the photoactivity of the TNC gradually decreased with a COD reduction of 27% and 11% in the second and third reaction cycle, respectively (Fig. 5a). A similar trend was observed for the reduction in CBZ degradation (23% and 9%) and UV_{280} (17% and 15%) measurements. These can be explained by catalyst deactivation by the PO_4^{3-} ions in particular, and will be discussed in detail in Section 3.3.

When the TNC photoactivity was compared with the composite nature of the TiO_2 crystallites on mesoporous TiO_2-K catalyst, it was seen that a high COD reduction rate was associated with the TNC fibrils. One of the reasons for such an inferior photoactivity in TiO_2-K is owing to the low surface-coverage of TiO_2-K catalysts with TiO_2 crystallites (Chong et al., 2009a). From Fig. 5b, however, the CBZ degradation by TiO_2-K catalysts as evidenced from both the HPLC and UV_{280} measurements showed a more constant and photostable removal of CBZ over two consecutive reaction cycles. Fig. 6b shows the HPSEC chromatogram for the similar removal in high AMW fraction removal of EOM. The higher stability associated with the TiO_2-K catalysts operation in SB-ASP mode over TNC might be attributed to the higher specific surface area of the mesoporous particles (35.24 $m^2\ g^{-1}$ to 15.70 $m^2\ g^{-1}$). The abrupt changes in the photocatalytic efficiency during the third reaction cycles with TiO_2-K catalyst might be owing to the low reaction turnover time, where its catalytic surface area was fully-saturated and prevent the subsequent treatment of new contaminants that are present in the fresh wastewater feed.

3.3. Effects of Inorganic Anions NO_3^- and PO_4^{3-} on SB-ASP Operation

The effects of anions on the efficient photo-oxidation of organic compounds are inevitable as these anions are often associated with the complex matrices of wastewater or might evolve during the progress of the photocatalytic reaction. In this section, we evaluated the changes in two important inorganic anions of NO_3^- and PO_4^{3-} during the photocatalytic oxidation of CBZ.

Previous studies on the photo-oxidation of organic compounds in the presence of PO_4^{3-} have concluded that such an anion remains strongly adsorbed onto the TiO_2 surface over a wide pH range, and further inhibits its photoactivity (Kerzhentsev et al., 1996; Abdullah et al., 1990). Further in-situ internal reflection infrared spectroscopy studies by Connor and McQuillan (1999) confirmed such strong binding of PO_4^{3-} on the TiO_2 surface, where they concluded that the PO_4^{3-} shows a fast adsorption and slow desorption process. On the contrary, NO_3^- was reported to have minimal inhibition of the TiO_2 surface but may act as an inner filter in UV screening of the photocatalyst particles (Abdullah et al., 1990).

Controlled experiments in Section 3.1 without CBZ revealed that in 2 h SBRT, the PO_4^{3-} removal is higher in TNC (15%) than the TiO_2-K (5%) catalyst used. During the first SB-ASP cycle with CBZ, the PO_4^{3-} removal for both TNC and TiO_2-K catalyst were 21% and 25%, respectively (Fig. 7). The subsequent second and third SB cycles, however, showed an abrupt reduction in PO_4^{3-} removal for both TiO_2 catalysts. Connor and McQuillan (1999) explained that there are specific sites on the surface of TiO_2 that bind only PO_4^{3-} and CO_3^{2-}. This means that the PO_4^{3-} inhibition does not entirely affect the CBZ degradation but causes only a partial reduction in total surface sites. These were evidenced from the unparallel CBZ and COD removal efficiency with its PO_4^{3-} removal at both second and third SB cycles, even the PO_4^{3-} removal abruptly dropped after the first cycle. The PO_4^{3-} reduction during the second cycle for both TNC and TiO_2-K catalysts was 3% and 10%, respectively, while approximately 1% removal was obtained for both catalysts in the third SB cycle. Simultaneously, the CBZ degradation for the second and third cycles using TNC and TiO_2-K was 23% and 46% in the second cycle and 10% and 17% in the third cycle, respectively. Thus, it can be concluded that the anionic PO_4^{3-} in the wastewater has a partial effect on photocatalyst fouling and deactivation for subsequent use. However, the phosphate fouling does not proportionally reduce the photoactivity as can be seen from the phosphate uptake (adsorption) at each SB cycles with the CBZ and COD removal efficiency.

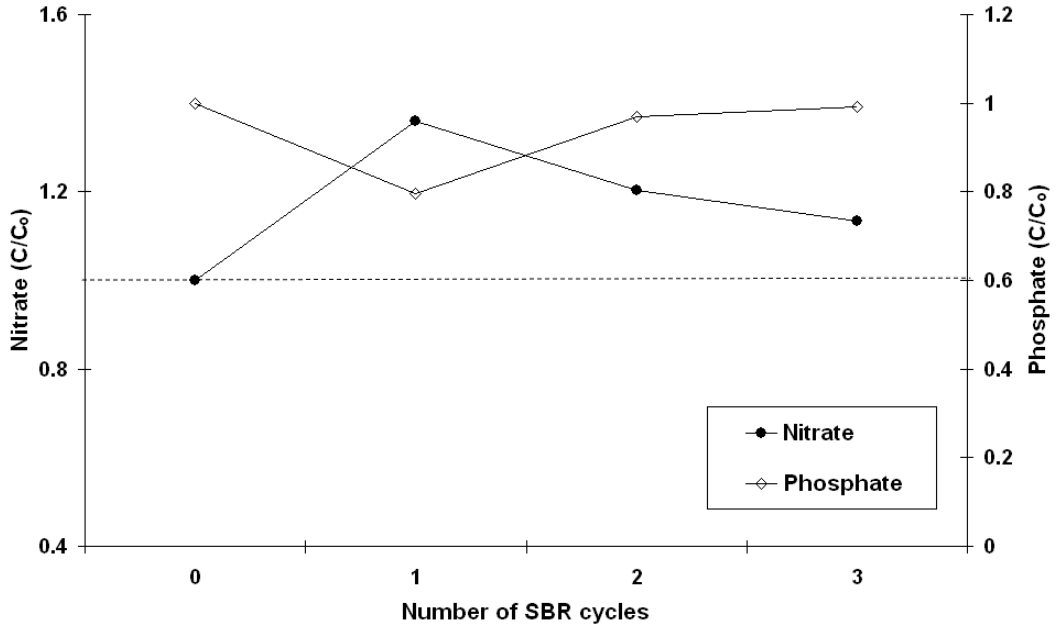

(a)

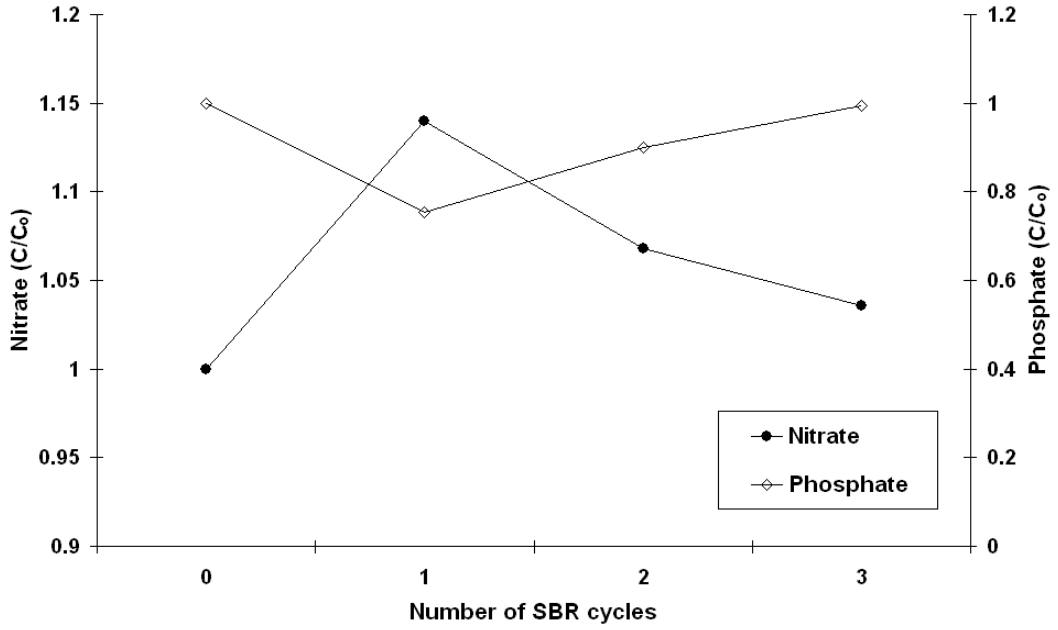

(b)

Figure 7: Changes in NO_3^- and PO_4^{3-} concentration during the SB-ASP operation over three reaction cycles.

The independent effects of NO_3^- on the photo-oxidation of CBZ could not be qualitatively evaluated in this study. It was, however, interesting to note that NO_3^- concentrations increased after each SB cycles using the two catalysts (Fig. 7). The extent of the NO_3^- evolution in this case was seen to strongly correlate to the amount of CBZ degraded during the 2 h reaction cycles. As CBZ is an amine compound, the increase in NO_3^- in this case might be owing to the partial photooxidation of CBZ and release of N atoms into the wastewater effluent. Prolonged oxidation of the N atoms during the photocatalytic reaction will contribute to an increase in the overall NO_3^- concentration. In this instance, the measurement of NO_3^- can be used as a relative indicator for the extent of CBZ degradation during the photooxidation process. From the SB-ASP operation using both catalysts, it can be concluded that the overall NO_3^- evolution rate was higher in TNC than TiO_2-K (Fig. 7).

4. Conclusion

The possible integration of a microfiltration module into the ASP for semi-continuous degradation of CBZ in secondary wastewater via the SBR operation mode has been successfully demonstrated. From this work, it can be shown that the SB-ASP operation with immobilized TiO_2 catalysts is a promising approach to enhance the biodegrability of persistent pharmaceuticals while retaining the photocatalysts for continuous use. It is expected that such SB-ASP systems could be operated in conjunction with a biological treatment process, so as to establish an integrated chemical-biological treatment process for wastewater reclamation and reuse, due to the combined removal capacity, better water quality and lower process operation costs.

When the pharmaceutical CBZ was degraded in the presence of high molecular weight EOM in wastewater, preferential attack on the EOM was found to be one of the key reasons for lowered degradation efficiency of CBZ. Inorganic PO_4^{3-} in the wastewater was also found to have a detrimental effect of photocatalyst fouling and deactivation of both TiO_2 catalysts used. However, it was found that the PO_4^{3-} fouling is site-specific and does not completely retard the photoactivity of the catalysts used. Also, the measured NO_3^- evolution rate from the degradation was found to strong correlate with the oxidation of CBZ in wastewater. In

conclusion, the TNC fibril has shown higher photoactivity and affinity for the degradation of CBZ in wastewater (but decreases abruptly after first cycle) while the mesoporous TiO_2-K catalysts shows higher adsorption capacity and photostability over the three assessed cycles for each catalyst. Further works need to be carried out to obtain a better understanding of the effects of different wastewater constituents on the degradation of pharmaceutical CBZ in complex wastewater effluent. This information is important for the optimization of the operation of SB-ASP (i.e. SBR cycle time, catalyst dosage, aeration rate) for a better treatment performance.

Acknowledgement

The authors would like to thank Ms. Vipasiri Vimonses and Dr. Giuseppe Laera for their technical assistances. This work was supported by the Australian Research Council Linkage Grant (LP0562153) and the Australian Water Quality Centre, SA Water Corporation, through the Water Environmental Biotechnology Laboratory (WEBL) at the University of Adelaide.

References

Abdullah, M., Low, G.K.C., Matthews, R.W., 1990. Effects of common inorganic anions on rates of photocatalytic oxidation of organic carbon over illuminated titanium dioxide. J. Phys. Chem. 94, 6820-6825.

Anderson, P.D., D'Aco, V.J., Shanahan, P., Chapra, S.C., Buzby, M.E., Cunningham, V.L., Duplessie, B.M., Hayes, E.P., Mastracco, F.J., Parke, N.J., Rader, J.C., Samuelian, J.H., Schwab, B.W., 2004. Screening analysis of human pharmaceutical compounds in US surface waters. Environ. Sci. Technol. 38, 838-859.

Belgiorno, V., Rizzo, L., Fatta, D., Rocca, C.D., Lofrano, G., Nikolaou, A., Naddeo, V., Meric, S., 2007. Review on endocrine disrupting-emerging compounds in urban wastewater: Occurrence and removal by photocatalysis and ultrasonic irradiation for wastewater reuse. Desalination 215, 166-176.

Benotti, M.J., Stanford, B.D., Wert, E.C., Snyder, S.A., 2009. Evaluation of a photocatalytic reactor membrane pilot system for the removal of pharmaceuticals and endocrine disrupting compounds from water. Wat. Res. 43, 1513-1522.

Chong, M.N., Vimonses, V., Lei, S., Jin, B., Chow, C., Saint, C., 2009a. Synthesis and characterisation of novel titania impregnated kaolinite nano-photocatalyst. Micro. Meso. Mater. 117, 233-242.

Chong, M.N., Lei, S., Jin, B., Saint, C., Chow, C.W.K., 2009b. Optimisation of an annular photoreactor process for degradation of Congo red using a newly synthesized titania impregnated kaolinite nano-photocatalyst**.** Sep. Purif. Technol. 67, 355-363.

Chong, M.N., Jin, B., Zhu, H.Y., Chow, C.W.K., Saint, C., 2009c. Application of H-titanate nanofibers for degradation of Congo red in an annular slurry photoreactor. Chem. Eng. J. 150, 49-54.

Chong, M.N., Jin, B., Chow, C.W.K., Saint, C.P., 2009d. A new approach to optimise an annular slurry photoreactor system for the degradation of Congo red: Statistical analysis and modelling. Chem. Eng. J. 152, 158-166.

Doll, T.E., Frimmel, F.H., 2004. Kinetic study of photocatalytic degradation of carbamazepine, clofibric acid, iomeprol and iopromide assisted by different TiO_2 materials – Determination of intermediates and reaction pathways. Wat. Res. 38, 955-964.

Doll, T.E., Frimmel, F.H., 2005a. Removal of selected persistent organic pollutants by heterogeneous photocatalysis in water. Catal. Today 101, 195-202.

Doll, T.E., Frimmel, F.H., 2005b. Photocatalytic degradation of carbamazepine, clofibric acid and iomeprol with P25 and Hombikat UV100 in the presence of natural organic matter (NOM) and other organic water constituents. Wat. Res. 39, 403-411.

Doll, T.E., Frimmel, F.H., 2005c. Cross-flow microfiltration with periodical back-washing for photocatalytic degradation of pharmaceutical and diagnostic residues-evaluation of the long term stability of the photocatalytic activity of TiO_2. Wat. Res. 39, 847-854.

Esplugas, S., Bila, D.M., Krause, L.G.T., Dezotti, M., 2007. Ozonation and advanced oxidation technologies to remove endocrine disrupting chemicals (EDCs) and pharmaceuticals and personal care products (PPCPs) in water effluents. J. Hazar. Mater. 149, 631-642.

Heberer, T., Dünnbier, U., Reilich, C., Stan, H.J., 1997. Detection of drugs and drug metabolites in groundwater samples of drinking water treatment plant. Fresenius Environ. Bull. 6, 438-443.

Huang, X., Leal, M., Li, Q., 2008. Degradation of natural organic matter by TiO_2 photocatalytic oxidation and its effect on fouling of low-pressure membranes. Wat. Res. 42, 1142-1150.

Huber, M.M., Canonica, S., Park, G.Y., von Gunten, U., 2003. Oxidation of pharmaceuticals during ozonation and advanced oxidation processes. Environ. Sci. Technol. 37, 1016-1024.

Kerzhentsev, M., Guillard, C., Herrmann, J.M., Pichat, P., 1996. Photocatalytic pollutant removal in water at room temperature: case study of the total degradation of the insecticide fenitrothion (phosphorothioic acid O,O-dimethyl-O-(3-methyl-4-nitro-phenyl) ester). Catal Today 27, 215-220.

Klavarioti, M., Mantzavinos, D., Kassinos, D., 2009. Removal of residual pharmaceuticals from aqueous systems by advanced oxidation processes. Environ. Int. 35, 402-417.

Kümmerer, K., 2009. The presence of pharmaceuticals in the environment due to human use – Present knowledge and future challenges. J. Environ. Management 90, 2354-2366.

Lin, C., Lin, K.S., 2007. Photocatalytic oxidation of toxic organohalides with TiO_2/UV: The effects of humic substances and organic mixtures. Chemosphere 66, 1872-1877.

Liu, S., Lim, M., Fabris, R., Chow, C., Drikas, M., Amal, R., 2008. TiO_2 photocatalysis of natural organic matter in surface water: Impact on trihalomethanes and haloacetic acid formation potential. Environ. Sci. Technol. 42, 6218-6223.

Low, G.K.C., McEvoy, S.R., Matthews, R.W., 1991. Formation of nitrate and ammonium ions in titanium dioxide mediated photocatalytic degradation of organic compounds containing nitrogen atoms. Environ. Sci. Technol. 25, 460.

Low, G.K.C., Zhang, M., 1992. Degradation of hazardous organics in water by titanium dioxide mediated photocatalytic oxidation. Proc. Emerging Technologies for Hazardous Waste Management, Atlanta, Georgia, Vol. 2, 507-510.

Malato, S., Fernández-Ibáñez, P. Maldonado, M.I. Blanco, J., Gernjak, W., 2009. Decontamination and disinfection of water by solar photocatalysis: Recent overview and trends. Catal. Today 147, 1-59.

Méndez-Arriaga, F., Esplugas, S., Giménez, J., 2008. Photocatalytic degradation of non-steroidal anti-inflammatory drugs with TiO_2 and simulated solar irradiation. Wat. Res. 42, 585-594.

Molinari, R., Pirillo, F., Loddo, V., Palmisano, L., 2006. Heterogeneous photocatalytic degradation of pharmaceuticals in water by using polycrystalline TiO_2 and a nanofiltration membrane reactor. Catal. Today 118, 205-213.

Muir, N., Nichols, J.D., Clifford, J.M., Skyes, J., 1997. Comparative bioavailability of aspirin and acetaminophen following single dose administration of soluble and plain tablets. Curr. Med. Res. Opin. 13, 491-500.

Putschew, A., Wischnack, S., Jekel, M., 2000. Occurrence of triiodinated X-ray contrast agents in the aquatic environment. Sci, Total Environ. 255, 129-134.

Radjenović, J., Petrović, M., Barceló, D., 2009. Fate and distribution of pharmaceuticals in wastewater and sewage sludge of the conventional activated sludge (CAS) and membrane bioreactor (MBR) treatment. Wat. Res. 43, 831-841.

Rizzo, L., Meric, S., Guida, M., Kassinos, D., Belgiorno, V., 2009. Heterogeneous photocatalytic degradation kinetics and detoxification of an urban wastewater treatment plant effluent contaminated with pharmaceuticals. Wat. Res. 43, 4070-4078.

Rosal, R., Rodríguez, A., Perdigón-Melón, J.A., Mezcua, M., Hernando, M.D., Letón, P., García-Calvo, E., Agüera, A., Fernández-Alba, A.R., 2008. Removal of pharmaceuticals and kinetics of mineralization by O_3/H_2O_2 in a biotreated municipal wastewater. Wat. Res. 42, 3719-3728.

Sacher, F., Lange, F.T., Brauch, H.J., Blankenhorn, I., 2001. Pharmaceuticals in groundwaters analytical methods and results of a monitoring program in Baden-Württemberg, Germany. J. Chromatogr. A 938, 199-210.

Ternes, T.A., 1998. Occurrence of drugs in German sewage treatment plants and rivers. Wat. Res. 32, 3245-3260.

Ternes, T.A., Meisenheimer, M., McDowell, D., Sacher, F., Brauch, H.J., Haist-Gulde, B., Preuss, G., Wilme, U., Zulei-Seibert, N., 2002. Removal of pharmaceuticals during drinking water treatment. Environ. Sci. Technol. 36, 3855-3863.

Zhu, H., Gao, X., Lan, Y., Song, D., Xi, Y., Zhao, J., 2004. Hydrogen titanate nanofibers covered with anatase nanocrystals: A delicate structure achieved by the wet chemistry reaction of the titanate nanofibers. J. Am. Chem. Soc. 126, 8380-8381.

Zwiener, C., Frimmel, F.H., 2000. Oxidative treatment of pharmaceuticals in water. Wat. Res. 34, 1881-1885.

CHAPTER 9

CONCLUSIONS AND FUTURE DIRECTION

1. Conclusions

1.1. Introduction

The application of heterogeneous semiconductor TiO_2 photocatalysis in water treatment is a sound and proven technology for the degradation of refractory organic compounds and inactivation of various microbial contaminants. One of the key technical problems that impede the further commercialisation of this advanced technology is the difficulty in post-separation of the fine commercial Degussa P25 TiO_2 particles (i.e. 30-50 nm) after treatment (Byrne et al., 1998). Fine particle size of the commercial TiO_2 presents various operational issues for a downstream separation unit if it is integrated with the aim to recover these particles. When the photocatalytic system is integrated with a membrane filtration module, serious pore blockage and gradual reduction in the permeate flux might be experienced with the further possibility of deteriorating the surface of the membrane used (Zhao et al., 2002). Similarly, long settling time might be attained when a sedimentation tank is used to recover the commercial TiO_2 particles (Aguado et al., 2002). If the TiO_2 particles are not fully recovered after the water treatment, the nanoparticles can cause potential risk to the environment and human health (Hund-Rinke and Simon, 2006).

This study was to synthesize a novel photocatalyst with high adsorption and photo-oxidation capacity that further permits the ease of post-separation after the water treatment process. Adsorption of the water pollutants onto the surface of the TiO_2 catalyst is a pre-requisite phase for promoting the surface interaction and subsequent high photocatalytic oxidation rate. Thus, immobilizing the TiO_2 particles onto larger supporting materials (in microns) for a slurry photocatalytic system operation is considered a viable solution to enhance the post-separation of the solid catalyst particles. Therefore, the aim of this study was to develop an efficient and cost-effective structured photocatalyst for slurry operation in a semiconductor photoreactor system. Comparison of the performance to another TiO_2 based catalyst with a fiber morphology was also performed, in order to assess the suitability of each immobilized catalyst in the batch and semi-continuous photoreactor operation. The research also focussed on the subsequent optimization and modelling of the photocatalytic treatment of water contaminated with various chemical and microbial contaminants (i.e. dye CR, pharmaceutical CBZ and *Escherichia coli*).

1.2. Major Achievements

Development of a novel photocatalyst via a reproducible synthesis method

A modified two step sol-gel method was developed to immobilize the nanosize TiO_2 crystallites onto the surface of the kaolin clay. The surface of the immobilizer K clay was pre-treated in a series of acidification-alkalization-thermal treatment to highly augment the specific surface area and porosity prior to TiO_2 immobilization. During the synthesis procedures, it was found that the concentration of nitric acid used had a profound effect on the eventual porosity of the TiO_2-K catalysts formed. The thickness of the TiO_2 crystallite layer formed on the K surface was also found to be highly dependent on the amount of K added in suspension. When the coated TiO_2-K was calcined, TiO_2 crystallites agglomerated into a large mesoporous structure with high specific surface area. The optimal temperature for the transition of anatase-to-rutile phase for the TiO_2-K catalysts was determined to be 650^oC. Photoactivity of the TiO_2-K catalysts was subsequently probed in a crude reactor system and found able to degrade 40 mg L^{-1} CR (~120mg COD L^{-1}) in 6 h of irradiation time. Simulated thermal cycles for recycle studies of the TiO_2-K catalysts showed that the catalyst particles were able to retain their initial photoactivity even after 5 reuse cycles.

Optimization of the photoreactor operating factors and its factor interactions

The optimization of the operation conditions using both the TiO_2-K and TNC catalysts was carried out in the ASP system. The operational parameters, including catalyst loadings, pH, aeration rate and CR concentration were optimized comprehensively in the ASP via conventional methods and the combined Taguchi-RSA approach. Results showed that the TiO_2-K was able to operate in a wide range of pH and was not constricted to the nominal range of pH<PZC (TiO_2) as in TNC. The PZC of TiO_2-K catalysts were determined to be highly basic of 9.5 to the slightly acidic in TNC of 4.6. Under the optimum operating conditions, the TiO_2-K catalysts were able to degrade 40 mg L^{-1} CR within 4 h of irradiation with a simultaneous 80% COD reduction while TNC-ASP system was able to achieve a 90% COD reduction for CR concentration of 60 mg L^{-1}. When the factor interactions were evaluated using coupling RSA-ANOVA, pH was not the dominant factor that affects the photoactivity in TiO_2-K catalysts but the initial CR concentration was the most important operational factor. In the TNC-ASP, on the other hand, the pH appeared to be a profound factor and greatly impacted with

other operational factors. This is one of few studies that have introduced the use of statistical analyses and an associated design of experiments approach to understand and optimise the photoreactor system.

Determination of photomineralization kinetic models of CR and its intermediate by-products

In this study, the LC-MS analysis method was used to study the possible photo-oxidation by-products formed during the CR degradation under a 7 h irradiation period. Experimental results showed that eight intermediate compounds were evolved along the irradiation period. The resultant MS intermediate peaks were then matched with both the NIST and NISTREP library data. These identified intermediates will provide a good basis for the development of the kinetic modelling and identification of proper photocatalytic reaction time.

Evaluation and development of photo-disinfection kinetics models

The photocatalytic inactivation of sewage isolated *E.coli* strain (ATCC 11775) using UVA-lamp driven ASP was successfully implemented in this study. At the optimum operating conditions of the ASP, a 5 log-reduction was achieved within 60 and 120 min for TNC and TiO_2-K catalyst, respectively. Different empirical photo-disinfection kinetic models were evaluated. It was found that the modified-Hom model gives a good approximation for the inactivation profiles with strong shoulder and tailing characteristics. In the case of TNC, the TNC loading has a significant impact on the DO level during the photocatalytic reaction. At the optimal TNC loading, the rapid volumetric generation rate of ROS resulted in enhancing the mass transfer and DO diffusion rate during the photo-disinfection reaction. This improvement of mass transfer and DO diffusion might be attributed to the thin fibril morphology of the TNC. Owing to this observation, an additional DO limiting term was added to the formulation of L-H mechanistic disinfection models for sub-optimal TNC loadings. Cross-validation of the formulated DO models showed the necessity for the inclusion of such a DO term in the sub-optimal TNC conditions.

Assessing the residual disinfecting effect of photocatalysis

In this study, Fe^{2+} at different concentrations was added to the reaction medium during the start of the irradiation experiments. After 2 h photocatalytic reaction, the UVA lamp was turned off, in order to assess the residual disinfecting effect (RDE) of the photocatalysis as a

result of constant dissociation of H_2O_2 formed during the photocatalytic reaction into $OH^{\cdot}$ radicals. It was found that the RDE at a constant Fe^{2+} concentration was highly dependent on the COD of the water quality. The photocatalytic reaction of TNC showed a preferential attack on the *E.coli* over the organic carbon that presents in the water. To ensure the biostability of the treated water using photocatalytic treatment, a prolong irradiation period needs to be ensured to degrade the COD at lower than 16 mg L^{-1}. Thus, if the photocatalytic treatment was targeted on the removal of microbes, sufficiently low organic carbon content has to be ensured to prevent the bacteria from utilizing the carbon sources for regrowth.

Development of sequential batch operation mode for semi-continuous wastewater treatment

The possible integration of a microfiltration module into the ASP system for semi-continuous treatment of CBZ in secondary wastewater via SBR mode was successfully implemented. The SB-ASP operation with immobilized TiO_2 catalysts proved to be a promising engineering solution to enhance the biodegrability of persistent pharmaceuticals while retaining the aged photocatalysts (without replacement) for continuous use. It is expected that such SB-ASP operation could be integrated with the biological treatment process to enhance treatment performance, due to their combined treatment efficiency, better water quality and low treatment costs.

Preferential adsorption and catalyst deactivation in wastewater effluent

It was found that the high molecular weight effluent organic effluent (EOM) in the wastewater was preferentially adsorbed and reacted prior to the degradation of the spiked surrogate pharmaceutical CBZ. This may be a result of higher number of reaction sites on the high molecular weight EOM than the spiked CBZ. Other than this, the presence of inorganic PO_4^{3-} in the wastewater was also determined to have a detrimental effect of photocatalyst fouling and deactivation on both TiO_2-K and TNC catalysts used. However, it was found that the PO_4^{3-} fouling is site specific and does not completely retard the photoactivity of the catalysts used. Compared to the two photocatalysts, the TNC fibril demonstrated a higher photoactivity and affinity for the degradation of CBZ in wastewater, while the mesoporous TiO_2-K catalysts showed a higher adsorption capacity and photostability during the SB-ASP operation.

1.3 Summary

This project has successfully developed a novel mesoporous photocatalyst, synthesis method and optimized the operational conditions in the ASP. Important scientific findings from the research included (1) identification of the intermediate by-products from the CR degradation, (2) evaluation and development of the photo-disinfection kinetic models, (3) assessment of the residual disinfecting effect of photocatalysis, (4) development of a sequential batch operation mode for semi-continuous wastewater treatment and (5) determination of organic species that has preferential adsorption and catalyst deactivation during wastewater treatment. The TiO_2-K photocatalyst developed in this study has a comparable photoactivity to those reported, but superior chemical and physical properties that surpass the commercial Degussa P25 TiO_2 catalyst. It is also worth noting that the performance of mesoporous TiO_2-K and TNC catalyst during the batch and SBR operation makes this photocatalytic water treatment process technically feasible due to the ease of post-separation and no blocking of the microfiltration module. Thus, the TiO_2-K-ASP and TNC-ASP systems can be a viable technology as a wastewater treatment process.

2. Future direction

2.1. Enhancement of Photoactivity and Response in TiO_2-K Catalyst

In order to promote the feasibility of photocatalytic water treatment technology in the near future, several key photocatalyst issues need to be taken into consideration, including (i) catalyst improvement for a high photooxidation efficiency that can utilize wider solar spectrum; (ii) catalyst immobilisation strategy to provide a cost effective solid-liquid separation; (iii) improvement of the surface coverage of immobilized TiO_2 crystallites. Currently, the utilization of solar energy is limited by the photo-efficiency of the TiO_2 catalyst bandgap to only 5% of the whole solar spectrum. Thus, if all the technical issues associated with the photocatalysts could be addressed, it is expected that the photocatalytic water treatment technology can be realised in the very near future.

2.2. Hybridization of Photocatalytic Water Treatment Process

At present, the applicability of the heterogeneous photocatalytic technology for water treatment is still limited by the slow photocatalytic turnover rate for organics degradation. In this instance, consideration should be given as to whether the photocatalytic process could be used as a pre-treatment step or stand-alone system. Owing to the non-selective reactivity on the non-biodegradable and soluble pollutants, the photocatalytic process could effectively be used as pre-treatment step to enhance the biodegradation ability of the recalcitrant organic pollutants prior to a biological water treatment plant. In such a way, the residence time and reaction volume for the biological treatment could be significantly reduced. If the photocatalytic process is used in a stand-alone treatment system, the residence time required might be prolonged for total bacterial inactivation or mineralization. As discussed, this is determined by the slow degradation rate, low photo-efficiency and need for continuous (without interruption) illumination to achieve certain total organic carbon removal or disinfection. For the stand-alone system, the site area requirement might be proportionally high owing to the increasing reaction volume required. The hybridization with other physical or chemical water treatment processes should be considered, in order to find a promising application of photocatalytic water treatment.

3. References

Aguado, J., van Grieken, R., López-Muñoz, M.J., Marugán, J., 2002. Removal of cyanides in wastewater by supported TiO_2-based photocatalysts. Catal. Today 75, 95-102.

Byrne, J.A., Eggins, B.R., Brown, N.M.D., McKinley, B., Rouse, M., 1998. Immobilisation of TiO_2 powder for the treatment of polluted water. Appl. Catal. B: Environ. 17, 25-36.

Hund-Rinke, K., Simon, M., 2006. Ecotoxic effect of photocatalytic active nanoparticles (TiO_2) on algae and daphnids (8 pp). Environ. Sci. Poll. Res. 13, 225-232.

Zhao, Y., Zhong, J., Li, H., Xu, N., Shi, J., 2002. Fouling and regeneration of ceramic microfiltration membranes in processing acid wastewater containing fine TiO_2 particles. J. Membr. Sci. 208, 331-341.